ACTIVATED CARBON MONOLITH CATALYSTS: A BRIDGE FROM GREEN CHEMICALS TO VALUE-ADDED PRODUCTS

by

MARYAM PIRMORADI

(Under the Direction of JAMES KASTNER)

ABSTRACT

This work investigated activated carbon monolith catalysts as a substitute for conventional packed bed reactors in furfural hydrogenation reactions. Comparing the powder, granular and monolith forms of Pd catalyst for furfural hydrogenation, monolith was the only catalyst that did not show external mass transfer resistance for both hydrogen and furfural, which contributed to a lower activity loss for this catalyst. Adding acetic acid to the reaction medium, an impurity of crude furfural, did not affect the conversion of furfural in presence of Pd on activated carbon monolith. Selective hydrogenation of furfural using bi-metal Pd-Cu and Pd-Fe on activated carbon monolith was studied. Adding a second metal to Pd shifted the selectivity of the catalyst from 2-methylfuran and 2-methyltetrahydrofuran to furfuryl alcohol and tetrahydrofurfuryl alcohol over the range of tested temperatures and pressures. A high space time yield of 272 g/Lcat/h tetrahydrofurfuryl alcohol and 143 g/Lcat/h furfuryl alcohol was achieved using Pd-Fe/ACM at 180 °C, 300 psig and liquid hourly space velocity of 15.38 h^{-1}. Selective hydrogenation of furfural to 5-hydroxy-2-pentanone over Pd-TiO_2 was also studied. TiO_2 added weak acid sites to Pd catalyst resulting in furan ring opening and

formation of 5-hydroxy-2-pentanone. The highest space time yield of 140 g/Lcat/h and selectivity of 39% was achieved for 5-hydroxy-2-pentanone in a short residence time at 180 °C and 300 psig. A kinetic model was developed for hydrogenation of furfural over Pd-TiO_2 using a two-site Langmuir-Hinshelwood mechanism. The reaction constants of 1.925, 0.506, 0.269 and 0.973 mol/gcat.h for consumption of furfural, formation of 2-methylfuran, formation of tetrahydrofurfuryl alcohol and formation of 5-hydroxy-2-pentanone were calculated from the model, respectively.

INDEX WORDS: Furfural, Hydrogenation, Activated Carbon Monolith, Packed Bed Reactor

ACTIVATED CARBON MONOLITH CATALYSTS: A BRIDGE FROM GREEN CHEMICALS TO VALUE-ADDED PRODUCTS

by

MARYAM PIRMORADI

BS, University of Tabriz, 2012

MS, University of Georgia, 2016

A Dissertation Submitted to the Graduate Faculty of The University of Georgia in Partial Fulfillment of the Requirements for the Degree

DOCTOR OF PHILOSOPHY

ATHENS, GEORGIA

2020

ACTIVATED CARBON MONOLITH CATALYSTS: A BRIDGE FROM GREEN CHEMICALS TO VALUE-ADDED PRODUCTS

by

MARYAM PIRMORADI

Major Professor:	James Kastner
Committee:	Mark Eiteman
	William Kisaalita
	Eric Ferreira

Electronic Version Approved:

Ron Walcott

Interim Dean of the Graduate School

The University of Georgia

May 2020

ACKNOWLEDGMENTS

First and foremost, I would like to thank my advisor, Dr. James Kastner for his support and expert guidance throughout my years in graduate school. His positive attitude and strong work ethic have been a great source of inspiration for me. Thank you Dr. Kastner for giving me the opportunity to work in your lab!

I would like to express my gratitude to the members of my committee, Dr. Mark Eiteman, Dr. William Kisaalita and Dr. Eric Ferreira for their expert suggestions and valuable feedback on my PhD work.

I owe my thanks to Nida Janulaitis for her contributions to analytical methods. I also thank Sarada Sripada for her support and contributions to FTIR analysis.

I am thankful to my family and friends for their unconditional love and encouragement. Thank you all!

TABLE OF CONTENTS

Page

LIST OF TABLES

Page

LIST OF FIGURES

Page

CHAPTER 1

INTRODUCTION

Monolith catalysts are a type of structured catalyst with a high number of small parallel capillary channels. Compared to its conventional packed bed counterpart, this honeycomb shape catalyst provides lower pressure drop and higher mass transfer rates due to a larger open frontal area and a shorter diffusion path. Unlike powder packed beds, monolith catalysts provide easy downstream filtration and separation. In addition, another advantage of using monolith catalysts is the easy scale-up of flow from one channel to the monolith structure. In other words, design for one capillary channel can be applied to all other channel in the monolith structure.

Activated carbon, obtained from renewable forest and agricultural resources, is a promising base material for production of monolith catalysts. Activated carbon provides a large surface area and a meso to micro pore distribution as a catalyst support. In addition, activated carbon supports provide advantages such as inertness, durability and easy recovery of precious metal from catalyst (by combustion). Therefore, manufacturing a monolith catalyst from activated carbon will allow all the benefits of both activated carbon and monolith structure in one single catalyst, known as activated carbon monolith catalyst. Activated carbon monolith catalysts, impregnated with precious metals and transition metals, can be promising catalysts for a series of continuous hydrogenation reactions.

Furfural is an abundant and inexpensive promising biomass-derived chemical that can form a series of value-added products through hydrogenation reactions. Over the past decades, dwindling of fossil resources along with their negative impact on the environment has brought

the attention to finding green and bio-based alternatives for fossil fuels. Therefore, hydrogenation of the bio-based furfural is an important industrial reaction due to forming valuable products that can be promising alternatives for fossil fuels. This hydrogenation reaction can result in products such as furfuryl alcohol (important monomer for furan resins), tetrahydrofurfuryl alcohol (solvent for agricultural, cleaning, coating and paint stripper formulations), 2-methyltetrahydrofuran and 2-methylfuran (promising alternative fuel and fuel additive) and cyclopentanone (precursor for aviation fuels, rubber chemicals and pharmaceuticals).

This work investigates heterogeneous continuous hydrogenation of aqueous furfural in presence of activated carbon monolith, powder, granular and crushed activated carbon monolith catalysts impregnated with precious metals in single or dual forms. The specific goals of this work were:

1. To compare Pd-supported activated carbon monolith to conventional Pd-supported granular and powder activated carbon for continuous aqueous furfural hydrogenation in terms of mass transfer, catalyst deactivation, product distribution as a function of temperature, pressure and residence time, Pd loading and Pd reduction temperature.
2. To perform comprehensive characterization of fresh and spent activated carbon monolith, granular and powder catalysts.
3. To determine the effect of adding a second metal (Fe and Cu) to Pd supported activated carbon monolith on product yield, selectivity and furfural conversion.
4. To determine the impact of impurities in crude furfural on product distribution and furfural conversion.

5. To synthesize a novel Pd-TiO_2 catalyst on activated carbon support and determine the effect of adding TiO_2 to Pd on formation of furan ring opening products in continuous furfural hydrogenation.
6. To develop a Langmuir-Hinshelwood rate law using Pd-TiO_2 on activated carbon for continuous hydrogenation of furfural in aqueous phase.

CHAPTER 2

BACKGROUND AND LITERATURE ANALYSIS

2.1 Activated Carbon Support

In addition to their key role in production of biofuels, biomasses from forest and agricultural resources are the important starting materials for production of activated carbon. Coconut shell, wood and coal are some of the main starting materials used in activated carbon production. Activated carbon is a type of processed carbon that demonstrates very high porosity due to possessing defective graphene layers.[1] This processed carbon has been widely used in the areas of catalysis, purification, filtration and medicine. Durability, inertness in reaction medium, stability in acid/base, high surface area and very well-developed porosity of activated carbon make it a promising catalyst support for chemical industry. One of the other advantages of activated carbon as catalyst support, specifically when used as a support for precious metals, is easy recovery of the metal by combustion of the catalyst.

2.1.1 Preparation of Activated Carbon

The preparation of activated carbon involves two steps: carbonization and activation. During the carbonization step, an organic/carbon-rich starting material undergoes heat treatment in an inert atmosphere to decrease impurities (mostly in form of gases and tars) and non-carbon compounds to result in a high carbon-content compound (char) with porosity. Due to the blockage of pores by impurities and residues during the heat treatment, an extra step of activation is required to develop porosity in activated carbon.[2] Chemical and physical activation are the two main methods of activating carbon.

2.1.2 Chemical Activation

During chemical activation, carbonization and activation occur simultaneously. In other words, prior to heat treatment in an inert atmosphere (carbonization step), the organic starting material is mixed with an activating agent such as nitric acid, sulfuric acid and phosphoric acid, zinc chloride and sodium hydroxide to prevent the formation of tar. After heat treatment in presence of the activating agent, the carbon material requires a washing step. During the washing step, all the remaining chemicals are removed from the carbon structure. Activating agent to starting material weight ratio (impregnation ratio), carbonization temperature, type of activating agent and type of starting material are some of the most important parameters affecting the development of porosity in activated carbon during chemical activation.[3] Giraldo et al. 2012 studied the effect of different impregnation ratios on development of porosity and surface area of activated carbon. They tested KOH and $ZnCl_2$ as activating agents for synthesizing activated carbon, obtained from coffee residue. With increasing the ratio of chemical agent to starting material weight from two to three, an increase in both pore volume and pore size was observed.[4] The increase in pore volume was explained by better removal of tars in presence of higher weights of chemical agent. In a study by Tsai et al. 2001, the effect of carbonization/activation temperature on porosity development of activated carbon was determined.[5] Waste corncob, the starting material, was carbonized and activated using KOH and K_2CO_3. By raising carbonization temperature from 500 to 800 °C, the BET surface area of activated carbon was raised from 0.1 to 1806 m^2/g with KOH and from 0.2 to 1541 m^2/g with K_2CO_3, respectively. The highest total pore volume of activated carbon treated with KOH and K_2CO_3 was also achieved at 800 °C (0.87 cm^3/g for KOH and 0.74 cm^3/g with K_2CO_3). Raising temperature during heat treatment increases the yield of gas and liquid products and decreases the yield of solid product/char.

Increasing temperature also increases the purity and quality of the solid product. The type of activating agent is an important parameter in porosity development of activated carbon. Donald et al. 2011 investigated the effect of activating agent on porosity development of activated carbon derived from Canadian peat.[6] A comparison between the N_2 desorption/ adsorption isotherms of $ZnCl_2$ and H_3PO_4 activated carbons indicated higher pore volume and lower surface area for the carbon that was activated with H_3PO_4. Carbon activation using H_3PO_4 developed a mesoporous structure whereas activation using $ZnCl_2$ resulted in micropores.

2.1.3 Physical Activation

Physical activation of activated carbon is usually a two-step process. First, the raw starting material undergoes carbonization and in a second step the carbon resulted from carbonization step is activated using steam, CO_2, air or a mixture of these in high temperatures (800-1000 °C). Steam and CO_2 react with carbon and result in carbon monoxide and other gases. In addition to carbonization temperature, activation temperature and type of starting material, type of activating gas can affect the porosity development of activated carbon. Amosa et al. 2014 prepared activated carbon using both CO_2 and steam.[7] They observed a surface area of 1185.3 m^2/g for carbon activated by steam, which was significantly higher comparing to carbon activated by CO_2 (surface area of 713 m^2/g). The significant difference between the surface areas was attributed to higher reaction rates in presence of steam. Compared to CO_2, steam molecules are smaller and can diffuse easier resulting in higher rates of reacting with carbon.

In general, both chemical and physical activation have some advantages and disadvantages. The advantages of using chemical activation compared to physical activation method are lower temperatures, one-step process, and shorter activation time, while the disadvantages are corrosion of instruments and requiring a washing step. Activated carbon

preparation process directly affects its properties such as surface area, pore volume, pore size distribution and surface chemical structure. It is possible to obtain different activated carbons from one biomass source simply by using different activation methods. Therefore, it is important to choose a suitable starting material and activation method for any desired purpose.

2.1.4 Chemical Composition and Surface Functional Groups

Surface chemistry of activated carbon has a significant effect on properties of activated carbon such as the charge, reactivity and hydrophobicity. The activated carbon matrix contains heteroatoms such as oxygen, hydrogen, nitrogen, chlorine, phosphorus and sulfur. These heteroatoms are bound to carbon atoms at the edges of graphene layers in form of functional groups such as carboxyl, carbonyl, phenols and others. The presence of these functional groups affects the acidity and basicity of activated carbon. The acidity of activated carbon is associated with the presence of functional groups such as carboxyl groups and lactones. Carbonyl, quinone and ether groups are responsible for basic properties of activated carbon. The preparation and activation process of activated carbon determines the concentration and amount of surface functional groups.[3] In other words, parameters such as type and concentration of activating agent, treatment temperature and the type of starting material have a great influence on the amount and type of surface functional groups. Prahas et al. 2008 determined the effect of activation temperature on surface chemistry of activated carbon (activated with H_3PO_4) prepared from jackfruit peel waste.[8] They observed that increasing activation temperature decreases the amount of acid surface group. Decreasing the amount of acid functional groups at high temperatures was attributed to degradation of several functional groups resulted in forming carbon monoxide and carbon dioxide. In order to change reactivity and other properties of activated carbon, the surface functional groups may be modified through different techniques.

For instance, oxidation treatments (using oxidizing gases or liquids) could increase the concentration of oxygen functional groups. In contrast, applying high temperatures (heat treatment in an inert atmosphere) could remove or decompose some of the functional groups. Figueiredo et al. 1999 reported that oxidation of activated carbon in gas phase (using 5% oxygen in nitrogen) increases the amount of hydroxyl and carbonyl groups while liquid phase oxidation (using nitric acid) improves the number of carboxyl groups.[9]

2.2 Monolith Catalysts

Monolith catalysts are honeycomb –shaped structures that have been mainly used in the automotive industry. The use of monolith catalysts in the automotive industry dates back to the mid-1970s when monolith catalysts were applied as catalytic converters for reduction of nitric oxides in exhaust gas.[10] Monolith structures, commonly fabricated using ceramic and metallic materials, provide a group of uniform straight thin channels that are separated through thin walls. For catalytic purposes, these ceramic or metallic structures are coated with a layer of catalyst such as palladium and platinum or catalyst support such as carbon, zeolites and silica. In order to assure the best adherence of the catalyst coat to the monolith structure, binders, additive, chemical and heat pretreatment are applied.[11] In comparison to conventional packed bed reactors, monolithic reactors provide lower pressure drop, high surface area to volume ratio, high mass transfer rates, easy scale up and filtration. Several research groups have investigated the application of monolith catalysts in both single and multiple phase reactions. Low temperature combustion of xylenes using Pd and Pt supported on carbon-coated monolith[12], hydrogenation of benzaldehyde to benzyl alcohol using Ni supported on γ-alumina-coated monolith[13], esterification of 1-octanol with hexanoic acid using zeolite-coated monolith[14], selective hydrogenation of fatty acid methyl esters using Pd supported on carbon coated monolith[15] and

hydrogenation of benzene to cyclohexene on Ru/alumina-coated monolith[16] are examples of reactions that have been performed using monolithic catalysts. Despite the benefits, monolith catalysts have not been commercialized for multiple phase reactions due to lack of experience in scale-up and high costs of extrusion of the monolith catalysts.[10]

2.2.1 Geometry Characterization

The geometry of monolith structures is characterized by cell density (cells per square inch/CSPI), open frontal area, geometric surface area and hydraulic diameter:

$$\text{Cell density} = \frac{1}{L^2} \qquad \text{Equation 2.1}$$

$$\text{Open Frontal Area (OFA)} = \frac{(L - t_W)^2}{L^2} \qquad \text{Equation 2.2}$$

$$\text{Geometric Surface Area (GSA)} = \frac{4(L - t_W)^2}{L^2} \qquad \text{Equation 2.3}$$

$$\text{Hydraulic Diameter} = \frac{4(\text{OFA})}{\text{GSA}} \qquad \text{Equation 2.4}$$

where L is width of channel (inch) and t_w is wall thickness (inch).[17]

Cell density and GSA are important factors in determining catalyst performance; OFA determines the void fraction (the high OFA of monolith catalysts provide low resistance against flow which further leads to high velocities of fluid throughout the channel) and hydraulic diameter defines the hydrodynamic behavior of the monolithic system.[17]

2.2.2 Pressure Drop

Lower pressure drop, compared to conventional packed bed reactors, is the most important advantage of monolith catalysts. During the fluid flow over a packed bed, a percentage of pressure is lost due to friction. This pressure loss results in energy loss and decreasing flow velocities. Pressure drop over packed beds is a challenging problem in designing reactors. Small

catalyst particle size provides high mass transfer rates during the reaction. On the other hand, employing small particle sizes results in higher pressure drop and a more difficult separation/filtration process. Therefore, selecting larger particle sizes decreases the pressure drop with sacrificing high mass transfer rates of the reaction. Monolith catalysts can provide high mass transfer rates (due to short diffusion path) and low pressure drops simultaneously. As mentioned in the previous section, monolith catalysts provide high open frontal area and hence lower flow resistance, which further leads to low pressure drop and high fluid velocities. Figure 2.1 (from Boger et al. 2004) compares pressure drops for monolith catalyst with particles having different shapes. For a multiphase monolithic reactor, operating under Taylor flow conditions, Kreutzer et al. 2005 suggested the following pressure drop correlations for each channel:[18]

$$\mathrm{fRe} = \frac{\left(\frac{\Delta P}{L} - \rho g \epsilon_L\right) d^2}{2 \mu U \epsilon_L} = 16\left[1 + \frac{17 d}{L_{slug}}\left(\frac{Re}{Ca}\right)^{1.3}\right] \qquad \text{Equation 2.5}$$

Where Re is Reynolds number ($\rho U d/\mu$), Ca is capillary number ($\mu d/\gamma$) where γ is surface tension, L_{slug} is the length of slug, L is length of monolithic reactor, ΔP is pressure drop, ϵ_L is liquid holdup, d is diameter of a single channel, U is sum of liquid and gas superficial velocities, μ is liquid viscosity, ρ is liquid density and f is friction factor.

Therefore, under Taylor flow conditions the pressure drop is a function of fluid properties, channel diameter, velocities, and length of bubble formed during the Taylor flow condition. It is possible to calculate the pressure drop of packed bed reactors through Ergun equation:[19]

$$\frac{dP}{dZ} = -\frac{G}{\rho g_c D_p}\left(\frac{1-\emptyset}{\emptyset^3}\right)\left[\frac{150(1-\emptyset)\mu}{D_p} + 1.75G\right] \qquad \text{Equation 2.6}$$

Where ∅ is porosity, G is superficial mass velocity (ρu), ρ is density, D_p is particle size, u is superficial velocity, P is pressure, Z is bed length and g_c is conversion factor for gravitational acceleration.

Bauer et al. 2011 compared the pressure drops of monolithic reactors and packed bed reactors in hydrogenation of alpha-methylstyrene using palladium.[20] In similar reaction conditions, using a monolithic reactor with 62 channels per square centimeter, 1.02 mm hydraulic diameter and wall thickness of 180 μm resulted in a 10 times smaller pressure drop compared to a conventional packed bed with catalyst spheres of 3.2 mm diameter.

2.2.3 Mass Transfer and Flow Patterns

A monolith catalyst consists of multiple parallel channels. Depending on the liquid and gas velocities and properties and channel geometry, a variety of flow patterns can occur in multiphase monolith reactors. At constant liquid velocities, with increasing gas velocity the flow pattern shifts from bubble flow to Taylor flow (where the elongated bubbles are separated through liquid slugs) to film flow (where liquid flows on the walls and gas flows in the center of the channel). With further increasing the gas velocity, annular flow appears with the continuous phase of a mist gas phase carrying small liquid drops inside. Due to low liquid velocities, compared to Taylor flow, film flow patterns are selected for reactions with longer residence times whereas Taylor flow patterns are usually selected for short residence time reactions.[21,22] Figure 2.2 (obtained from Moulijn et al. 2011) demonstrates different flow regimes in monolith channels.[23] Internal mass transfer resistance in monolithic reactors is usually negligible due to very thin channel walls and hence short diffusion length.[24] Roy et al. 2004 applied a diffusion length for calculation of Thiele modulus (∅) and internal effectiveness factor ($\eta_{internal}$) in monolithic reactors (an equivalent diffusion length as if the catalyst was pellet).[25] The equivalent

diffusion length (L) for monolith was calculated using (volume of the catalyst)/(surface area of the catalyst):

$$L = \frac{(1-OFA)Vchannel}{(GSA)Vchannel} = \frac{(1-OFA)}{(GSA)} \quad \text{for monolith catalyst} \qquad \text{Equation 2.7}$$

$$\emptyset = \frac{L\sqrt{k\, C_A^{n-1}}}{D_e} \quad \text{for an n order reaction} \qquad \text{Equation 2.8}$$

$$\eta_{internal} = \frac{\tanh(\emptyset)}{\emptyset} \qquad \text{Equation 2.9}$$

Where D_e is effective diffusivity, k is reaction rate constant and C_A is the concentration of species A.

2.2.4 Carbon-based Monolith Catalyst Supports

In general, ceramic and metallic materials are the base material in production of monolith structures. For catalytic purposes, the monolith structures are coated with layers of catalyst or catalyst support (known as coated monolith catalyst).[26] In addition to the coating method, preparation of monolith catalysts is also possible through extrusion of the support material (known as integral monolith catalyst). Activated carbon is a promising catalyst support that provides very well-developed porosity and high surface area for catalyst particles. Activated carbon-coated ceramic and metallic monolith structures have been employed as catalyst supports for catalysts such as precious metals. However, there are some disadvantages associated with using activated carbon-coated ceramic or metal catalyst support such as durability and inertness. One solution to overcome these issues is using the renewable integrated carbon materials. In addition to solving durability and inertness issue, employing activated carbon monolith catalysts as a support for precious metals offers easy recovery of the metal by a combustion step.

2.2.5 Carbon Monolith Preparation

Figure 2.3 is a schematic of monolith catalyst preparation methods (from Nijhuis et al. 2001).[27] Monolith extrusion is the first step in manufacturing of both integral and coated type monolith catalysts. Preparation of coated-type monolith catalysts involves extrusion of the inert material followed by coating with the desired catalysts support or catalyst while the integral type monolith catalysts is directly obtained from extrusion of the catalyst or the catalyst support. Manufacturing of integral type carbon monolith involves mixing of carbon particles such as activated carbon or carbon precursor such as resins, a binder (preferably inert) and an extrusion aid such as water followed by extrusion step. After extrusion, the extrudate goes under a drying step followed by carbonization and activation (The activation and carbonization steps are employed in a case where a carbon precursor such as resins is used for extrusion as opposed to activated carbon particles).[28] After preparation of the monolith support, the active phase is deposited through conventional methods used in preparation of regular granulated catalysts. The main three methods for deposition of metals on activated carbon monolith supports are impregnation, ion exchange and deposition precipitation.[27] There are two types of impregnation; dry and wet. During dry impregnation, a solution of active metal with a volume equal to the total pore volume of the monolith support is prepared and added to the support. As a result, the pores of catalyst support draw the solution with capillary action. This type of impregnation method is challenging for monolith structures since a small amount of solution (exactly equal to the total pore volume) is applied which might not be able to wet the entire surface of the structure and leave the center of the monolith catalyst dry. For monolith catalysts, wet impregnation is preferable since higher amounts of solution are applied and after liquid adsorption, the excess amount of solution is dried. Ion exchange is another active site deposition method where a

solution of metal salt complexes is prepared and added to the catalyst support. As a result, the metal complexes (ions) react with active surface groups of the support. Deposition-precipitation method is possible through placing the monolith in a metal salt solution and adding a second salt as a precipitating agent slowly. Therefore, the first salt starts depositing on the support surface.

2.3 Heterogeneous Hydrogenation Reactions

Hydrogenation reactions are among the most important reactions for organic synthesis. These reactions play a key role in industry of pharmaceuticals, fine chemicals, food, etc. Hydrogenation reactions can occur in presence of hydrogen gas (H_2) or other hydrogen donors such as alcohols which is known as transfer hydrogenation. In general, there are two major catalyst groups involved in heterogeneous hydrogenation reactions; first, precious metals such as platinum and palladium and second, transition base metals such as nickel and copper.[29] These metal catalysts can actively adsorb the hydrogen atoms from hydrogen gas. The adsorbed hydrogen atoms are further added to the unsaturated bond of the other reactants. Hydrogenation of acids to alcohols using rhenium and ruthenium, alkenes to alkanes using palladium and nickel and aromatic and aliphatic aldehydes to alcohols using ruthenium and palladium are examples of wide range of heterogeneous hydrogenation reactions.[29]

2.3.1 Furfural: a green feedstock for hydrogenation

Furfural, an aldehyde of furan, is a biomass-derived chemical. Acid hydrolysis of hemicellulose-rich biomasses such as corn stover, wheat bran, or corncobs results in xylose. In a second step, catalytic dehydration of xylose yields furfural. The global production of furfural is 300,000 tons per year[30] with market price of 1000 US dollars per ton.[31] Furfural hydrogenation can result in a series of valuable upgraded products such as furfuryl alcohol (important monomer for furan resins), tetrahydrofurfuryl alcohol (solvent for agricultural, cleaning, coating and paint

stripper formulations), 2-methyltetrahydrofuran, 2-methylfuran (promising alternative fuels) and cyclopentanone (precursor for aviation fuels, rubber chemicals and pharmaceuticals).[32]

Several research groups have investigated hydrogenation of furfural in both vapor and liquid phase. Hydrogenation to furfuryl alcohol and 2-methylfuran using carbon supported-copper catalyst at temperatures of 200 to 300 °C [33], silica supported-copper at temperatures of 230 to 290 °C [34], Cu/Zn/Al/Ca/Na = 59:33:6:1:1 (atomic ratio) and Cu/Cr/Ni/Zn/Fe = 43:45:8:3:1 (atomic ratio) at temperatures of 200 to 300 °C [35] and SBA-15 silica supported-copper at temperatures of 170 to 270 °C [36] are examples of furfural hydrogenation in vapor phase. Hydrogenation to furfuryl alcohol and 2-methylfuran over carbon supported-ruthenium at temperatures of 120 to 200 °C using alcohol (as an hydrogen donor) under 2.04 MPa nitrogen pressure [37], over Ni–Co–B amorphous alloy catalyst at 100 °C and 1 MPa (in ethanol) [38] and over metal oxides supported-platinum at temperatures of 50 to 70 °C (in alcohol solvents)[39] are examples of liquid phase hydrogenation of furfural.

All of the mentioned hydrogenation products of furfural, except for cyclopentanone, are obtained through hydrogen attack to a double bond on furan ring or aldehyde group. In addition to the hydrogen attack to a double bond, hydrogenation of furfural to cyclopentanone involves an acid catalyzed rearrangement of the furan ring, also known as Piancatelli rearrangement, to 4-hydroxy-2-cyclopentenone. The name of the reaction comes from Giovanni Piancatelli, who with coworkers discovered the rearrangement of 2-furylcarbinols into 4-hydroxycyclopentenones in presence of acid catalysts.[40] These researchers observed that for more reactive reactants weaker Lewis acids are required. After furfuryl alcohol rearrangement, 4-hydroxy-2-cyclopentenone undergoes fast hydrogenation and dehydration steps to form cyclopentanone (due to high reactivity). Further hydrogenation of cyclopentanone in reaction medium can result in formation

of cyclopentanol. Hronec et al. 2014 investigated the rearrangement of furfuryl alcohol to 4-hydroxy-2-cyclopentenone in water at temperatures of 110 to 200 °C.[41] Hronec et al. 2014 reported that the yield of 4-hydroxy-2-cyclopentenone increased with increasing temperature due to presence of hydrogen ions, resulted from natural dissociation of water to hydrogen and hydroxyl ions at high temperatueres, which acted as an acid catalyst for the rearrangement step. However, adding acetic acid and hydrochloric acid to the reaction medium decreased the yield of product and increased the furfuryl alcohol conversion. In another study, Hronec et al. 2012 investigated the effect of solvent type on furfural rearrangement.[42] n-Decanol, water and 2-propanol were tested in presense of precious metal catalysts at temperatures of 160 to 175 °C. Only water demonstrated high cyclopentanone yields and the two other alcohols were selective towards 2-methylfuran and and tetrahydrofufuryl alcohol which confirms the key role of water in ring rearrangement.

2.4 Multifunctional Catalysts

Heterogeneous multifunctional catalysts usually offer two or more active sites where each active site plays an independent role in the reaction system. Multifunctional catalysts can play a crucial role in multi-step selective reactions where each active site involves promoting a different step of the reaction. Metal-acid (for hydrogenation and ring opening/rearrangement) and bimetal catalysts (for promoting the hydrogenation steps) are the two multifunctional catalysts of interest in this project:

2.4.1 Metal-acid catalysts

As discussed in *section 2.3.1*, obtaining cyclopentanone requires a ring rearrangement step of furan ring (known as Piancatelli rearrangement). This step involves opening of the furan ring to an unstable intermediate in presence of a weak Lewis acid site and rearranging to 4-

hydroxy-2-cyclopentenone (4HCP). It has been previously reported in literature that using water as a reaction solvent can promote the furfural ring rearrangement step since water can act as a donor of H^+.[41] Further hydrogenation steps of 4HCP will result in cyclopentanone (CP). On the other hand, during furfuryl alcohol ring rearrangement in presence of hydrogen, hydrogen can quickly attack the unstable intermediate of the rearrangement reaction and form 4-oxopentanal where another valuable hydrogenation product, 5-hydroxy-2-pentanone, is formed with a further hydrogenation step.[43] 5-hydroxy-2-pentanone works as an important building block in synthesis of multiple medications and one further hydrogenation step of 5-hydroxy-2-pentanone, generates 1,4-pentanediol, which is another important chemical for controlled drug delivery and biodegradable polyesters.[43] Therefore, a metal-acid catalyst that catalyzes the hydrogenation step (through metal active sites) and rearrangement/opening step (through active acid sites) can be employed to achieve these products in furfural hydrogenation. In a study by Zhang et al. 2016, Au metal and TiO_2 as a support was applied for a selective hydrogenation of furfural to cyclopentanone in water at 160 °C and 4 MPa of hydrogen. TiO_2 initiates weak Lewis acid sites, promoting the Piancatelli rearrangement, and gold particles are responsible for selective hydrogenation step.[44] Nearly 100% selectivity of cyclopentanone was achieved after 70 minutes of residence time. In another study by Ohyama et al. 2014, Au supported on Nb_2O_5 (source of Lewis acid sites) catalyst was employed to achieve 3-hydroxymethylcyclopentanone (a cyclopentanone derivative) from 5-hydroxymethylfurfural at 140 °C and 8 MPa for residence time of 12 hours.[45] Ohyama et al. 2016 also tested Pt/SiO_2 catalyst in presence of different metal oxides such as Ta_2O_5, ZrO_2, Nb_2O_5, TiO_2, Al_2O_3, SiO_2–Al_2O_3, CeO_2, La_2O_3, and hydrotalcite for synthesizing 3-hydroxymethylcyclopentanone from 5-hydroxymethylfurfural at 140 °C and 4 MPa of hydrogen.[46] Metal oxides containing Lewis acid sites resulted in highest yield of 3-

hydroxymethylcyclopentanone. Pt/SiO_2 in presence of Ta_2O_5 catalysts resulted in highest yield of 82%. Fang et al. 2015 achieved 86% selectivity of cyclopentanone from furfural hydrogenation using ruthenium supported on MIL-101 (a metal-organic framework with Lewis acid sites) at 160 °C and 4 MPa of hydrogen for 2.5 hours.[47] Cr^{3+} of the MIL-101 support initiated the weak Lewis acid sites for rearrangement.

2.4.2 Bimetallic catalysts

Bimetallic catalysts have long played a key role in chemical industry. In comparison to monometallic catalysts, bimetallic catalysts demonstrate higher activity and stability and better selectivity. Generally, adding a second metal to a monometallic catalyst can improve the catalytic properties mostly through complex metal interactions. Alonso et al. 2012 stated that these interactions can promote the catalyst functionality through five different effects.[48] First a geometric effect, where the local atomic arrangement at the active sites is modified through adding a second metal to the monometallic catalyst.[49] Second, an electron effect, where electron transfer between metals promotes the electron structure of the catalyst through changing d-band properties of the metals (which leads to a change in the bond strength/weakness between the metal and reactants).[50] Third, a stabilizing effect, where adding the second metal stabilizes the first metal by preventing the deposition of carbon compounds on the surface and sintering. Fourth, a synergistic effect, where both metals are involved in the reaction system through chemical bonding and transition pathways. Finally, the last effect is a bi-functional effect where each metal independently plays its own significant and different role in the reaction system. The bi-functional effect is probably the most prominent effect of bimetallic catalysts in terms of their ability to promote desired pathways through one metal and block unwanted pathways through the other in reaction systems.

Due to high activity, enhanced stability and modified selectivity, bimetallic catalysts have been used in many chemical reactions. Oxidation, hydrogenation, and hydrogenolysis reactions are some of the most important reactions utilizing bimetallic catalysts. Bianchi et al. 2005 reported selective oxidation of glycerol using bimetallic catalysts based on Pt, Pd an Au metals where using bimetallic catalyst resulted in higher activity and better control of product distribution than monometallic catalyst.[51] In another example, Wang et al. 2014 reported hydrogenolysis of 5-hydroxymethylfurfural to 2,5-dimethylfuran using Pt-Co bimetallic catalyst achieving 98% yield of the desired product, significantly higher than monometallic catalyst.[52] Since the focus of this research is on selective hydrogenation reactions, examples of hydrogenation reactions using bimetallic catalysts will be explained extensively in the next section.

2.4.3 Bimetallic catalysts in selective hydrogenation

Hydrogenation reactions can occur through adding hydrogen to unsaturated bonds such as C=O and C=C. Metal catalysts can promote the hydrogenation reactions through producing adsorbed hydrogen atom from hydrogen molecule, which can further be added to the unsaturated carbon-carbon or carbon-oxygen bonds. The importance of selective hydrogenation is the most obvious in cases where adsorbed hydrogen atom can attack different unsaturated bonds of a compound simultaneously. For example, unsaturated aldehydes contain both C=C and C=O bonds in their structure, hence designing a catalyst for selective hydrogenation towards a specific product can be challenging.

Due to the five effects explained in the previous section, bimetallic catalysts can perform better than monometallic catalysts in terms of modified selectivity towards desired unsaturated bonds and higher activity. Several research groups have reported successful design and

utilization of bimetallic catalysts for selective hydrogenation. Santori et al. 2002 studied the effect of adding tin to silica-supported platinum on hydrogenation of benzaldehyde and butanone. They reported that adding tin to Pt/SiO_2 catalyst promotes C=O hydrogenation and inhibits C=C hydrogenation route.[53] In another study by Hammoudeh et al. 2003, adding tin to silica-supported palladium increased the rate constant ratio in hydrogenation of cinnamaldehyde to cinnamyl alcohol and from there to phenylpropanal and suppressed the hydrogenation route to saturated aldehydes.[54] Bachiller-Baeza et al. 2001 reported adding iron to activated carbon-supported ruthenium increased the selectivity of citral hydrogenation towards unsaturated alcohols.[55] Borgna et al. 2004 also reported that hydrogenation of crotonaldehyde using Co-Pt/SiO_2 had higher selectivity towards crotyl alcohol than Pt/SiO_2.[56] Selective hydrogenation of acrolein using gold-indium supported by zinc oxide[57] and selective hydrogenation of acetophenone using Ni-Pt supported by Y zeolite[58] are other examples of selective hydrogenation of ketones and unsaturated aldehydes in presence of bimetallic catalysts. Bimetallic catalysts have also been used in selective hydrogenation of carboxylic acid such as levulinic acid to gamma-valerolactone using a Sn-Ru catalyst.[59]

2.4.4 Bimetallic catalysts; selective hydrogenation of furfural

Several research groups have studied the use of bimetallic catalysts towards selective hydrogenation of furfural. Fulajtarova et al. 2015, studied hydrogenation of aqueous furfural to furfuryl alcohol over Cu-Pd catalysts.[61] The most active catalyst was the catalyst with $MgO/Mg(OH)_2$ support and prepared through electroless deposition. Fulajtarova et al. 2015 also reported that the adsorption of C=O groups on the catalyst is associated with Cu active sites. As a result, the interaction between adsorbed C=O groups on Cu and adsorbed H atoms on Pd becomes easier. In another study by Thompson et al. 2016, $Pd\text{-}Re/Al_2O_3$ performed with higher

activity and better selectivity of furfuryl alcohol than Pd/Al_2O_3.[62] Regarding synthesizing cyclopentanone from furfural using bimetallic catalysts, Yang et al. 2013 reported Ni-Cu supported by SBA-15 silica enhanced the selectivity of cyclopentanone and the conversion of furfural (at 160 °C and 4 MPa) to 62% and nearly 100%, respectively while the Ni/SBA-15 catalyst result in approximately 39% selectivity and 46% conversion in the similar reaction condition.[60] Testing 10, 30, 50 and 80 percent molar ratios of Cu/Ni indicated that the highest conversion of furfural and selectivity of cyclopentanone was achieved at 50% molar ratio. Rearrangement of the furan ring was independent of the first hydrogenation step and occurred from furfuryl alcohol. Hronec et al. 2016 also tested carbon supported Pd-Cu catalysts, prepared by different methods, for selective hydrogenation of furfural to cyclopentanone in water.[63] The three methods used for preparation of the catalyst were reductive deposition precipitation, co-impregnation and electroless plating (these methods will be explained in the next section). The highest selectivity of cyclopentanone was achieved with the catalyst that was prepared with electroless plating. Catalyst characterization indicated that in the electroless plating method, copper appeared in Cu^+ oxidation form as Cu_2O where Cu^+ played a key role in adsorption of C=O groups. In the optimum condition, the selectivity of 92.1% cyclopentanone was achieved.

2.4.5 Preparation methods

There are several methods for preparation of supported bimetallic catalysts. In this section, a summary of five of the most important and commonly used methods will be reviewed.

2.4.6 Incipient wetness impregnation

This method has been used for synthesis of both monometallic and bimetallic catalysts. In this method, the active metal precursors are dissolved in a solvent (most of the time deionized water) then a volume of solution equal to the total pore volume of the catalyst support is added to

the catalyst support and capillary action draws the solution into the catalyst pores.[64] The amount of metals dissolved in the solution is calculated based on the desired metal loading. Wetness impregnation can be performed simultaneously or separately. In other words, in simultaneous impregnation the solution contains both metals whereas in separate impregnation, one metal solution is added to the catalyst first then the catalyst is dried and the second metal solution is added. Lorengan et al. 2010 reported that in preparation of Pt/Ni catalyst using incipient wetness impregnation, simultaneous impregnation resulted in higher activity of catalyst due to a better bond between metals.[65]

2.4.7 Electroless deposition

Electroless deposition method involves a controlled chemical reaction to catalytically/autocatalytically deposit a metal salt on pre-existing metal surfaces.[66] The process can be either catalytic meaning the deposition of the second metal salt in the solution on pre-existing metal surface on a support or autocatalytic meaning the deposition of metal salt on a just reduced and deposited metal on the surface. Catalytic process is a more common process which involves adding the pre-existing metal on support (first metal is added to the support usually through wet impregnation method) to the second metal salt solution (solvent mostly deionized water). In addition to metal salt, the solution contains a reducing agent such as formaldehyde, a pH adjuster and an ionic adjuster. Then the solution is stirred under a controlled pH condition until deposition is completed. After deposition, the solution is filtered, and the catalyst is dried. Several studies, mentioned in the previous sections, reported higher activities of bimetallic catalysts prepared with electroless deposition method than other methods. One of the advantages of using this method is that the size and composition of the metals can be controlled.

2.4.8 Reductive deposition precipitation

This method is similar to electroless deposition method except that for adding the second metal hydrogen gas is utilized as the reducing agent. The hydrogen atoms are adsorbed at the metal particles of a pre-existing metal surface on support, then the adsorbed hydrogen atoms react with the second metal precursor.[67]

2.4.9 Slurry synthesis method

This method is one of the conventional methods in preparing both monometallic and bimetallic catalysts. In this method, all of the catalyst components including catalyst support and metal salt solution (in deionized water) form a slurry. Similar to incipient wetness impregnation method the amount of metal is calculated based on the desired metal loading. The slurry is stirred until the adsorption equilibrium point followed by filtering, washing, drying and calcining. This method is usually used when high metal loadings are desired.

2.4.10 Organometallic precursors

Using organometallic precursors in preparation of bimetallic catalysts result in uniform bimetallic particles whereas the conventional incipient wetness impregnation method perform poorly in uniformity due to the separation of metal ions during the capillary draw into the pores.[68] Using a solution containing bimetallic ligands results in uniform bimetallic particles. In this method, an organobimetallic cluster (such as $[PPh_4]_2[Ru_5PtC(CO)_{15}]$) solution is added to the support (in spinning mode). After adsorption of the clusters, the solvent is removed by heating in vacuum and clusters are activated under oxygen and heat.[68] In this way, both of the metals are deposited simultaneously with uniform bimetallic particles.

These five methods, explained above, are some of the most relevant methods for preparation of bimetallic catalysts on supports. Each of these methods appear to have their

advantages; the organometallic cluster method results in good uniformity, electroless deposition and reductive deposition methods give controlled composition and particle size, slurry method is suitable for high metal loading and the conventional incipient wet impregnation seems to have the easiest procedure among all of the mentioned methods.

2.5 Catalyst Deactivation

Catalyst deactivation is the decay in selectivity and activity of the catalyst over time due to chemical, mechanical and thermal processes. Catalyst deactivation, a(t), is also defined as the ratio of reaction rate at time t to reaction rate at time 0 (a(t) = $-r_{A(t)}$ $-r$ A $t=0$ Equation 2.1).[69]

$$a(t) = \frac{-r_{A(t)}}{-r_{A(t=0)}} \qquad \text{Equation 2.1}$$

In general, observed reaction rate constant (K_{obs}) is an indicator of catalysts activity. K_{obs} is equal to effectiveness factor (η) multiplied by C_t (number of active sites) multiplied by intrinsic reaction rate constant (K_{int})[70]:

$$K_{obs} = \eta\, C_t\, K_{int} \qquad \text{Equation 2.11}$$

Therefore, any change in number of sites, effectiveness factor and intrinsic kinetics of the reaction affects the catalyst's activity. According to Moulijn et al. 2001, heterogeneous catalysts deactivation mechanisms can be categorized into five main groups.[70]

2.5.1 Poisoning

Poisoning is defined as chemical adsorption of reactants, intermediates, products or contaminants on active sites of the catalyst. In addition to blocking the active sites, poisoning can change the geometry and electron structure of the surface. At the beginning of poisoning, the poison can adsorb at the most active sites first, known as selective poisoning or at the least active

sites, known as antiselective poisoning. In addition, there is a third condition where the decay in activity is linear with concentration of adsorbed poison, which is known as nonselective poisoning.[71] The main classes of catalyst poisons are group VA and VIA (i.e., N, P, As, O, S) through forming shielded structures, group VII A (i.e., F, Cl, Br, I) through forming halides, toxic heavy metals (i.e., Pb, Hg, Sn, Zn) through forming alloys and molecules that have the ability to adsorb at the surface sites with multiple bonds (i.e. CO and NO).[71] For hydrogenation reactions on metal catalysts such as nickel, platinum and palladium, compounds of sulfur, phosphorus, arsenic, zinc, mercury, lead and halides are known to be poisoning to the catalyst system. In order to prevent poisoning prior to reaction, some methods such as feed purifying, and using guard beds and additives to adsorb poison can be applied. In order to regenerate the catalysts after poisoning some techniques have been applied. For example for sulfur poisoned nickel catalysts, regeneration treatment with steam at temperatures of 700 to 800 °C was observed to recover more than 80% of the activity through the following reaction.[72]

$$Ni - S + H_2O \xrightarrow{700\,^{\circ}C} NiO + H_2\,S$$

2.5.2 Sintering

At reaction temperatures higher than 500 °C, surface area of the supported metal catalyst decays due to crystalline growth of active sites and catalyst support. Due to surface migration or volatilization of the particles at high temperatures, a group of small particles can unify and form one single large particle resulting in loss of surface area. Temperature, metal-support interaction, catalysts promoters, porosity and reaction atmosphere are important parameters affecting the sintering process. With increasing temperature and decreasing strength of metal-support interaction, the mobility of particles increases resulting in accelerating the sintering process. In general, porous materials have less tendency to sinter and presence of water vapor in reaction

medium facilitates particle migration and, hence sintering. Utilizing temperatures lower than melting point of metal, thermal stabilizers such as Ba, Zn and La to the catalyst and not using water vapor in reaction atmosphere can prevent or slow the sintering process. In order to regenerate the catalyst after sintering, oxychlorination method has been employed. In oxychlorination method, the sintered catalyst goes under a treatment of HCl and low concentrations of oxygen at average temperature of 500 °C for 1 to 4 hours. Therefore, metal oxide molecules start forming, separating and moving away from the large particle. This regeneration process is known as redispersion. Figure 2.4 demonstrates redispersion of alumina supported platinum (from Bartholomew et al. 2011).[29]

2.5.3 Coking

One other possible and common deactivation mechanism of catalysts is formation of coke. During the reaction, carbon species from reactants form and deposit on the active sites of catalysts resulting in blockage of the active sites. Polymerization and dehydrogenation of organic compound in the reactant are the two major sources of coking. Coke can decrease the activity through forming a mono or multilayer, surrounding the metal particle and clogging the pores of catalyst.[73] The regeneration of coked catalysts/coke removal is usually performed through gasification with gases like oxygen, hydrogen, steam and carbon dioxide at high temperatures.[74]

$$C + O_2 \rightarrow CO_2$$

$$C + H_2O \rightarrow CO + H_2$$

$$C + CO_2 \rightarrow 2CO$$

$$C + 2H_2 \rightarrow CH_4$$

Coke removal of carbon catalysts with high temperature gasification method can cause degradation to the carbon structure of the catalyst. In addition to the conventional gasification

method, low temperature regeneration using ozone treatment[75], solvents, surfactants, and photocatalysts[76] have been suggested in the literature.

2.5.4 Mechanical deactivation

Mechanical deactivation occurs due to several reasons. Thermal stress from consecutive heating and cooling of the catalyst, presence of hot spot in catalyst bed during the reaction, collision of catalyst particles under turbulent flow, gravitational stress and crushing under mechanical load can cause mechanical degradation.[71] Employing supports with high toughness and methods of catalysts preparation that ensure high strength bonding between the catalyst and support can decrease the mechanical deactivation of the catalyst.

2.5.5 Corrosion/Leaching

In liquid phase reactions, leaching of the active site/metal particles into the liquid results in loss of activity. The pH of liquid phase, reaction temperature and the bond strength between metal and the support are parameters that influence the catalysts leaching. In addition to accelerating the leaching process, high acidity/basicity of the reaction medium can cause corrosion to the catalyst so that sometimes very high or low pH can lead to the dissolve of catalyst.

References

1. Marsh, H.; Reinoso, F. R., *Activated carbon*. Elsevier: 2006

2. Serp, P.; Figueiredo, J. L., *Carbon materials for catalysis*. John Wiley & Sons: 2009.

3. Yahya, M. A.; Al-Qodah, Z.; Ngah, C. W. Z., Agricultural bio-waste materials as potential sustainable precursors used for activated carbon production: A review. *Renewable and Sustainable Energy Reviews* **2015,** *46*, 218-235.

4. Giraldo, L.; Moreno-Piraján, J. C., Synthesis of activated carbon mesoporous from coffee waste and its application in adsorption zinc and mercury ions from aqueous solution. *Journal of Chemistry* **2012,** *9* (2), 938-948.

5. Tsai, W.; Chang, C.; Wang, S.; Chang, C.; Chien, S.; Sun, H., Cleaner production of carbon adsorbents by utilizing agricultural waste corn cob. *Resources, conservation and recycling* **2001,** *32* (1), 43-53.

6. Donald, J.; Ohtsuka, Y.; Xu, C. C., Effects of activation agents and intrinsic minerals on pore development in activated carbons derived from a Canadian peat. *Materials Letters* **2011,** *65* (4), 744-747.

7. Amosa, M. K.; Jami, M. S.; Alkhatib, M.; Jimat, D. N.; Muyibi, S. A., Comparative and optimization studies of adsorptive strengths of activated carbons produced from steam-and CO2-activation for BPOME treatment. *Advances in Environmental Biology* **2014,** *8* (3), 603-612.

8. Prahas, D.; Kartika, Y.; Indraswati, N.; Ismadji, S., Activated carbon from jackfruit peel waste by H 3 PO 4 chemical activation: pore structure and surface chemistry characterization. *Chemical Engineering Journal* **2008,** *140* (1), 32-42.

9. Figueiredo, J. L.; Pereira, M. F. R., The role of surface chemistry in catalysis with carbons. *Catalysis Today* **2010,** *150* (1-2), 2-7.

10. Boger, T.; Heibel, A. K.; Sorensen, C. M., Monolithic catalysts for the chemical industry. *Industrial & engineering chemistry research* **2004,** *43* (16), 4602-4611

11. Tomašić, V.; Jović, F., State-of-the-art in the monolithic catalysts/reactors. *Applied Catalysis A: General* **2006,** *311*, 112-121.

12. Pérez-Cadenas, A. F.; Kapteijn, F.; Moulijn, J. A.; Maldonado-Hodar, F. J.; Carrasco-Marín, F.; Moreno-Castilla, C., Pd and Pt catalysts supported on carbon-coated monoliths for low-temperature combustion of xylenes. *Carbon* **2006,** *44* (12), 2463-2468.

13. Nijhuis, T.; Kreutzer, M.; Romijn, A.; Kapteijn, F.; Moulijn, J., Monolithic catalysts as more efficient three-phase reactors. *Catalysis Today* **2001,** *66* (2), 157-165.

14. Nijhuis, T.; Beers, A.; Kapteijn, F.; Moulijn, J., Water removal by reactive stripping for a solid-acid catalyzed esterification in a monolithic reactor. *Chemical engineering science* **2002,** *57* (9), 1627-1632.

15. Pérez-Cadenas, A. F.; Kapteijn, F.; Zieverink, M. M. P.; Moulijn, J. A., Selective hydrogenation of fatty acid methyl esters over palladium on carbon-based monoliths. *Catalysis Today* **2007,** *128* (1-2), 13-17.

16. Zhao, Y.; Zhou, J.; Zhang, J.; Li, D.; Wang, S., Selective hydrogenation of benzene to cyclohexene on a Ru/Al2O3/cordierite monolithic catalyst: Effect of mass transfer on the catalytic performance. *Industrial & Engineering Chemistry Research* **2008,** *47* (14), 4641-4647.

17. Govender, S.; Friedrich, H. B., Monoliths: A Review of the Basics, Preparation Methods and Their Relevance to Oxidation. *Catalysts* **2017,** *7* (2), 62.

18. Kreutzer, M. T.; Eijnden, M. G. v. d.; Kapteijn, F.; Moulijn, J. A.; Heiszwolf, J. J., The pressure drop experiment to determine slug lengths in multiphase monoliths. *Catalysis Today* **2005,** *105* (3-4), 667-672.

19. Ergun, S., Fluid flow through packed columns. *Chem. Eng. Prog.* **1952,** *48*, 89-94.

20. Bauer, T.; Haase, S., Comparison of structured trickle-bed and monolithic reactors in Pd-catalyzed hydrogenation of alpha-methylstyrene. *Chemical engineering journal* **2011,** *169* (1), 263-269.

21. Cybulski, A.; Moulijn, J. A., *Structured catalysts and reactors*. CRC press: 2005.

22. Bauer, T.; Schubert, M.; Lange, R.; Abiev, R. S., Intensification of heterogeneous catalytic gas-fluid interactions in reactors with a multichannel monolithic catalyst. *Russian Journal of Applied Chemistry* **2006,** *79* (7), 1047-1056.

23. Moulijn, J. A.; Kreutzer, M. T.; Alexander Nijhuis, T.; Kapteijn, F., 5 Monolithic Catalysts and Reactors: High Precision with Low Energy Consumption. *Advances in Catalysis* **2011,** *54*, 249.

24. Andersson, B.; Irandoust, S.; Cybulski, A., Modeling of monolith reactors in three-phase processes. *Structured catalysts and reactors* **1998**, 267.

25. Roy, S.; Heibel, A. K.; Liu, W.; Boger, T., Design of monolithic catalysts for multiphase reactions. *Chemical Engineering Science* **2004,** *59* (5), 957-966.

26. Kreutzer, M. T.; Du, P.; Heiszwolf, J. J.; Kapteijn, F.; Moulijn, J. A., Mass transfer characteristics of three-phase monolith reactors. *Chemical Engineering Science* **2001,** *56* (21), 6015-6023.

27. Nijhuis, T. A.; Beers, A. E.; Vergunst, T.; Hoek, I.; Kapteijn, F.; Moulijn, J. A., Preparation of monolithic catalysts. *Catalysis Reviews* **2001,** *43* (4), 345-380.

28. Vergunst, T.; Linders, M. J.; Kapteijn, F.; Moulijn, J. A., Carbon-based monolithic structures. *Catalysis Reviews* **2001,** *43* (3), 291-314.

29. Bartholomew, C. H.; Farrauto, R. J., *Fundamentals of industrial catalytic processes*. John Wiley & Sons: 2011.

30. Dashtban, M.; Gilbert, A.; Fatehi, P., Production of furfural: overview and challenges. *J Sci Technol Forest Prod Process* **2012,** *2* (4), 4.

31. Machado, G.; Leon, S.; Santos, F.; Lourega, R.; Dullius, J.; Mollmann, M. E.; Eichler, P., Literature review on furfural production from lignocellulosic biomass. *Natural Resources* **2016,** *7* (03), 115.

32. Yan, K.; Wu, G.; Lafleur, T.; Jarvis, C., Production, properties and catalytic hydrogenation of furfural to fuel additives and value-added chemicals. *Renewable and Sustainable Energy Reviews* **2014,** *38*, 663-676.

33. Rao, R. S.; Baker, R. T. K.; Vannice, M. A., Furfural hydrogenation over carbon-supported copper. *Catalysis Letters* **1999,** *60* (1-2), 51-57.

34. Sitthisa, S.; Sooknoi, T.; Ma, Y.; Balbuena, P. B.; Resasco, D. E., Kinetics and mechanism of hydrogenation of furfural on Cu/SiO 2 catalysts. *Journal of catalysis* **2011,** *277* (1), 1-13.

35. Zheng, H.-Y.; Zhu, Y.-L.; Teng, B.-T.; Bai, Z.-Q.; Zhang, C.-H.; Xiang, H.-W.; Li, Y.-W., Towards understanding the reaction pathway in vapour phase hydrogenation of furfural to 2-methylfuran. *Journal of Molecular Catalysis A: Chemical* **2006,** *246* (1), 18-23.

36. Vargas-Hernández, D.; Rubio-Caballero, J.; Santamaría-González, J.; Moreno-Tost, R.; Merida-Robles, J.; Perez-Cruz, M.; Jimenez-Lopez, A.; Hernandez-Huesca, R.; Maireles-Torres, P., Furfuryl alcohol from furfural hydrogenation over copper supported on SBA-15 silica catalysts. *Journal of Molecular Catalysis A: Chemical* **2014,** *383*, 106-113

37. Panagiotopoulou, P.; Vlachos, D. G., Liquid phase catalytic transfer hydrogenation of furfural over a Ru/C catalyst. *Applied Catalysis A: General* **2014,** *480*, 17-24.

38. Luo, H.; Li, H.; Zhuang, L., Furfural hydrogenation to furfuryl alcohol over a novel Ni–Co–B amorphous alloy catalyst. *Chemistry Letters* **2001,** *30* (5), 404-405.

39. Taylor, M. J.; Durndell, L. J.; Isaacs, M. A.; Parlett, C. M.; Wilson, K.; Lee, A. F.; Kyriakou, G., Highly selective hydrogenation of furfural over supported Pt nanoparticles under mild conditions. *Applied Catalysis B: Environmental* **2016,** *180*, 580-585.

40. Piancatelli, G.; Scettri, A.; Barbadoro, S., A useful preparation of 4-substituted 5-hydroxy-3-oxocyclopentene. *Tetrahedron Letters* **1976,** *17* (39), 3555-3558.

41. Hronec, M.; Fulajtárová, K.; Soták, T., Kinetics of high temperature conversion of furfuryl alcohol in water. *Journal of Industrial and Engineering Chemistry* **2014,** *20* (2), 650-655.

42. Hronec, M.; Fulajtarová, K.; Liptaj, T., Effect of catalyst and solvent on the furan ring rearrangement to cyclopentanone. *Applied Catalysis A: General* **2012,** *437-438*, 104-111.

43. Mironenko, R. M.; Talsi, V. P.; Gulyaeva, T. I.; Trenikhin, M. V.; Belskaya, O. B., Aqueous-phase hydrogenation of furfural over supported palladium catalysts: effect of the support on the reaction routes. Reaction Kinetics, Mechanisms and Catalysis 2019, 126 (2), 811-827.

44. Zhang, G.-S.; Zhu, M.-M.; Zhang, Q.; Liu, Y.-M.; He, H.-Y.; Cao, Y., Towards quantitative and scalable transformation of furfural to cyclopentanone with supported gold catalysts. *Green Chemistry* **2016,** *18* (7), 2155-2164.

45. Ohyama, J.; Kanao, R.; Esaki, A.; Satsuma, A., Conversion of 5-hydroxymethylfurfural to a cyclopentanone derivative by ring rearrangement over supported Au nanoparticles. *Chem Commun (Camb)* **2014,** *50* (42), 5633-6

46. Ohyama, J.; Kanao, R.; Ohira, Y.; Satsuma, A., The effect of heterogeneous acid–base catalysis on conversion of 5-hydroxymethylfurfural into a cyclopentanone derivative. *Green Chemistry* **2016,** *18* (3), 676-680.

47. Fang, R.; Liu, H.; Luque, R.; Li, Y., Efficient and selective hydrogenation of biomass-derived furfural to cyclopentanone using Ru catalysts. *Green Chemistry* **2015,** *17* (8), 4183-4188.

48. Alonso, D. M.; Wettstein, S. G.; Dumesic, J. A., Bimetallic catalysts for upgrading of biomass to fuels and chemicals. *Chem Soc Rev* **2012,** *41* (24), 8075-98.

49. Kim, D.; Resasco, J.; Yu, Y.; Asiri, A. M.; Yang, P., Synergistic geometric and electronic effects for electrochemical reduction of carbon dioxide using gold-copper bimetallic nanoparticles. *Nat Commun* **2014,** *5*, 4948.

50. Hu, S.; Scudiero, L.; Ha, S., Electronic effect on oxidation of formic acid on supported Pd–Cu bimetallic surface. *Electrochimica Acta* **2012,** *83*, 354-358.

51. Bianchi, C. L.; Canton, P.; Dimitratos, N.; Porta, F.; Prati, L., Selective oxidation of glycerol with oxygen using mono and bimetallic catalysts based on Au, Pd and Pt metals. *Catalysis Today* **2005,** *102-103*, 203-212.

52. Wang, G. H.; Hilgert, J.; Richter, F. H.; Wang, F.; Bongard, H. J.; Spliethoff, B.; Weidenthaler, C.; Schuth, F., Platinum-cobalt bimetallic nanoparticles in hollow carbon nanospheres for hydrogenolysis of 5-hydroxymethylfurfural. *Nat Mater* **2014,** *13* (3), 293-300.

53. Santori, G. F.; Casella, M. L.; Ferretti, O. A., Hydrogenation of carbonyl compounds using tin-modified platinum-based catalysts prepared via surface organometallic chemistry on metals (SOMC/M). *Journal of Molecular Catalysis A: Chemical* **2002,** *186* (1), 223-239.

54. Hammoudeh, A.; Mahmoud, S., Selective hydrogenation of cinnamaldehyde over Pd/SiO2 catalysts: selectivity promotion by alloyed Sn. *Journal of Molecular Catalysis A: Chemical* **2003,** *203* (1-2), 231-239.

55. Bachiller-Baeza, B.; Guerrero-Ruiz, A.; Wang, P.; Rodrıguez-Ramos, I., Hydrogenation of citral on activated carbon and high-surface-area graphite-supported ruthenium catalysts modified with iron. *Journal of Catalysis* **2001,** *204* (2), 450-459.

56. Borgna, A.; Anderson, B. G.; Saib, A. M.; Bluhm, H.; Hävecker, M.; Knop-Gericke, A.; Kuiper, A.; Tamminga, Y.; Niemantsverdriet, J., Pt− Co/SiO2 Bimetallic Planar Model Catalysts for Selective Hydrogenation of Crotonaldehyde. *The Journal of Physical Chemistry B* **2004,** *108* (46), 17905-17914.

57. Mohr, C.; Hofmeister, H.; Radnik, J.; Claus, P., Identification of active sites in gold-catalyzed hydrogenation of acrolein. *Journal of the American Chemical Society* **2003,** *125* (7), 1905-1911.

58. Malyala, R.; Rode, C.; Arai, M.; Hegde, S.; Chaudhari, R., Activity, selectivity and stability of Ni and bimetallic Ni–Pt supported on zeolite Y catalysts for hydrogenation of acetophenone and its substituted derivatives. *Applied Catalysis A: General* **2000,** *193* (1), 71-86.

59. Wettstein, S. G.; Bond, J. Q.; Alonso, D. M.; Pham, H. N.; Datye, A. K.; Dumesic, J. A., RuSn bimetallic catalysts for selective hydrogenation of levulinic acid to γ-valerolactone. *Applied Catalysis B: Environmental* **2012,** *117-118*, 321-329.

60. Yang, Y.; Du, Z.; Huang, Y.; Lu, F.; Wang, F.; Gao, J.; Xu, J., Conversion of furfural into cyclopentanone over Ni–Cu bimetallic catalysts. *Green Chemistry* **2013,** *15* (7), 1932.

61. Fulajtárova, K.; Soták, T.; Hronec, M.; Vávra, I.; Dobročka, E.; Omastová, M., Aqueous phase hydrogenation of furfural to furfuryl alcohol over Pd–Cu catalysts. *Applied Catalysis A: General* **2015,** *502*, 78-85.

62. Thompson, S. T.; Lamb, H. H., Palladium–Rhenium Catalysts for Selective Hydrogenation of Furfural: Evidence for an Optimum Surface Composition. *ACS Catalysis* **2016,** *6* (11), 7438-7447.

63. Hronec, M.; Fulajtárová, K.; Vávra, I.; Soták, T.; Dobročka, E.; Mičušík, M., Carbon supported Pd–Cu catalysts for highly selective rearrangement of furfural to cyclopentanone. *Applied Catalysis B: Environmental* **2016,** *181*, 210-219.

64. Richardson, J., Principles of Catalyst Development in "Fundamental and Applied Catalysis" Series (MV Twigg, MS Spencer, Eds.). Plenum Press, New York: 1989.

65. Lonergan, W. W.; Vlachos, D. G.; Chen, J. G., Correlating extent of Pt–Ni bond formation with low-temperature hydrogenation of benzene and 1, 3-butadiene over supported Pt/Ni bimetallic catalysts. *Journal of Catalysis* **2010,** *271* (2), 239-250.

66. Schaal, M. T.; Metcalf, A. Y.; Montoya, J. H.; Wilkinson, J. P.; Stork, C. C.; Williams, C. T.; Monnier, J. R., Hydrogenation of 3, 4-epoxy-1-butene over Cu–Pd/SiO 2 catalysts prepared by electroless deposition. *Catalysis today* **2007,** *123* (1), 142-150.

67. Ekou, T.; Vicente, A.; Lafaye, G.; Especel, C.; Marecot, P., Bimetallic Rh-Ge and Pt-Ge catalysts supported on TiO 2 for citral hydrogenation: I. Preparation and characterization of the catalysts. *Applied Catalysis A: General* **2006,** *314* (1), 64-72.

68. Koh, A. C.; Chen, L.; Leong, W. K.; Ang, T. P.; Johnson, B. F.; Khimyak, T.; Lin, J., Ethanol steam reforming over supported ruthenium and ruthenium–platinum catalysts: Comparison of organometallic clusters and inorganic salts as catalyst precursors. *international journal of hydrogen energy* **2009,** *34* (14), 5691-5703.

69. Fogler, H. S., Elements of chemical reaction engineering. **1999**.

70. Moulijn, J. A.; Van Diepen, A.; Kapteijn, F., Catalyst deactivation: is it predictable?: What to do? *Applied Catalysis A: General* **2001,** *212* (1), 3-16.

71. Bartholomew, C., Catalyst deactivation and regeneration. *Kirk-Othmer Encyclopedia of Chemical Technology* **2003**.

72. Hashemnejad, S. M.; Parvari, M., Deactivation and regeneration of nickel-based catalysts for steam-methane reforming. *Chinese Journal of catalysis* **2011,** *32* (1), 273-279.

73. Albers, P.; Pietsch, J.; Parker, S. F., Poisoning and deactivation of palladium catalysts. *Journal of Molecular Catalysis A: Chemical* **2001,** *173* (1), 275-286.

74. Trimm, D., The regeneration or disposal of deactivated heterogeneous catalysts. *Applied Catalysis A: General* **2001,** *212* (1), 153-160.

75. Alvarez, P.; Beltran, F.; Gomez-Serrano, V.; Jaramillo, J.; Rodrıguez, E., Comparison between thermal and ozone regenerations of spent activated carbon exhausted with phenol. *Water research* **2004,** *38* (8), 2155-2165.

76. Sheintuch, M.; Matatov-Meytal, Y. I., Comparison of catalytic processes with other regeneration methods of activated carbon. *Catalysis Today* **1999,** *53* (1), 73-80.

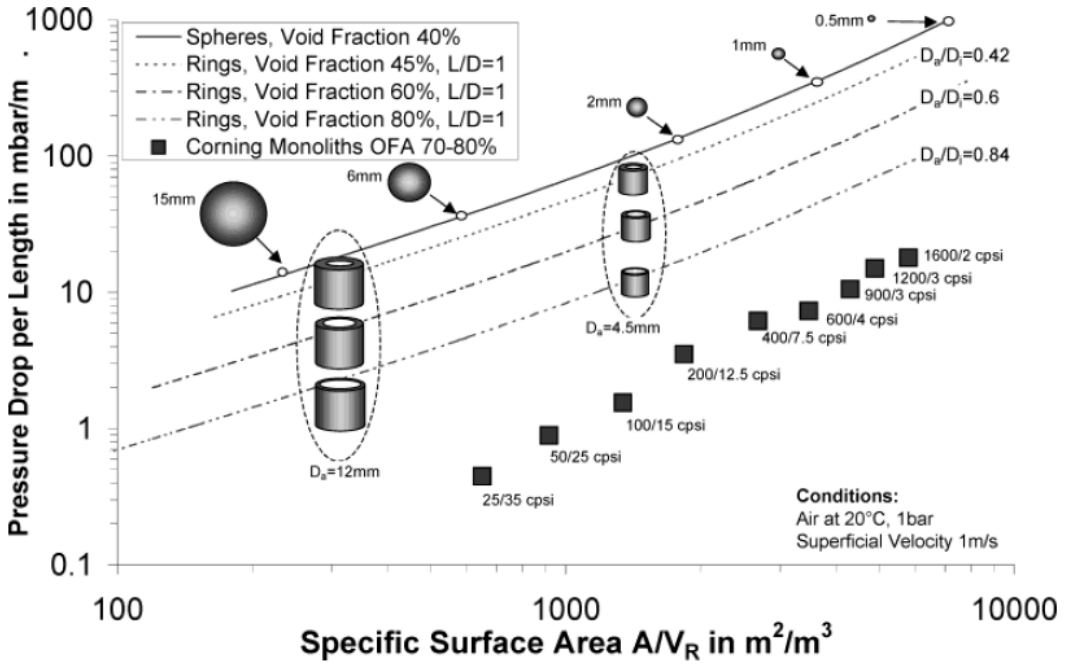

Figure 1.1. Pressure drop vs specific geometric surface area of monolithic structures, spheres, and rings.[10]

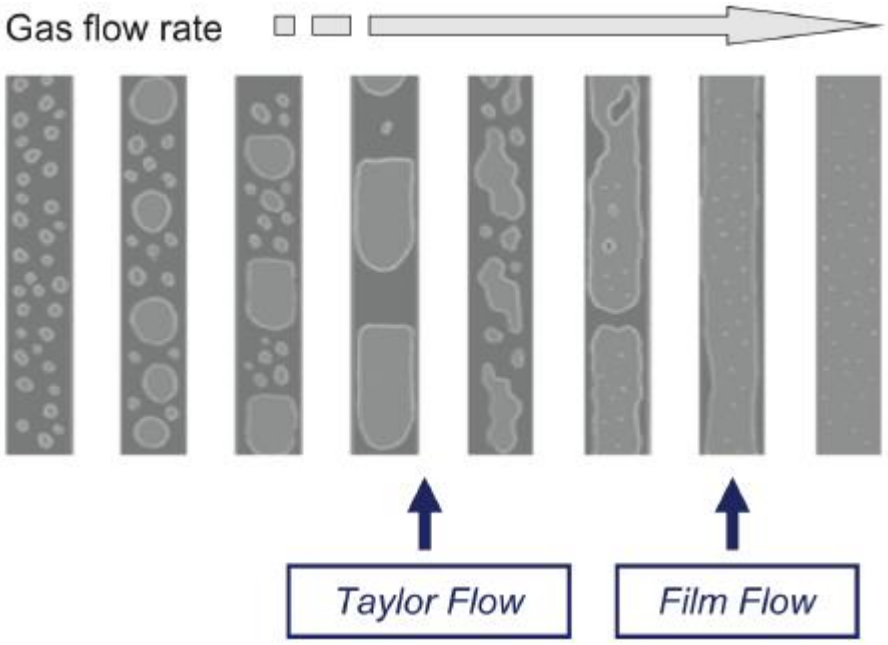

Figure 2.2. Flow patterns inside monolith channels.[23]

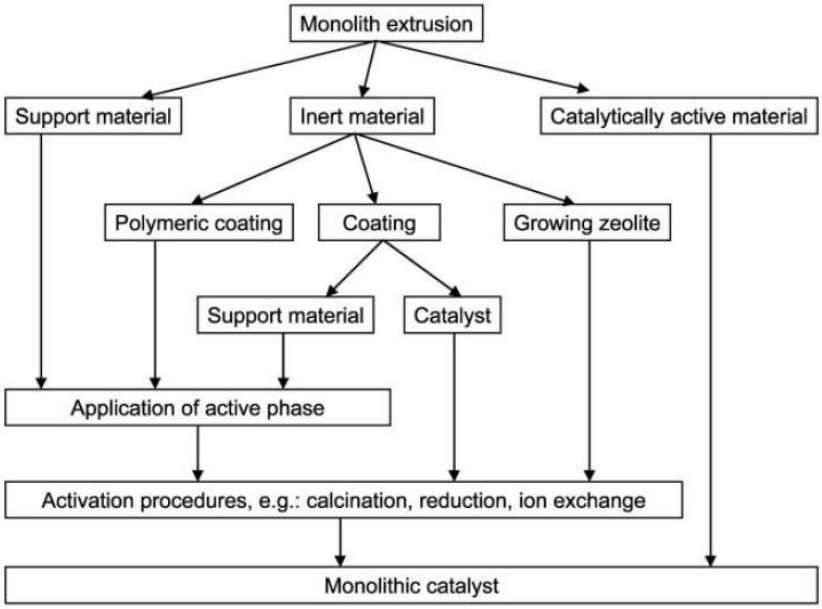

Figure 2.3. Preparation methods of monolith catalysts.[27]

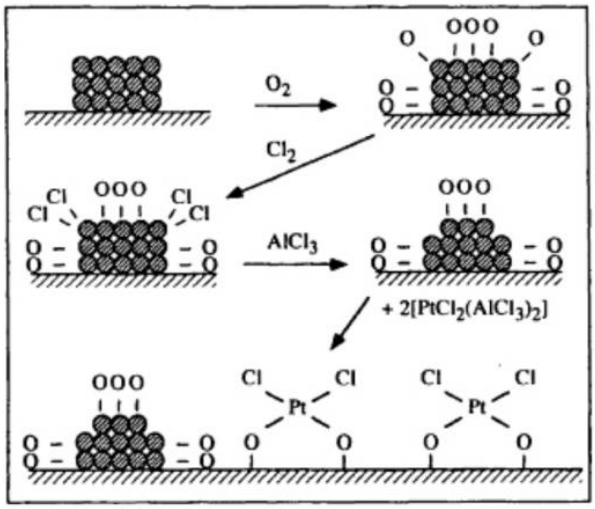

Figure 2.4. Redispersion of Pt/Al_2O_3 with oxygen and chlorine.[29]

CHAPTER 3

CONTINUOUS HYDROGENATION OF AQUEOUS FURFURAL USING A METAL SUPPORTED ACTIVATED CARBON MONOLITH COMPARED TO GRANULAR AND POWDER FORMS [1]

[1] Pirmoradi, M, Janulaitis, N, Gulotty Jr., R.J., Kastner, J.R., 2020. Submitted to *ACS Omega*

Abstract

Continuous hydrogenation of aqueous furfural (4.5%) was studied using powder (Powder C), granular (GAC) and monolith form (ACM) of activated carbon Pd catalysts. A sequential reaction pathway was observed with ACM achieving the highest selectivity and space time yields (STY) for furfuryl alcohol (~30%, 70–80 g/L-cat/h, 7–15 1/h LHSV), 2-methylfuran (~25 %, 50 g/L-cat/h, 7–15 1/h LHSV) and tetrahydrofurfuryl alcohol (35–40%, 15–32 g/L-cat/h, < 7 1/h LHSV). From liquid hourly space velocity (LHSV) 3 to 6 1/h Powder C generated the highest selectivity and STY for 5-hydroxy-2-pentanone (16–20%, 30–40 g/L-cat/h) and cyclopentanone (6–8%, 10–11 g/L-cat/h), potentially due to weak acid sites. ACM showed lower loss of activity and metal leaching over the course of the reactions and was not limited by H_2 external mass transfer resistance. Acetic acid (1%) did not significantly affect furfural conversion and product yields using ACM, whereas lower furfural conversion was observed using GAC. Limited metal leaching combined with high metal dispersion and H_2 mass transfer rates in the composite carbon catalyst (ACM) provided advantages over granular and powder forms in continuous processing.

Keywords: Activated Carbon, Monolith Catalyst, Palladium, Hydrogenation, Furfural, Continuous, Packed Bed Reactor

3.1 Introduction

The negative economic and environmental impact of petroleum utilization in the chemical industry has been a concern for a long time. Issues such as toxicity, climate change and acid rain are some unavoidable impacts of petroleum carbon sources. Therefore, finding suitable bio-renewable replacements for petroleum-based resources is one of the most important aims of the chemical industry. Furfural, an aldehyde of furan, is a biomass-derived chemical that can be generated by a two-step acid hydrolysis of hemicellulose-rich biomasses such as corn stover, wheat bran, or corncobs. The first step generates xylose and in the second step, catalytic dehydration of xylose yields furfural. The global production of furfural is ~ 300,000 tons per year[1] with a market price of 1,000 US dollars per ton.[2] Furfural hydrogenation can result in a series of valuable upgraded products such as furfuryl alcohol (important monomer for furan resins), tetrahydrofurfuryl alcohol (solvent for agricultural, cleaning, coating and paint stripper formulations), 2-methyltetrahydrofuran and 2-methylfuran (promising alternative fuel and fuel additive) and cyclopentanone (precursor for aviation fuels, rubber chemicals and pharmaceuticals).

Several research groups have investigated hydrogenation of furfural in both vapor and liquid phase. Examples of furfural hydrogenation in the vapor phase to furfuryl alcohol and 2-methylfuran include the use of a carbon supported copper catalyst at temperatures of 200 to 300 °C, silica supported copper at temperatures of 230 to 290 °C, Cu/Zn/Al/Ca/Na (59:33:6:1:1atomic ratio) and Cu/Cr/Ni/Zn/Fe (43:45:8:3:1, atomic ratio) at temperatures of 200 to 300 °C, and SBA-15 silica supported copper at temperatures of 170 to 270 °C.[3-6] Examples of liquid phase hydrogenation of furfural to furfuryl alcohol and 2-methylfuran include carbon

supported-ruthenium at temperatures of 120 to 200 °C using 2-propanol as a hydrogen donor under 2.04 MPa nitrogen pressure, over Ni–Co–B amorphous alloy catalyst at 100 °C and 1 MPa (in ethanol), and metal oxides supported-planitum at temperatures of 50 to 70 °C (in methanol and n-butanol).[7-9] Hydrogenation of furfural to cyclopentanone involves a fast hydrogenation step to furfuryl alcohol followed by an acid catalyzed rearrangement of the furan ring, also known as Piancatelli rearrangement, to 4-hydroxy-2-cyclopentenone. In 1976, Giovanni Piancatelli and coworkers discovered the rearrangement of 2-furylcarbinols into 4-hydroxycyclopentenones in presence of acid catalysts (2:1 acetone-water mixture, with the type of acid not reported).[10, 11] Piancatelli et al. 1976 observed that for more reactive reaction substrates weaker Lewis acids are required. After furfuryl alcohol rearrangement, 4-hydroxy-2-cyclopentenone undergoes fast hydrogenation and dehydration steps to form cyclopentanone (due to high reactivity). Further hydrogenation of cyclopentanone can result in formation of cyclopentanol. Hronec et al. 2014 investigated the rearrangement of furfuryl alcohol to 4-hydroxy-2-cyclopentenone in water at temperatures of 110 to 200 °C and reported that the yield of 4-hydroxy-2-cyclopentenone increased with increasing temperature.[12] They suggested that due to the presence of hydrogen ions resulting from the dissociation of water to hydrogen and hydroxyl ions at high temperatures the aqueous medium acted as an acid catalyst for the rearrangement step. In another study, Hronec et al. 2012 investigated the effect of solvent type on furfural rearrangement in which n-decanol, water and 2-propanol were tested in presence of precious metal catalysts at temperatures of 160 to 175 °C.[13] Only in the presence of water were high cyclopentanone yields reported. Use of alcohols as the solvent increased selectivity towards 2-methylfuran and tetrahydrofurfuryl alcohol, which confirms the key role of water in ring

rearrangement leading to cyclopentanone. Further hydrogenation of all of the mentioned products can lead to production of long chain alcohols.

Activated carbon (AC) is often used as a support in catalytic hydrogenation, since it can be synthesized from renewable carbon sources and is stable in acidic, basic, and aqueous environments.[14,15,16] Often powdered forms are used in batch slurry reactors or granular forms are used in trickle bed reactors, but these forms are difficult to use in continuous processing.[14] There is much interest in continuous processing since it can reduce costs, relative to batch processes.[17] The powdered forms can undergo attrition and are difficult to recover and reuse continuously.[14,17] High flow rates in trickle bed systems can cause large pressure drops, and H_2 external and internal mass transfer can be rate limiting if a large particle size is used to minimize pressure drop. Activated carbon formed into monoliths used as supports can overcome problems using powdered and granular forms in continuous processing.

Monolith catalysts are honeycomb shaped structures that have been mainly used in the automotive and environmental industry for air pollution control. The use of monolith catalysts in the automotive industry dates back to the mid-1970s when monolith catalysts were applied as catalytic converters for reduction of nitric oxides in exhaust gas.[18] Monolith structures, commonly fabricated using ceramic and metallic materials, provide a group of uniform straight channels that are separated through thin walls. For catalytic purposes, these ceramic or metallic structures are coated with a layer of catalyst such as palladium and platinum or catalyst support such as carbon, zeolites and silica. In order to assure the best adherence of the catalyst coat to the monolith structure, binders, additive, chemical and heat pretreatment are applied.[19] Compared to conventional packed bed reactors, monolithic reactors provide lower pressure drop, high surface

area to volume ratio, high mass transfer rates, and easy scale up and filtration.[19] Activated carbon is a promising catalyst support that provides well developed porosity and high surface area for catalyst particles. Activated carbon-coated ceramic and metallic monolith structures have been employed as catalysts supports for catalysts such as precious metals. However, there are some disadvantages associated with using activated carbon-coated ceramic or metal catalyst support such as durability and inertness. One solution to overcome these issues is to use renewable integrated carbon materials. In addition to solving durability and inertness issues, employing activated carbon monolith catalysts as a support for precious metals offers easy recovery of the metal by a combustion step.

This work focuses on continuous aqueous phase hydrogenation of furfural using metal supported activated carbon monolith catalysts compared to traditional granular and fine powered carbons. Activated carbon monolith (ACM) catalysts, derived from woody biomass, are impregnated with precious metals and employed for furfural hydrogenation reactions. Advantages of using ACM catalysts include low pressure drop, high mass transfer rates, high surface area to volume ratio, ease of scale-up, high stability in various reaction solutions, and that the material is made from renewable carbon sources.

In this work we use ACM catalysts for continuous furfural hydrogenation in an aqueous and acidic environment, with low metal loadings to achieve high conversions and space time yields with limited leaching. Although activated carbon monoliths have distinct advantageous as a catalyst support, there is little information on the use of these structured catalysts highlighting their advantages.

3.2 Experimental Method

Materials and Catalysts: Furfural was purchased from Sigma-Aldrich (99%). Desired concentrations of furfural solution were prepared using deionized water. Activated carbon monolith (ACM) catalysts and Pd/GAC (~ 3 mm particle size) were provided by Applied Catalysts (Laurens, SC). The 3 mm particle size of the GAC was selected, since this size is typically used in industrial scale trickle beds to minimize pressure drop and promote heat transfer for hydrogenations.[20] Both the ACM and Pd/GAC were designed to have 0.8% Pd and are thus labeled as 0.8% Pd/ACM and 0.8% Pd/GAC. ACM is manufactured by coextrusion of 50% activated carbon and 50% ceramic binder and has recently been used for the hydrogenation of nitrobenzene to aniline, and ketones to alcohols.[21, 22] Images of the ACM cores used in this work can be seen in previous literature[22] and the graphical abstract. The monolith properties (1 in * 1 in cores) have been reported previously and the surface area of the blank ACM is 598 m^2/g with a pore volume of 0.45 cm^3/g.[22] 5% Pd on powder activated carbon (Pd/Powder C, ~ 0.25 mm particle size) was purchased from Alfa Aesar (Type 87L, Dry) and was selected since this catalyst type is commonly used in hydrogenations.[13] For the effect of metal loading studies (0.8, 2.5, and 5 wt% Pd), different concentrations of $Pd(NO3)_2.2H_2O$ (purchased from Sigma-Aldrich, 40% Pd basis) were prepared using deionized water and added to crushed monolith catalysts or cACM (particle size of 0.5 to 1 mm), via a wet impregnation method (a defined mass of $Pd(NO3)_2.2H_2O$ was dissolved in 5 ml of DI water, then added dropwise to 5.5 g of cACM). The mixture was dried at 120 °C for two hours followed by H_2 reduction at 250 °C for 4 hours. The palladium catalysts were reduced in 100 ml/min flowing H_2 (100%) at 250 °C for four hours

inside the packed bed reactor (PBR) prior to reaction. Elemental analysis of the catalysts indicated Pd loadings different from original designs (Table S3.1).

Catalyst Characterization: Surface area analysis and pore size analysis were performed as previously described.[22,23] Micropore analysis was performed using the t-method of de Boer [24] (t is the statistical thickness of an adsorbed film [t (Å) = $[13.99/\log(Po/P)+0.034]^{1/2}$]) and the BET surface area data extended to higher pressures (Quantachrome, AUTOSORB-1C; Boynton Beach, Florida). Scanning Electron Microscopy / Energy Dispersive X-Ray Spectroscopy (SEM/EDS) was performed using FEI TENEO with 150 mm Oxford XMaxN detector at 10 kV. X-ray diffraction (XRD) was performed on a PANalytical X'Pert PRO using a Cu-Ka radiation source (l = 1.5418 Å) with step size of 0.02° and 2θ range of 15° to 80°. Ammonia-TPD analysis was performed to determine the quantity and strength of acid sites as previously described.[23] To obtain strong acid site density for Pd/ACM (Table 3.1), the peak area of the Pd/GAC desorption curve from 300 to 500 °C was subtracted from the Pd/ACM peak area over the same range. TPR analysis was performed to determine the reducibility of the catalyst and CO pulse titration was performed to determine the dispersion and particle size of metal on the fresh catalysts.[23] A 1:1 CO to Pd stoichiometry was assumed in calculating dispersion. Dispersion was estimated from the pulse titration data as described in past work.[22] The average particle size of the active metal for fresh catalyst was estimated from CO pulse titration using the equation below,

$$d = \frac{100\ L\ *\ S\ *\ f}{ASA\ *\ \rho}$$

where d is average crystallite size (Å), ASA the active metal surface area (m^2/g), ρ the metal

density, and f the shape factor (6 was used assuming spherical particles).

TGA analysis in air was used to estimate tar and coke formation on the catalysts (Discovery TGA from TA Instruments). Air flow over the sample (10-25 mg in ceramic pans) was set at 25 mL/min with a balance flow rate at 10 mL/min (N_2). The temperature of the sample was equilibrated at 40 °C before ramping at a rate of 10 °C/min to 800 °C. Elemental analysis of fresh and spent catalysts was performed following the Environmental Protection Agency (EPA) ICP method 200.8. Concentrated HNO_3 was added (5 ml) to the sample (~ 0.1g) for microwave digestion following protocols listed in EPA method 3051A. Digested solutions were analyzed by inductively coupled plasma optical emission spectroscopy (ICP-OES, Spectro Arcos FHS16 AMETEK ICP-OES).

Analytical: Once the liquid sample was collected from the reactor, it was analyzed in triplicate using gas chromatography with flame ionization detection (GC-FID, HP 5890 Series II) with HP Innowax column (30 m x 0.25 mm x 0.25mm). The GC-FID was operated with the method of inlet temperature 230 °C, detector temperature 240 °C, initial oven temperature of 45 °C for 2.5 minutes followed by a ramp of 10 °C/min for 15.5 minutes and then held at 200 °C for 3 minutes. 1 μL of sample is injected on the GC-FID in triplicate. The concentrations of furfural (FUR, 99%), furfuryl alcohol (FA, 98%), tetrahydrofurfuryl alcohol (THFA, 98%), 2-methylfuran (2MF, 99%), 2-methyltetrahydrofuran (2MTHF, 99%), cyclopentanol (CPO, 99%), cyclopentanone (CP, 95%), 5-hydroxy-2-pentanone (5H2P, 95%), and 1,4-pentanediol (1,4PD, 99%) were determined using 4-point standard curves (chemicals purchased from Sigma-Aldrich, each point run in triplicate). All standards were prepared in DI water, except for 2MF which was prepared with ethanol as the solvent. The presence of all intermediates and products were

confirmed using GC/MS (HP-6890 with HP Innowax column, same method as for GC/FID, 1 μl injection volume, 25:1 split ratio, 0.8 ml/min, 10-500 mass units, MSD ChemStation D.03.00.611 with NIST 2008 database for identification). Neat compounds identified by GC/MS were purchased (standards) and then were then matched with retention times of our products on a GC/FID. A typical progression of reactant conversion and product formation is shown in a series of GC/FID chromatograms in the supporting information.

Catalytic Reactions: Furfural hydrogenation reactions were performed in a continuous reactor system, designed by Parr Instrument Company. Liquid (0.5–16 ml/min) and gas flow (100 ml/min) entered the stainless-steel tube (1 in inner diameter) downwards and concurrently through a T-junction. Gas flow rate was controlled by Brooks Delta II Smart Mass Flow Controller. Liquid feedstock was pumped into the reactor using a Scientific Systems LD-Class HPLC pump. The liquid product was collected in a stainless-steel vessel with a cooling jacket attached to a Brookfield TC-602 water bath at 7 °C. Reactor temperature was controlled by a Thermcraft Lab-Temp 1760-watt furnace and a Parr 4875 Power Controller. Reactor pressure was controlled using a TESCOM back pressure regulator. Cores of activated carbon monolith catalyst (4 cores) were wrapped in Teflon tape and loaded into the center of the reactor. These four ACM cores were 4 inches (10 cm) in packing height at a total weight of 15 g. The GAC and powdered forms of the Pd loaded catalysts (5 g each) were placed between two layers of quartz wool. To determine the optimum conditions for furfural hydrogenation in a continuous reactor system, a series of experiments at temperatures ranging from 120 to 180 °C, pressures of atmospheric to 300 psi (0.1–2.1 MPa), and liquid flow rates of 0.5 to 16 mL/min were performed. The order of performing reactions to determine the effect of different reaction

parameters on product distribution for GAC and ACM was as follows: first, testing varying liquid flow rates, second, testing varying pressures, third, testing varying temperatures and fourth, acetic acid effect. For the powder form of catalyst, four reactions at different flow rates were performed.

Key kinetic parameters were calculated in the following manner. Conversion (X), yield (Y), selectivity (S), weighted hourly space velocity (WHSV), liquid hourly space velocity (LHSV), space time yield (STY) and the catalyst to mass rate ratio (W/F) were calculated using the following equations. $X_A = 1\text{-}F_{Aout}/F_{Ain}$, where F_A is the molar rate for species A (e.g., $F_{Aout} = C_{Aout} Q_{out}$; C_{Aout} is the measured concentration and is the measured volumetric flowrate). $Y_A = F_{Aout}/ F_{Tin}$, where $F_{Tin} = \sum F_i$ and i is species. $S_A = F_{Aout}/(F_{Tin}- F_{Tout})$. WHSV was calculated as $[MW_A* F_{Ain}]/W$, where W is catalyst mass and MW is the molecular weight. LHSV was calculated as $[Q_{in}*\rho_{cat}]/W$ and GHSV as $[Q_{gas,in}*\rho_{cat}]/W$, where ρ_{cat} is the bulk density of the catalyst. Space time yield (STY) was calculated as $F_{Aout} \rho_{cat} MW_A / W$ (g/L-catalyst/h).

3.3 Results and Discussion

3.3.1 Catalyst Characterization

Untreated Pd/ACM (0.8 wt% Pd) catalyst had similar surface area and pore volume compared to ACM only, but there were differences between the powder and granular forms of activated carbon (Table 3.1, S3.1 and S3.2). The surface area and pore volume for Pd/ACM was lower than Pd/GAC, but similar to Pd/Powder C (Table 3.1). These data do suggest that the surface properties of the activated carbon were changed, and the resultant material differentiated (Pd/ACM) by processing and extrusion into monolith supports. Most notably, the Pd/ACM did have a significantly smaller micro-pore volume, higher Pd dispersion, and resultant smaller

active particle size compared to the GAC and powder supports (Table 3.1, S3.1 and S3.2).

Reducibility of the metal catalysts was determined by hydrogen consumption of the catalyst versus temperature using TPR analysis. All Pd catalysts showed a negative peak between 45 to 75 °C (Fig. S3.3-B). These peaks are indicative of PdHx (Pd hydride) decomposition due to freely available PdO and have been reported on Pd supported catalysts in the range from 60 to 80 °C.[25-27] The ACM support (without Pd) also showed a negative peak at 48 °C, which we attribute to an unknown off-gas component potentially due to the binder. TPR analysis of the 0.8% Pd/ACM catalyst demonstrates two additional peaks at temperatures of 205 °C and 287 °C, which is an indicator for reduction of Pd oxide to Pd metal (Figure S3.3). Pd^{2+} reduction to Pd° has been shown to range from 130-227 °C on activated carbons and can depend on the pretreatment method.[25] The peak at 287 °C could be due to Pd interaction with the binder component alumina. For example, TPR analysis of Pd/Al_2O_3 catalysts have indicated reduction of PdO at 295 and 350 °C (either prepared from H_2PdCl_4 or $Pd(NO_3)_2$).[27,28] We attribute the peak at ~470 °C to hydrogen reaction with oxygen functional groups on the carbon surface or a gasification reaction with the carbon. CO and CO_2 TPD analysis of activated carbons in helium suggest peak evolution at temperatures > 300 °C can occur due to decomposition of oxygen functional groups.[29]

Pd/Powder C showed three additional peaks, one small peak at 75 °C after the negative peak (Fig. S3.3-B), and two broad peaks (relative to Pd/ACM) centered around 350 °C (Fig. S3.3) and 560 °C. The positive peak at 75°C is indicative of further PdO reduction and has been reported on activated carbon and Al_2O_3 supports.[26-27, 30] Similar to Pd/ACM analysis, we attribute

the peaks at 350 and 560 °C to hydrogen reaction with oxygen functional groups on the carbon surface or a gasification reaction with the carbon. After the negative peak at 50 °C, Pd on granular activated carbon demonstrated two small broad peaks at temperatures of 125 °C and 350 °C (attributed to thermal reaction with carbon). Compared to the Pd/GAC, the Pd/ACM appeared to have a higher peak hydrogen reduction temperature (205 and 287 °C vs. 125 °C) and higher H_2 consumption (Figure S3.3). The peak at 125 °C for Pd/GAC is at the low end of the range reported for PdO reduction on many activated carbons (127-227 °C).[25] Some Pd on activated carbon materials only show the low temperature negative peak (50-80 °C) with the associated H_2 consumption peak (75-100 °C), which has been suggested to be due to a weak interaction of PdO with carbon.[26-27] These differences may be attributed to the different metal-support interactions in ACM from the other two catalysts, since the ACM support is manufactured from activated carbon, binders and other additives. SEM-EDS analysis indicates some co-location of Pd with Al and Si suggesting interaction with ceramic binder, but much of the Pd appears to be distributed on carbon (Figure S3.4). TPR analysis of the ACM only (no Pd present) did indicate a small background H_2 consumption over the entire temperature range, possibly due to the metal oxides (e.g., Al_2O_3) present in the binder (Figure S3.3). However, the background H_2 consumption could also be due to the carbon reacting with H_2. A shift to higher peak hydrogen temperatures and higher H_2 consumption in the Pd/ACM could be due to interaction with the binder in the ACM and its higher Pd dispersion then the other two carbon catalysts (Table 3.1). It is generally recognized that oxygen functional groups (e.g., carboxylic, phenolic, and laconic groups) in activated carbon can provide nucleation sites for metallic crystallites.[31] Increased oxygen

functional group density reportedly leads to increased metal dispersion, a reduction in particle size, and resistance to sintering.[32] Thus, smaller particle size or higher dispersion could shift the TPR peaks to higher temperatures. Smaller particles could have increased interaction with the support in the Pd/ACM catalyst resulting in the higher dispersion and thus significant change in the TPR curves. This effect has been noted for Pd/Al_2O_3 and indicated for Pd on carbon catalysts.[27,33-34] For example, higher Pd dispersion on Al_2O_3 due to stronger interaction with the support leads to a TPR peak at 350 °C.[3] Calcination of the Pd/Al_2O_3 in air eliminated this TPR peak (350 °C) which was indicated to be due to enlargement of the PdO particles and reduced interaction with the support allowing PdO reduction at room temperature.[27] Also, such a peak (350 °C) was not observed for Pd/SiO_2 and Pd/C in this work and was suggested to be due a lack of interaction with these supports.[27] Similarly, increased oxygen groups in carbon which provide anchoring/adsorption sites for Pd (via C-O groups) lead to an increase in the H_2-TPR peak (~183 °C), increased Pd interaction with the support and increased Pd dispersion, compared to non-functionalized carbon (~137 and ~175 °C, maximum peak).[33-34 (data not shown)]

Additionally, such shifts in TPR profiles have been observed in carbon encapsulated metal oxide supports (e.g., Al_2O_3, ZrO_2) when active metals have been deposited.[35,36] For example, Ni on carbon covered Al_2O_3 showed a shift in peak hydrogen consumption from ~250 to ~400 °C, relative to Ni on AC, and better stability towards hydrogenation of nitrobenzene to aniline.[35] Carbon encapsulated ZrO_2 deposited with Ru was shown to increase the metal support strength minimizing Ru leaching in aqueous, acidic environments, when hydrogenating levulinic

acid to γ-valerolactone.[36] Again, a shift to higher peak hydrogen consumption temperatures was observed for the Ru/carbon encapsulated ZrO_2 versus Ru on AC.[36]

Ammonia-TPD analysis of the unreduced Pd/ACM and Pd/Powder C catalysts demonstrated a peak at 200-260 °C, suggesting the presence of weak acid sites, potentially due to metal oxides in the carbon or binders used in the ACM (Figure 3.1). The Pd/GAC catalyst did not show any peaks during ammonia desorption (Figure 3.1). Upon H_2 reduction of the Pd/ACM the weak acid sites disappeared, suggesting metal oxides acting as weak acid sites were reduced during the pretreatment step to generate Pd metal (Figure 3.1). A smaller strong acid site was observed in the Pd/ACM (300-500 °C) upon H_2 reduction, again probably due to the binder in the ACM, since the GAC which was used in the synthesis of the ACM showed no observable peaks. The TPD for H_2 reduced Pd/GAC was the same as for the unreduced Pd/GAC catalyst (Figure 3.1). Upon H_2 reduction the Pd/Powder C did show a small weak acid site which shifted in desorption from 200-260 °C to 100 to 200 °C. When comparing TPD analysis of the three H_2 reduced catalysts the presence of this weak acid site in the Pd/Powder C and strong acid site in the Pd/ACM was the most noticeable differences (bottom plot Figure 3.1).

XRD analysis indicated the presence of graphite with sharp peaks at 2θ of 21° and 26° for both powder and monolith form of catalyst whereas GAC indicated broader peaks implying a more amorphous carbon structure (Figure S3.5). The Pd/Powder C XRD did indicate a peak at 40 ° (2θ) suggesting Pd (111). XRD results for GAC and ACM before and after impregnation with Pd did not indicate a significant change, which suggests that Pd is well dispersed on both GAC and ACM. We believe the lack of Pd or PdO peaks for Pd/ACM and GAC was due to the low Pd loading and high dispersion. We also performed XRD on the spent catalysts (pre-

reduced with H_2 and reacted) and observed little difference (Figure S3.5). The only noticeable difference was an increase in the peak at 40 ° (2θ) for Pd/Powder C and the formation of a new peak at 47 ° (2θ) indicative of Pd (200 or 110). Overall, the XRD analysis indicates no change in the Pd/ACM and Pd/GAC catalysts and further reduction of PdO in the Pd/Powder C catalysts. The XRD analysis of the Pd/ACM and Pd/GAC was indicative of low Pd loading and high dispersion.

3.3.2 Temperature Effect

Since little work has been conducted on continuous hydrogenation of furfural for the synthesis of furfuryl alcohol, tetrahydrofurfuryl alcohol, and cyclopentanone using activated carbon monoliths, we wanted to determine the effect of temperature and pressure on selectivity and space time yields or conversion. Further, these results would allow us to determine optimum reactions parameters to compare furfural reaction kinetics between a commercially available Pd on carbon catalyst (5% Pd/Powder C) with the base carbon support or Pd/GAC (used to generate the activated carbon monoliths) and the Pd/ACM. Thus, in a set of experiments, Pd/GAC and Pd/ACM were employed to determine the effect of temperature on furfural hydrogenation. Increasing temperature increases furfural conversion for GAC only. At all temperatures, furfural conversion was higher than 90% percent for ACM and increasing temperatures increased conversion for GAC supported catalysts. The highest carbon closure for ACM was achieved at 180 °C (~90%) and carbon closure never exceeded 64% for the Pd/GAC catalyst (Figure S3.6). The presence of internal and external mass transfer resistance for GAC (please refer to section 3.3.8 Mass transfer effect), limiting hydrogen transport and adsorption on active sites, and oligomerization of furfural at high temperatures in water leads to formation of tar and coke,

resulting in low carbon closure for GAC. Increasing temperatures reduced FA selectivity and increased selectivity for all products. At all temperatures, FA selectivity was higher using Pd/ACM compared to the Pd/GAC catalyst (Figure 3.2).

3.3.3 Pressure Effect

After a series of reaction studies varying temperature indicated that a temperature of 180 °C would generate high furfural conversions, and high carbon closures and product selectivity, the effect of pressure was studied at this temperature. For the GAC catalyst, as the total pressure (and thus hydrogen partial pressure) was increased, THFA reached peak selectivity between 100 to 200 psig (0.7–1.4 MPa) and declined at the highest pressure (Figure 3.3). FA selectivity was low at all pressures for the GAC catalyst, suggesting this compound is an intermediate to THFA formation. For the Pd/ACM catalyst, FA, THFA, and 2MF selectivity increased with pressure and was significantly higher at 300 psig compared to the Pd/GAC (Figure 3.3). The selectivity of 5H2P increased linearly with pressure for both catalysts (Figure 3.3) and the cyclopentanone (CP) levels were low under all conditions. As discussed later, the type and level of acid sites in the catalysts, combined with pressure may have played a role in 5H2P production and selectivity over CP formation. Water under subcritical conditions, and Lewis acids, may act as catalysts in promoting a Piancatelli rearrangement to 5H2P or CP from furfuryl alcohol.[10,12] Since reaction rates were higher at 180 °C and the selectivity of the Piancatelli rearrangement product, 5H2P, the highest at 300 psig, we decided to conduct future reaction experiments under these conditions (180 °C, 300 psig or 2.1 MPa).

3.3.4 Liquid Hourly Space Velocity Effect

In the next set of experiments, the effect of liquid residence time on furfural hydrogenation over 5% Pd/Powder C, 0.8% Pd/GAC and 0.8% Pd/ACM was determined (the H_2 gas flow was held constant at 100 ml/min). In general, the 0.8% Pd/ACM had higher carbon closure for similar residence times compared to the other catalysts (Figure S3.7). Except for 2MTHF, 5H2P and CP, the selectivity of FA, THFA, and 2MF were significantly higher using Pd/ACM (Figure 3.4). 2MTHF selectivity changed little with LHSV, and there was little difference between the catalysts in 2MTHF selectivity. These same trends were observed for space time yield or STY of products, i.e., the ACM catalyst generated the highest FA, 2MF and THFA space time yields at residence times between 0.07–0.53 h among the three catalysts (Figure 3.5). The selectivity and STY plots demonstrate that at short contact time or high flow rates the primary products of the reactions in presence of the three catalysts are furfuryl alcohol and 2-methylfuran (Figures 3.4 and 3.5). A high furfuryl alcohol STY at short contact time indicates that the furfural to furfuryl alcohol (FA) reaction occurs at a fast rate. In a second fast hydrogenolysis step, furfuryl alcohol forms 2-methylfuran (2MF) and in a further hydrogenation step, 2-methyltetrahydrofuran (2MTHF) is formed from 2MF.

Interestingly, comparing the selectivity and STYs of the three catalysts, Pd/Powder C showed the highest selectivity and STY towards 5H2P and cyclopentanone (CP), whereas the lowest CP selectivity was observed using ACM and GAC catalyst. As LHSV decreased there was a significant increase in the 5-hydroxy-2-pentanone (5H2P) selectivity and then decline at very long residence times (Figure 3.5). 5H2P STY was significantly higher between a 0.16-0.3 h liquid residence time when using Pd/Powder C compared to ACM and GAC (Figure 3.5). The

results from the temperature, pressure, and liquid residence time effect studies suggest Pd/GAC and Pd/ACM promoted the formation of 2MF from furfural and Pd/Powder C the formation of CP and 5H2P via a speculative reaction pathway requiring acid catalysis for the ketone(s) formation (Figure 3.6). Given the distinct differences in end products between the two catalyst forms, the possible differences in catalyst structure that may have promoted different reaction pathways were next explored.

3.3.5 Palladium Loading Effect

In reactions with multiple products and side reactions, the size of the active metal particle can affect product selectivity. Past work on furfural hydrogenation using palladium catalysts suggested that the product distribution can be controlled by particle size and differences in product selectivity can be attributed to metal dispersion.[37] Given the possibility that Pd particle size may have effected product selectivity, a series of catalysts were prepared with higher Pd loading, lower dispersion, and thus larger particle size. Originally it was considered to change the Pd particle size by increasing the H_2 reduction temperature anticipating a reduction in dispersion and increase in particle size. However, a series of CO pulse titrations with increasing H_2 reduction temperature had little effect on the 0.8 wt% Pd on GAC and ACM, except at temperatures greater than 350 °C. The 5% Pd/Powder C reduced at higher temperatures did see a significant reduction in dispersion (30 to 14% from 150 to 450 °C – Figure S3.8). Thus, we decided to increase the Pd loading and reduce in H_2 at 250 °C. These catalysts were prepared by crushing the base ACM support and loading Pd via wet impregnation. Our rationale for this preparation method was to compare these catalysts with the 5% Pd on carbon powder and GAC materials, more easily. Additionally, in future experiments it was anticipated to develop bi-metal

catalysts and felt this technique would be easier to use for the ACM material to screen activity. Subsequently, once an optimum metal loading and bi-metal ratio were determined the monolith structure could be synthesized and tested. As indicated in Table 3.2, increasing the Pd loading did reduce the surface area, pore volume, and metal dispersion. The most significant observed effects were for THFA and 2MTHF; THFA selectivity and reaction rate declined with increased Pd loading and 2MTHF selectivity and reaction rate increased with increased Pd loading (Figure S3.9, data not shown for rates [both r, mmol/g-cat/h and STY, g/L-cat/h]). These results suggest that Pd loading had limited effect on CP and 5H2P formation and the hydration/dehydration/rearrangement of FA.

3.3.6 Acetic Acid Effect

Industrial production of furfural involves acid hydrolysis of biomass followed by a dehydration step in presence of an acid catalyst at temperatures of 200 to 240 °C. After several steam stripping steps, this process can result in furfural concentrations up to 99%. These purifying steps are high in energy consumption and are not cost effective. Therefore, one approach to reduce the process cost is to use crude furfural (~5 wt % before purification) with impurities or a feed generated from a single distillation step.[38] The impurities associated with crude furfural are water and carboxylic acids, such as acetic acid. The presence of these impurities in the reaction medium can impact catalyst activity, selectivity and reaction pathways. In this work the effect of acetic acid on product distribution was determined for both ACM and GAC supports (Figure 3.7). Adding acetic acid did not significantly affect furfural conversion, and 2MF and THFA selectivity (the primary products of the reaction) using Pd/ACM, but it did lower FA selectivity. Using Pd/GAC a lower furfural conversion and higher 2MF and THFA

yields were achieved. The presence of acetic acid lowered the 5H2P selectivity when using both Pd/ACM and Pd/GAC. Acetic acid was converted using both Pd/ACM and Pd/GAC, but conversion was significantly higher using Pd/GAC (95 vs. 63%). The products of acetic acid transformation could not be confirmed and ethanol, a possible direct reduction product, was not observed.

3.3.7 Catalyst Coking and Metal Leaching

After the furfural hydrogenation experiments, catalysts were collected and analyzed for changes in surface properties. Time on stream (TOS) analysis indicated high furfural conversions for all three catalysts during the course of reactions, although conversion is not a good indicator of catalyst activity (Figure S3.10). Analyzing the activity data, there was a smaller reduction in surface area, pore volume, and micro-pore area for Pd/ACM (Table 3.1). However, there was a significant reduction in surface area and micro-pore area for the Pd/GAC and Pd/Powder C catalysts, probably due to the oligomerization of furfural on the catalyst surface and pores (originated from external mass transfer resistance of hydrogen, refer to section 3.3.8). After the reactions, the surface areas of Pd/GAC, Pd/Powder C and Pd/ACM decreased by 95%, 50% and 23%, respectively (Table 3.1). The reduction in micro-pore area was most noticeable when comparing t-plots between fresh and used catalysts (Figure S3.11). The Pd/GAC catalyst lost all micro-pore area and the surface area was reduced by ~94% (using the lower reported surface area). Similarly, the micro-pore area in Pd/Powder C reduced by ~83% and the surface area by ~50%.

Since surface area declined significantly for the Pd/GAC and Pd/Powder C catalysts, TGA analysis was also performed to estimate tar/coke levels (Figure 3.8). Compared to their

fresh counterparts over the 200 to 400°C range, Pd/GAC (~16.5%) and Pd/Powder C (~7.8%) had the largest mass loss, compared to Pd/ACM (5.7%). The % mass loss over the 400 to 600°C range for the Pd/ACM (0%) was smaller compared to the Pd/Powder C (31%) and Pd/GAC (3%). It is speculated that the coke formed on the Pd/ACM may have deposited in/on an area which did not affect furfural or H_2 chemisorption on the Pd metal particles, potentially due to the ceramic binder. Finally, elemental analysis of the spent catalyst indicated leaching of Pd from the GAC (~99%) and powder support (40%), but a lower loss from the ACM (20%) (Table S3.1). Since the last set of reactions on GAC and ACM were performed in presence of acetic acid, we speculate that much of the leaching may have occurred during this reaction due to presence of an acid. We acknowledge that the Pd/GAC spent catalyst did have a measurable CO uptake indicating the presence of Pd (Table 3.1) and its TOS was longer than the Pd/ACM (Figure S3.10). This observation suggests the possibility of error in the Pd analysis of the Pd/GAC due to the limited sample size. Direct comparison between the Pd/ACM and Pd/Powder C catalyst is a better assessment, since the TOS for Pd/ACM was longer and Pd loading lower, yet leaching was lower. We also acknowledge that longer time on stream studies are needed to determine the time effect on product selectivity and reaction rates, and to develop regeneration methods.

3.3.8 Mass Transfer Effect

The mass transfer analysis indicated higher mass transfer rates of H_2, resulting in less coke formation, higher carbon closures and higher product selectivity for FA, THFA, and 2MF in presence of Pd/ACM, compared to the other two forms Pd catalyst. Calculating the gas to liquid velocity (Q_g/Q_l) ratios (6.3 to 200) indicated film or annular flow (liquid superficial velocity varied from 1.6 to $53*10^{-5}$ m/s and the gas velocity was $3.3*10^{-3}$ m/s). Film or annular

flow occurs from Q_g/Q_l equal 6 to 200.[39,42] Monolith reactors, under Taylor flow conditions, have three mass transfer steps - gas to solid through a very thin film, gas to a liquid slug with circulating eddies, and from the liquid slug to the solid.[40, 41] Given our Q_g to Q_l ratio (film flow condition), H_2 transport was considered from the gas phase to the solid through a thin film. Mears and Weisz-Prater criteria were applied for mass transfer analysis (Details in Appendix A).[43] The Mears criterion calculations for hydrogen in presence of Pd/GAC and Pd/Powder C and greater than 0.15, indicating the system is limited by external mass transfer resistance (Table S3.2). Mears criterion analysis for hydrogen in presence of Pd/ACM ranged from 2 to $4*10^{-5}$, indicating hydrogen external mass transfer *was not rate limiting* (Table S3.2). The internal mass transfer analysis (Wiesz-Prater criterion) for the three catalysts indicated that the only catalyst with internal mass transfer resistance for H_2 was Pd/GAC showing large C_{WP} values at all liquid hourly space velocities (Table S3.3).[44] The lower carbon closures and product selectivity for Pd/GAC and Pd/Powder C compared to the Pd/ACM is explained by larger Mears and Weisz-Prater values for Pd/GAC and Pd/Powder C.

3.4 Comparison to Literature

As mentioned earlier, little work has been performed on continuous furfural hydrogenation using palladium catalysts, especially in aqueous systems. One recent work using 5-hydroxymethyl furfural (HMF) is included, which is analogous to furfural.[49] No work on the use of activated carbon monolith catalysts for furfural hydrogenation could be found. Table 3.3 demonstrates a comparison of selectivity and space time yield of furfural hydrogenation products between this work and previously reported literature. All the reported works in Table 3.3 employed a Pd on activated carbon or carbon catalyst for furfural or HMF hydrogenation. Batch

processing at high pressures (≥ 30 bar) and long residence times in water produced Piancatelli rearrangement products (CP and 5H2P, entries A, I, J). Using isopropanol (as an organic solvent) eliminated the Piancatelli rearrangement products resulting in high selectivity towards FA and THFA (entry D, Table 3.3). In continuous processing, little Piancatelli rearrangement products were produced regardless of the solvent used. For example, using ethyl acetate at 150°C produced a high THFA selectivity (entry C, Table 3.3). Using cyclopentyl methyl ether as a solvent at the same temperature gave predominately FA and THFA (entry D, Table 3.3). When using water in continuous processing, the products were predominately FA, THFA, and 2MF (entries E,F,G). Continuous hydrogenation of HMF using a Pd/GAC catalyst produced primarily DMTHF (analogues to FA) and DHMTHF (analogues to THFA) at similar STY's compared to furfural hydrogenation, and no Piancatelli rearrangement products were observed (entry K, Table 3.3). Taken together this analysis suggests that water under subcritical conditions can act as a weak acid and catalyze the Piancatelli rearrangement of FA to CP or 5H2P if given long enough residence times. In continuous processing it is possible that a higher number of weak acid sites are needed, especially on the catalyst surface, to promote the Piancatelli rearrangement in shorter process times.

Thus, the low cyclopentanone or 5H2P yields using Pd/ACM might be attributed to a limited number of weak acid sites on the catalyst and a much shorter contact time for furfuryl alcohol ring rearranging to CP or 5H2P. Comparing the results of three catalysts employed in this work, the powder form of catalyst had higher 5H2P and CP yields possibly due to the presence of weak acid sites after H_2 reduction, contrary to the Pd/ACM and Pd/GAC. The NH_3-TPD results for our reduced Pd/Powder C catalyst suggest the presence of a small weak acid

peak at about 150 °C. Liu et al. 2018 suggest weak acid sites as a reason for the formation of 1,4-pentanediol (through 5-hydroxy-2-pentanone) from furfural in water using Ru on mesoporous carbon.[50]

Overall the Pd/ACM generated much higher STY's of FA, THFA, and 2MF from aqueous furfural with very low Pd loading compared to previous work (Table 3.3). The absence of furfural and H_2 external mass transfer resistance in Pd/ACM resulted in lower loss of activity and coke formation. Despite the previous reported works, where high yields of 2MF and THFA were achieved in presence of organic solvents, the results of using activated carbon monolith catalyst in aqueous furfural hydrogenation indicate that this catalyst was able to achieve a high yield of 2MF and THFA (and FA at lower LHSV's) using only water, an inexpensive, environmentally friendly and safe solvent. Comparing the NH_3-TPD analysis and product selectivity between the Pd/ACM and Pd/Powder C catalysts does suggest it would be fruitful to add/increase the number of weak acid sites, especially Lewis acid sites, to Pd/ACM. Since Lewis acids are known to promote the Piancatelli rearrangement of furfuryl alcohol (FA)[10,11] and ours and other work indicates that furfural conversion to FA is fast, it is theorized that Lewis acid sites on Pd/ACM would overcome the potentially rate limiting Piancatelli rearrangement step in continuous processing and generate higher selectivity of 5H2P or CP. If the Piancatelli step is promoted (via Lewis acid sites) and over hydrogenation to 2MF and THFA reduced (potentially by adding a second metal to reduce H_2 chemisorption) one may successfully increase 5H2P or CP selectivity and STY's from furfural in continuous processing.

Since activated carbon does not have strong acid or Brønsted acid sites, without treatment, we assume the strong acid sites observed in the Pd/ACM are due to alumina in the

binder (Table 3.1). As noted in our discussion, the consensus in the literature is that Lewis acid sites or weak acid sites promote the Piancatelli rearrangement of furfural alcohol (generated from furfural) in the presence of water.[10,11,51] When stronger acids are used resinification of the furfural occurs. Thus, the strong acid sites present in the Pd/ACM could have induced oligomerization/resinification of furfural leading to the coke formation. Coke formation on the Pd/GAC was probably due to limited H_2 mass transfer and thermal degradation of the furfural. Substituted furans such as 5-hydroxy-methyl furfural require Bronsted acid or moderate to strong Lewis acid sites to promote the Piancatelli rearrangement.[51] Blocking the strong acid sites in the Pd/ACM and adding weak Lewis acid sites should promote the formation of Piancatelli rearrangement products.

3.5 Conclusions

Comparing the results of the three catalysts, activated carbon monolith showed highest selectivity toward FA, THFA, and 2MF resulting in the highest STY's of these products, along with the least percent of metal leaching and activity loss, which makes this catalyst a promising alternative to other forms of carbon catalysts. Among the three catalysts, activated carbon monolith was the only catalyst that did not show an external mass transfer resistance for hydrogen, which contributed to its lower level of coking. The presence of acetic acid in reaction medium did not affect the furfural conversion using Pd/ACM, suggesting Pd/ACM can be used to process crude furfural. Using water as a safe alternative to organic solvents resulted in high yields and selectivity of FA, THFA and 2MF using the activated monolith carbon catalyst. Finally, compared to most Pd/GAC catalysts used in the literature to process furfural, the Pd/ACM accomplished these results at much lower Pd loadings (~1 wt% versus 3-10 wt%).

In general, this work demonstrated the prolonged hydrogenation of furfural using Pd/ACM catalyst in an aqueous and acidic environment with low metal loadings and high space time yields of furfuryl alcohol and 2-methylfuran, due to limited Pd leaching and higher H_2 mass transfer rates. These results with the metal/ACM have implications for a wider range of reactants (or substrates) generated in microbial fermentations or acid hydrolysis of biomass requiring catalytic upgrading – e.g., hydrogenation of 5-hydroxymethyl furfural, xylose to xylitol, glucose to sorbitol, succinic acid to butanediol, levulinic acid to γ-valerolactone, and muconic acid to adipic acid.

ASSOCIATED CONTENT

Supporting Information (Appendix A)

The following results are presented, 1) catalyst adsorption isotherms, 2) effect of temperature on furfural conversions, 3) effect of liquid residence times on furfural conversions, 4) effect of H_2 reduction temperature on Pd dispersion, 5) SEM-EDS pictures, and 6) XRD analysis.

ACKNOWLEDGMENTS

Support for this research and Maryam Pirmoradi's PhD in Biochemical Engineering and support of Nida Janulaitis (undergraduate research) was provided by a USDA-NIFA Grant (Carbon Monolith Catalysts from Wood for Biobased Platform Chemicals: 2017-67021-26136). The authors acknowledge and thank Dr. Yiping Zao, Sarada Sripada and Yanjun Yang for their contribution in performing XRD analysis.

References

1. Dashtban, Mehdi., Allan Gilbert, and Pedram Fatehi. "Production of furfural: overview and challenges." J Sci Technol Forest Prod Process 2, no. 4 (2012): 44-53.

2. Machado, Grazielle, Sabrina Leon, Fernando Santos, Rogério Lourega, Jeane Dullius, Maria Elizabete Mollmann, and Paulo Eichler. "Literature review on furfural production from lignocellulosic biomass." Natural Resources 7, no. 03 (2016): 115-129.

3. Rao, Rajeev S., R. Terry K. Baker, and M. Albert Vannice. "Furfural hydrogenation over carbon-supported copper." Catalysis letters 60, no. 1-2 (1999): 51-57.

4. Sitthisa, Surapas, Tawan Sooknoi, Yuguang Ma, Perla B. Balbuena, and Daniel E. Resasco. "Kinetics and mechanism of hydrogenation of furfural on Cu/SiO_2 catalysts." Journal of catalysis 277, no. 1 (2011): 1-13.

5. Zheng, Hong-Yan, Yu-Lei Zhu, Bo-Tao Teng, Zong-Qing Bai, Cheng-Hua Zhang, Hong-Wei Xiang, and Yong-Wang Li. "Towards understanding the reaction pathway in vapour phase hydrogenation of furfural to 2-methylfuran." Journal of Molecular Catalysis A: Chemical 246, no. 1-2 (2006): 18-23.

6. Vargas-Hernández, D., J. M. Rubio-Caballero, J. Santamaría-González, R. Moreno-Tost, J. M. Mérida-Robles, M. A. Pérez-Cruz, A. Jiménez-López, R. Hernández-Huesca, and P. Maireles-Torres. "Furfuryl alcohol from furfural hydrogenation over copper supported on SBA-15 silica catalysts." Journal of Molecular Catalysis A: Chemical 383 (2014): 106-113.

7. Panagiotopoulou, Paraskevi, and Dionisios G. Vlachos. "Liquid phase catalytic transfer hydrogenation of furfural over a Ru/C catalyst." Applied Catalysis A: General 480 (2014): 17-24.

8. Luo, Hongshan, Hexing Li, and Li Zhuang. "Furfural hydrogenation to furfuryl alcohol over a novel Ni–Co–B amorphous alloy catalyst." Chemistry Letters 30, no. 5 (2001): 404-405.

9. Taylor, Martin J., Lee J. Durndell, Mark A. Isaacs, Christopher MA Parlett, Karen Wilson, Adam F. Lee, and Georgios Kyriakou. "Highly selective hydrogenation of furfural over supported Pt nanoparticles under mild conditions." Applied Catalysis B: Environmental 180 (2016): 580-585.

10. Piancatelli, G., A. Scettri, and S. Barbadoro. "A useful preparation of 4-substituted 5-hydroxy-3-oxocyclopentene." Tetrahedron Letters 17, no. 39 (1976): 3555-3558.

11. Piutti, Claudia, and Francesca Quartieri. "The piancatelli rearrangement: New applications for an intriguing reaction." Molecules 18, no. 10 (2013): 12290-12312.

12. Hronec, Milan, Katarína Fulajtárová, and Tomáš Soták. "Kinetics of high temperature conversion of furfuryl alcohol in water." Journal of Industrial and Engineering Chemistry 20, no. 2 (2014): 650-655.

13. Hronec, Milan, Katarina Fulajtarová, and Tibor Liptaj. "Effect of catalyst and solvent on the furan ring rearrangement to cyclopentanone." Applied Catalysis A: General 437 (2012): 104-111.

14. Bartholomew, Calvin H., and Robert J. Farrauto. Fundamentals of industrial catalytic processes. John Wiley & Sons, 2011.

15. Bravo-Suárez, J. J., R. V. Chaudhari, and B. Subramaniam. "Design of heterogeneous catalysts for fuels and chemicals processing: An overview." Novel materials for catalysis and fuels processing 1132 (2013): 3-68.

16. Auer, E., A. Freund, J. Pietsch, and T. Tacke. "Carbons as supports for industrial precious metal catalysts." Applied Catalysis A: General 173, no. 2 (1998): 259-271.

17. Amara, Zacharias, Martyn Poliakoff, Rubén Duque, Daniel Geier, Giancarlo Franciò, Charles M. Gordon, Rebecca E. Meadows, Robert Woodward, and Walter Leitner. "Enabling the scale-up of a key asymmetric hydrogenation step in the synthesis of an API using continuous flow solid-supported catalysis." Organic Process Research & Development 20, no. 7 (2016): 1321-1327.

18. Boger, Thorsten, Achim K. Heibel, and Charles M. Sorensen. "Monolithic catalysts for the chemical industry." Industrial & engineering chemistry research 43, no. 16 (2004): 4602-4611.

19. Tomašić, Vesna, and Franjo Jović. "State-of-the-art in the monolithic catalysts/reactors." Applied Catalysis A: General 311 (2006): 112-121.

20. Azarpour, A. and G. Zahedi. "Performance analysis of crude terephthalic acid hydropurification in an industrial trickle-bed reactor experiencing catalyst deactivation." Chemical Engineering Journal (2012) **209**: 180-193.

21. Gulotty Jr, Robert J., Stephanie Rish, Andrew Boyd, Lee Mitchell, Scott Plageman, Corinne McGill, Joseph Keller, Jeter Starnes, John Stadalsky, and George Garrison. "Run Parameters for a Continuous Hydrogenation Process Using ACMC-Pd To Replace Commercial

Batch Reactor Processes." Organic Process Research & Development 22, no. 12 (2018): 1622-1627.

22. Weber, Justin, Aaron Thompson, Jared Wilmoth, Robert J. Gulotty Jr, and James R. Kastner. "Coupling Red-Mud Ketonization of a Model Bio-Oil Mixture with Aqueous Phase Hydrogenation Using Activated Carbon Monoliths." Energy & Fuels 31, no. 9 (2017): 9529-9541.

23. Weber, Justion; Aaron Thompson, Jared Wilmoth, Vidya S. Batra, Nida Janulaitis, James R. Kastner. Effect of metal oxide redox state in red mud catalysts on ketonization of fast pyrolysis oil derived oxygenates. Applied Catalysis B: Environmental 241 (2019) 430–441.

24. De Boer, J. H., B. G. Linsen, Th Van der Plas, and G. J. Zondervan. "Studies on pore systems in catalysts: VII. Description of the pore dimensions of carbon blacks by the t method." Journal of Catalysis 4, no. 6 (1965): 649-653.

25. M. Gurrath, T. Kuretzky, H.P. Boehm, L.B. Okhlopkova, A.S. Lisitsyn, V.A. Likholobov. Palladium catalysts on activated carbon supports: Influence of reduction temperature, origin of the support and pretreatments of the carbon surface. Carbon 38 (2000) 1241–1255.

26. S. Biniak, R. Diduszko, W. Gac, M. Pakuła, A. S´wiatkowski. Reduction and oxidation of a Pd/activated carbon. catalyst: evaluation of effects. Reac Kinet Mech Cat (2010) 101:331–342.

27. F. Pinna, F. Menegazzo, M. Signoretto, P. Canton, G. Fagherazzi, N. Pernicone. Consecutive hydrogenation of benzaldehyde over Pd catalysts. Influence of supports and sulfur poisoning. Applied Catalysis A: General 219 (2001) 195–200.

28. Qiuchen Yang, Ruijun Hou, Kening Sun. Tuning butene selectivities by Cu modification on Pd-based catalyst for the selective hydrogenation of 1,3-butadiene. Journal of Catalysis 374 (2019) 12–23.

29. Issa I. Salame and Teresa J. Bandosz. Surface Chemistry of Activated Carbons: Combining the Results of Temperature-Programmed Desorption, Boehm, and Potentiometric Titrations. Journal of Colloid and Interface Science 240, 252–258 (2001).

30. M. Martin-Martinez∗, L.M. Gómez-Sainero, J. Bedia, A. Arevalo-Bastante, J.J. Rodriguez. Enhanced activity of carbon-supported Pd–Pt catalysts in the hydrodechlorination of dichloromethane. Applied Catalysis B: Environmental 184 (2016) 55–63.

31. E. Auer, A. Freund, J. Pietsch*, T. Tacke. Carbons as supports for industrial precious metal catalysts. Applied Catalysis A: General 173 (1998) 259±271.

32. C. PRADO-BURGUETE, A. LINARES~OLANO, F. RoDRiGuEz-REINoso, AND C. SALINAS-MARTiNEZ DE LECEA. The Effect of Oxygen Surface Groups of the Support on Platinum Dispersion in Pt/Carbon Catalysts. JOURNAL OF CATALYSIS 115,98-106 (1989)

33. Tieyong Xu, Qunfeng Zhang, Jie Cen, Yizhi Xiang, Xiaonian Li. Selectivity tailoring of Pd/CNTs in phenol hydrogenation by surface modification: Role of C-O oxygen species. Applied Surface Science 324 (2015) 634–639.

34. Guangxin Yang, Jiuxuan Zhang, Hong Jiang, Yefei Liu, Rizhi Chen. Turning surface properties of Pd/N-doped porous carbon by trace oxygen with enhanced catalytic performance for selective phenol hydrogenation to cyclohexanone Applied Catalysis A, General 588 (2019) 117306.

35. Venkateshwarlu, V.; Mohan, V.; Rao, M. Venkata; Nagaiah, P.; Raju, B. David; Rao, K. S. Rama. (2016). "Advantage of carbon coverage over Al_2O_3 as support for Ni/C-Al_2O_3 catalyst in vapour phase hydrogenation of nitrobenzene to aniline." Catalysis Communications 86: 1-4.

36. Cao, Wenxiu; Luo, Wenhao; Ge, Hongguang; Su, Yang; Wang, Aiqin; Zhang, Tao. (2017). "UiO-66 derived Ru/ZrO2@C as a highly stable catalyst for hydrogenation of levulinic acid to γ-valerolactone." Green Chemistry 19(9): 2201-2211.

37. Date, Nandan S., Narayan S. Biradar, Rajeev C. Chikate, and Chandrashekhar V. Rode. "Effect of Reduction Protocol of Pd Catalysts on Product Distribution in Furfural Hydrogenation." ChemistrySelect 2, no. 1 (2017): 24-32.

38. Mariscal, R., P. Maireles-Torres, M. Ojeda, I. Sádaba, and M. López Granados. "Furfural: a renewable and versatile platform molecule for the synthesis of chemicals and fuels." Energy & environmental science 9, no. 4 (2016): 1144-1189.

39. Bauer, T., R. Guettel, S. Roy, M. Schubert, M. Al-Dahhan, and R. Lange. "Modelling and simulation of the monolithic reactor for gas–liquid–solid reactions." Chemical Engineering Research and Design 83, no. 7 (2005): 811-819.

40. Kawakami, Koei, Kyosuke Kawasaki, Fumihide Shiraishi, and Koichiro Kusunoki. "Performance of a honeycomb monolith bioreactor in a gas-liquid-solid three-phase system." Industrial & Engineering Chemistry Research 28, no. 4 (1989): 394-400.

41. Mogalicherla, Aswani Kumar, and Deepak Kunzru. "Effect of gas and liquid superficial velocities on the performance of monolithic reactors." Industrial & Engineering Chemistry Research 49, no. 4 (2010): 1631-1641.

42. Han, Youngbae, and Naoki Shikazono. "Measurement of the liquid film thickness in micro tube slug flow." International Journal of Heat and Fluid Flow 30, no. 5 (2009): 842-853.

43. Fogler, H.S., 1986. Elements of Chemical Reaction Engineering. Prentice-Hall, Englewood Cliffs, New Jersey.

44. Mukherjee, S.; Albert Vannice, M.A. Solvent effects in liquid-phase reactions. I. Activity and selectivity during citral hydrogenation on Pt/SiO2 and evaluation of mass transfer effects. J.Catal. 243 (2006) 108–130.

45. Mironenko, Roman M., Valentin P. Talsi, Tatiana I. Gulyaeva, Mikhail V. Trenikhin, and Olga B. Belskaya. "Aqueous-phase hydrogenation of furfural over supported palladium catalysts: effect of the support on the reaction routes." Reaction Kinetics, Mechanisms and Catalysis (2018): 1-17.

46. Garcia-Olmo, Antonio J., Alfonso Yepez, Alina M. Balu, Antonio A. Romero, Yingwei Li, and Rafael Luque. "Insights into the activity, selectivity and stability of heterogeneous catalysts in the continuous flow hydroconversion of furfural." Catalysis Science & Technology 6, no. 13 (2016): 4705-4711.

47. Ouyang, Weiyi, Alfonso Yepez, Antonio A. Romero, and Rafael Luque. "Towards industrial furfural conversion: Selectivity and stability of palladium and platinum catalysts under continuous flow regime." Catalysis Today 308 (2018): 32-37.

48. Wang, Yantao, Pepijn Prinsen, Konstantinos S. Triantafyllidis, Stamatia A. Karakoulia, Pantelis N. Trikalitis, Alfonso Yepez, Christophe Len, and Rafael Luque. "Comparative Study of Supported Monometallic Catalysts in the Liquid-Phase Hydrogenation of Furfural: Batch Versus Continuous Flow." ACS Sustainable Chemistry & Engineering 6, no. 8 (2018): 9831-9844.

49. Lima, Sérgio, David Chadwick, and Klaus Hellgardt. "Towards sustainable hydrogenation of 5-(hydroxymethyl) furfural: a two-stage continuous process in aqueous media over RANEY® catalysts." RSC Advances 7, no. 50 (2017): 31401-31407.

50. Liu, Fei, Qiaoyun Liu, Jinming Xu, Lei Li, Yi-Tao Cui, Rui Lang, Lin Li et al. "Catalytic cascade conversion of furfural to 1, 4-pentanediol in a single reactor." Green Chemistry 20, no. 8 (2018): 1770-1776.

51. J. Ohyama, A. Satsuma. Chapter 5: Reductive Conversion of 5-Hydroxymethylfurfural in Aqueous Solutions by Furan Ring Opening and Rearrangement. Z. Fang et al. (eds.), Production of Biofuels and Chemicals with Bifunctional Catalysts, Biofuels and Biorefineries 8, https://doi.org/10.1007/978-981-10-5137-1_5.

Table 3.1. Physical properties of the carbon catalysts

Catalysts	Pd/ACM	Pd/ACM	Pd/GAC	Pd/GAC	Pd/Powder C	Pd/Powder C
Properties	(Fresh)	(Spent) [d]	(Fresh)	(Spent) [d]	(Fresh)	(Spent) [d]
Metal Loading (wt.%)	1.2	0.95 [21%][e]	0.56	0.09 [83%][e]	4.8	2.9 [39%][e]
Bulk Density (g/cm^3)	0.28	NP	0.22	NP	0.25	NP
Surface Area (m^2/g)	608	470	805-914	45	686	341
Pore Volume (cm^3/g)	0.45	0.46	0.43	NM	0.47	0.46
Average Pore Size (radius, Å)	29.8	39.3	21.6	NM	27.5	54.2
Pd Dispersion, % (μmoles CO/g) [a]	47 (53.2)	NP (7.8)	39 (20.5)	NP (9.7)	17.7 (79.8)	NP (20.8)
Pd Particle Size (nm) [b]	2.4	13	2.8	NM	6.3	14.7
Micro-pore area (m^2/g) [c]	14	0.0	625-737	0.0	349	44
Micro-Pore Volume (cm^3/g) [c]	0.005	0.0	0.33	0.0	0.18	0.03
Weak Acid Sites [f] (μmoles NH_3/g) -155°C	0.0	NP	0.0	NP	86	NP
Strong Acid Sites [f] (μmoles NH_3/g) -390°C	239	NP	0.0	NP	0.0	NP

[a], CO Pulse Titration, 1:1 stoichiometry assumed, Reduced with 100% H_2 at 250 °C for 2 h

[a], Particle size and dispersion calculations were not performed (NP) for the spent catalysts due to possible coking effect on CO uptake and low Pd metal content measured by ICP for the spent Pd/GAC

[b], Particle size estimated from dispersion via CO pulse titration; [c,] Estimated from t-plot analysis

[d], Spent catalysts from furfural hydrogenation

[e], % Pd loss via leaching in brackets

[f], Estimated from NH_3-TPD for H_2 reduced catalysts, estimated peak desorption temperature. ACM is activated carbon monolith, GAC is granular activated carbon, Powder is from Alfa Aesar

NM – not measurable, probably below detection limit; NP – not performed

Table 3.2. Physical properties of carbon catalysts with different palladium loadings using crushed ACM

Catalysts / **Properties**	0.8Pd/cACM (Fresh)	2.5Pd/cACM (Fresh)	5.0Pd/cACM (Fresh)
Metal Loading (wt.%)	0.3	2.4	5.6
Bulk Density (g/cm^3)	0.28	0.28	0.28
Surface Area (m^2/g)	844	761	628
Micropore Area (m^2/g)[a]	33.6	44.7	37.5
Pore Volume (cm^3/g)[b]	0.732	0.659	0.545
Average Pore Size (radius, Å)	17.34	17.32	17.34
Pd Dispersion (%)[c]	72	26	8
Pd Particle Size (Å)[d]	15.6	42.4	145.5

[a], Estimated using the de Boer equation

[b], Total pore volume at P/Po = 0.992

[c], CO Pulse Titration, 1:1 stoichiometry assumed, Reduced with 100% H_2 at 250 °C for 2 h

[d], Particle size estimated from dispersion via CO pulse titration

cACM is crushed activated carbon monolith

Table 3.3. Comparison of selectivity and space time yield for products of furfural hydrogenation reactions using carbon supported catalysts

							Selectivity %							
Entry	**Pd Catalyst**	**Reactor Mode**	**Solvent**	**T (°C)**	**P (bar)**	**Conversion (%)**	**FA**	**THFA**	**2MF**	**2MTHF**	**CP**	**5H2P**	**STY[a] (g/L/h)**	**Reference**
A	1% Pd/CNT	B	water	150	30	98	0	1.7	NR	5.7	49.4	3.1	-	45
B	5% Pd/AC	C	EtOAc	90	50	99	0	0	75	NR	NR	NR	-	46
C	10%Pd/AC	C	EtOAc	150	90	99	0	75	NR	NR	NR	NR		47
D	3% Pd/AC	C	CPME	150	50	97	25	56	5	<10	NR	NR		48
E	5% Pd/Powder C	C	water	180	20	100	6	11	6	3.5	6	16	~20,~25[b]	This work
F	0.8 % Pd/GAC	C	water	180	20	98	15	10	9	5	1	6	~35,~25[b]	This work
G	0.8% Pd/ACM	C	water	180	20	97	31	24	27	3	1	6	71,58	This work
H	3% Pd/AC	B	i-PrOH	200	30	47	33	52	5	NR	NR	NR	-	48
I	5% Pd/C	B	water	160	30	97.8	0	2.1	2.4	6	69	NR	-	13
J	5% Pd/C	B	water	175	80	100	0	36	3	10	39	NR	-	13
K	10%Pd/C (HMF)	C	water	90	90	100	21 DMTHF	17 DHMHF	-	-	-	-	33, 30	49

NR: Not reported; C: Continuous; B: Batch; HMF: Hydroxymethyl furfural

FA: Furfuryl Alcohol; THFA: tetrahydrofurfuryl alcohol; 2MF: 2-methylfuran; 2MTHF: 2-methyltetrahydrofuran; CP: cyclopentanone; 5H2P, 5-hydroxy-2-pentanone

CPME: cyclopentyl methyl ether; EtOAc: ethyl acetate; i-PrOH: isopropanol

DMTHF: 2,5- dihydroxymethylfuran; DHMTHF: 2,5-bis(hydroxymethyl) tetrahydrofuran

[a], space time yield for FA or DMTHF and THFA or DHMTHF respectively at LHSV of 8 1/h

[b], approximated from curve fit of data at LHSV of 8 1/h

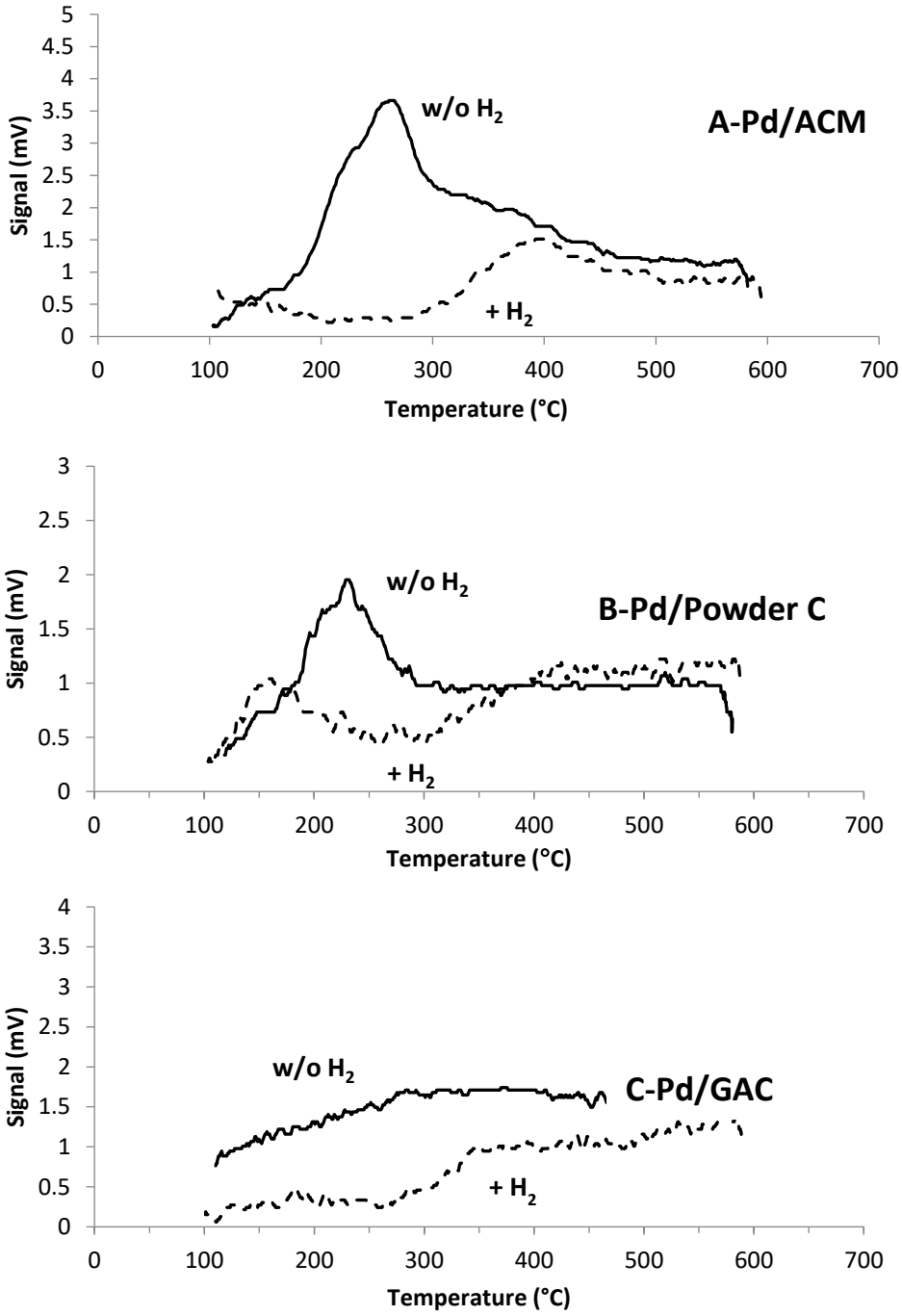

Figure 3.1. Ammonia TPD analysis of Pd on carbon catalysts pre-reduced with H_2 (100% H_2 for 2 h at 250 °C) and without H_2 reduction. A moving average is reported for the overlay of the NH_3-TPD (H_2 reduced carbons) in the bottom plot.

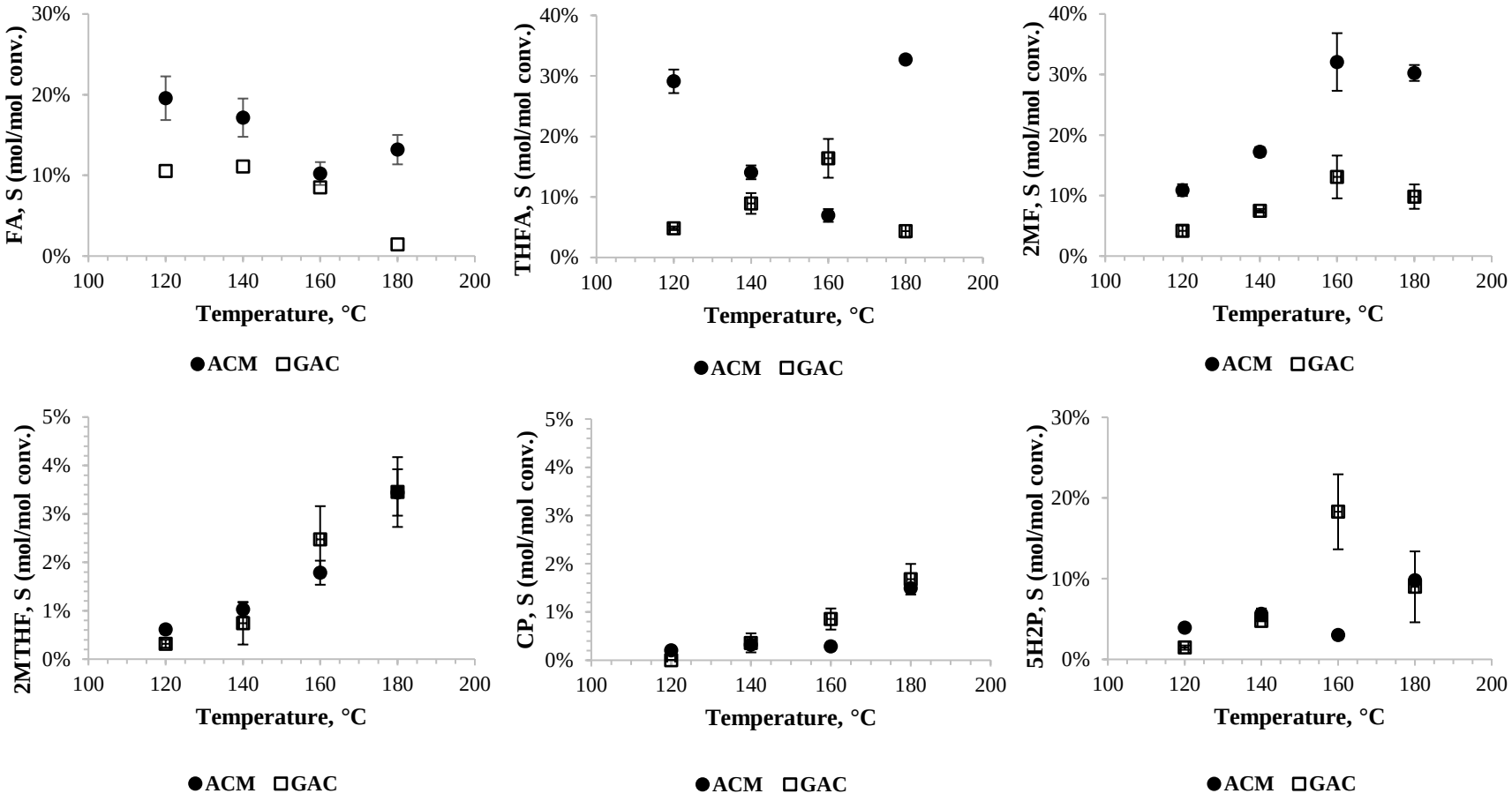

Figure 3.2. Effect of reaction temperature on product selectivity (FA, furfuryl alcohol; THFA, tetrahydrofurfuryl alcohol; 2MF, 2-methylfuran; 2MTHF, 2-methyltetrahydrofuran; 5H2P, 5-hydroxy-2-pentanone; CP, cyclopentanone). All reactions were conducted at 180 °C, 300 psig (2.04 MPa), and 1.32 1/h LHSV with 0.8% Pd on GAC or ACM.

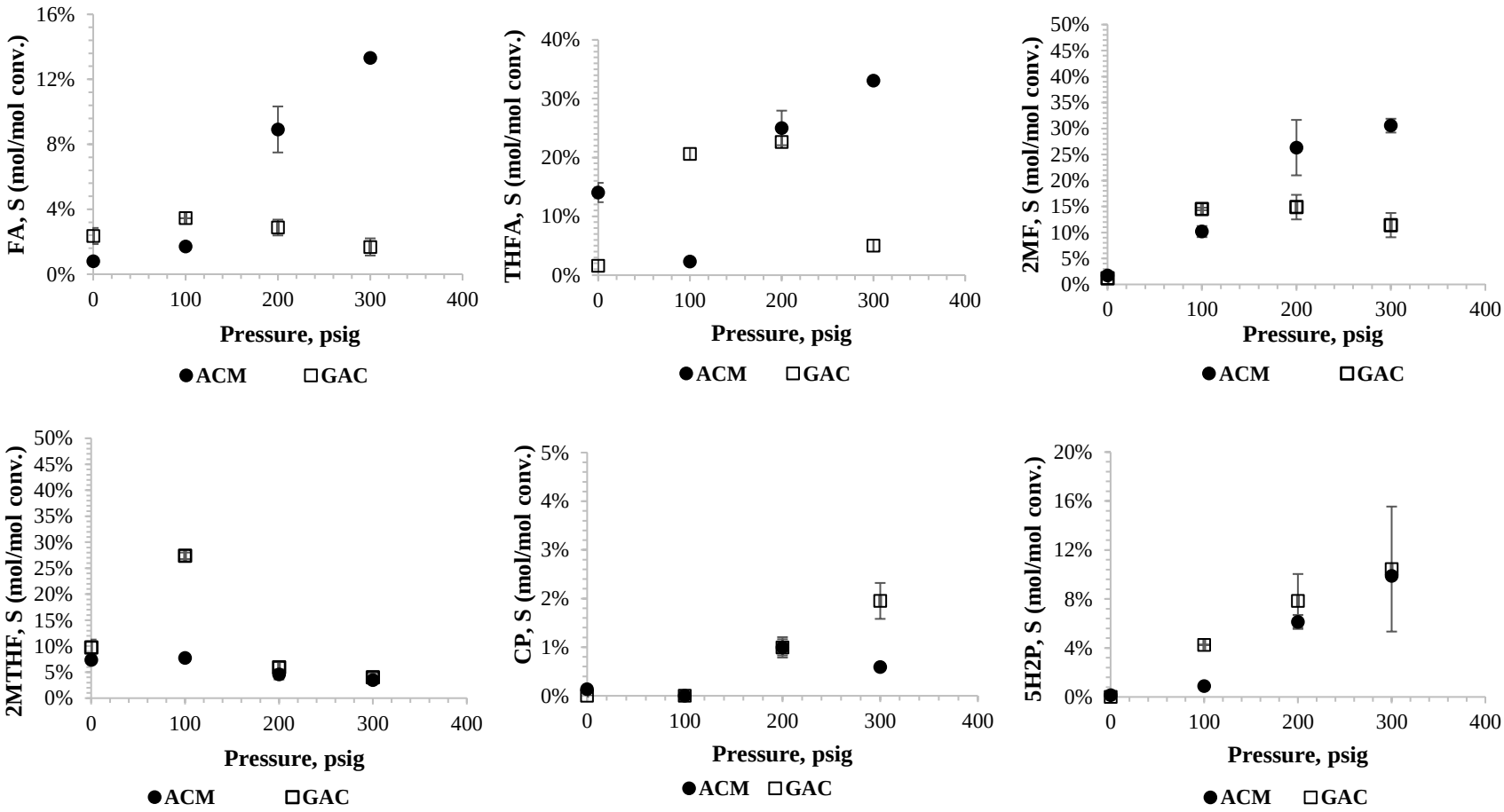

Figure 3.3. Effect of reaction pressure on product selectivity (FA, furfuryl alcohol; THFA, tetrahydrofurfuryl alcohol; 2MF, 2-methylfuran; 2MTHF, 2-methyltetrahydrofuran; 5H2P, 5-hydroxy-2-pentanone; CP, cyclopentanone). All reactions were performed at 180 °C and 1.32 1/h LHSV using 0.8% Pd on GAC or ACM.

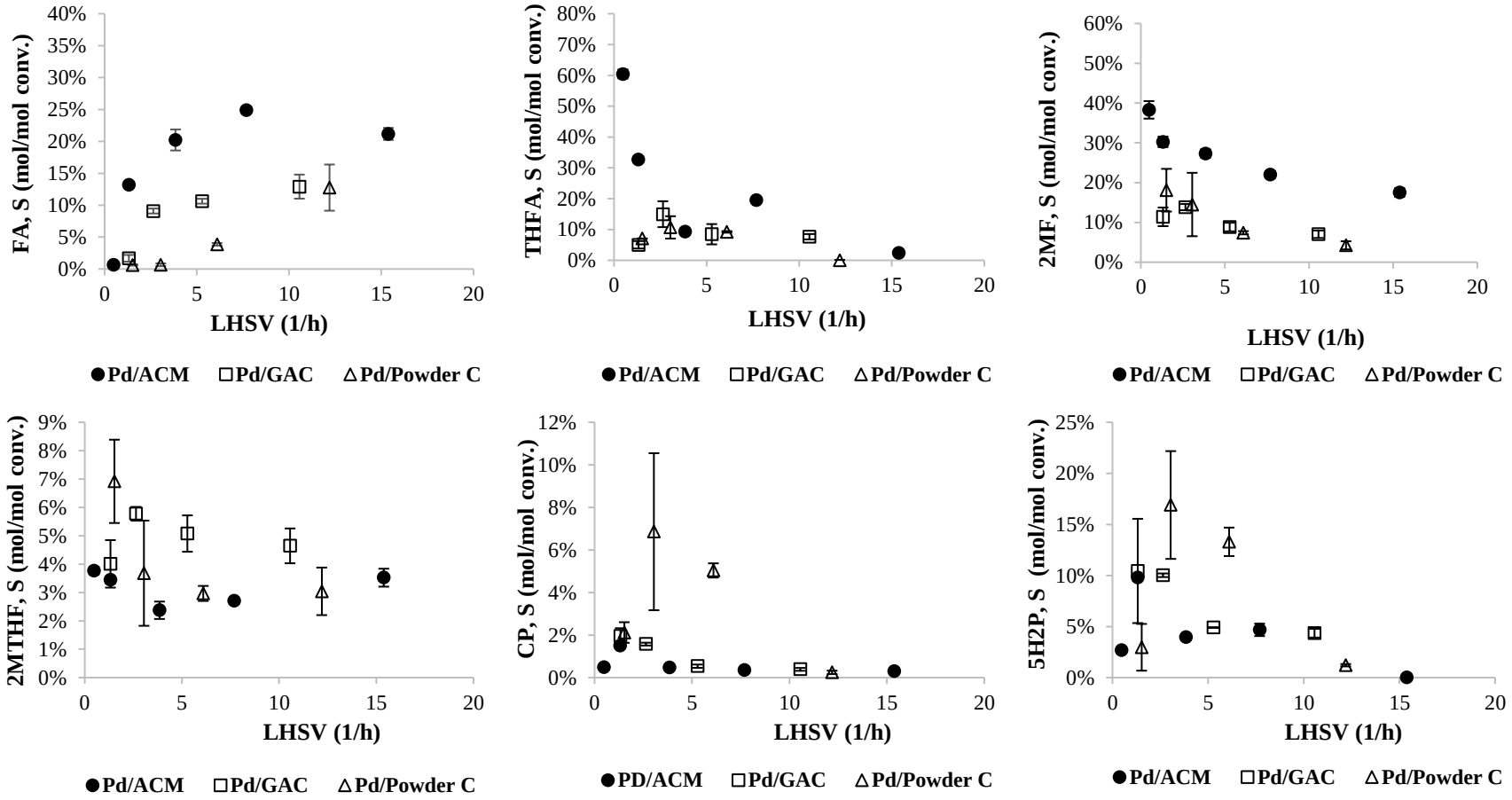

Figure 3.4. Effect of liquid hourly space velocity (LHSV, 1/h) on product selectivity using Pd on carbon catalysts at T=180 °C and P=300 psig (FA, furfuryl alcohol; THFA, tetrahydrofurfuryl alcohol; 2MF, 2-methylfuran; 2MTHF, 2-methyltetrahydrofuran; 5H2P, 5-hydroxy-2-pentanone; CP, cyclopentanone).

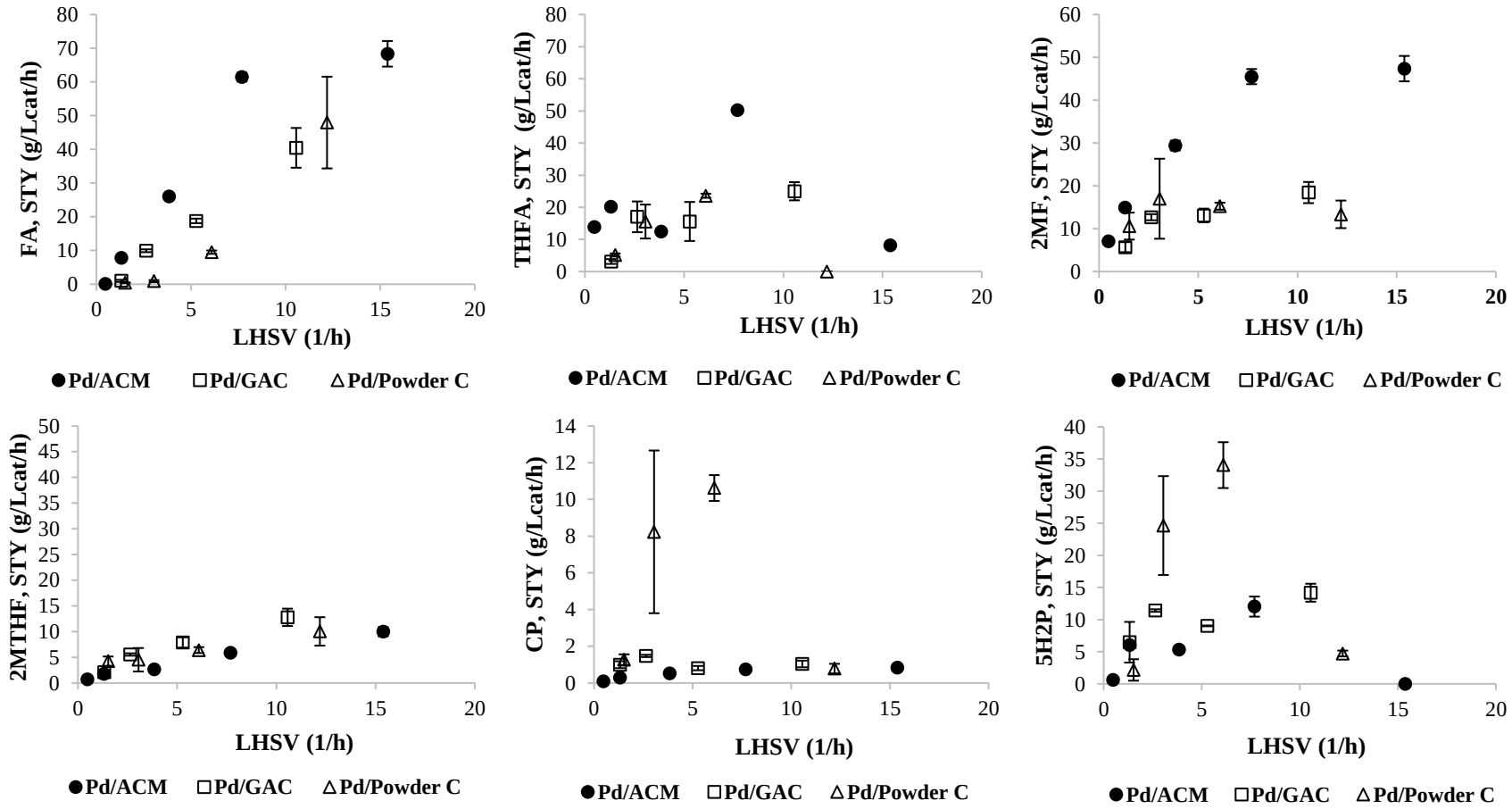

Figure 3.5. Effect of liquid residence time on space time yields (STY, g/L-cat/h) using Pd on carbon catalysts at T= 180 °C and P=300 psig (FA, furfuryl alcohol; THFA, tetrahydrofurfuryl alcohol; 2MF, 2-methylfuran; 2MTHF, 2-methyltetrahydrofuran; 5H2P, 5-hydroxy-2-pentanone; CP, cyclopentanone).

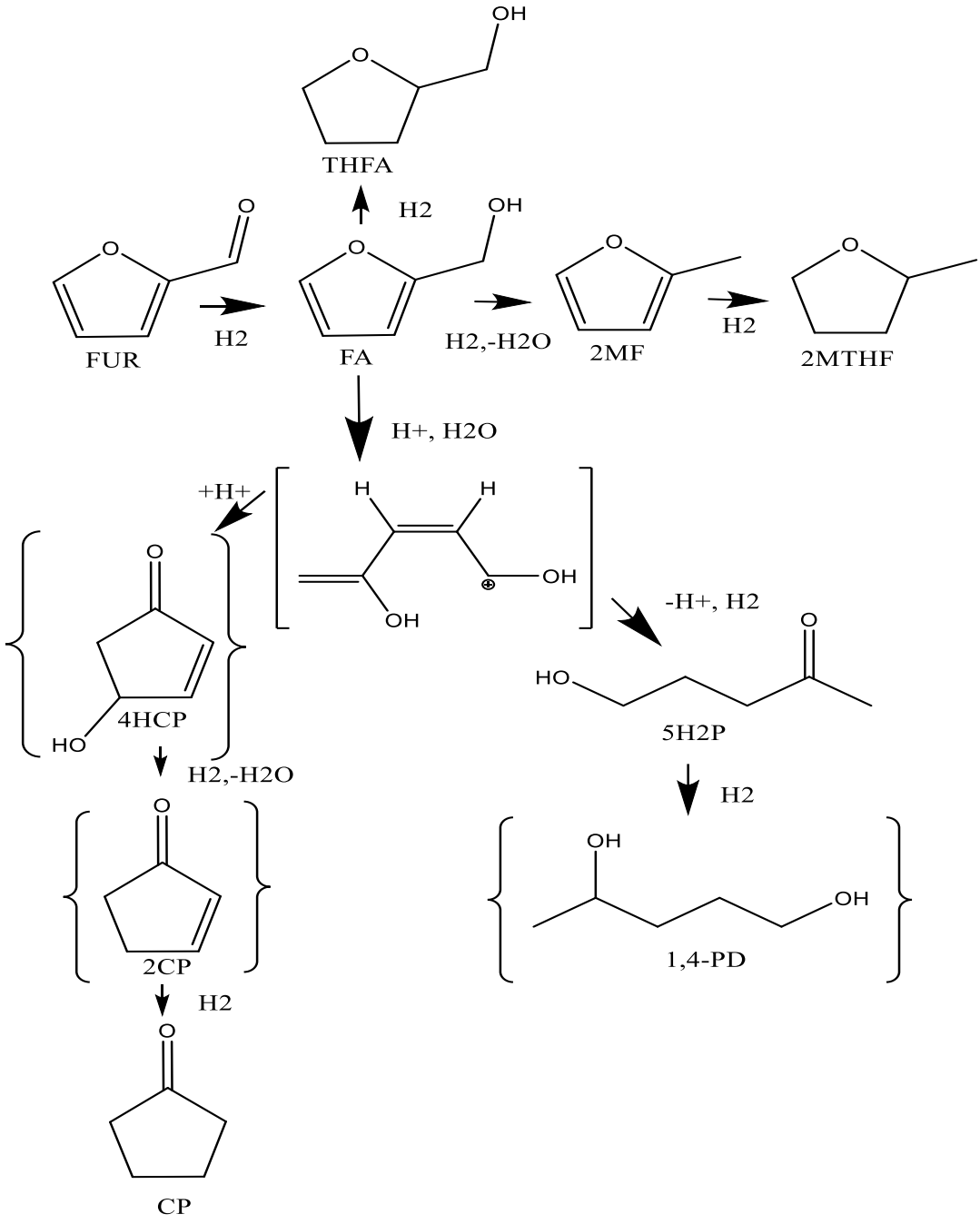

Figure 3.6. Speculative pathway for furfural (FUR) hydrogenation, dehydration, and Piancatelli rearrangement reactions to 2-methylfuran (2MF), cyclopentanone (CP), and 5-hydroxy-2-pentanone (5H2P) FA, furfuryl alcohol; THFA, tetrahydrofurfuryl alcohol; 2MTHF, 2-methyltetrahydrofuran; 2-cyclopentenone (2CP); 4HCP, 4-hydroxy-2-cyclopentenone; 1,4-PD, 1,4-pentanediol (Mironenko et al., 2019; Liu et al., 2018). [ ], indicates a possible short lived intermediate; {}, indicates anticipated product or intermediate not observed.

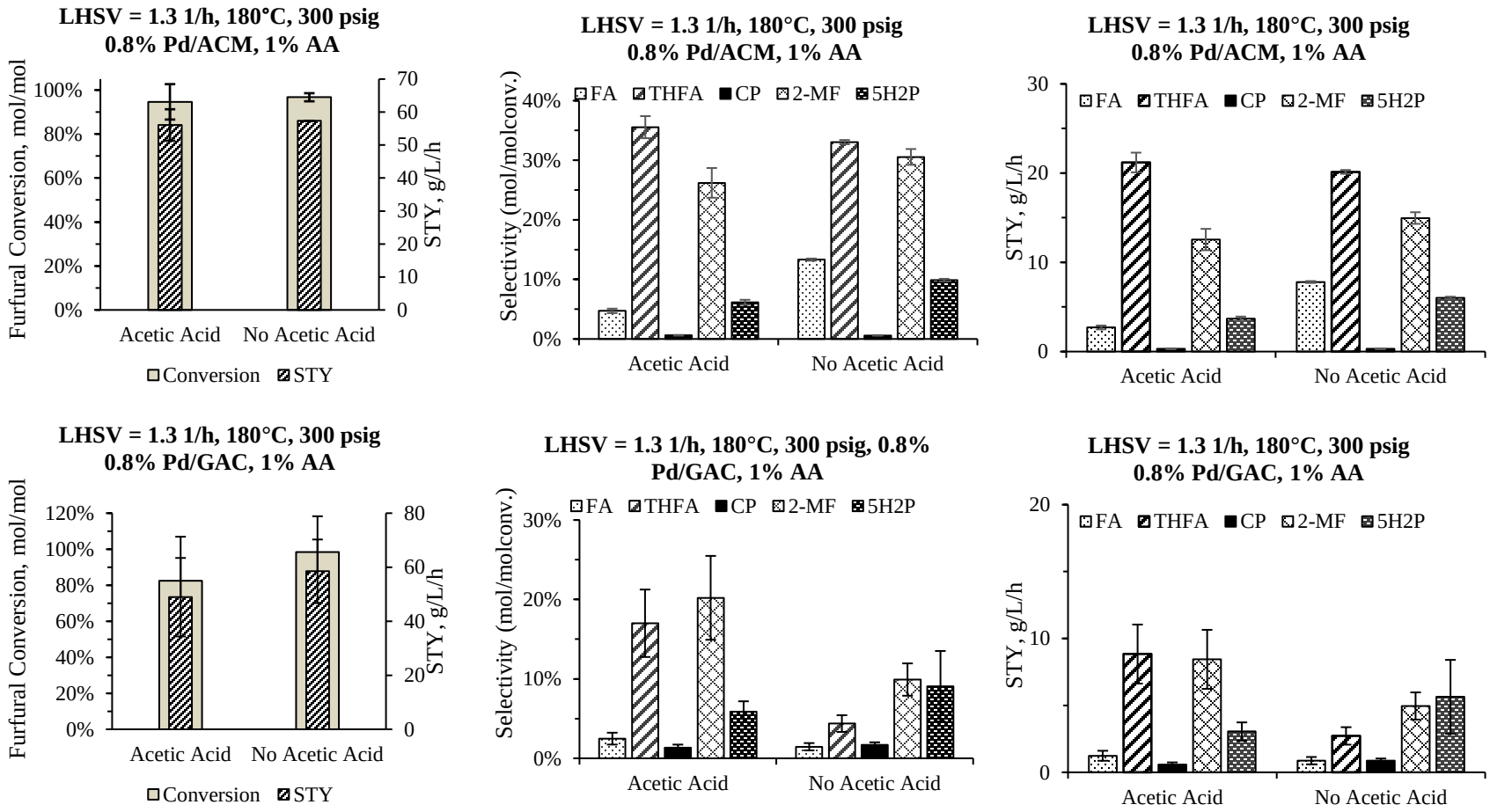

Figure 3.7. Effect of acetic acid (1 wt%) on product selectivity and space time yield using carbon supported catalysts (FA, furfuryl alcohol; THFA, tetrahydrofurfuryl alcohol; 2MF, 2-methylfuran; 2MTHF, 2-methyltetrahydrofuran; 5H2P, 5-hydroxy-2-pentanone; CP, cyclopentanone). Reactions were performed at 180 °C, 300 psig (2.07 MPa), and LHSV 1.3 h^{-1}.

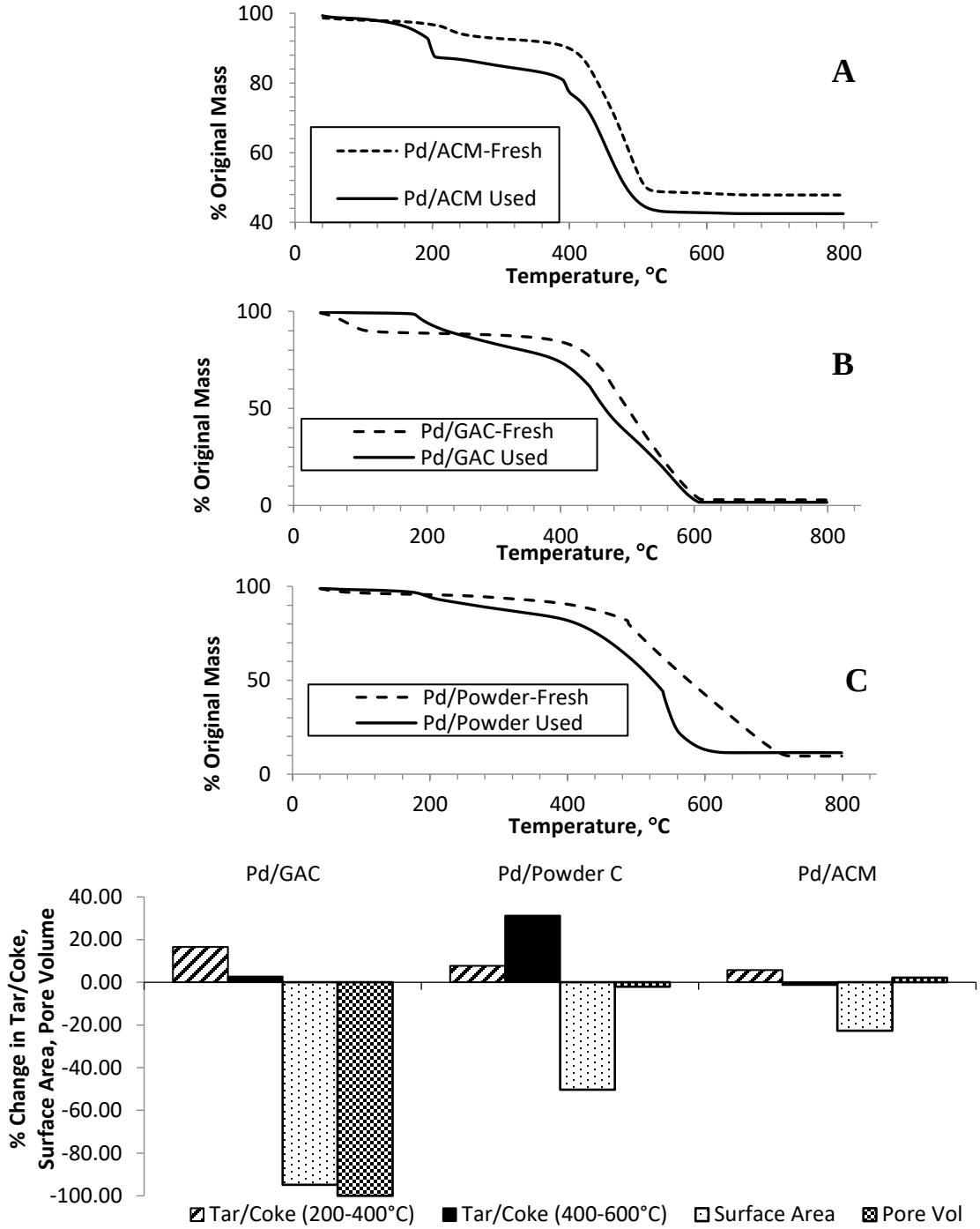

Figure 3.8. TGA analysis of spent catalysts compared to unreacted materials – A) Pd/ACM, B) Pd/GAC, and C) Pd/Powder C (% original mass is % loss in mass relative to the starting mass) and the change in tar/coke relative to the fresh catalyst, surface area, and pore volume (bottom) of the spent catalysts relative to the fresh catalyst.

CHAPTER 4

BI-METAL ACTIVATED CARBON MONOLITH CATALYSTS FOR SELECTIVE HYDROGENATION OF FURFURAL[1]

[1] Pirmoradi, M, Janulaitis, N, Gulotty Jr., R.J., Kastner, J.R., 2020. To be submitted to *Industrial and Engineering Chemistry Research.*

Abstract

Activated carbon monolith (ACM) catalysts were impregnated with Pd, Pd-Cu and Pd-Fe for continuous hydrogenation of aqueous furfural. The effect of temperature, pressure and liquid residence time on product selectivity and space time yield was determined. Adding a second metal to Pd/ACM shifted the selectivity of the catalyst from 2-methylfuran (2MF) and 2-methyltetrahydrofuran (2MTHF) to furfuryl alcohol (FA) and tetrahydrofurfuryl alcohol (THFA) over the range of tested temperatures and pressures. A high space time yield of 272 g/Lcat/h THFA and 143 g/Lcat/h FA was achieved using Pd-Fe/ACM at 180 °C and 300 psig. The effect of acetic acid, an impurity present in crude furfural, on furfural conversion and product selectivity was determined. The surface area analysis indicated a relatively low loss of surface area over 13 hydrogenation reactions on each catalyst. The presence of a second metal on the monolith catalyst stabilized Pd particles, reduced leaching, and altered product selectivity.

Keywords: Bi-metallic catalysts, furfural, selective hydrogenation, activated carbon monolith

4.1 Introduction

Monolith catalysts, commonly fabricated using ceramic and metallic materials, are a type of structured catalyst with a shape of honeycomb, providing a high number of parallel channels with small diameter.[1] Compared to conventional packed bed reactors, monolith catalysts provide lower pressure drop and higher mass transfer rates due to a larger open frontal area and a shorter diffusion path. Several research groups have investigated the application of monolith catalysts in both single and multiple phase reactions. Low temperature combustion of xylenes using Pd and Pt supported on carbon-coated monolith[2], hydrogenation of benzaldehyde to benzyl alcohol using Ni supported on γ-alumina-coated monolith[3], esterification of 1-octanol with hexanoic acid using zeolite-coated monolith[4], selective hydrogenation of fatty acid methyl esters using Pd supported on carbon coated monolith[5] and hydrogenation of benzene to cyclohexene on Ru/alumina-coated monolith[6] are examples of reactions that have been performed using monolithic catalysts.

Activated carbon, obtained from renewable forest and agricultural resources, is a promising base material for production of monolith catalysts due to providing a large surface area and a well-defined pore distribution as a catalyst support. In addition, activated carbon supports provide advantages such as inertness, durability, and easy recovery of precious metal from catalysts (by combustion). Therefore, manufacturing a monolith catalyst from activated carbon will allow all the benefits of both activated carbon and a monolithic structure in one single catalyst, known as activated carbon monolith catalyst. Activated carbon monolith catalysts, impregnated with precious metals and transition metals, can be promising catalysts for

series of continuous hydrogenation reactions. Furfural (derived from lignocellulosic biomass) is an abundant green feedstock for continuous hydrogenation reaction systems.

Hydrogenation of furfural (FUR) results in several value-added products such as furfuryl alcohol (FA), tetrahydrofurfuryl alcohol (THFA), 2-methyltetrahydrofuran (2MTHF) and 2-methylfuran (2MF), cyclopentanone (CP) and 5-hydroxy-2-pentanone (5H2P). In general, there are two major catalyst groups involve in heterogeneous hydrogenation reactions; first, precious metals such as platinum and palladium and second, transition base metals such as iron and copper.[7] These metal catalysts can actively adsorb the hydrogen atoms from hydrogen gas. The adsorbed hydrogen atoms are further added to the unsaturated bond of the other reactants. Compared to monometallic catalysts, bi-metallic catalysts demonstrate higher activity and stability and better selectivity mainly due to metal-metal interactions. Adding a second metal to a mono-metallic catalyst can enhance the selectivity of the catalyst by modifying atomic arrangement at the metal active site, stabilize the catalyst by reducing the deposition of carbon compounds, changing d-band properties, and formation of a synergistic effect.[8-10] Moreover, each metal independently can play its own significant and different role in the reaction system. This feature is a very important for selective hydrogenation reactions where the catalyst can promote desired pathways through one metal and block unwanted pathways through the other. Several research groups have reported successful design and utilization of bi-metallic catalysts for selective hydrogenation. Santori et al. 2002 studied the effect of adding tin to silica-supported platinum on hydrogenation of benzaldehyde and butanone. They reported that adding tin to Pt/SiO_2 catalyst promotes C=O hydrogenation and inhibits C=C hydrogenation route.[11] In

another study by Hammoudeh et al. 2003, adding tin to silica-supported palladium increased the rate constant ratio in hydrogenation of cinnamaldehyde to cinnamyl alcohol and from there to phenylpropanal and suppressed the hydrogenation route to saturated aldehydes.[12] Bachiller-Baeza et al. 2001 reported adding iron to activated carbon- supported ruthenium increased the selectivity of citral hydrogenation towards unsaturated alcohols.[13] Borgna et al. 2004 also reported that hydrogenation of crotonaldehyde using Co-Pt/SiO_2 had higher selectivity towards crotyl alcohol than Pt/SiO_2.[14] Selective hydrogenation of acrolein using gold-indium supported by zinc oxide[15] and selective hydrogenation of acetophenone using nickel-platinum supported by Y zeolite[16] are other examples of selective hydrogenation of ketones and unsaturated aldehydes in presence of bi-metallic catalysts. Bi-metallic catalysts have also been used in selective hydrogenation of carboxylic acid such as levulinic acid to gamma-valerolactone using a tin-ruthenium catalyst.[17] Regarding the hydrogenation of furfural using bi-metallic catalysts, Fulajtarova et al. 2015, studied hydrogenation of aqueous furfural to furfuryl alcohol over Pd-Cu catalysts with supports of carbon, MgO/$Mg(OH)_2$ and hydrotalcite.[18] The catalyst with carbon support achieved 100% conversion with 90% selectivity of furfuryl alcohol. Fulajtarova et al. 2015 also reported that the adsorption of C=O groups on the catalyst is associated with Cu active sites. As a result, the interaction between adsorbed C=O groups on Cu and adsorbed H atoms on Pd becomes easier.[18] In another study by Thompson et al. 2016, Pd-Re/Al_2O_3 performed with higher activity and better selectivity of furfuryl alcohol than Pd/Al_2O_3.[19] Yang et al. 2013 reported Ni-Cu supported by SBA-15 silica enhanced the selectivity of cyclopentanone and the conversion of furfural (at 160 °C and 4 MPa) to 62% and nearly 100%, respectively while the Ni/SBA-15 catalyst result in approximately 39% selectivity and 46% conversion in the similar

reaction condition.[20] Testing 10, 30, 50 and 80 percent molar ratios of Cu/Ni indicated that the highest conversion of furfural and selectivity of cyclopentanone was achieved at 50% molar ratio. Rearrangement of the furan ring was independent of the first hydrogenation step and occurred from furfuryl alcohol. Hronec et al. 2016 also tested carbon supported Pd-Cu catalysts, prepared by different methods, for selective hydrogenation of furfural to cyclopentanone in water.[21] The three methods used for preparation of the catalyst were reductive deposition precipitation, co-impregnation and electroless plating (these methods will be explained in the next section). The highest selectivity of cyclopentanone was achieved with the catalyst that was prepared with electroless plating. Catalyst characterization indicated that in the electroless plating method, copper appeared in Cu^{+} oxidation form as Cu_2O where Cu^{+} played a key role in adsorption of C=O groups. In the optimum condition, the selectivity of 92.1% cyclopentanone was achieved.

The focus of this work is to employ activated carbon monolith structures as a support for precious and transition metals of Pd, Pd-Cu and Pd-Fe catalysts in a continuous furfural hydrogenation system. The furfural hydrogenation reaction is important from industrial point of view since it can form series of valuable products. The monolith structure can be a promising industrial replacement for conventional granular catalysts due to providing higher mass transfer rates, significant lower pressure drops and easy scale-up. In general, the novel aspects of this work are 1) employing activated carbon monolith catalysts for continuous aqueous furfural hydrogenation, 2) using a structured catalyst as a support for bimetals, 3) synthesis of a bimetal

carbon monolith catalyst to alter furfural hydrogenation pathways, 4) determining the effect of acidic reaction medium (crude furfural stimulant) on furfural hydrogenation.

4.2 Methods and Materials

Catalysts and Reactions: Activated carbon monolith catalysts with nominal metal loadings (wt%) of 0.8% Pd on activated carbon monolith (Pd/ACM), 0.8% Pd-1.6% Cu on activated carbon monolith (Pd-Cu/ACM) and 0.8% Pd-1.6% Fe on activated carbon monolith (Pd-Fe/ACM) were provided by Applied Catalysts (Laurens, SC). Each monolith structure has diameter and length of 1 inch, 529 cells/in^2, wall thickness of 0.01 inch, cell spacing of 0.0435 inch, geometric surface area of 70.84 in^2/in^3 and open frontal area of 0.593 in. Details on activated carbon monolith (ACM) production procedure and pictures of ACM have been previously demonstrated in literature.[22, 23] 4 cores of activated carbon monolith (ACM) were loaded in a Parr Packed Bed Reactor System (details have been previously described).[22] ACM catalysts were reduced for 4 hours prior to reaction in 100 mL/min flow of pure hydrogen at 250 °C. Next, aqueous furfural hydrogenation reactions were conducted at liquid flow rates of 0.5 to 16 mL/min, temperatures of 120 to180 °C and pressures of atm to 300 psig using a feedstock of 44 g/L furfural (purchased from Sigma-Aldrich, 99%) dissolved in DI water. After each reaction, liquid samples were recovered and analyzed using Gas Chromatography-Flame Ionization Detection (GC-FID), with a method previously described.[22] The concentrations of FUR (99%, Sigma-Aldrich), FA (98%, Sigma-Aldrich), THFA (98%, Sigma-Aldrich), 2MF (99%, Sigma-Aldrich), 2MTHF (99%, Sigma-Aldrich), CP (95%, Sigma-Aldrich) and 5H2P (95%, Sigma-Aldrich) were measured according to a four point standard curve (each point run in triplicate). 2MF standard solution was prepared using ethanol and all the other standard solutions were

prepared using DI water. Gas Chromatography-Mass Spectrometry (GC-MS) confirmed the presence of all the above compounds in the reaction samples with the following method: HP-6890 with HP Innowax column, same method as for GC/FID, 1 μl injection volume, 25:1 split ratio, 0.8 ml/min, 10-500 mass units, MSD ChemStation D.03.00.611 with NIST 2008 database for identification.

Catalysts Characterization: Hydrogen-Temperature Programmed Reduction (H_2-TPR) for determining reduction temperatures, Ammonia-Temperature Programmed Desorption (NH_3-TPD) for determining acid site density, CO pulse titration for determining dispersion and CO uptake and surface area analysis were performed as previously described.[22] Scanning Electron Microscopy / Energy Dispersive X-Ray Spectroscopy (SEM/EDS) was performed using FEI TENEO with 150 mm Oxford XMaxN detector at 10 kV. TGA analysis in air was used to estimate tar and coke formation on the catalysts (Discovery TGA from TA Instruments). Air flow over the sample (10-25 mg in ceramic pans) was set at 25 mL/min with a balance flow rate at 10 mL/min (N_2). The temperature of the sample was equilibrated at 40 °C before ramping at a rate of 10°C/min to 800 °C. Elemental analysis of fresh and spent catalysts was performed following the Environmental Protection Agency (EPA) ICP method 200.8. Concentrated HNO_3 was added (5 ml) to the sample (~ 0.1g) for microwave digestion following protocols listed in EPA method 3051A. Digested solutions were analyzed by inductively coupled plasma optical emission spectroscopy (ICP-OES, Spectro Arcos FHS16 AMETEK ICP-OES). X-ray diffraction (XRD) was performed on a PANalytical X'Pert PRO using a Cu-Ka radiation source (l = 1.5418 Å) with step size of 0.02° and 2θ range of 15° to 80°.

4.3 Results and Discussion

4.3.1 Catalyst Characterization

The reduction temperature of metal oxides on Pd/ACM, Pd-Cu/ACM and Pd-Fe/ACM catalysts was determined using H_2-TPR (Figure 4.1). The TPR analysis of mono-metallic Pd/ACM catalyst indicated two peaks at approximately 205 and 287 °C. Adding Cu to the Pd/ACM catalyst shifted the peak/reduction temperatures to 220 and 320 °C. Adding Fe to the mono-metallic Pd/ACM catalyst also increased the reduction temperature to approximately 250 and 400 °C. Normally, the reduction temperature of Cu and Fe mono-metal on carbon is close to 400 °C[24] and 550 °C[25], respectively. A shift to higher Pd reduction temperatures in the TPR peaks can be attributed to metal-metal interactions on bi-metal catalysts.[24, 25] Śrębowata et al. 2011 reported a shift to higher temperature peaks from Pd/C to Pd-Cu/C due to strong metal interactions.[24] Espro et al. 2017 also reported the same effect with Pd-Fe catalysts.[25] Wettstein et al. 2012 observed a shift to higher temperatures in TPR peaks when comparing Ru/C and Ru-Sn/C catalysts due to a similar effect.[17] The shift to higher temperature peaks is indicative of Pd stabilization due to interaction with the second metals.[26] Pd-Cu/ACM and Pd-Fe/ACM demonstrated a different reduction behavior from Pd/ACM. The Pd-Cu/ACM and Pd-Fe/ACM TPR peaks were broader with limited separation between peaks, which also indicates the two metals are reducing simultaneously with close interaction to each other.[27] SEM-EDS images of bi-metal catalysts indicate that in most regions on the catalyst support, Pd and the second metal (Fe or Cu) particles are located very close to each other, while at other regions metal particles are present in form of a mono-metal **(**Figure 4.2**)**. SEM-EDS images also indicate that Pd particles at

some regions on the catalyst are located close to Al and Si particles from ceramic binder but most of the Pd is located close to carbon substrate (Figure 4.2, S4.1, S4.2 and S4.3).

NH_3-TPD analysis was performed to determine the acid site density on each catalyst. The NH_3-TPD results of Pd/ACM and Pd-Cu/ACM catalysts indicated a peak approximately at 400 °C (strong acid site) whereas Pd-Fe/ACM indicated three peaks at approximately 400, 525 and 575 °C where the highest temperature peak with a smaller peak area represents carbon off-gassing carbon dioxide and carbon monoxide (Figure 4.3). Comparing the NH_3-TPD results of 0.8% Pd/ACM to the conventional granular 0.8% Pd on granular activated carbon (Pd/GAC) of the same carbon source, with no binder in the carbon structure, the presence of 400 °C peak for the three ACM catalysts is attributed to presence of mineral binder in the monolith structure. An acid site density of 406, 401 and 184 micro-moles NH_3/g was calculated at 400 °C for Pd/ACM, Pd-Cu/ACM and Pd-Fe/ACM, respectively and an acid site density of 38 micro-moles NH_3/g was calculated for Pd-Fe/ACM at 525 °C (Table 4.1).

The results of BET and BJH analysis indicated that most of the physical properties of untreated Pd/ACM, Pd-Cu/ACM and Pd-Fe/ACM were similar (Table 4.1 and Figure 4.4). The only significant difference observed in physical properties of the three catalysts was that the micro-pore volume of Pd-Fe/ACM catalyst was higher than the micro-pore volume of the other two catalysts. ICP-MS/elemental analysis was performed to determine the accurate metal loading of each catalyst. The nominal weight percent of metal on each activated carbon monolith catalyst was 0.8% Pd, 0.8%Pd-1.6%Cu and 0.8%Pd-1.6%Fe for Pd/ACM, Pd-Cu/ACM and Pd-Fe/ACM, respectively and ICP/MS results indicated metal loadings of 1.2% Pd, 0.65% Pd-1.7% Cu and

0.5%-1.71% Fe for Pd/ACM, Pd-Cu/ACM and Pd-Fe/ACM, respectively. XRD analysis of catalysts indicated two sharp peaks of graphite at 2θ of 20° and 26° (Figure S4.4). Comparing the XRD plots of blank ACM to Pd/ACM catalyst, adding metal to the ACM structure at the low loadings did not add a significant peak to XRD plot, implying that Pd particles are very well dispersed on the ACM structure.[28] Comparing fresh Pd/ACM to fresh Pd-Cu/ACM XRD patterns, no significant change in number and location of peaks was observed, implying that adding Cu to Pd/ACM catalyst did not change the crystalline structure.[29] Pd-Fe/ACM XRD pattern showed less number of peaks at higher 2θ. XRD results for fresh and spent catalyst also did not show a significant change in the location of peaks.

4.3.2 Effect of Temperature on Product Distribution

The effect of temperature on furfural conversion, product selectivity and product yield was determined over the temperatures of 120 to 180 °C (pressure of 300 psig and LHSV of 1.32 1/hr) using Pd/ACM, Pd-Cu/ACM and Pd-Fe/ACM (Figure 4.5). At all temperatures approximately complete conversion of furfural (higher than 90%) was achieved using Pd/ACM and Pd-Fe/ACM whereas using Pd-Cu/ACM over the temperatures of 120 to 160 °C resulted in approximately 80% furfural conversion and complete conversion at temperature of 180 °C. For all the three ACM catalysts, increasing temperature decreased the selectivity of furfuryl alcohol (FA), which is a very fast forming hydrogenation product of furfural. Therefore, with increasing temperature the formed FA converts to other side products resulting in lower FA selectivity at high temperatures. 2-Methylfuran (2MF), the direct hydrogenation product of furfuryl alcohol, had an increasing selectivity with increasing temperature. For Pd-Cu/ACM and Pd-Fe/ACM,

increasing the temperature from 120 to 180 °C, increased 2MF selectivity from 0% to 12% and 1% to 10%, respectively whereas higher 2MF selectivities were achieved using Pd/ACM, increasing from 11% at 120 °C to 31% at 180 °C. Tetrahydrofurfuryl alcohol (THFA), another hydrogenation product of FA, had an increasing selectivity from 12% to 44% in presence of Pd-Cu/ACM and decreasing selectivity from 42% to 31% in presence of Pd-Fe/ACM over the increasing temperature of 120 to 180 °C. Using Pd/ACM at 140 and 160 °C less than 10% selectivity of THFA was observed whereas at 120 and 180 °C the selectivity of approximately 30% THFA was achieved. 2-Methyltetrahydrofuran (2MTHF) which is a side product that can be formed in hydrogenation of tetrahydrofurfuryl alcohol, 2-methylfuran and 5-hydroxy-2-pentanone was determined in very low selectivity (less than 6%) with all three catalysts. Very small amounts of cyclopentanone (CP) was formed using all three catalysts. 5-hydroxy-2-pentanone (5H2P), one of the side products of acid catalyzed rearrangement of FA to 4-hydroxy-2-cyclopentanone, was observed among the reaction products. Using Pd-Cu/ACM, an increasing selectivity of 5H2P from 0 to 5% with increasing temperature over 120 to 180 °C. Using Pd-Fe/ACM, the 5H2P selectivity increased from 4 to 8 % over 120 to 160 °C and dropped to 2% at 180 °C. Pd/ACM resulted in selectivity of 4% at 120 °C to 12% at 180 °C. In general, it can be concluded that the bi-metal catalysts were selective towards THFA whereas Pd/ACM indicated higher selectivity towards 2MF over the tested range of temperature.

4.3.3 Effect of Hydrogen Pressure on Product Distribution

Hydrogen pressures of atmospheric to 300 psig (20 bar) were tested to determine the effect of pressure on product selectivity, yield and furfural conversion (Figure 4.6). Since the complete conversion of furfural was achieved at 180 °C for all three ACM catalysts, the effect of

pressure studies were conducted under 180 °C and LHSV of 1.32 1/h. Approximately complete conversion (higher that 90%) was achieved using Pd/ACM at all hydrogen pressures whereas using Pd-Cu/ACM and Pd-Fe/ACM, an increasing conversion of approximately 80% at atmospheric to complete conversion at 300 psig was achieved. Using Pd-Fe/ACM, THFA selectivity reached a maximum selectivity at 200 psig (increased from 10% at atmospheric to 60%) then dropped to 31% at 300 psig. The highest selectivity of THFA using Pd-Cu/ACM (49%) also achieved at 200 psig whereas only 25% selectivity of THFA was achieved using Pd/ACM at 200 psig. 2MF selectivity increased with increasing pressure for both Pd /ACM and Pd-Fe/ACM to a maximum of 31% and 10%, respectively. Using Pd-Cu/ACM, 2MF selectivity increased from 1% to 16% from atmospheric to 200 psig and dropped to 12% at 300 psig. For all three catalysts, low 2MTHF selectivities were determined (less than 10%). Generally, 2MTHF yields decreased over increasing pressure. 5H2P selectivity using Pd-Fe/ACM catalyst increased from 1% at atmospheric to 9% at 200 psig then decreased to 2% at 300 psig. An increasing 5H2P yield of 0 to 10% was achieved using Pd/ACM. The highest 5H2P selectivity using Pd-Cu/ACM was 5% at 300 psi. Using all three catalysts less than 2% CP selectivity was observed.

4.3.4 Effect of Liquid Hourly Space Velocity on Product Distribution

Effect of liquid hourly space velocity (LHSV) on furfural conversion, product selectivity and yield was determined by testing liquid flow rates ranging from 0.5 mL/min (LHSV of 0.48 1/h) to 16 mL/min (LHSV of 15.38 1/h) at 180 °C and 300 psig (Figure 4.7 and Figure 4.8). Complete conversion of furfural was achieved at the lowest LHSV or the longest contact time. Increasing LHSV or decreasing contact time decreased furfural conversion for all three catalysts.

At the highest LHSV (15.38 1/h) the conversions of 51%, 56% and 84% were determined for Pd/ACM, Pd-Cu/ACM and Pd-Fe/ACM, respectively. Using Pd-Fe/ACM, FA selectivity increased from 1% at 0.48 1/h to 24% at 15.38 1/h. At 15.38 1/h a FA space time yield (STY) of 143 g/Lcat/h was achieved. Longer contact times or lower LHSVs lead to higher conversion of FA to other products and therefore lower selectivity of FA. Using Pd/ACM and Pd-Cu/ACM, increasing LHSV also increased FA selectivity to a maximum at 7.69 1/h and then slightly dropped at 15.38 1/hr. In presence of Pd/ACM, THFA selectivity declined from 60% at 0.48 1/h to 2% at 15.38 1/h. Using Pd-Fe/ACM, THFA selectivity increased from 12% at 0.48 1/hr to 44% at 15.38 1/hr where the highest STY of 272 g/Lcat/h was achieved. In presence of Pd-Cu/ACM, THFA selectivity reached a maximum of 43% at 1.32 1/h and then dropped to approximately 19% at 15.38 1/hr whereas the THFA STY increased from 1 g/Lcat/h at 0.48 1/h to 80 g/Lcat/h at 15.38 1/h. Over increasing LHSV of 0.48 to 15.35 1/h, the 2MF selectivity of Pd/ACM decreased from 38% to 18% whereas the 2MF STY increased from 3 g/Lcat/h at 0.48 1/h to 47 g/Lcat/h at 15.38 1/h. Using Pd-Fe/ACM, 2MF did not change significantly whereas an increasing STY pattern was observed (highest of 58.39 g/Lcat/h at 15.38 1/h). The highest selectivity of 2MF using Pd-Cu/ACM was 19 % at 7.69 1/h, but a clear pattern of 2MF selectivity was not observed, although the 2MF STY increased from 2 g/Lcat/h at 0.48 to 42 g/Lcat/h at 7.69 g/Lcat/h and then dropped to 24 g/Lcat/h at 15.38 1/h. Less than 2% 2MTHF selectivity was determined at all LHSVs using Pd-Cu/ACM and Pd-Fe/ACM. A selectivity of 4% 2MTHF at 0.48 1/h was observed for Pd/ACM. Very low CP selectivity (less than 3%) and CP STY (less than 6 g/Lcat/h) were determined in the presence of all three catalysts. In the presence of Pd-Fe/ACM, 5H2P STY in increased from 0.14 g/Lcat/h at 0.48 1/h to 40 g/Lcat/h at

15.38 1/h. Comparing the three catalysts, higher product STYs were achieved using Pd-Fe/ACM at the highest LHSV or lowest contact time, most significantly for THFA and 5H2P. Based on the available Pd sites, turnover frequency of 248, 624 and 802 1/h at the highest LHSV was calculated for Pd/ACM, Pd-Cu/ACM and Pd-Fe/ACM.

4.3.5. Effect of Impurities on Product Distribution

In this work, furfural with 99% purity was employed for all the reactions. In real industrial work, achieving this purity is extremely costly due to several steam stripping steps of crude furfural. Therefore, using crude furfural for hydrogenation reactions can be cost effective. Furfural is produced using biomass hydrolysis followed by a dehydration step, resulting in approximately 5% furfural. Acetic acid with approximately 1% concentration is one of the most significant impurities in this reaction. Therefore, we decided to determine the effect of acetic acid, present in crude furfural, on product selectivity of furfural hydrogenation. Using Pd/ACM, presence of 1% acetic acid did not significantly changed furfural conversion or product selectivity (Figure 4.9). Using Pd-Cu/ACM, furfural conversion decreased from 97% to 88% in presence of acetic. THFA showed the most significant change in product selectivity, decreasing from 43% to 27%. 2MF selectivity also increased from 11% to 17% in presence of acetic. Using Pd-Fe/ACM in the presence of acetic acid, furfural conversion decreased from 98% to 93% and 5H2P selectivity increased from 2% to 9%. Cyclopentanone selectivity also slightly increased. The increase in selectivity of these two products implies that acetic acid promoted the FA acid catalyzed rearrangement using Pd-Fe/ACM.

4.3.6. Catalyst Activity Analysis

After 13 furfural hydrogenation experiments on each catalyst (total of approximately 280 minutes of reaction time), the catalyst was recovered for activity analysis. The surface area analysis indicated surface area loss of 22%, 31% and 35% for Pd/ACM, Pd-Cu/ACM and Pd-Fe/ACM, respectively. All three catalysts lost 100% of their micro-pore volume. The higher surface area loss in Pd-Fe/ACM is attributed to presence of higher initial micro-pore volume compared to the other two catalysts, contributing to coke formation. Therefore, in order to determine the amount of coke formed on spent catalysts TGA analysis was performed. The TGA results indicated that the highest mass loss at 40-300 °C occurred in presence of Pd-Fe/ACM (Figure 4.10). Next ICP-MS was performed on spent catalysts to determine the percent of metal leaching. The ICP-MS results indicated Pd loss of 20% for Pd/ACM, Pd loss of 10% and Cu loss of 0% for Pd-Cu/ACM, Pd loss of 14% and Fe loss of 37% for Pd-Fe/ACM. These results imply that adding a second metal stabilized Pd particles and reducing leaching, a common problem with Pd on carbon catalysts.[30]

4.3.7. Discussion

Significantly higher CO uptakes of the spent Pd-Cu/ACM and Pd-Fe/ACM compared to Pd/ACM coupled with TPR results where higher temperature reduction peaks were observed for Pd-Cu/ACM and Pd-Fe/ACM, indicate that adding a second metal stabilized Pd and prevented the migration of Pd particles during a series of catalytic reactions at relatively high temperatures. Adding a second metal to Pd catalyst also increased the turnover frequency of catalyst, significantly. The CO uptake and thus Pd dispersion was the highest for fresh and spent Pd-

Fe/ACM. The spent Pd-Fe/ACM showed higher CO uptake than the fresh catalyst due to a significant Fe loss after hydrogenation reactions. As previously reported in literature, furfural can adsorb at Pd, Cu and Fe sites.[31] Pd is usually active towards C=C bonds and Cu is active towards C=O bonds.[18] Therefore, with adsorption of furfural at both metal active sites, it was expected that the presence of Cu and Fe on the surface along with Pd would change the product selectivity. As shown in Figure 4.5 and Figure 4.6, using Pd/ACM, a higher selectivity of 2MF and 2MTHF was observed, whereas adding the second metal (Cu and Fe) resulted in higher selectivity of FA and THFA at lower pressures and temperatures. Higher selectivity of FA using bi-metals can be attributed to the fact that Cu and Fe promote the hydrogenation of C=O bond. These results are consistent with previous works in literature where adding Cu to Ni and Pd catalysts increased THFA and FA selectivity due to adsorption of C=O bond at Cu site, resulting in a synergistic effect, where different active sites act on different substrates during the reaction, upon formation of bi-metal alloys.[18, 32, 33] In order to prevent sintering of the Pd in our work, the reduction temperature of 250 °C for all the three catalysts was applied prior to reaction, which potentially resulted in incomplete reduction of the metals since TPR peaks were observed at 220 and 320 °C for Pd-Cu/ACM and 250 and 400 °C for Pd-Fe/ACM. The presence of these ions can also promote the formation of furfuryl alcohol through adsorption of furan ring at the ion site.[34] In general, adding a transition metal to Pd improved the selectivity towards FA and THFA due to changing the adsorbing bond at the active site. These transition metals also improved the stability of Pd and catalyst turnover frequency and reduced leaching.

4.4 Conclusions

For the first time, bi-metal activated carbon monolith catalysts were employed for continuous hydrogenation of furfural. The bi-metal carbon monolith structures of Pd-Cu and Pd-Fe were compared with the mono-metal Pd monolith structure. Adding Cu and Fe to the Pd catalyst changed the selectivity from 2MF and 2MTHF to FA and THFA. A high space time yield of 272 g/Lcat/h for THFA and 143 g/Lcat/h for FA, the highest reported space time yields in aqueous phase furfural hydrogenation to the best of our knowledge, was determined using Pd-Fe/ACM at 180 °C and 300 psig. Catalyst activity analysis indicated that adding a second metal reduced leaching of Pd particles which can be attributed to metal-metal interactions indicated by SEM-EDS images. Adding acetic acid to the feedstock solution did not significantly affect furfural conversion in presence of Pd/ACM and Pd-Fe/ACM and lowered furfural conversion by 9% in presence of Pd-Cu/ACM. In general, these results indicate that the activated carbon monolith catalysts, impregnated with bi-metals for selective hydrogenation of furfural, are promising substitutes for conventional packed beds, which leads to easier scale-up in reactor design, lower pressure drop and higher mass transfer rates. The use of activated carbon monolith is not limited to hydrogenation of furfural and can be extended to multiple three-phase reactions.

ASSOCIATED CONTENT

Supporting Information (Appendix B)

The following results are presented, 1) SEM and XRD analysis, 2) furfural conversion and carbon closure, 3) effect of temperature and pressure on product space time yield, 4) effect of acetic acid on furfural conversion.

ACKNOWLEDGMENTS

Support for this research and Maryam Pirmoradi's PhD in Biochemical Engineering and support of Nida Janulaitis (undergraduate research) was provided by a USDA-NIFA Grant (Carbon Monolith Catalysts from Wood for Biobased Platform Chemicals: 2017-67021-26136). Authors thank Dr. Yiping Zhao and Sarada Sripada for their contribution in performing XRD analysis.

References

1. Boger, T.; Heibel, A. K.; Sorensen, C. M., Monolithic catalysts for the chemical industry. Industrial & engineering chemistry research 2004, 43 (16), 4602-4611.

2. Pérez-Cadenas, A. F.; Kapteijn, F.; Moulijn, J. A.; Maldonado-Hodar, F. J.; Carrasco-Marín, F.; Moreno-Castilla, C., Pd and Pt catalysts supported on carbon-coated monoliths for low-temperature combustion of xylenes. Carbon 2006, 44 (12), 2463-2468.

3. Nijhuis, T.; Kreutzer, M.; Romijn, A.; Kapteijn, F.; Moulijn, J., Monolithic catalysts as more efficient three-phase reactors. Catalysis Today 2001, 66 (2), 157-165.

4. Nijhuis, T.; Beers, A.; Kapteijn, F.; Moulijn, J., Water removal by reactive stripping for a solid-acid catalyzed esterification in a monolithic reactor. Chemical engineering science 2002, 57 (9), 1627-1632.

5. Pérez-Cadenas, A. F.; Kapteijn, F.; Zieverink, M. M. P.; Moulijn, J. A., Selective hydrogenation of fatty acid methyl esters over palladium on carbon-based monoliths. Catalysis Today 2007, 128 (1-2), 13-17.

6. Zhao, Y.; Zhou, J.; Zhang, J.; Li, D.; Wang, S., Selective hydrogenation of benzene to cyclohexene on a Ru/Al2O3/cordierite monolithic catalyst: Effect of mass transfer on the catalytic performance. Industrial & Engineering Chemistry Research 2008, 47 (14), 4641-4647.

7. Bartholomew, C. H.; Farrauto, R. J., Fundamentals of industrial catalytic processes. John Wiley & Sons: 2011.

8. Alonso, D. M.; Wettstein, S. G.; Dumesic, J. A., Bimetallic catalysts for upgrading of biomass to fuels and chemicals. Chemical Society Reviews 2012, 41 (24), 8075-8098.

9. Kim, D.; Resasco, J.; Yu, Y.; Asiri, A. M.; Yang, P., Synergistic geometric and electronic effects for electrochemical reduction of carbon dioxide using gold–copper bimetallic nanoparticles. Nature communications 2014, 5, 4948.

10. Hu, S.; Scudiero, L.; Ha, S., Electronic effect on oxidation of formic acid on supported Pd–Cu bimetallic surface. Electrochimica Acta 2012, 83, 354-358.

11. Santori, G. F.; Casella, M. L.; Ferretti, O. A., Hydrogenation of carbonyl compounds using tin-modified platinum-based catalysts prepared via surface organometallic chemistry on metals (SOMC/M). Journal of Molecular Catalysis A: Chemical 2002, 186 (1), 223-239.

12. Hammoudeh, A.; Mahmoud, S., Selective hydrogenation of cinnamaldehyde over Pd/SiO2 catalysts: selectivity promotion by alloyed Sn. Journal of Molecular Catalysis A: Chemical 2003, 203 (1-2), 231-239.

13. Bachiller-Baeza, B.; Guerrero-Ruiz, A.; Wang, P.; Rodrıguez-Ramos, I., Hydrogenation of citral on activated carbon and high-surface-area graphite-supported ruthenium catalysts modified with iron. Journal of Catalysis 2001, 204 (2), 450-459.

14. Borgna, A.; Anderson, B. G.; Saib, A. M.; Bluhm, H.; Hävecker, M.; Knop-Gericke, A.; Kuiper, A.; Tamminga, Y.; Niemantsverdriet, J., Pt− Co/SiO2 Bimetallic Planar Model Catalysts for Selective Hydrogenation of Crotonaldehyde. The Journal of Physical Chemistry B 2004, 108 (46), 17905-17914.

15. Mohr, C.; Hofmeister, H.; Radnik, J.; Claus, P., Identification of active sites in gold-catalyzed hydrogenation of acrolein. Journal of the American Chemical Society 2003, 125 (7), 1905-1911.

16. Malyala, R.; Rode, C.; Arai, M.; Hegde, S.; Chaudhari, R., Activity, selectivity and stability of Ni and bimetallic Ni–Pt supported on zeolite Y catalysts for hydrogenation of acetophenone and its substituted derivatives. Applied Catalysis A: General 2000, 193 (1), 71-86.

17. Wettstein, S. G.; Bond, J. Q.; Alonso, D. M.; Pham, H. N.; Datye, A. K.; Dumesic, J. A., RuSn bimetallic catalysts for selective hydrogenation of levulinic acid to γ-valerolactone. Applied Catalysis B: Environmental 2012, 117-118, 321-329.

18. Fulajtárova, K.; Soták, T.; Hronec, M.; Vávra, I.; Dobročka, E.; Omastová, M., Aqueous phase hydrogenation of furfural to furfuryl alcohol over Pd–Cu catalysts. Applied Catalysis A: General 2015, 502, 78-85.

19. Thompson, S. T.; Lamb, H. H., Palladium–Rhenium Catalysts for Selective Hydrogenation of Furfural: Evidence for an Optimum Surface Composition. ACS Catalysis 2016, 6 (11), 7438-7447.

20. Yang, Y.; Du, Z.; Huang, Y.; Lu, F.; Wang, F.; Gao, J.; Xu, J., Conversion of furfural into cyclopentanone over Ni–Cu bimetallic catalysts. Green Chemistry 2013, 15 (7), 1932-1940.

21. Hronec, M.; Fulajtárová, K.; Vávra, I.; Soták, T.; Dobročka, E.; Mičušík, M., Carbon supported Pd–Cu catalysts for highly selective rearrangement of furfural to cyclopentanone. Applied Catalysis B: Environmental 2016, 181, 210-219.

22. Weber, J.; Thompson, A.; Wilmoth, J.; Gulotty Jr, R. J.; Kastner, J. R., Coupling Red-Mud Ketonization of a Model Bio-Oil Mixture with Aqueous Phase Hydrogenation Using Activated Carbon Monoliths. Energy & Fuels 2017, 31 (9), 9529-9541.

23. Gulotty Jr, R. J.; Rish, S.; Boyd, A.; Mitchell, L.; Plageman, S.; McGill, C.; Keller, J.; Starnes, J.; Stadalsky, J.; Garrison, G., Run Parameters for a Continuous Hydrogenation Process Using ACMC-Pd To Replace Commercial Batch Reactor Processes. Organic Process Research & Development 2018, 22 (12), 1622-1627.

24. Śrębowata, A.; Lisowski, W.; Sobczak, J. W.; Karpiński, Z., Hydrogen-assisted dechlorination of 1, 2-dichloroethane on active carbon supported palladium–copper catalysts. Catalysis today 2011, 175 (1), 576-584.

25. Espro, C.; Gumina, B.; Paone, E.; Mauriello, F., Upgrading lignocellulosic biomasses: Hydrogenolysis of platform derived molecules promoted by heterogeneous Pd-Fe catalysts. Catalysts 2017, 7 (3), 78.

26. Jiang, H.; Tzou, M.; Sachtler, W., Dispersion and catalysis of platinum in bimetal/zeolite catalysts. Applied catalysis 1988, 39, 255-265.

27. Da Silva, A.; Jordao, E.; Mendes, M.; Fouilloux, P., Effect of metal-support interaction during selective hydrogenation of cinnamaldehyde to cinnamyl alcohol on platinum based bimetallic catalysts. Applied Catalysis A: General 1997, 148 (2), 253-264.

28. Mane, R.; Patil, S.; Shirai, M.; Rayalu, S.; Rode, C., Influence of carbon based supports on selectivity behavior of diols and propanol in Ru catalyzed glycerol hydrogenolysis. Applied Catalysis B: Environmental 2017, 204, 134-146.

29. Du, J.; Zhang, J.; Sun, Y.; Jia, W.; Si, Z.; Gao, H.; Tang, X.; Zeng, X.; Lei, T.; Liu, S., Catalytic transfer hydrogenation of biomass-derived furfural to furfuryl alcohol over in-situ prepared nano Cu-Pd/C catalyst using formic acid as hydrogen source. Journal of catalysis 2018, 368, 69-78.

30. Albers, P.; Pietsch, J.; Parker, S. F., Poisoning and deactivation of palladium catalysts. Journal of molecular catalysis A: Chemical 2001, 173 (1-2), 275-286.

31. Jaatinen, S. K.; Karinen, R. S.; Lehtonen, J. S., Liquid Phase Furfural Hydrotreatment to 2‐Methylfuran with Carbon Supported Copper, Nickel, and Iron Catalysts. ChemistrySelect 2017, 2 (1), 51-60.

32. Liu, L.; Lou, H.; Chen, M., Selective hydrogenation of furfural to tetrahydrofurfuryl alcohol over Ni/CNTs and bimetallic CuNi/CNTs catalysts. International Journal of Hydrogen Energy 2016, 41 (33), 14721-14731.

33. Lesiak, M.; Binczarski, M.; Karski, S.; Maniukiewicz, W.; Rogowski, J.; Szubiakiewicz, E.; Berlowska, J.; Dziugan, P.; Witońska, I., Hydrogenation of furfural over Pd–Cu/Al2O3 catalysts. The role of interaction between palladium and copper on determining catalytic properties. Journal of Molecular Catalysis A: Chemical 2014, 395, 337-348.

34. Seo, G.; Chon, H., Hydrogenation of furfural over copper-containing catalysts. Journal of Catalysis 1981, 67 (2), 424-429.

Table 4.1. Physical properties of the activated carbon monolith catalyst

Catalysts	Pd/ACM	Pd/ACM	Pd-Cu/ACM	Pd-Cu/ACM	Pd-Fe/ACM	Pd-Fe/ACM
Properties	(Fresh)	(Spent)[a]	(Fresh)	(Spent)	(Fresh)	(Spent)
Metal Loading (wt.%)[b]	1.2 Pd	0.95 Pd	0.65 Pd-1.7 Cu	0.58 Pd-1.7 Cu	0.50 Pd-1.71 Fe	0.43 Pd-1.07 Fe
Surface Area (m^2/g)	608	469	562	385	627	405
Pore Volume (cm^3/g)	0.45	0.46	0.504	0.399	0.544	0.415
Average Pore Size (radius, Å)	29.8	39.3	35.91	41.4	34.8	41
Micro-Pore Volume[c], (cm^3/g)	0.005	0	0.00923	0	0.0247	0
Acid Sites at 400 °C, (μmoles NH_3/g)	239	NP	231	NP	14	NP
Acid Sites at 525 °C, (μmoles NH_3/g)	0	NP	0	NP	38	NP
CO Uptake[d] (μmoles CO/μmoles Pd)	0.465	0.089	0.408	0.361	0.633	0.724

[a], Spent catalysts from 13 furfural hydrogenation experiments
[b], Calculated from elemental analysis/ICP-MS
[c], Estimated from t-plot analysis
[d], CO uptake from CO pulse titration at 40 °C, CO was assumed to adsorb only to Pd
ACM is activated carbon monolith
NP – not performed

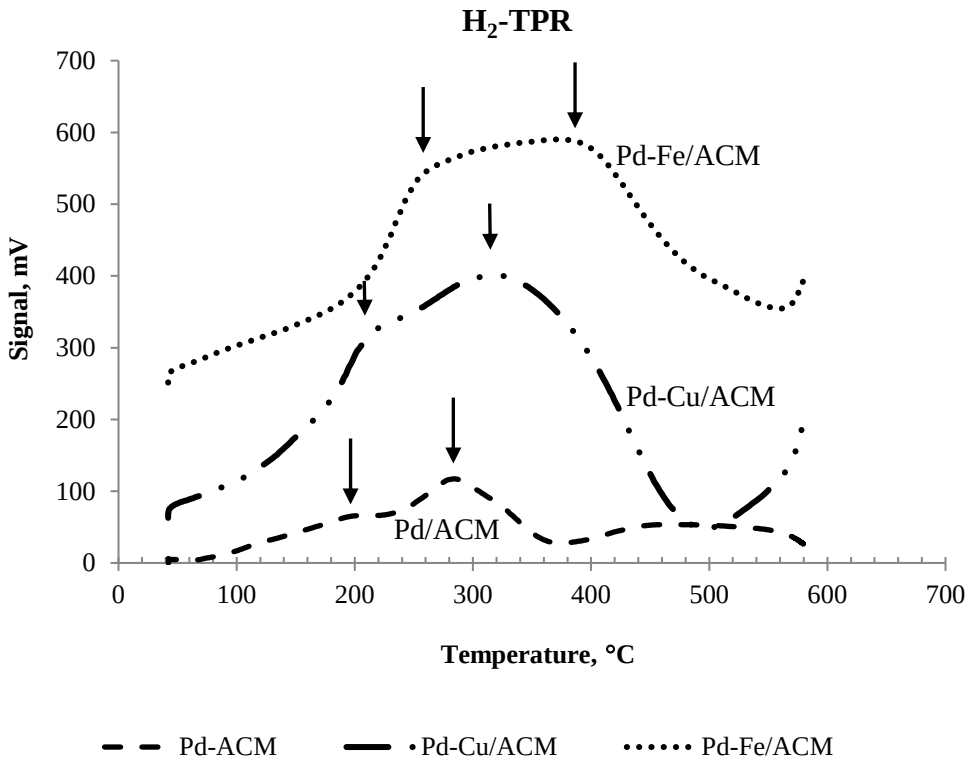

Figure 4.1. Temperature programmed hydrogen reduction of activated carbon catalysts.

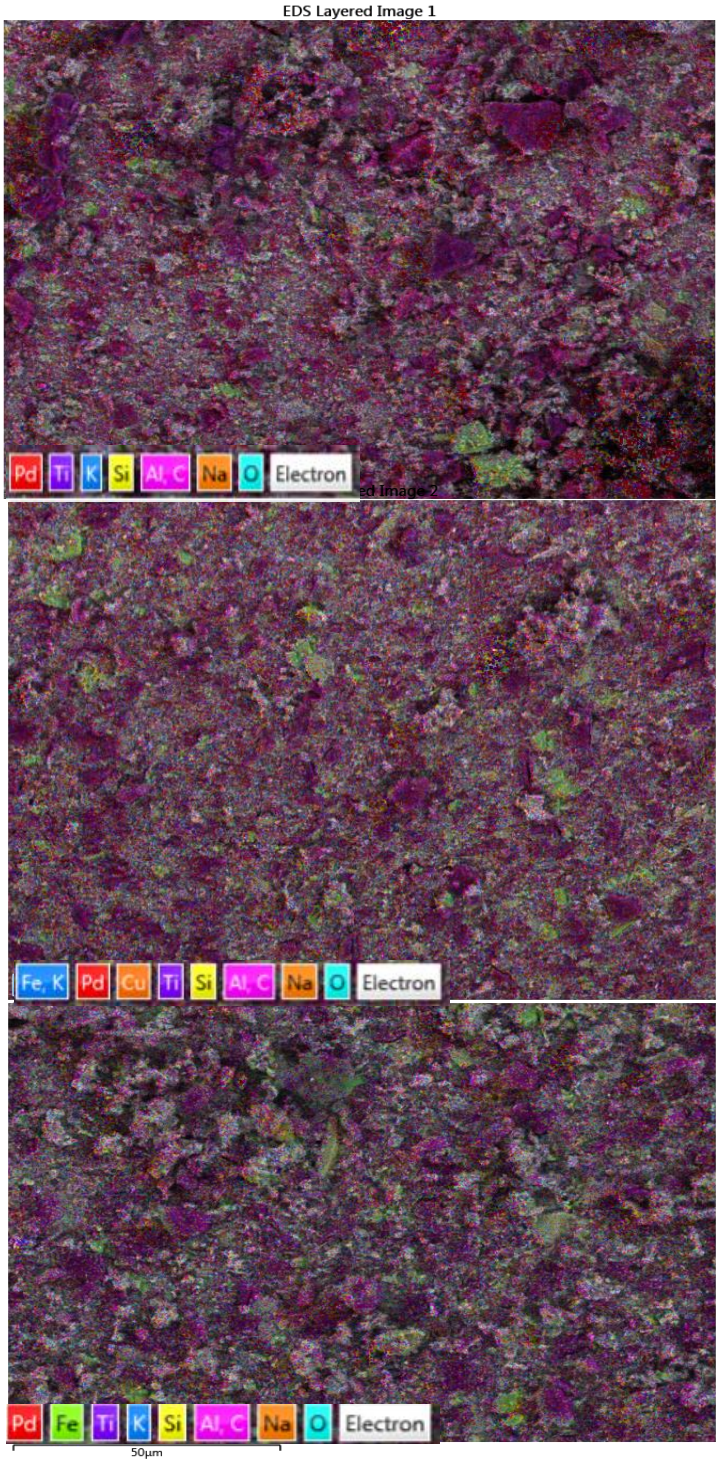

Pd/ACM

Figure 4.2. SEM-EDS images of Pd/ACM, Pd-Cu/ACM and Pd-Fe/ACM. (for expanded SEM analysis, please see Figures S4.2, S4.3 and S4.4 in Appendix B).

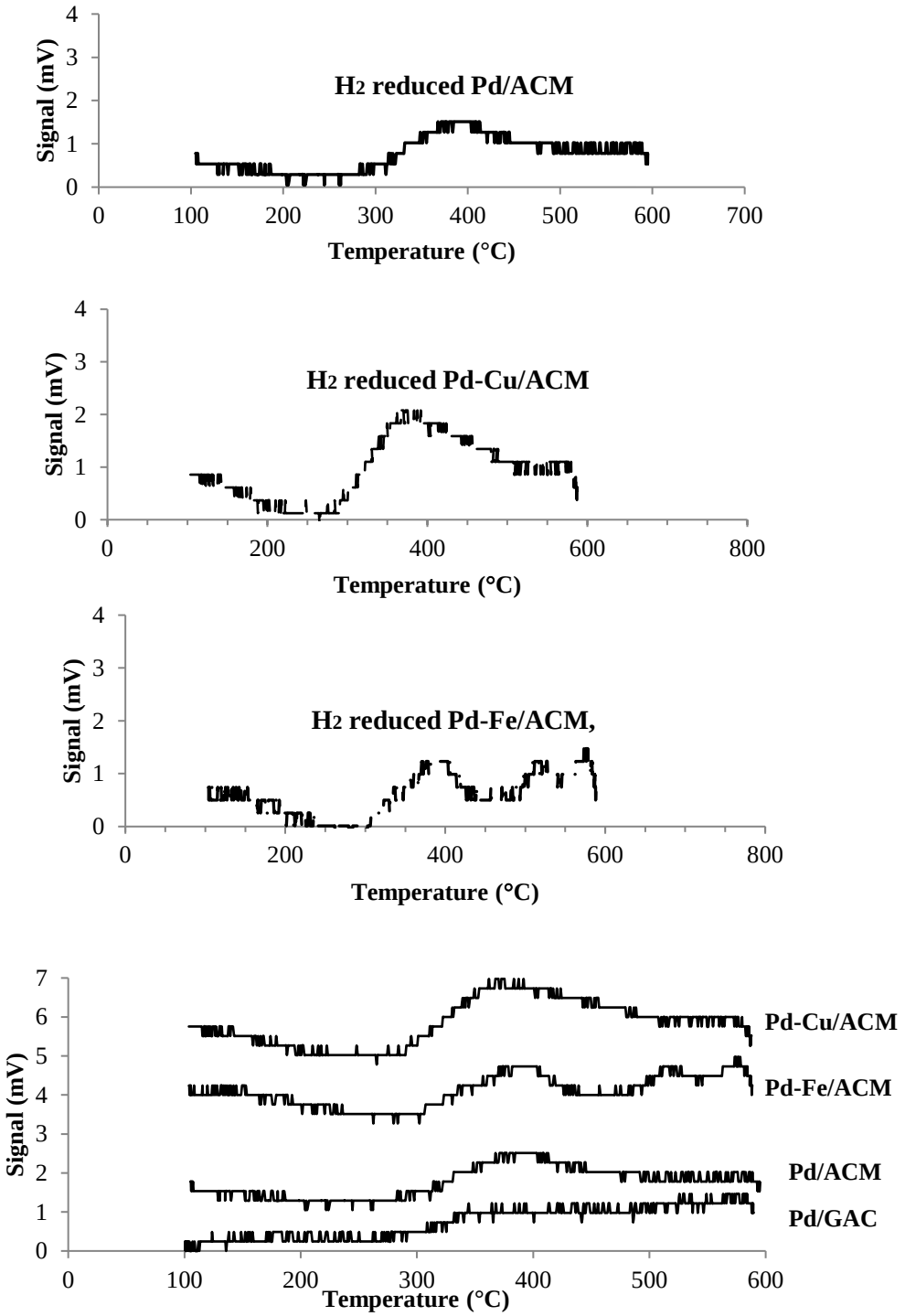

Figure 4.3. Ammonia TPD analysis of bi-metal carbon monolith catalysts pre-reduced with H_2 (100% H_2 for 2 h at 250 °C). Pd/GAC stands for 0.8% Pd on Granular activated carbon without binder in the structure.

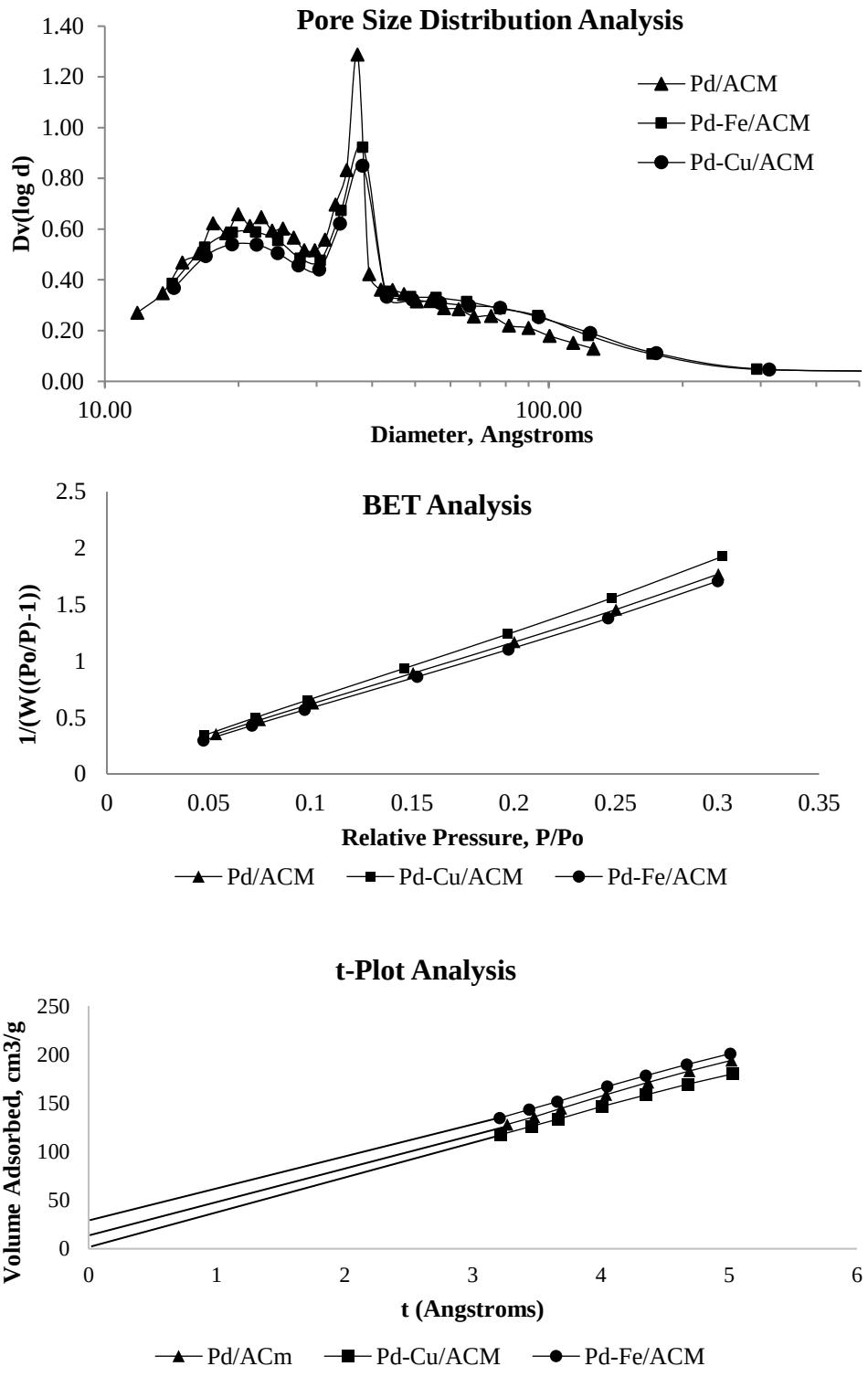

Figure 4.4. BJH, t-plot and BET analysis of fresh ACM catalysts.

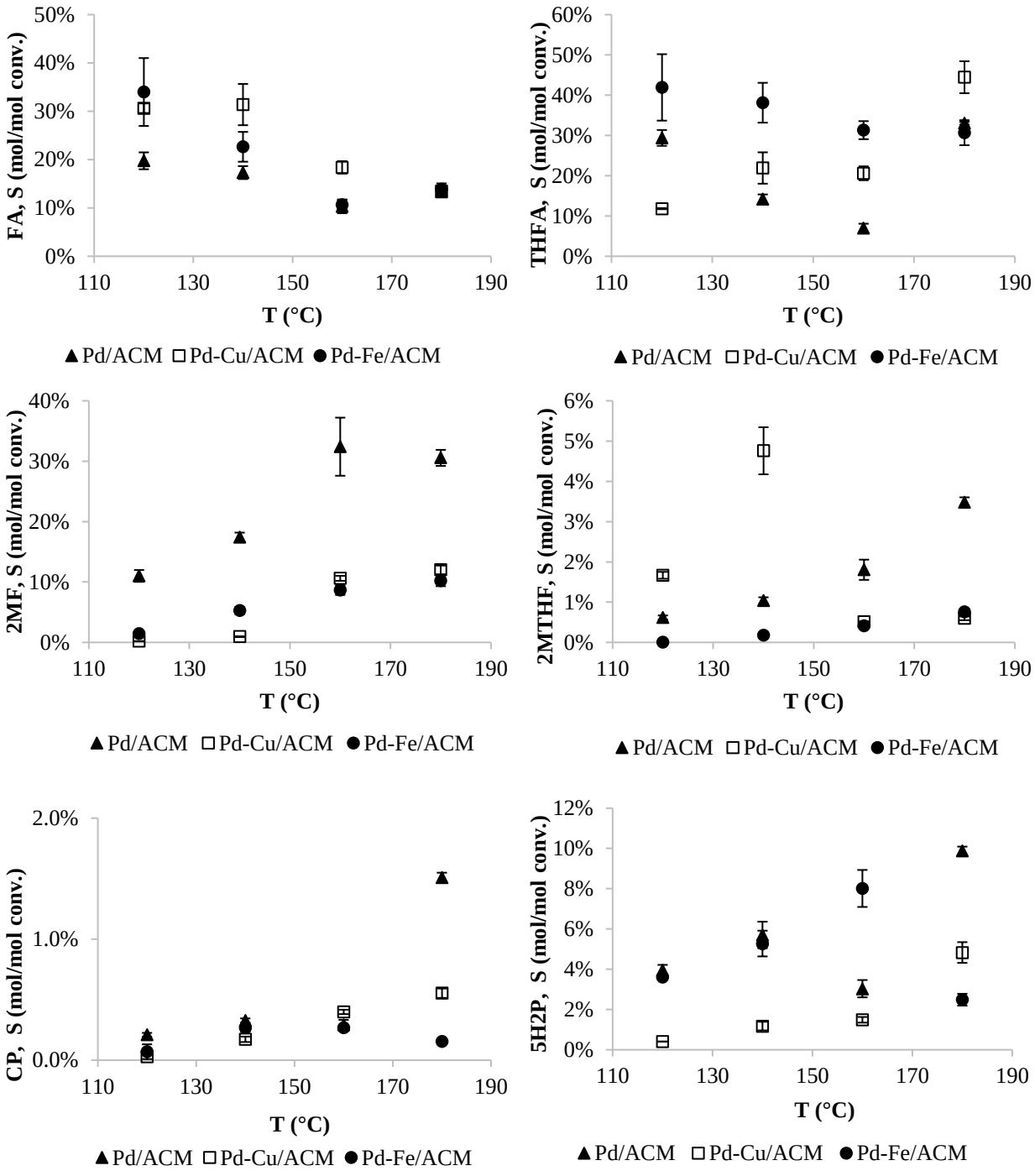

Figure 4.5. Effect of reaction temperature on product selectivity (FA, furfuryl alcohol; THFA, tetrahydrofurfuryl alcohol; 2MF, 2-methyl furan; 2MTHF, 2-methyl tetrahydrofuran; 5H2P, 5-hydroxy-2-pentanone; CP, cyclopentanone). Reaction Condition: P=300 psig , LHSV =1.32 1/h, 4 cores of ACM catalyst.

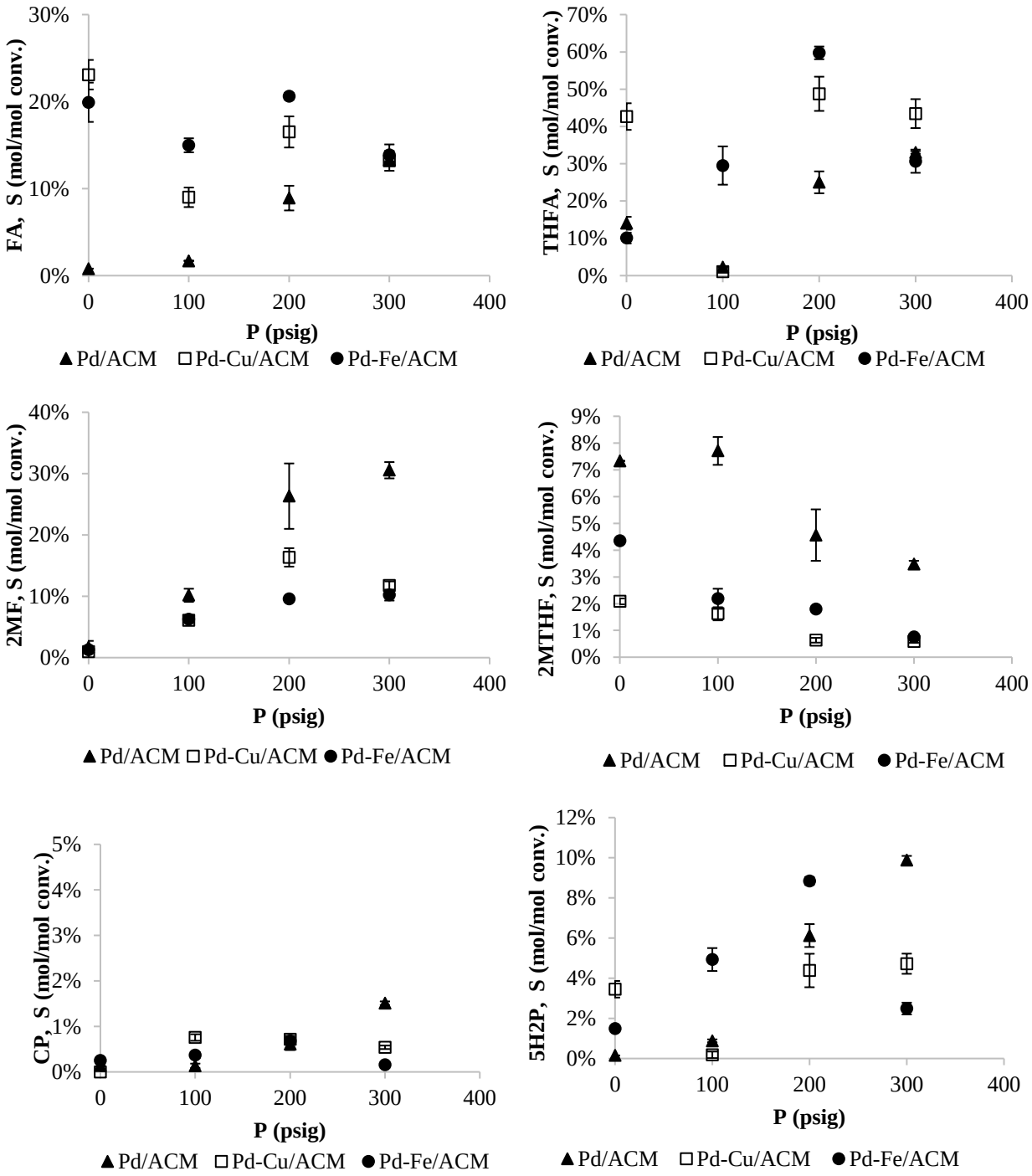

Figure 4.6. Effect of hydrogen pressure on product selectivity. Reaction Condition: T=180 °C, LHSV =1.32 1/h, 4 cores of ACM catalyst.

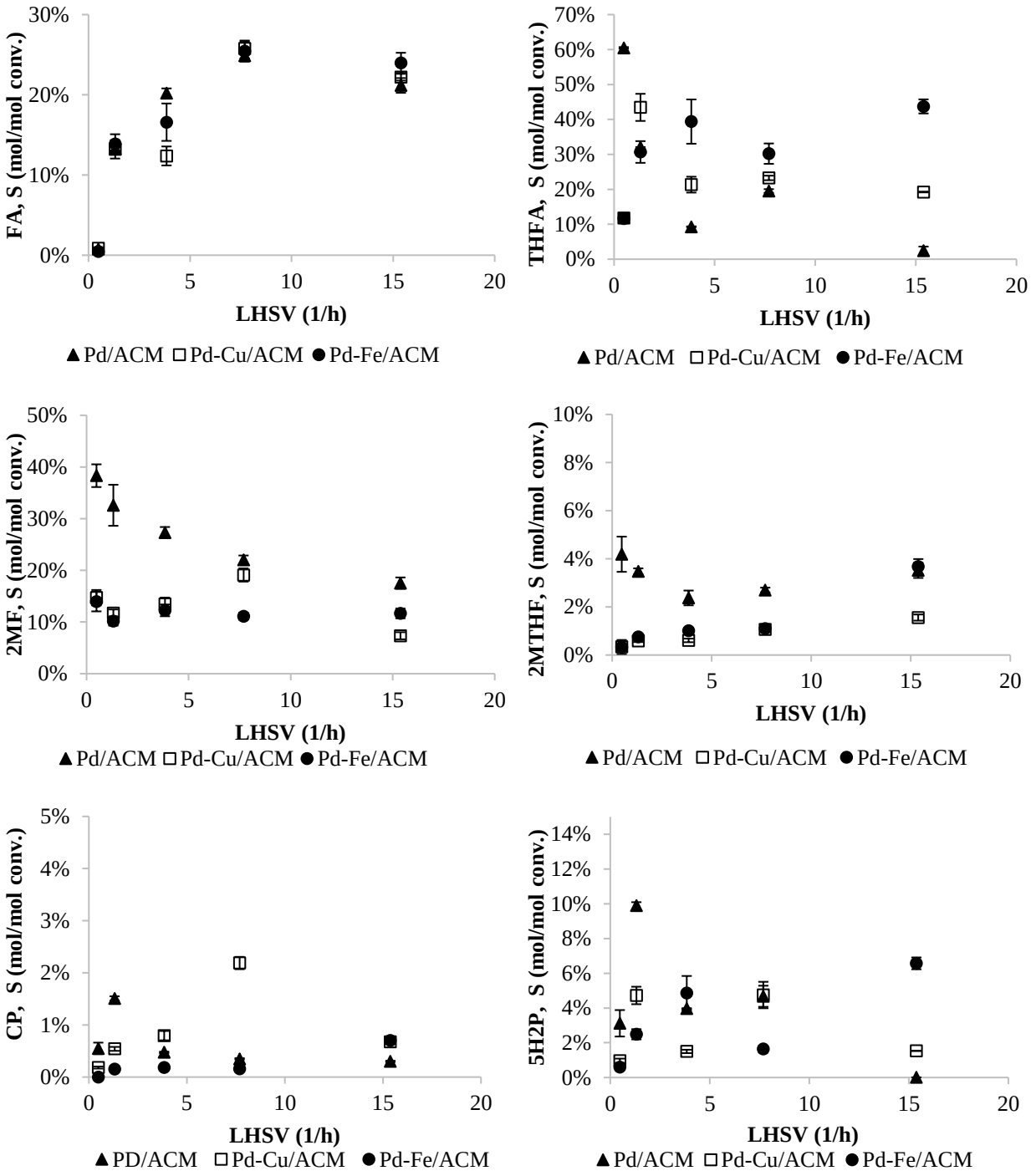

Figure 4.7. Effect of liquid hourly space velocity (LHSV) on product selectivity. P = 300 psig, T = 180 °C, 4 cores of ACM.

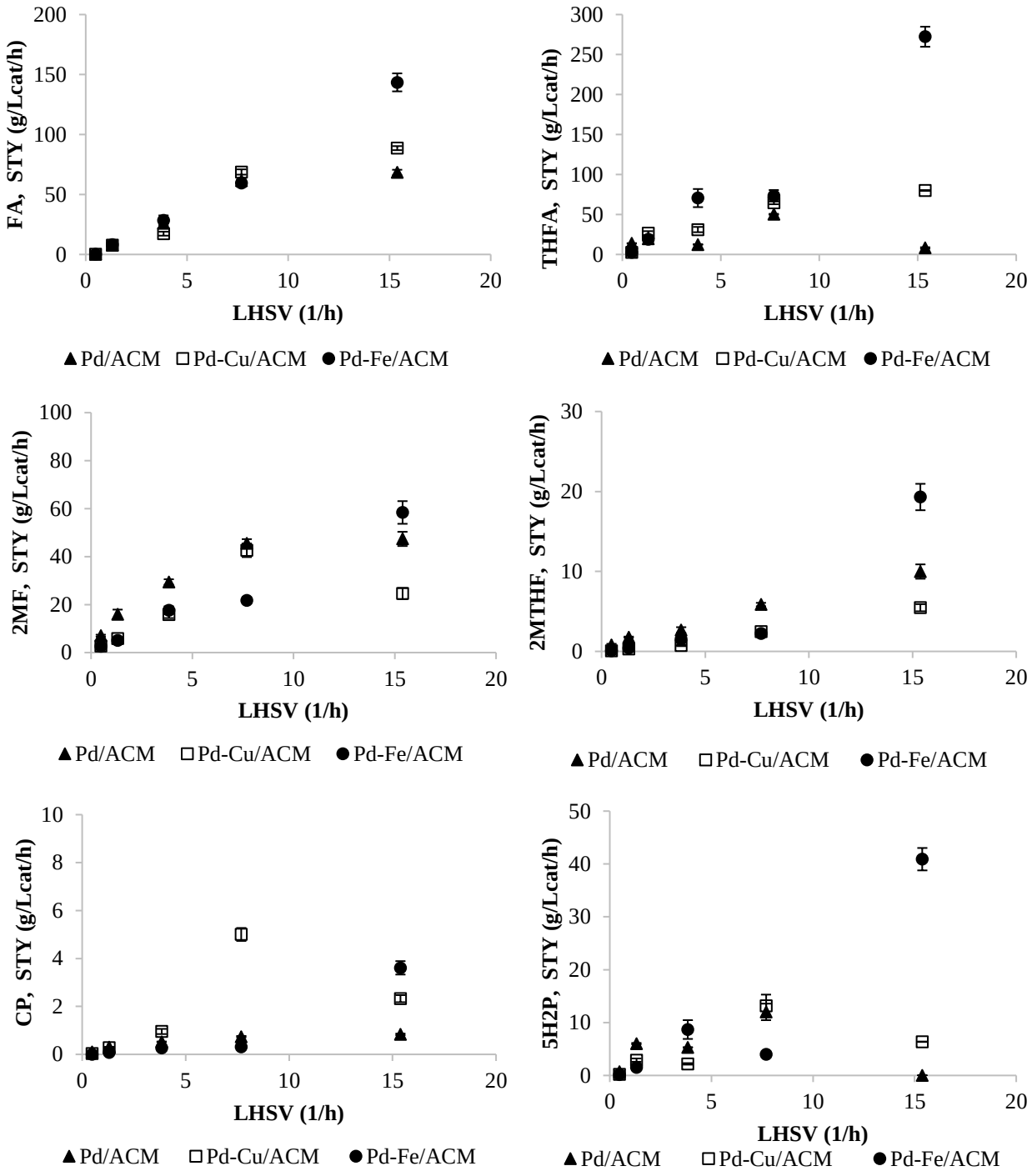

Figure 4.8. Effect of LHSV on product STY. P = 300 psig, T = 180 °C, 4 cores of ACM.

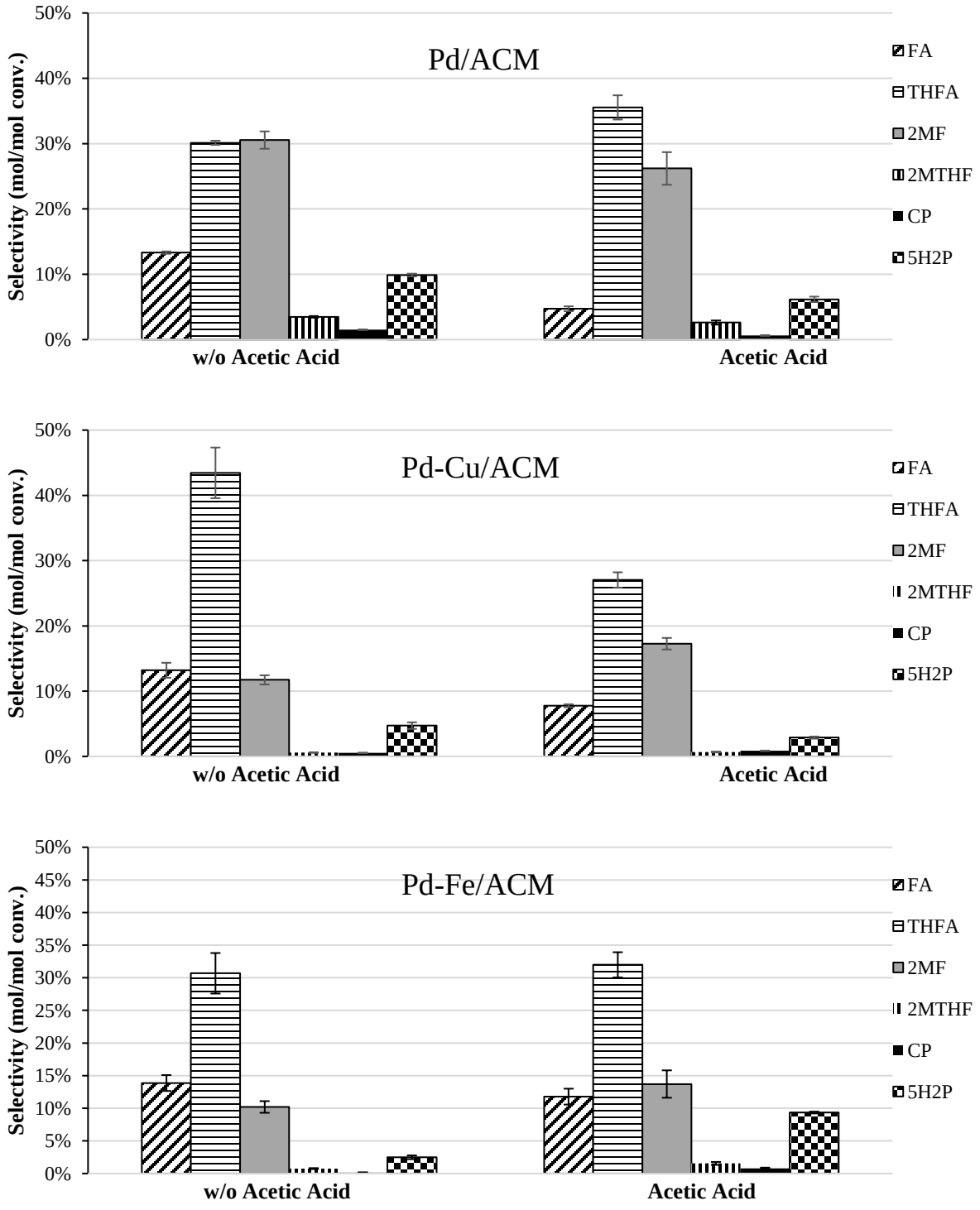

Figure 4.9. Effect of acetic acid on product selectivity and furfural conversion using monolith catalysts. P = 300 psig, T = 180 °C, LHSV = 1.32 1/h, 4 cores of ACM, 5% furfural, 1% acetic acid (aqueous).

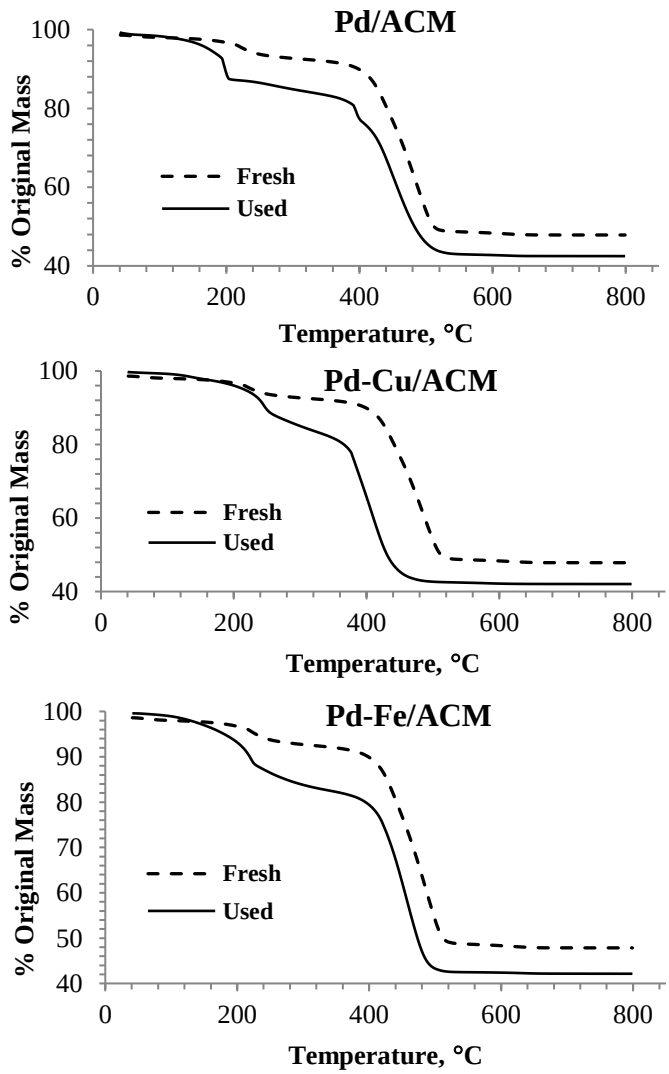

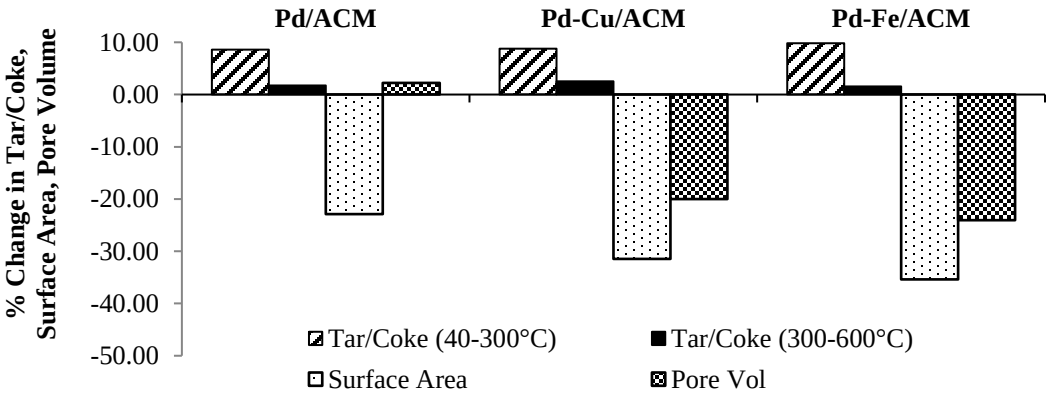

Figure 4.10. TGA analysis for fresh and spent catalysts.

CHAPTER 5

BI-FUNCTIONAL METAL-ACID ON CARBON CATALYST FOR SELECTIVE CONTINUOUS FURFURAL HYDROGENATION: A Pd-TiO_2 ON ACTIVATED CARBON CATALYST [1]

[1] Pirmoradi, M, Gulotty Jr., R.J., Kastner, J.R., 2020. To be submitted to *Applied Catalysis A: General*

Abstract

The effect of weak acid sites, coupled with Pd, on furfural hydrogenation was determined. Pd-TiO_2, Pd-Cu and Pd-Fe catalysts were employed for continuous selective hydrogenation of furfural using crushed form of activated carbon monolith support. Effect of reaction parameters on product selectivity and furfural conversion was determined. NH_3-TPD of the three catalysts indicated weak and strong acid sites for Pd-TiO_2 and strong acid sites for Pd-Cu and Pd-Fe. The presence of weak acid sites on Pd-TiO_2 catalyst contributed to furan ring opening and resulted 140 g/Lcat/h and 39% selectivity of 5-hydroxy-2-pentanone, a hydrogenation product of furan ring opening, in a short residence time at 180 °C and 300 psig. Pyridine-FTIR coupled with NH_3-TPD analysis indicated that furan ring opening is independent of the type of weak acid site. Pd-Cu and Pd-Fe catalysts were selective towards tetrahydrofurfuryl alcohol and furfuryl alcohol. 259 g/Lcat/h and 42% selectivity of furfuryl alcohol was achieved in presence of Pd-Cu catalyst at 180 °C and 300 psig.

Keywords: Titanium dioxide, weak acid site, hydrogenation, furfural

5.1 Introduction

Furfural is an inexpensive, abundant and biomass-derived aldehyde of furan. Hydrogenation of this chemical results in multiple value-added products such as furfuryl alcohol (FA), tetrahydrofurfuryl alcohol (THFA), 2-methylfuran (2MF) and 2-methyltetrahydrofuran (2MTHF). FA is obtained from furfural through one step hydrogenation of the aldehyde group to alcohol. Hydrogen can further attack the formed alcohol group and result in 2MF through elimination of a water molecule. THFA can also be achieved through hydrogenation of FA ring double bonds. Cyclopentanone (CP) and 5-hydroxy-2-pentanone (5H2P) are two other valuable products of furfural hydrogenation. CP is a precursor for production of jet fuels, rubber chemicals and pharmaceuticals.[1] 5H2P works as an important building block in synthesis of multiple medications.[2] With one further hydrogenation step of 5H2P, 1,4-pentanediol, an important linear diol for controlled drug delivery, cosmetics industry and biodegradable polymer fabrication, is achieved.[3, 4] Obtaining CP requires a ring rearrangement step of FA's furan ring (known as Piancatelli rearrangement).[5] This step involves opening of the furan ring into an unstable intermediate in presence of a weak Lewis acid site and rearranging to 4-hydroxy-2-cyclopentenone (4HCP).[6] It has been previously reported that using water as a reaction solvent can promote the furfural ring rearrangement/opening step since water can act as a donor of H^+.[7, 8] Further hydrogenation and water elimination steps of 4HCP will result in CP. On the other hand, during furfural hydrogenation in presence of an acid catalyst, the formed unstable intermediate from ring opening step can undergo hydrogenation at the C=C bond to form 4-oxopentanal, a linear product, where a further hydrogenation step result in 5H2P (Figure 5.1).[2] Therefore, the

unstable intermediate compound will not undergo cyclization and ring rearrangement does not happen.

Heterogeneous multifunctional catalysts usually offer two or more active sites where each active site plays an independent role in the reaction system. Multifunctional catalysts can play a crucial role in multi-step selective reactions where each active site involves promoting a different step of the reaction. Metal-acid (for hydrogenation and ring arrangement/opening) and bimetal catalysts (for selective hydrogenation steps) are the two multifunctional catalysts of interest in hydrogenation of furfural. Several studies investigated the application of metal-acid catalysts for furfural ring rearrangement. In a study by Zhang et al. 2016, Au metal and TiO_2 as a support was applied for a selective hydrogenation of furfural to cyclopentanone in water at 160 °C and 4 MPa of hydrogen. TiO_2 initiates weak Lewis acid sites, promoting the Piancatelli rearrangement, and gold particles are responsible for selective hydrogenation step.[9] Nearly 100% selectivity of cyclopentanone was achieved after 70 minutes of residence time. In another study by Ohyama et al. 2014, Au supported on Nb_2O_5 (source of Lewis acid sites) catalyst was employed to achieve 3-hydroxymethylcyclopentanone (a cyclopentanone derivative) from 5-hydroxymethylfurfural at 140 °C and 8 MPa for residence time of 12 hours.[10] Ohyama et al. 2016 also tested Pt/SiO_2 catalyst in presence of different metal oxides such as Ta_2O_5, ZrO_2, Nb_2O_5, TiO_2, Al_2O_3, SiO_2–Al_2O_3, CeO_2, La_2O_3, and hydrotalcite for synthesizing 3-hydroxymethylcyclopentanone from 5-hydroxymethylfurfural at 140 °C and 4 MPa of hydrogen.[11] Metal oxides containing Lewis acid sites resulted in highest yield of 3-hydroxymethylcyclopentanone. Pt/SiO_2 in presence of Ta_2O_5 catalysts resulted in highest yield of 82%. Fang et al. 2015 achieved 86% selectivity of cyclopentanone from furfural

hydrogenation using ruthenium supported on MIL-101 (a metal-organic framework with Lewis acid sites) at 160 °C and 4 MPa of hydrogen for 2.5 hours.[12] Cr^{3+} of the MIL-101 support initiated the weak Lewis acid sites for rearrangement. The role of bimetallic catalysts for selective hydrogenation of furfural is also important. One advantage of using bimetallic catalysts for furfural hydrogenation is that by providing two different metal active sites, bimetallic catalysts can promote adsorption of hydrogen (through one site) and C=O (through the second site). For example, Fulajtarova et al. 2015 reported that in hydrogenation of furfural to furfuryl alcohol using a Cu-Pd catalysts, the adsorption of C=O groups on the catalyst is associated with Cu active sites whereas the H atoms are adsorbed on Pd active sites.[13] This mechanism offers an easier interaction between the adsorbed species. In another study by Liu et al. 2016, a selective hydrogenation of furfural to THFA was achieved using Ni-Cu/CNT whereas using Ni only, the catalyst was selective towards furfuryl alcohol only.[14]

Very few studies have investigated the possibility of continuous 5H2P formation from furfural. As mentioned earlier, 5H2P is an important building block and a precursor for 1,4-pentanediol, an important chemical for drug delivery and biodegradable polymer purposes. Furfural can be an inexpensive and green substrate for production of 5H2P. Furfural's commercial unit price is approximately 1/6 of 5H2P. This study will focus on comparing bimetal catalysts supported on activated carbon for selective hydrogenation of furfural. Pd-TiO_2, generating weak acid sites, is employed for promoting furan ring opening and formation of 5H2P and the results will be compared to Pd-Fe and Pd-Cu catalysts, providers of strong acid sites.

5.2 Methods and Materials

Materials and Catalysts: 45 gL^{-1} aqueous furfural (Sigma-Aldrich, 99%) was prepared for each reaction. 0.8% Pd-1.6% Cu and 0.8% Pd-1.6%Fe on activated carbon catalysts were supplied by Applied Catalysts (Laurens, SC) in a form of monolith structure, manufactured by coextrusion of 50% activated carbon and 50% ceramic binder. Pd-TiO_2 catalyst was not available in the form monolith structure. Therefore, to compare the three catalysts directly, Pd-Cu and Pd-Fe monolith structures were crushed and sieved to a particle size of $0.5 < d < 1$ mm. In order to prepare 0.8% Pd-5% TiO_2 catalyst, a blank activated carbon monolith structure was crushed and sieved into a particle size of $0.5 < d < 1$ mm. In the next step, direct air-hydrolysis method was employed to deposit TiO_2 particles on activated carbon support.[15] Therefore, titanium (IV) isopropoxide (Sigma-Aldrich, 99.999%) was dissolved in isopropanol under nitrogen atmosphere. The solution was added to crushed activated carbon monolith under stirring condition. The final sample was dried at 120 °C for 2 hours followed by calcination at 300 °C under 100% flow of N_2 (100 ml/min) for 4 hrs. After sample cool down, incipient wetness impregnation method was employed to deposit Pd particles on the catalyst.[16] Therefore, Pd(ll) nitrate dihydrate (Sigma-Aldrich, 40% Pd basis) was dissolved in DI water and added to the sample. The sample was dried at 120 °C for 2 hours followed by reduction at 250 °C under 100% flow of H_2 (100 ml/min) for 4 hours.

Catalyst Characterization: Surface area analysis and pore size analysis were performed as previously described.[17] Micropore analysis was performed using the t-method of de Boer[18] (t is the statistical thickness of an adsorbed film [$t\ (Å) = [13.99/\log(Po/P)+0.034]^{1/2}$]) and the BET surface area data extended to higher pressures (Quantachrome, AUTOSORB-1C; Boynton

Beach, Florida). Ammonia-TPD analysis was performed to determine the quantity and strength of acid sites as previously described. FTIR analysis were performed to determine the type of acid sites. The FTIR spectra was obtained using a Thermo Scientific Nicolet 6700 FTIR spectrometer in the wave number range of 4000-399 cm^{-1}. The catalyst samples were diluted in finely powdered KBr. 3 to 4 mg of sample was mixed with 300 to 400 mg of KBr and pressed into a disc in a hydraulic press (Carver.Inc; Pressure: 20,000 pounds/ 9 metric tons, Time: 10 min). The disc was placed into the sample holder on the KBr FTIR apparatus. After setting the experimental conditions (resolution:6 ; number of scans : 64) the background was collected for 5-10 minutes to avoid peaks of carbon dioxide and moisture in the spectrum. Prior to KBr dilution, pyridine treatment was performed to determine the type of acid site. The sample was degassed at 150 °C for 2 hours. Next, 50 mg of sample was suspended in 3 mL of 5% pyridine in dry hexane. The mixture was stirred for 1 hour followed by filtering and drying at 100 °C for 1 hour.

TPR analysis was performed to determine the reducibility of the catalyst, and CO pulse titration was performed to determine the CO uptake of Pd at 40 °C.[17] TGA analysis in air was used to estimate tar and coke formation on the catalysts (Discovery TGA from TA Instruments). Air flow over the sample (10-25 mg in ceramic pans) was set at 25 mL/min with a balance flow rate at 10 mL/min (N_2). The temperature of the sample was equilibrated at 40 °C before ramping at a rate of 10 °C/min to 800 °C. Elemental analysis of fresh and spent catalysts was performed following the Environmental Protection Agency (EPA) ICP method 200.8. Concentrated HNO_3 was added (5 ml) to the sample (~ 0.1g) for microwave digestion following protocols

listed in EPA method 3051A. Digested solutions were analyzed by inductively coupled plasma optical emission spectroscopy (ICP-OES, Spectro Arcos FHS16 AMETEK ICP-OES).

Analytical: Once the liquid sample was collected from the reactor, it was analyzed in triplicate using gas chromatography with flame ionization detection (GC-FID, HP 5890 Series II) with HP Innowax column (30 m * 0.25 mm * 0.25mm). The GC-FID was operated with the method of inlet temperature 230 °C, detector temperature 240 °C, initial oven temperature of 45 °C for 2.5 minutes followed by a ramp of 10 °C/min for 15.5 minutes and then held at 200 °C for 3 minutes. 1 μL of sample is injected on the GC-FID in triplicate. The concentrations of furfural (FUR, 99%), furfuryl alcohol (FA, 98%), tetrahydrofurfuryl alcohol (THFA, 98%), 2-methylfuran (2MF, 99%), 2-methyltetrahydrofuran (2MTHF, 99%), cyclopentanol (CPO, 99%), cyclopentanone (CP, 95%), 5-hydroxy-2-pentanone (5H2P, 95%), and 1,4-pentanediol (1,4PD, 99%) were determined using 4-point standard curves (chemicals purchased from Sigma-Aldrich, each point run in triplicate). All standards were prepared in DI water, except for 2MF which was prepared with ethanol as the solvent. The presence of all intermediates and products were confirmed using GC/MS (HP-6890 with HP Innowax column, same method as for GC/FID, 1 μl injection volume, 25:1 split ratio, 0.8 ml/min, 10-500 mass units, MSD ChemStation D.03.00.611 with NIST 2008 database for identification).

Catalytic Reactions: Furfural hydrogenation reactions were performed in a continuous reactor system, designed by Parr Instrument Company, as described previously.[17] 5 g of crushed activated carbon monolith (CACM) was placed between two layers of quartz wool. To determine the optimum conditions for furfural hydrogenation in a continuous reactor system, a series of experiments at temperatures ranging from 120 to 180 °C, pressures of atmospheric to 300 psi

(0.1-2.1 MPa), and liquid flow rates of 0.5 to 6 mL/min were performed using Pd-TiO_2 on crushed activated carbon monolith (Pd-TiO_2 /CACM), Pd-Cu on crushed activated carbon monolith (Pd-Cu/CACM) and Pd-Fe on crushed activated carbon monolith (Pd-Fe/CACM).

5.3 Results and Discussion

5.3.1 Catalyst Characterization

NH_3-TPD results showed strong acid site peaks between 300-500 °C for all three catalysts, attributed to the monolith binder. In addition, Pd-TiO_2/CACM demonstrated weak acid sites at approximately 150 °C whereas Pd-Fe/CACM results indicated strong acid sites at 525 °C (Figure 5.2 and Table 5.1). In order to determine the type of acid sites FTIR spectra were recorded for each catalyst. The FTIR spectra of CACM support (Figure S5.1) shows a band around 1385 cm^{-1}, associated with -COOH in activated carbon support.[19] The bands around 1530, 1550 and 1640 cm^{-1} are associated with pyridine adsorption at Bronsted acid sites, attributed to the presence of metal oxides in the CACM binder.[19-21] Pd-Cu/CACM, Pd-Fe/CACM and Pd-TiO_2/CACM FTIR spectra (Figure 5.3, 5.4 and 5.5) showed additional bands around 1618 cm^{-1}, associated with Lewis acid sites, and 1480 cm^{-1}, associated with both Lewis and Bronsted acid sites.[11, 22] All three catalysts indicated both Brønsted and Lewis acid sites. Figure 5.6 shows SEM-EDS images of Pd-TiO_2/CACM (The SEM-EDS images of the other two catalysts have been shown in Figures S4.3 and S4.4). Most of the Pd particles are located close to TiO_2 particles. Due to high reactivity of titanium (IV) isopropoxide, employed for Pd-TiO_2/CACM synthesis, with moisture in the air, at some regions TiO_2 particles were formed quickly, resulting in large TiO_2 particles. Therefore, at some regions on Pd-TiO_2/CACM catalyst the density of TiO_2 particles is high. Figure 5.7 indicates TPR analysis of the three catalysts. Pd-

Cu/CACM indicated peaks at 220 and 320 °C and Pd-Fe/CACM demonstrated two peaks at 250 and 400 °C. Pd-TiO_2/CACM showed one small negative, one positive and one sharp negative peak at 42, 44 and 63 °C, respectively (Figure S5.2). The negative peaks are attributed to decomposition of palladium hydride (β-PdH), formed during the positive peak at 44 °C or initial purge of hydrogen during TPR, due to the presence of freely available PdO on the surface of the catalyst.[23] This effect has been associated with presence of large Pd particles since small Pd particles usually have stronger interaction with the catalyst support and do not react with hydrogen in low temperatures.[24] The lack of negative peaks in Pd-Cu/CACM and Pd-Fe/CACM TPR can indicate an interaction between Pd and the second metal which prevents the larger Pd particles from reacting with hydrogen at low temperature. Pd-TiO_2/CACM showed 5 additional peaks at 180, 220, 315, 422 and 525 °C. The peaks at 180 and 220 °C are associated with the reduction of Pd^{2+} to Pd on carbon.[25] The peak at 315 °C represents the reduction of Pd on the binder component such as silica or alumina.[26] The peaks at 422 and 525 °C may be associated with partial reduction of TiO_2 particles as it has been reported that the presence of Pd° can lower the reduction temperature of TiO_2 due to the role of Pd° in providing dissociated hydrogen for TiO_2 through hydrogen spillover effect.[24] Surface area analysis of the three catalysts indicated a slightly higher pore volume and surface area for Pd-TiO_2/CACM (Figure 5.8 and Table 5.1). Pd-TiO_2/CACM and Pd-Fe/CACM also demonstrated a higher micro-pore volume where after series of catalytic reactions 100% and 30% of the volume was lost, respectively (Table 5.1).

5.3.2 Effect of Temperature and Pressure on Hydrogenation Products

A series of reaction temperatures ranging from 120 to 180 °C (at 1.32 1/h LHSV, 300 psig) were tested to determine the effect of this parameter on selectivity and yield of products

(Figure 5.9). In presence of all three catalysts, FA selectivity decreased with increasing temperatures. THFA selectivity increased to a maximum of 37% for Pd-TiO_2/CACM, 44% for Pd-Fe/CACM and 59% for Pd-Cu/CACM at temperature of 140 °C then decreased with increasing temperature. In presence of all three catalysts, the highest selectivity of 2MF was achieved at 180 °C, with Pd-TiO_2/CACM achieving the highest 2MF selectivity of 38%. Pd-TiO_2/CACM also achieved the highest 2MTHF and CP selectivity although less than 5% of these two products were determined for all catalysts over the range of tested temperatures. The highest selectivity of 17% was achieved for 5H2P at 140 °C in presence of Pd-TiO_2/CACM.

A second series of reactions were performed to determine the effect of pressure, ranging from atm to 300 psig at 1.32 1/h LHSV and 180 °C, on selectivity and space time yield of products (Figure 5.10). The highest FA selectivity in presence of all three catalysts was determined at atmospheric pressure. Comparing the FA selectivity of the three catalyst at atmospheric pressure, Pd-Cu/CACM achieved the highest selectivity of 38% whereas Pd-TiO_2/CACM and Pd-Fe/CACM resulted in 11% and 14% FA selectivity, respectively. At pressures higher than atmospheric pressure, less than 5% of FA selectivity was determined for all the catalysts. Pd-Cu/CACM also achieved the highest THFA selectivity of 37% at 200 psig. In presence of Pd-Fe/CACM, THFA selectivity reached a maximum of 24 % at 100 psig and did not change significantly with increasing pressure. The highest selectivity of THFA in presence of Pd-TiO_2/CACM was 24%, achieved at 300 psig. 2MF selectivity increased with increasing pressures. At 300 psig, the 2MF selectivity of 38%, 25% and 16% for Pd-TiO_2/CACM, Pd-Cu/CACM and Pd-Fe/CACM were achieved, respectively. Except at 100 psig in presence of Pd-Fe/CACM where a 2MTHF selectivity of 14% was achieved, at all tested pressures less than

10% of 2MTHF and CP selectivity was determined. At 200 psig, 5H2P selectivity reached a maximum of 24%, 23% and 16% in presence of Pd-Fe/CACM, Pd-Cu/CACM and Pd-TiO_2, respectively and then decreased with increasing pressure to 300 psig.

5.3.3 Effect of Liquid Residence Time

Next, the effect of liquid flow rate on furfural conversion, product selectivity and space time yield were determined (Figure 5.11 and Figure 5.12). Flow rates of 0.5 to 6 mL/min, resulting in LHSVs of 1.32 to 15.8 1/h, were tested under 180 °C and 300 psig condition. High furfural conversions (90% or higher) were achieved for all three catalysts at LHSVs of 1.32, 3.96 and 7.92 1/h. At 15.8 1/h, conversions of 86%, 85% and 76% were achieved for Pd-Cu/CACM, Pd-TiO_2/CACM and Pd-Fe/CACM, respectively. In presence of all three catalysts, FA selectivity decreased with increasing residence time or decreasing LHSV. The highest FA selectivity of 42%, 32% and 30% for Pd-Cu/CACM, Pd-Fe/CACM and Pd-TiO_2/CACM at 15 1/h LHSV, the shortest residence time. A high FA space time yield of 260 g/Lcat/h was achieved in presence of Pd-Cu/CACM. THFA selectivity decreased with decreasing residence time. At LHSVs of 3.96 and 7.92 1/h, Pd-Fe/CACM demonstrated a significantly higher selectivity compared to the other two catalysts. At all residence times, Pd-TiO_2/CACM achieved the highest 2MF selectivity of 38% at the longest residence time among all three catalysts. In general, 2MF selectivity increased with increasing residence time. Very low selectivity of 2MTHF (less than 5%) was determined using Pd-TiO_2/CACM and Pd-Cu/CACM. Using Pd-Fe/CACM the 2MTHF selectivity increased to 11% at LHSV of 3.96 1/h then decreased with increasing LHSV. Less than 4% of CP selectivity was determined in presence of all three catalysts. Among the three catalysts, the highest 5H2P selectivity was achieved in presence of Pd-TiO_2/CACM at LHSVs of 3.96, 7.92

and 15.8 1/h. At 7.92 1/h 39% of 5H2P selectivity and 140 g/Lcat/h yield was achieved in presence of Pd-TiO_2/CAM whereas at the same LHSV the other two catalysts demonstrated approximately 11% selectivity and 43 g/Lcat/h yield (Figure 5.12).

5.3.4 Effect of Acetic Acid

Effect of acetic acid, an impurity present in crude furfural, on product distribution was determined. In presence of 1% acetic acid and Pd-TiO_2/CACM, furfural conversion did not change significantly while selectivity of CP and 5H2P increased and selectivity of other products decreased. Adding acetic acid to reaction medium in presence of Pd-Cu/CACM and Pd-Fe/CACM also increased 5H2P and CP selectivity and decreased 2MF selectivity with no significant change in furfural conversion (Figure 5.13). In presence of Pd-Fe/CACM and acetic acid, in addition to an increased selectivity of CP and 5H2P, THFA selectivity also increased. The increase in selectivity of these products in presence of acetic acid and Pd-Fe/CACM is attributed to the difference in carbon closure and recovered liquid from reaction. In the reaction with no acetic acid 53% of carbon was recovered whereas in presence of acetic acid 94% carbon closure was observed.

5.3.5 Discussion

NH_3-TPD results indicated the presence of both weak and strong acid sites for Pd-TiO_2/CACM whereas the other two catalysts demonstrated only strong acid sites (Figure 5.2 and Table 5.1). FTIR analysis indicated the presence of both Lewis and Bronsted acid sites in all three catalysts. As indicated in section 4.3.5, using Pd-Cu and Pd-Fe supported on activated carbon monolith structure, adding Fe and Cu to Pd shifted the selectivity of catalyst from 2MF to FA and THFA due to adsorption of C=O at Fe and Cu sites. Therefore, it was expected to see

similar selectivity effect using the crushed form of the bimetal monolith catalysts. Incorporating TiO_2 in Pd catalyst demonstrated the highest 2MF and 5H2P selectivity at the three shortest residence times among the three catalysts. Higher 5H2P selectivity in presence of TiO_2 is attributed to presence of weak acid sites at 150 °C, demonstrated by NH_3-TPD results, regardless of the type of the acid site. The weak acid sites can promote furan ring opening and further hydrogenation steps result in formation of 5H2P. Liu et al. 2015 also reported that presence of weak acid sites in Ni-bearing hierarchical Y zeolites promoted the furfural ring rearrangement whereas zeolites with medium-strong acid sites demonstrated lower yield of ring rearrangement product with higher furfural conversion.[27] Zhang et al. 2016 reported a high yield of furfural rearrangement ring product in presence of TiO_2, known to provide weak Lewis acid sites.[9]

5.4 Conclusions

Pd-TiO_2 catalyst demonstrated weak acid sites due to presence of TiO_2 and strong acid sites due to presence of mineral binders in the catalyst support. Regardless of the type of the acid site, the presence of weak acid sites promoted furan ring opening and increased the yield of 5H2P. A high yield of 140 g/Lcat/h and 39% selectivity of 5H2P was achieved using Pd-TiO_2 catalyst. The Pd-Cu and Pd-Fe catalysts demonstrated only strong acid sites in catalyst structure and showed selectivity towards FA and THFA. A high 259 g/Lcat/h and 42% selectivity of furfuryl alcohol was achieved in presence of Pd-Cu catalyst at 180 °C and 300 psig.

ASSOCIATED CONTENT

Supporting Information (Appendix C)

The following results are presented, 1) FTIR and expanded TPR analysis 2) furfural conversion and carbon closure, 2) effect of temperature and pressure on product space time yield, 3) effect of acetic acid on furfural conversion.

ACKNOWLEDGMENTS

Support for this research and Maryam Pirmoradi's PhD in Biochemical Engineering was provided by a USDA-NIFA Grant (Carbon Monolith Catalysts from Wood for Biobased Platform Chemicals: 2017-67021-26136). Authors acknowledge and thank Sarada Sripada for her contributions to FTIR analysis.

References

1. Hronec, M.; Fulajtarová, K., Selective transformation of furfural to cyclopentanone. *Catalysis Communications* **2012,** *24*, 100-104.

2. Mironenko, R. M.; Talsi, V. P.; Gulyaeva, T. I.; Trenikhin, M. V.; Belskaya, O. B., Aqueous-phase hydrogenation of furfural over supported palladium catalysts: effect of the support on the reaction routes. *Reaction Kinetics, Mechanisms and Catalysis* **2019,** *126* (2), 811-827.

3. Heller, J.; Barr, J.; Ng, S.; Shen, H.-R.; Gurny, R.; Schwach-Abdelaoui, K.; Rothen-Weinhold, A.; van de Weert, M., Development of poly (ortho esters) and their application for bovine serum albumin and bupivacaine delivery. *Journal of controlled release* **2002,** *78* (1-3), 133-141.

4. Liu, F.; Liu, Q.; Xu, J.; Li, L.; Cui, Y.-T.; Lang, R.; Li, L.; Su, Y.; Miao, S.; Sun, H., Catalytic cascade conversion of furfural to 1, 4-pentanediol in a single reactor. *Green chemistry* **2018,** *20* (8), 1770-1776.

5. Minai, M., Process for preparing oxocyclopentene derivatives. Google Patents: 1990.

6. Piancatelli, G.; Scettri, A.; Barbadoro, S., A useful preparation of 4-substituted 5-hydroxy-3-oxocyclopentene. *Tetrahedron Letters* **1976,** *17* (39), 3555-3558.

7. Hronec, M.; Fulajtarová, K.; Liptaj, T., Effect of catalyst and solvent on the furan ring rearrangement to cyclopentanone. *Applied Catalysis A: General* **2012,** *437*, 104-111.

8. Yang, Y.; Du, Z.; Huang, Y.; Lu, F.; Wang, F.; Gao, J.; Xu, J., Conversion of furfural into cyclopentanone over Ni–Cu bimetallic catalysts. *Green Chemistry* **2013,** *15* (7), 1932-1940.

9. Zhang, G.-S.; Zhu, M.-M.; Zhang, Q.; Liu, Y.-M.; He, H.-Y.; Cao, Y., Towards quantitative and scalable transformation of furfural to cyclopentanone with supported gold catalysts. *Green Chemistry* **2016,** *18* (7), 2155-2164.

10. Ohyama, J.; Kanao, R.; Esaki, A.; Satsuma, A., Conversion of 5-hydroxymethylfurfural to a cyclopentanone derivative by ring rearrangement over supported Au nanoparticles. *Chem Commun (Camb)* **2014,** *50* (42), 5633-6.

11. Ohyama, J.; Kanao, R.; Ohira, Y.; Satsuma, A., The effect of heterogeneous acid–base catalysis on conversion of 5-hydroxymethylfurfural into a cyclopentanone derivative. *Green Chemistry* **2016,** *18* (3), 676-680.

12. Fang, R.; Liu, H.; Luque, R.; Li, Y., Efficient and selective hydrogenation of biomass-derived furfural to cyclopentanone using Ru catalysts. *Green Chemistry* **2015,** *17* (8), 4183-4188.

13. Fulajtárova, K.; Soták, T.; Hronec, M.; Vávra, I.; Dobročka, E.; Omastová, M., Aqueous phase hydrogenation of furfural to furfuryl alcohol over Pd–Cu catalysts. *Applied Catalysis A: General* **2015,** *502*, 78-85.

14. Liu, L.; Lou, H.; Chen, M., Selective hydrogenation of furfural to tetrahydrofurfuryl alcohol over Ni/CNTs and bimetallic CuNi/CNTs catalysts. *International Journal of Hydrogen Energy* **2016,** *41* (33), 14721-14731.

15. El-Sheikh, A. H.; Newman, A. P.; Al-Daffaee, H.; Phull, S.; Cresswell, N.; York, S., Deposition of anatase on the surface of activated carbon. *Surface and Coatings Technology* **2004,** *187* (2-3), 284-292.

16. Toebes, M. L.; van Dillen, J. A.; de Jong, K. P., Synthesis of supported palladium catalysts. *Journal of Molecular Catalysis A: Chemical* **2001,** *173* (1-2), 75-98.

17. Weber, J.; Thompson, A.; Wilmoth, J.; Gulotty Jr, R. J.; Kastner, J. R., Coupling Red-Mud Ketonization of a Model Bio-Oil Mixture with Aqueous Phase Hydrogenation Using Activated Carbon Monoliths. *Energy & Fuels* **2017,** *31* (9), 9529-9541.

18. De Boer, J.; Linsen, B.; Van der Plas, T.; Zondervan, G., Studies on pore systems in catalysts: VII. Description of the pore dimensions of carbon blacks by the t method. *Journal of Catalysis* **1965,** *4* (6), 649-653.

19. Yang, R.; Li, G.; Hu, C., The preparation of Fe/wood-based activated carbon catalyst for phenol hydroxylation from Fe 2+ and Fe 3+ precursors. *Catalysis Science & Technology* **2015,** *5* (4), 2486-2495.

20. Bossola, F.; Pereira-Hernández, X. I.; Evangelisti, C.; Wang, Y.; Dal Santo, V., Investigation of the promoting effect of Mn on a Pt/C catalyst for the steam and aqueous phase reforming of glycerol. *Journal of catalysis* **2017,** *349*, 75-83.

21. Busca, G., The surface acidity of solid oxides and its characterization by IR spectroscopic methods. An attempt at systematization. *Physical Chemistry Chemical Physics* **1999,** *1* (5), 723-736.

22. Topaloğlu Yazıcı, D.; Bilgic, C., Determining the surface acidic properties of solid catalysts by amine titration using Hammett indicators and FTIR-pyridine adsorption methods. *Surface and Interface Analysis* **2010,** *42* (6-7), 959-962.

23. Biniak, S.; Diduszko, R.; Gac, W.; Pakuła, M.; Świątkowski, A., Reduction and oxidation of a Pd/activated carbon catalyst: evaluation of effects. *Reaction Kinetics, Mechanisms and Catalysis* **2010,** *101* (2), 331-342.

24. Shen, W.-J.; Okumura, M.; Matsumura, Y.; Haruta, M., The influence of the support on the activity and selectivity of Pd in CO hydrogenation. *Applied Catalysis A: General* **2001,** *213* (2), 225-232.

25. Gurrath, M.; Kuretzky, T.; Boehm, H.; Okhlopkova, L.; Lisitsyn, A.; Likholobov, V., Palladium catalysts on activated carbon supports: Influence of reduction temperature, origin of the support and pretreatments of the carbon surface. *Carbon* **2000,** *38* (8), 1241-1255.

26. Pinna, F.; Menegazzo, F.; Signoretto, M.; Canton, P.; Fagherazzi, G.; Pernicone, N., Consecutive hydrogenation of benzaldehyde over Pd catalysts: influence of supports and sulfur poisoning. *Applied Catalysis A: General* **2001,** *219* (1-2), 195-200.

27. Liu, C.-Y.; Wei, R.-P.; Geng, G.-L.; Zhou, M.-H.; Gao, L.-J.; Xiao, G.-M., Aqueous-phase catalytic hydrogenation of furfural over Ni-bearing hierarchical Y zeolite catalysts synthesized by a facile route. *Fuel Processing Technology* **2015,** *134*, 168-174.

Table 5.1. Physical properties of the catalysts

Catalysts	Pd-TiO_2/CACM	Pd-TiO_2/CACM	Pd-Cu/CACM	Pd-Cu/CACM	Pd-Fe/CACM	Pd-Fe/CACM
Properties	(Fresh)	(Spent)[a]	(Fresh)	(Spent)	(Fresh)	(Spent)
Surface Area (m^2/g)	736	348	562	501	627	566
Pore Volume (cm^3/g)	0.63	0.36	0.50	0.51	0.54	0.54
Average Pore Size (radius, Å)	34.2	42.3	35.9	40.8	34.8	38.4
Micro-Pore Volume[c], (cm^3/g)	0.022	0	0.009	0.011	0.024	0.017
Acid Sites at 150 °C, (μmoles NH_3/g)	50	NP	0	NP	0	NP
Acid Sites at 400 °C, (μmoles NH_3/g)	36	NP	231	NP	14	NP
Acid Sites at 525 °C, (μmoles NH_3/g)	0	NP	0	NP	38	NP
CO uptake[d] (μmoles CO/μmoles Pd)	0.46	0.89	0.40	0.33	0.63	0.63

[a], Spent catalysts from 13 furfural hydrogenation experiments
[b], Calculated from elemental analysis/ICP-MS
[c], Estimated from t-plot analysis
[d], CO uptake from CO pulse titration at 40 °C
CACM is crushed activated carbon monolith
NP is not performed

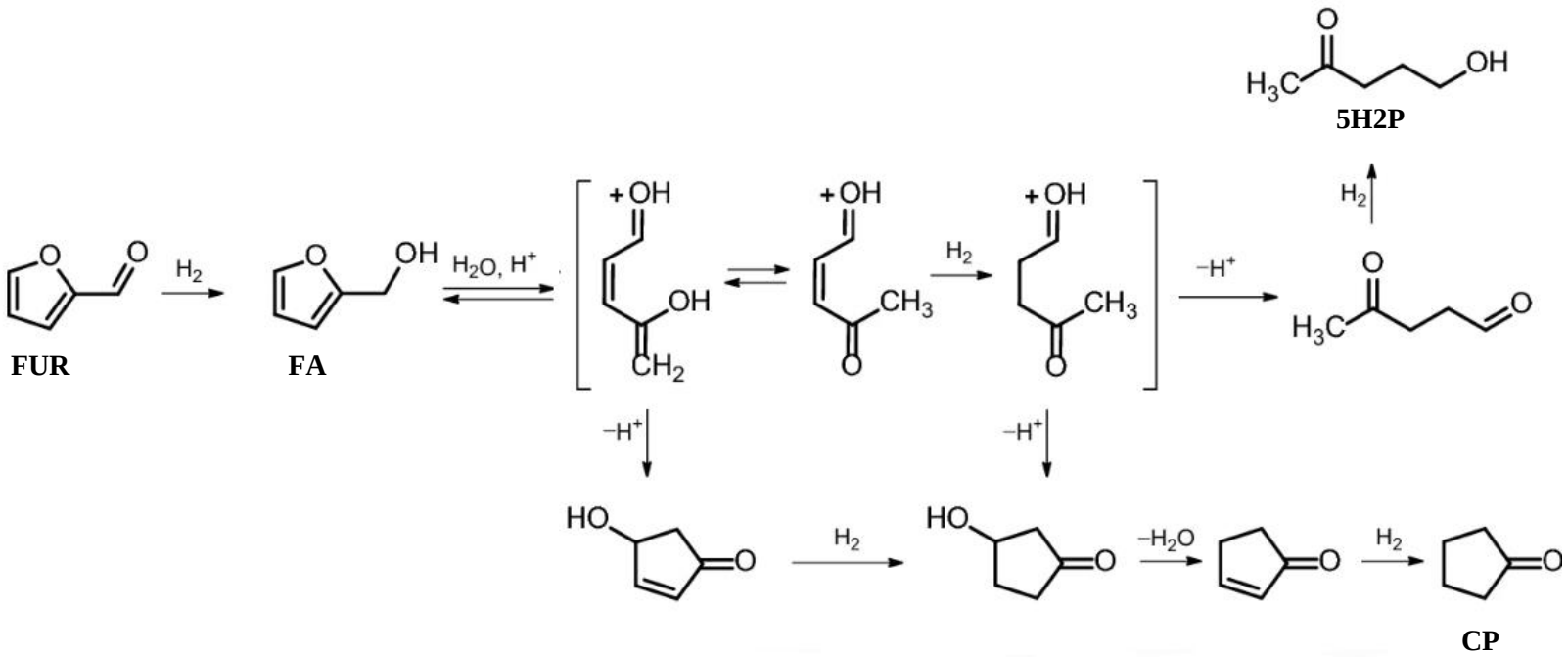

Figure 5.1. Ring opening pathway of furfuryl alcohol in presence of hydrogen.[2]

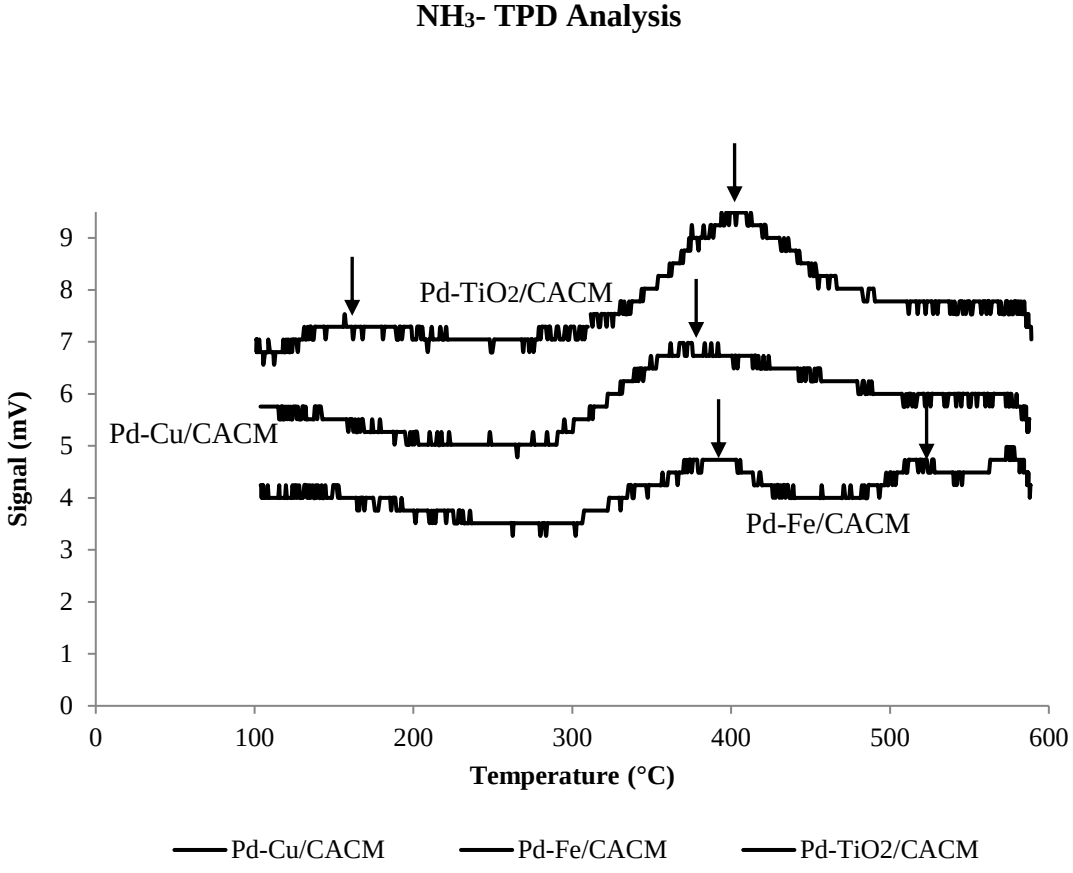

Figure 5.2. Ammonia TPD analysis of bi-metal carbon catalysts pre-reduced with H_2 (100% H_2 for 2 h at 250 °C).

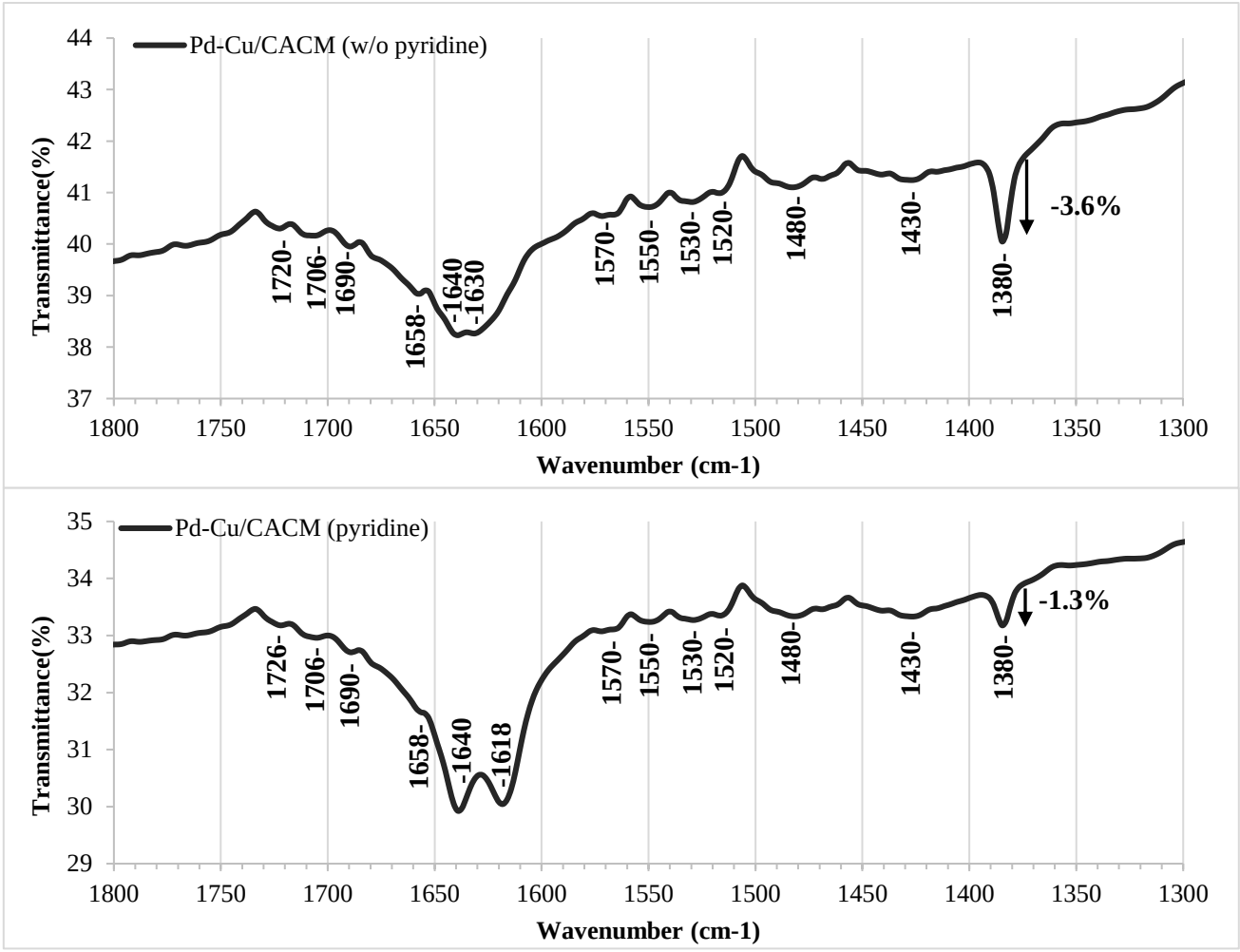

Figure 5.3. FTIR analysis of Pd-Cu/CACM.

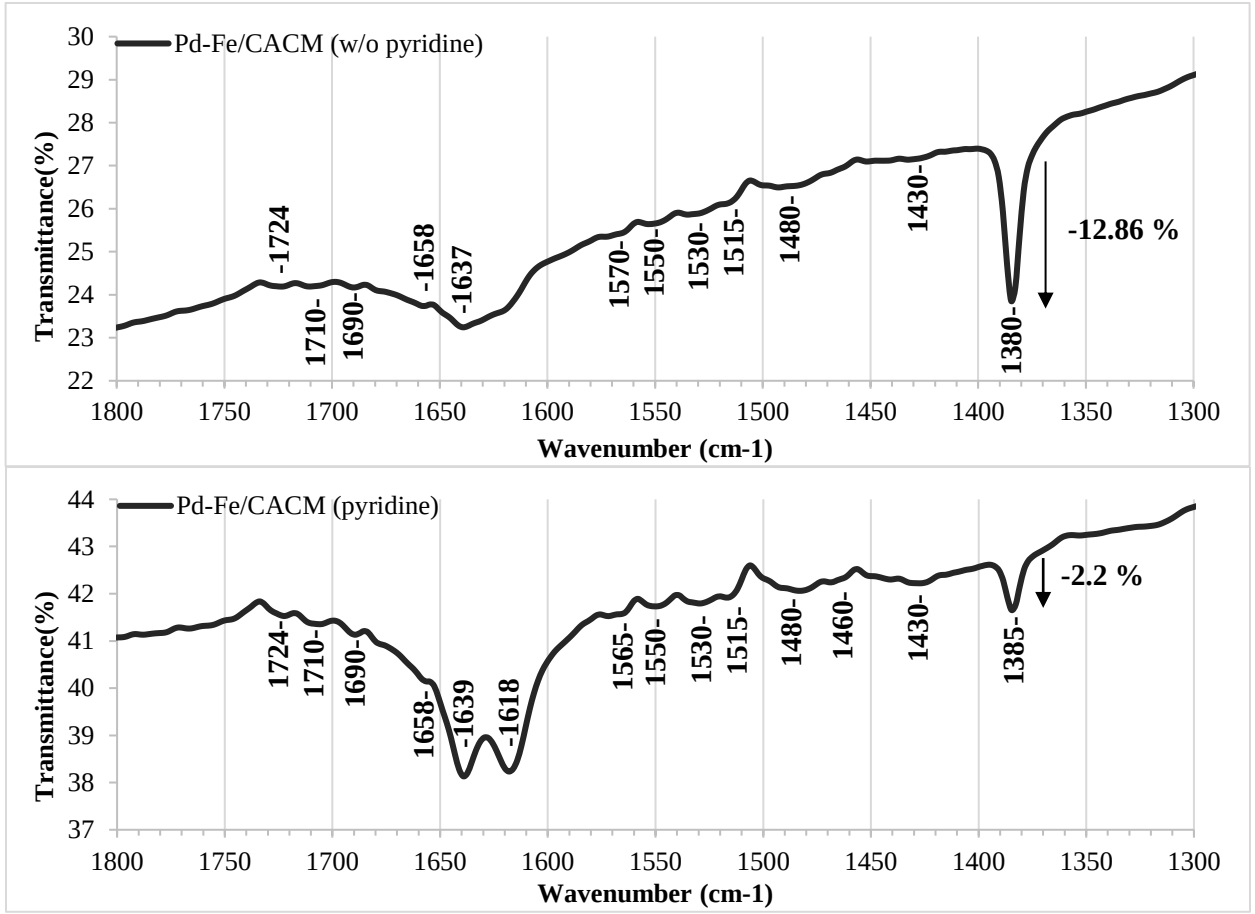

Figure 5.4. FTIR analysis of Pd-Fe/CACM.

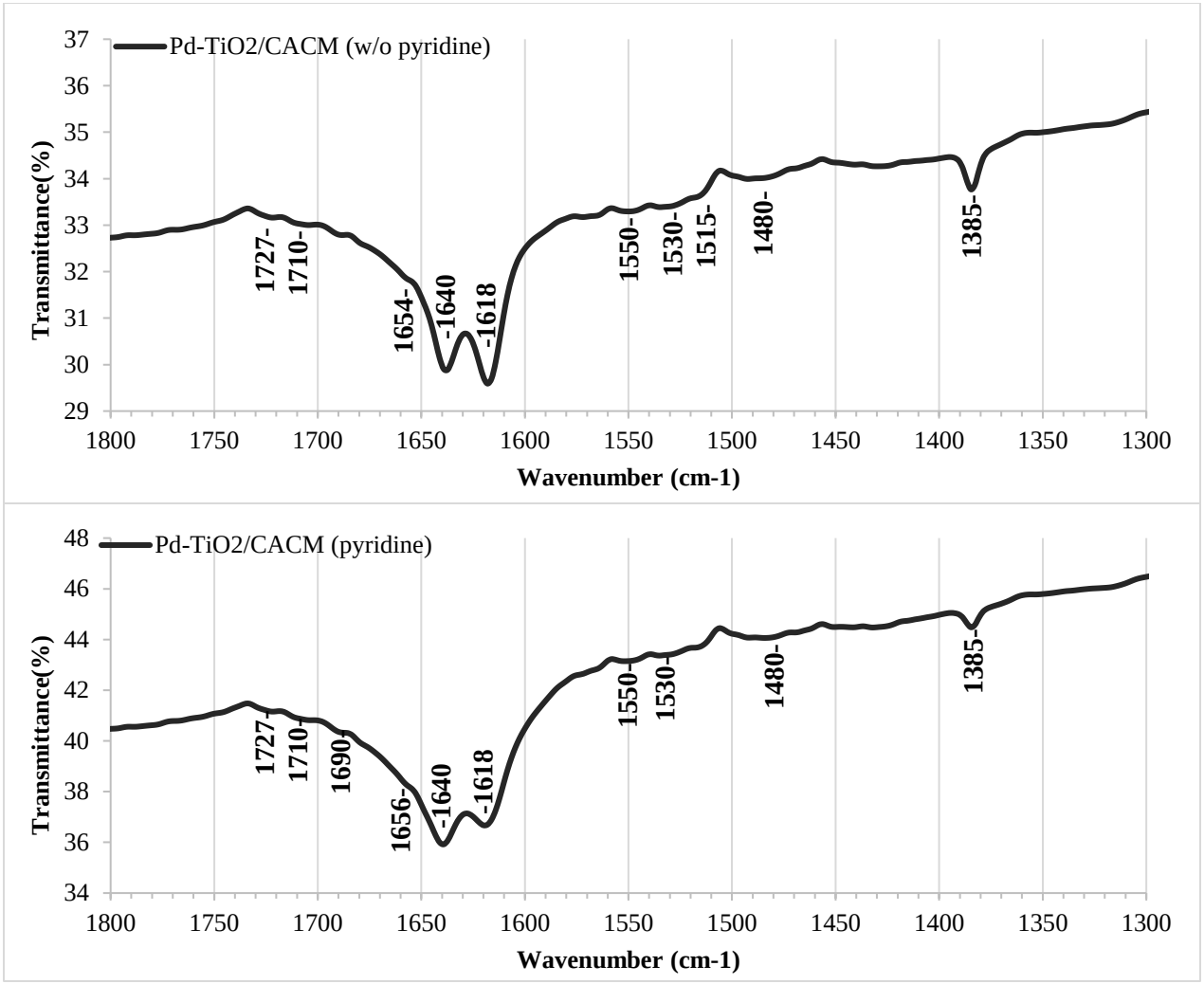

Figure 5.5. FTIR analysis of Pd-TiO_2/CACM.

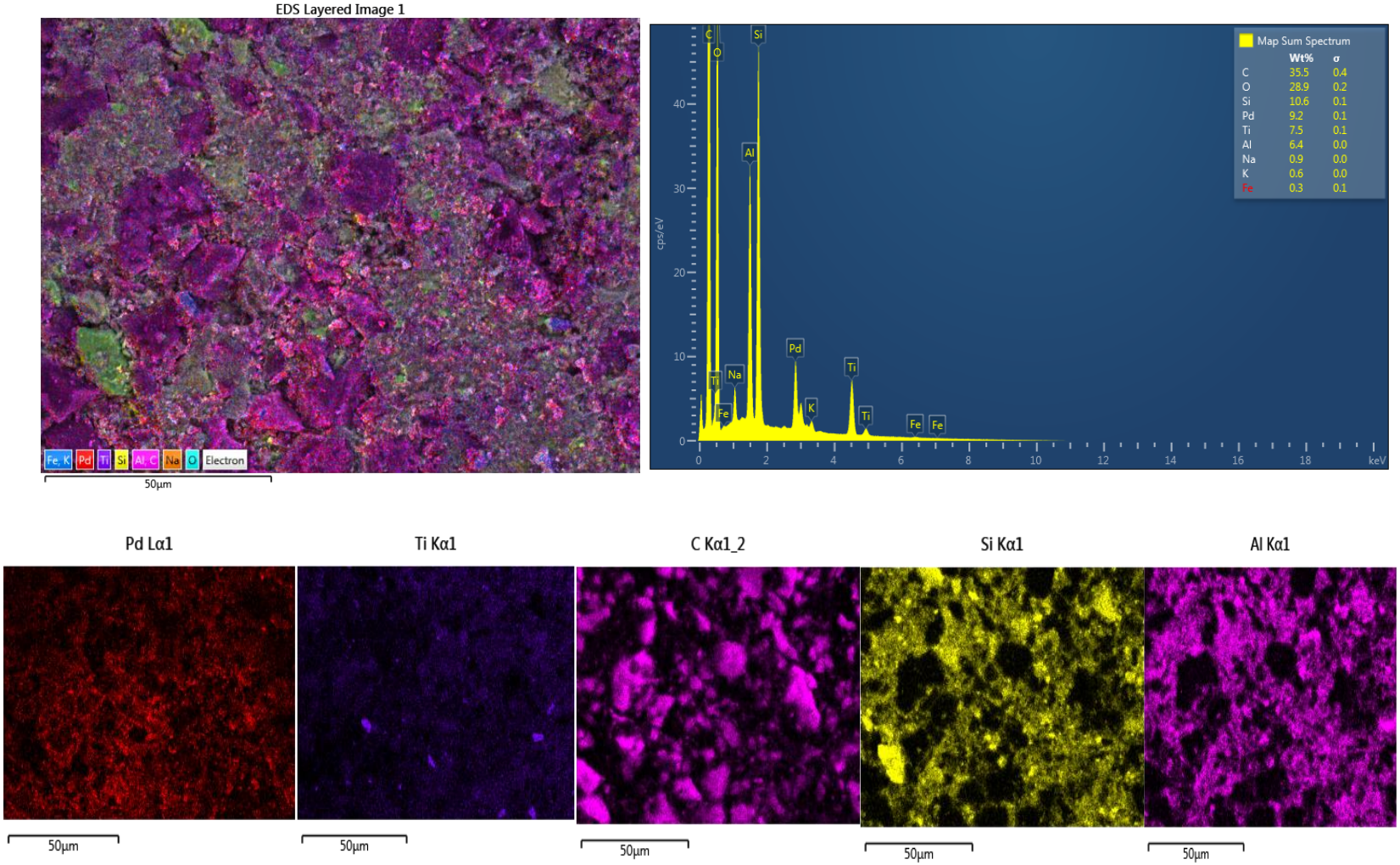

Figure 5.6. SEM-EDS images of Pd-TiO_2/CACM.

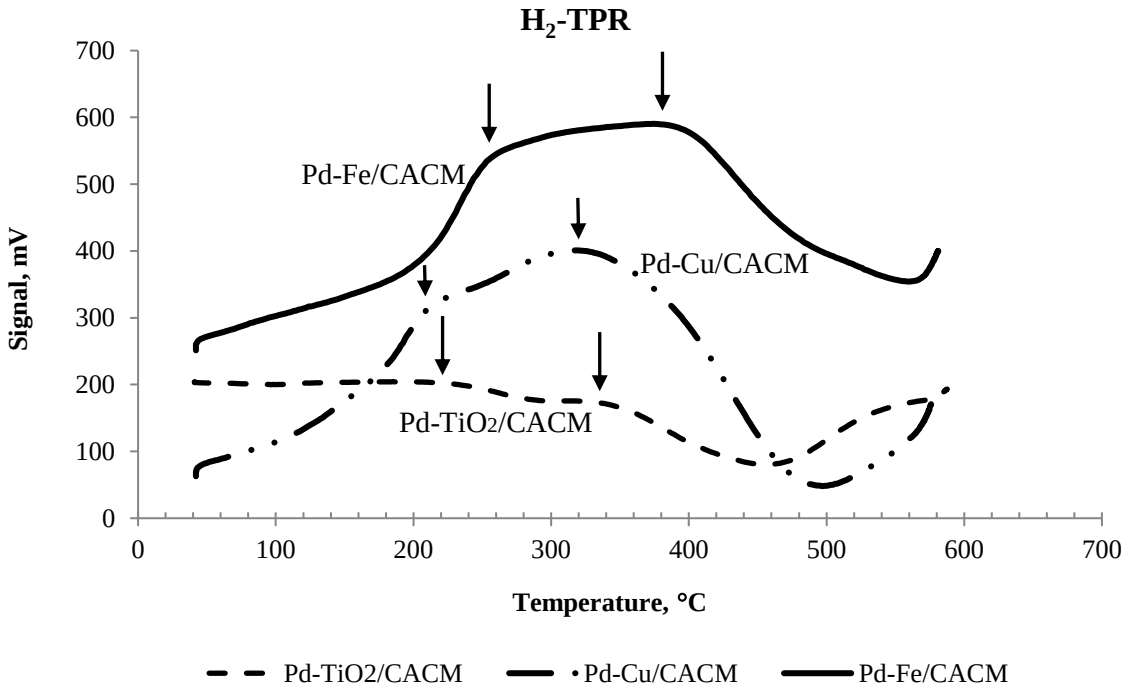

Figure 5.7. Temperature programmed hydrogen reduction of activated carbon catalysts.

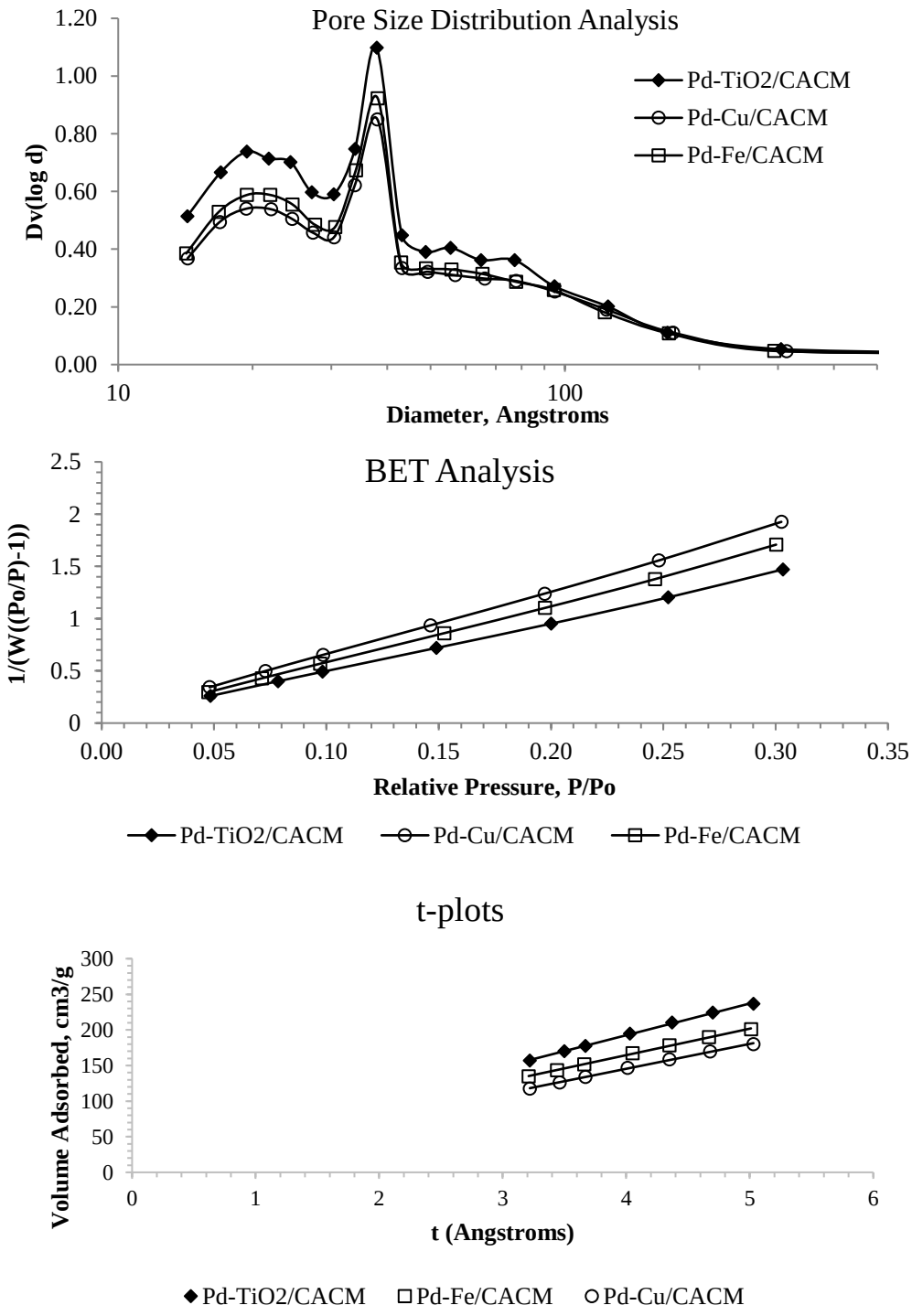

Figure 5.8. BJH, t-plot and BET analysis of fresh catalysts.

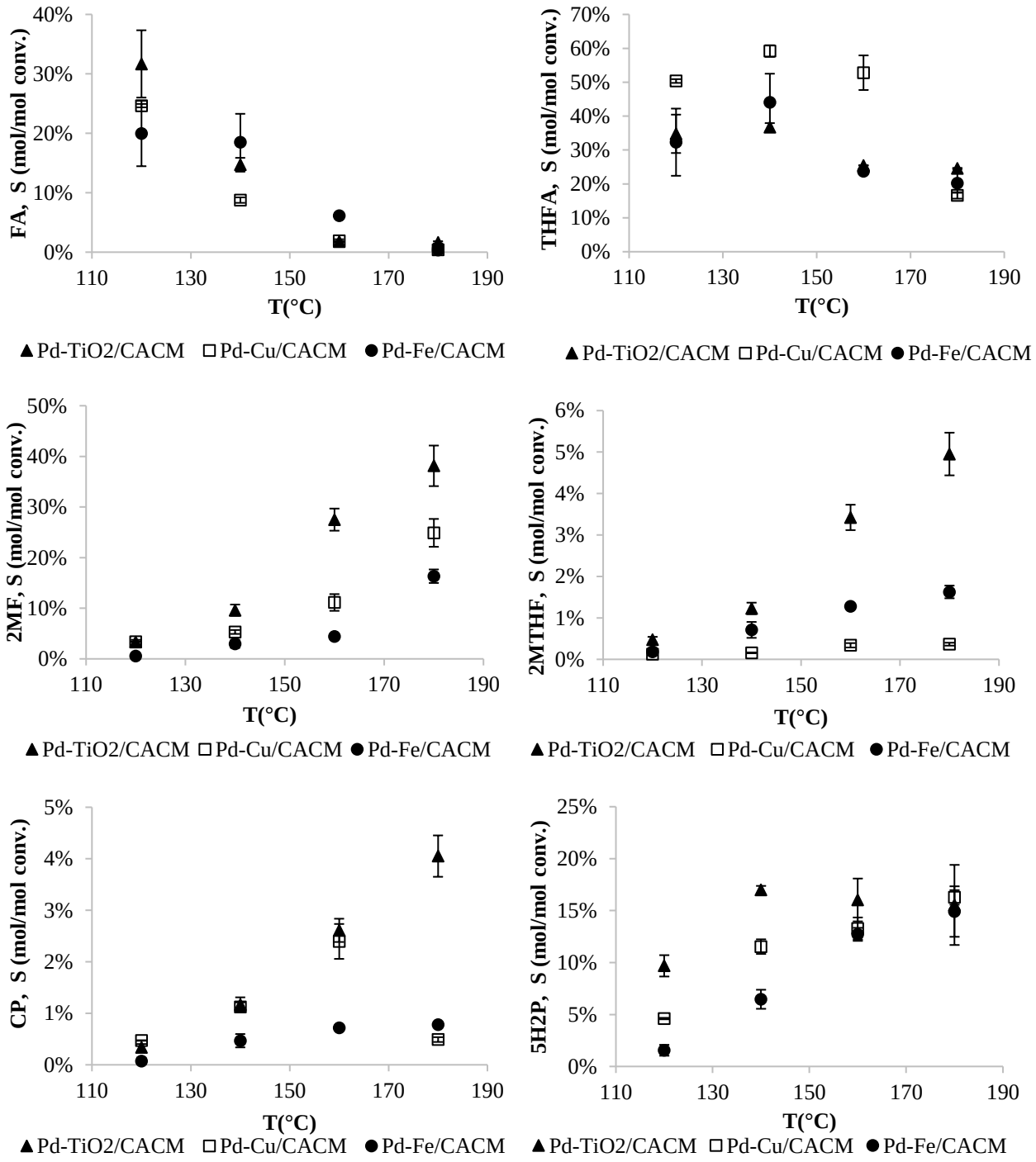

Figure 5.9. Effect of reaction temperature on product selectivity. Reaction Condition: P=300 psig , LHSV =1.32 1/h, 5 g of catalyst.

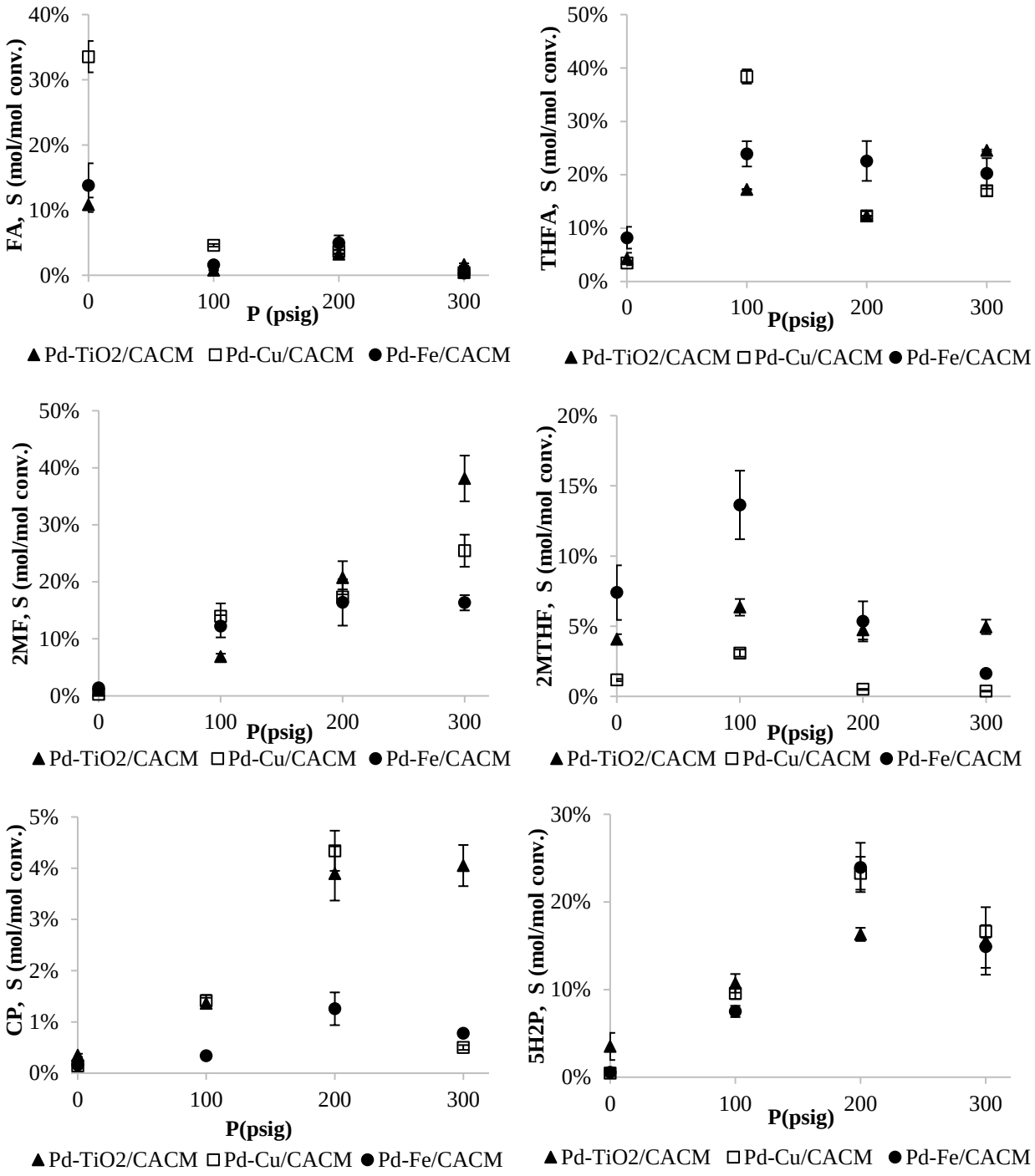

Figure 5.10. Effect of hydrogen pressure on product selectivity. Reaction Condition: T=180 °C, LHSV =1.32 1/h, 5 g of catalyst.

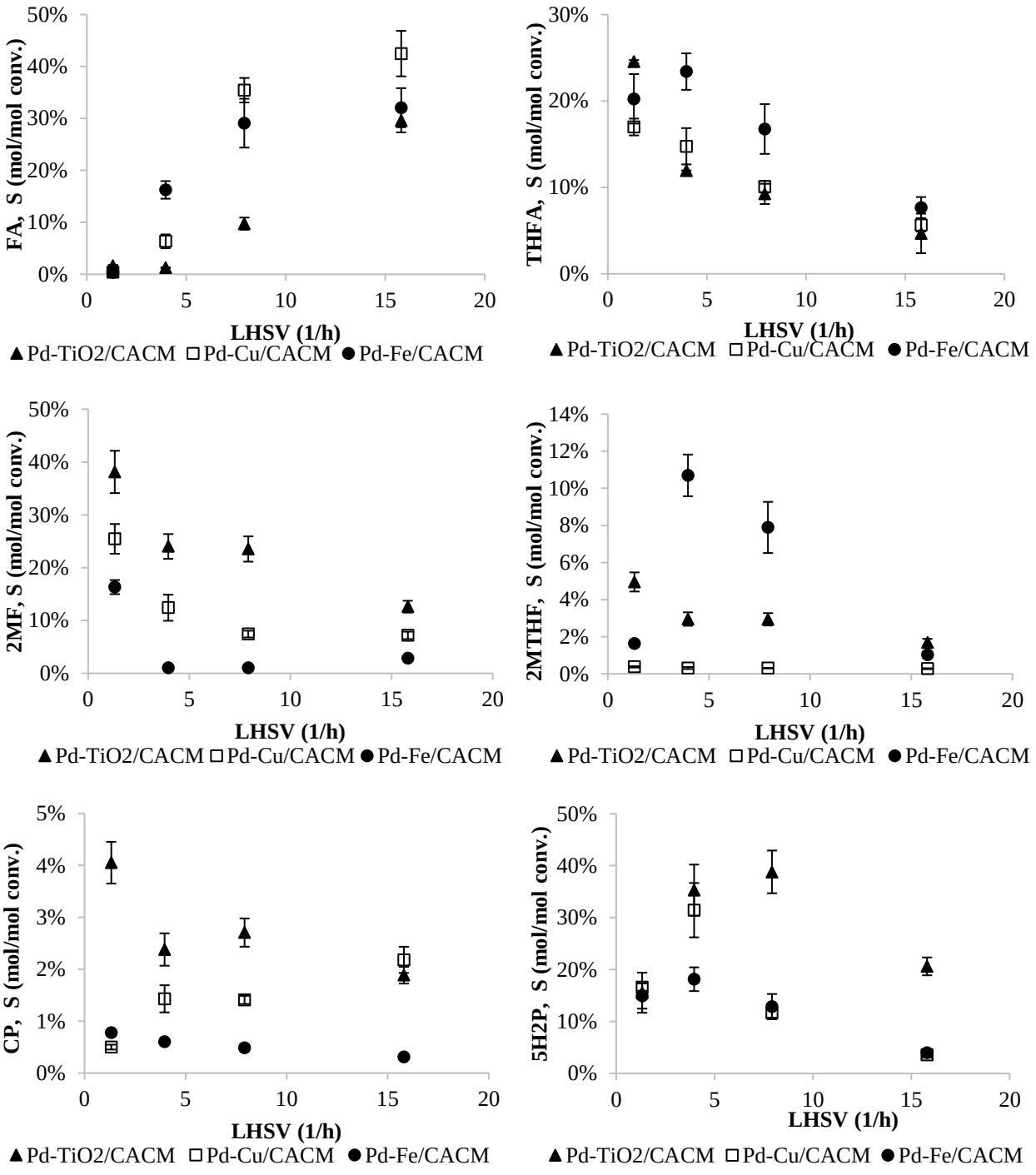

Figure 5.11. Effect of liquid hourly space velocity (LHSV) on product selectivity. P = 300 psig, T = 180 °C, 5 g of catalyst.

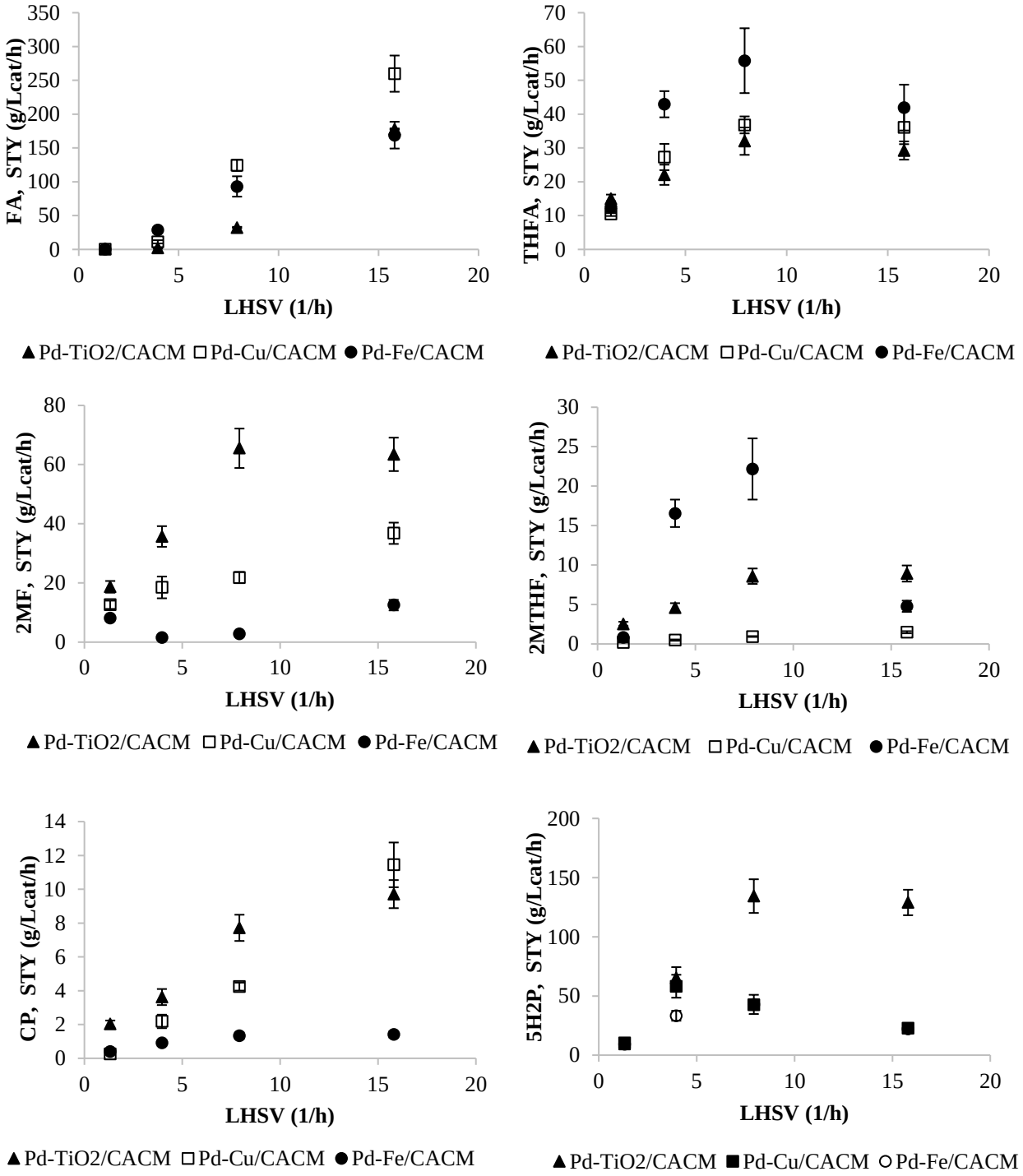

Figure 5.12. Effect of LHSV on product STY. P = 300 psig, T = 180 °C, 5 g of catalyst.

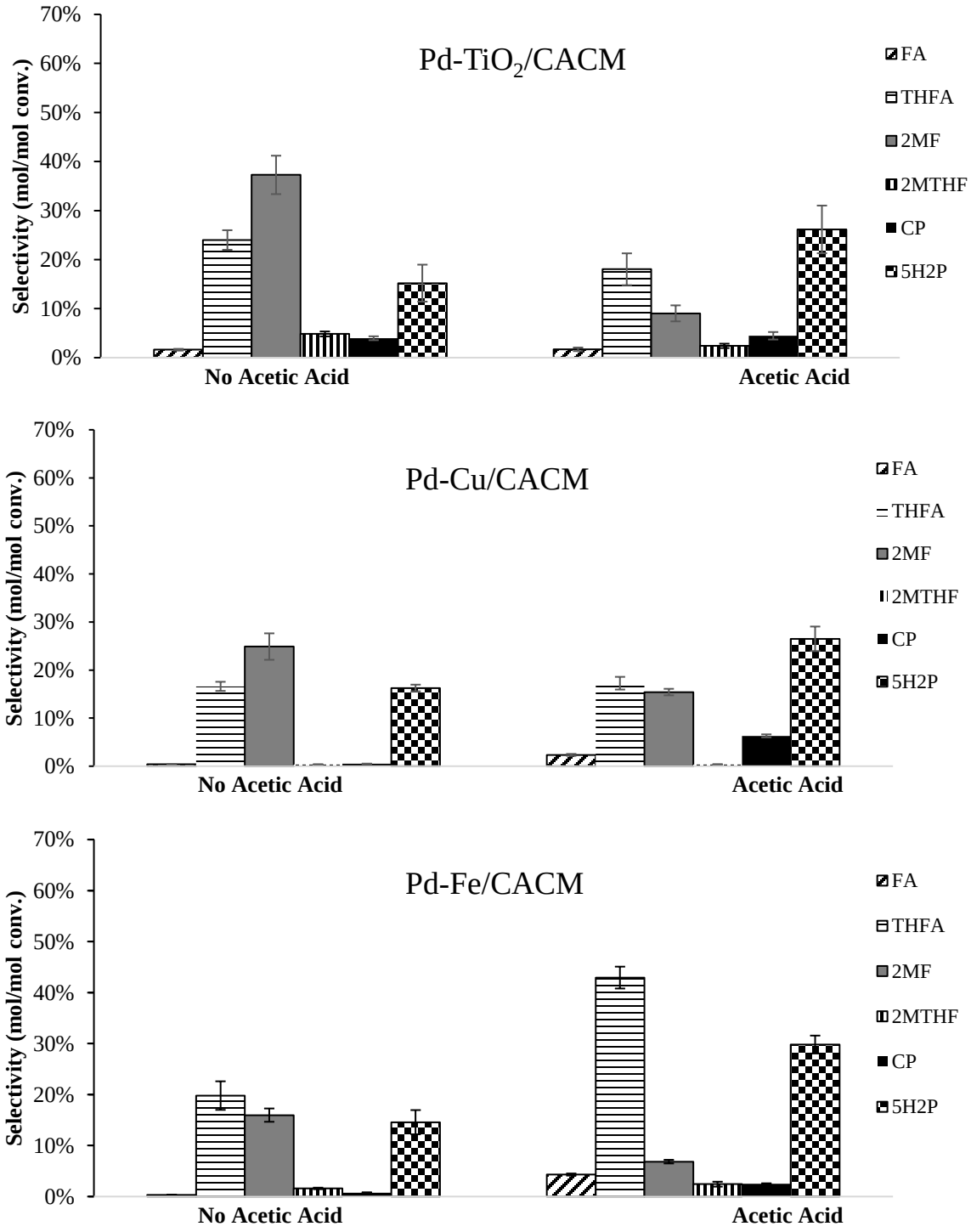

Figure 5.13. Effect of acetic acid on product selectivity and furfural conversion using ACM catalysts. P = 300 psig, T = 180 °C, LHSV = 1.32 1/h, 5 g of catalyst, 5% furfural, 1% acetic acid (aqueous).

CHAPTER 6

KINETICS OF MULTI-STEP FURFURAL HYDROGENATION OVER Pd-TiO_2 CATALYST USING LANGMUIR-HINSHELWOOD MECHANISM [1]

[1] Pirmoradi, N, Gulotty Jr., R.J., Kastner, J.R., 2020.
To be submitted to *Chemical Engineering Research and Design.*

Abstract

The multi-step hydrogenation of furfural (FUR) to furfuryl alcohol (FA), 2-methylfuran (2MF), tetrahydrofurfuryl alcohol (THFA) and 5-hydroxy-2-pentanone (5H2P) kinetics over Pd-TiO_2 catalyst at 180 °C was studied. A Langmuir-Hinshelwood model with two active sites (a metal site for hydrogenation steps and an acid site for ring opening step) was applied to fit the kinetic data. The kinetic parameters of the reaction system were obtained using non-linear regression of experimental data. The kinetic model showed an acceptable agreement with the experimental data with R^2 of 0.91 and residual sum of squares of 0.02. Adsorption constants of 2-methylfuran and tetrahydrofurfuryl alcohol were significantly lower than the adsorption constants of the other three compounds. Reaction rate constant of 1.925 mol/gcat.h for furfural consumption was predicted by the model. Reaction rates of 0.506 mol/gcat.h, 0.269 mol/gcat.h and 0.973 mol/gcat.h were predicted for formation of 2-methylfuran, tetrahydrofurfuryl alcohol and 5-hydroxy-2-pentanone, respectively.

Keywords: Kinetics, Langmuir-Hinshelwood mechanism, furfural, continuous hydrogenation, activated carbon

6.1 Introduction

Hydrogenation of furfural is an important industrial reaction due to forming series of valuable products that can be promising alternatives for fossil fuels. Furfural is an inexpensive bio-based chemical that is industrially produced through acid hydrolysis of biomasses rich in hemicellulose.[1] Furfural hydrogenation leads to formation of several valuable products such as furfuryl alcohol, tetrahydrofurfuryl alcohol, 2-methylfuran, cyclopentanone and 5-hydroxy-2-pentanone. Hydrogenation reactions usually occur in presence of a precious metal active site.[2] In order to form cyclopentanone and 5-hydroxy-2-pentanone from furfural, a furfuryl alcohol ring opening/rearrangement step, independent of the hydrogenation step, is required. This step is known to require a weak acid site.[3] In this work, Pd-TiO_2, a metal-acid catalyst, supported on activated carbon support is employed to study conversion of aqueous furfural as a function of liquid residence time. Developing a reaction rate law allows designing an efficient industrial scale reactor system. By determining the reaction rate law, coupled with heat and transfer model, the amount of catalyst required for a specified product concentration is calculated. The rate equation of heterogeneous hydrogenation reactions usually follow Langmuir-Hinshelwood approach.[4] This approach considers three steps in a heterogeneous catalytic reaction. These three steps are first, chemisorption of reactants at the active sites (single or dual), second, surface reaction and third, desorption of products from the surface. In order to determine the rate law using the experimental data, one of these steps is usually assumed to be rate limiting. Following the suggested furfural hydrogenation pathway[5], shown in Figure 3.6, Langmuir-Hinshelwood mechanism is employed to develop a rate law based on metal and acid active sites present on the carbon catalyst.

6.2 Experimental Approach

Materials and Catalysts: aqueous furfural (Sigma-Aldrich, 99%) was prepared for each reaction. Activated carbon support was supplied by Applied Catalysts (Laurens, SC) in a form of monolith structure, manufactured by coextrusion of 50% activated carbon and 50% ceramic binder. Each monolith structure was crushed and sieved to a particle size of $250 < d < 320$ μm. Mears and Weisz-Prater criterion were applied to verify that there is no internal and external mass transfer resistance present during the reactions. In order to prepare 0.8% Pd-5% TiO_2 catalyst, direct air-hydrolysis method was employed to deposit TiO_2 particles on activated carbon support.[6] Therefore, 2.19 g titanium (IV) isopropoxide (Sigma-Aldrich, 99.999%) was dissolved in 6 mL isopropanol under nitrogen atmosphere. The solution was added to 7 g of crushed activated carbon monolith under stirring condition. The final sample was dried at 120 °C for 2 hours followed by calcination at 300 °C under 100% flow of N_2 (100 ml/min) for 4 hours. After sample cool down, incipient wetness impregnation method was employed to deposit Pd particles on the catalyst.[7] 0.141 g of Pd(ll) nitrate dihydrate (Sigma-Aldrich, 40% Pd basis) was dissolved in DI water and added to the sample. The sample was dried at 120 °C for 2 hours followed by reduction at 250 °C under 100% flow of H_2 (100 ml/min) for 4 hours.

Catalyst Characterization: Surface area analysis and pore size analysis were performed as previously described.[8] Micropore analysis was performed using the t-method of de Boer[9] (t is the statistical thickness of an adsorbed film [$t\ (Å) = [13.99/\log(Po/P)+0.034]^{1/2}$]) and the BET surface area data extended to higher pressures (Quantachrome, AUTOSORB-1C; Boynton Beach, Florida). Ammonia-TPD analysis was performed to determine the quantity and strength of acid sites as previously described. TPR analysis was performed to determine the reducibility

of the catalyst and CO pulse titration was performed to determine the CO uptake of Pd at 40 °C. [8] TGA analysis in air was used to estimate tar and coke formation on the catalysts (Discovery TGA from TA Instruments). Air flow over the sample (10-25 mg in ceramic pans) was set at 25 mL/min with a balance flow rate at 10 mL/min (N_2). The temperature of the sample was equilibrated at 40 °C before ramping at a rate of 10°C/min to 800 °C. Elemental analysis of fresh and spent catalysts was performed following the Environmental Protection Agency (EPA) ICP method 200.8. Concentrated HNO_3 was added (5 ml) to the sample (~ 0.1g) for microwave digestion following protocols listed in EPA method 3051A. Digested solutions were analyzed by inductively coupled plasma optical emission spectroscopy (ICP-OES, Spectro Arcos FHS16 AMETEK ICP-OES).

Analytical: Once the liquid sample was collected from the reactor, it was analyzed in triplicate using gas chromatography with flame ionization detection (GC-FID, HP 5890 Series II) with HP Innowax column (30 m x 0.25 mm x 0.25mm). The GC-FID was operated with the method of inlet temperature 230 °C, detector temperature 240 °C, initial oven temperature of 45 °C for 2.5 minutes followed by a ramp of 10 °C/min for 15.5 minutes and then held at 200 °C for 3 minutes. 1 μL of sample is injected on the GC-FID in triplicate. The concentrations of furfural (FUR, 99%), furfuryl alcohol (FA, 98%), tetrahydrofurfuryl alcohol (THFA, 98%), 2-methylfuran (2MF, 99%), 2-methyltetrahydrofuran (2MTHF, 99%), cyclopentanol (CPO, 99%), cyclopentanone (CP, 95%), 5-hydroxy-2-pentanone (5H2P, 95%), and 1,4-pentanediol (1,4PD, 99%) were determined using 4-point standard curves (chemicals purchased from Sigma-Aldrich, each point run in triplicate). All standards were prepared in DI water, except for 2MF which was prepared with ethanol as the solvent. The presence of all intermediates and products were

confirmed using GC/MS (HP-6890 with HP Innowax column, same method as for GC/FID, 1 μl injection volume, 25:1 split ratio, 0.8 ml/min, 10-500 mass units, MSD ChemStation D.03.00.611 with NIST 2008 database for identification).

Catalytic Reactions: Furfural hydrogenation reactions were performed in a continuous reactor system, designed by Parr Instrument Company, as described previously.[8] Crushed activated carbon monolith catalyst was placed between two layers of quartz wool. Fresh catalyst was used for each run. In order to determine the kinetics of furfural hydrogenation, a series of reactions at 180 °C, 300 psig and 100 mL/min H_2 flow with different liquid residence times were performed.

6.3 Results and Discussion

6.3.1 Developing a rate law

With the suggested pathway for furfural (FUR) hydrogenation to furfuryl alcohol (FA), tetrahydrofurfuryl alcohol (THFA), 2-methylfuran (2-MF), 2-methyltetrahydrofuran (2-MTHF), 5-hydroxy-2-pentanone (5H2P), 4-hydroxy-2-pentanone (4-HCP), 2-cyclopentenone (2-CP) and cyclopentanone (CP) in Figure 3.6 over a metal-acid catalyst, the Langmuir-Hinshelwood mechanism can be applied with the assumptions of dissociative adsorption of hydrogen at the metal active site, rate-limiting role of surface reactions, and presence of 2 different active sites (S_1 for the metal, S_2 for the acid site). Since $r_{adsorption} = - r_{desorption}$ and $K_{adsorption} = 1/K_{desorption}$, all the adsorption and desorption steps are combined in one category, therefore:

Adsorption/desorption steps:

$$H_{2(g)} + 2S_1 \overset{K_{H_2}}{\Longleftrightarrow} 2H.S_1$$

$$\mathrm{FUR} + \mathrm{S}_1 \overset{\mathrm{K_{FUR}}}{\Longleftrightarrow} \mathrm{FUR.S}_1$$

$$\mathrm{FA.S}_1 \overset{\frac{1}{\mathrm{K_{FA1}}}}{\Longleftrightarrow} \mathrm{FA} + \mathrm{S}_1$$

$$\mathrm{FA.S}_2 \overset{\frac{1}{\mathrm{K_{FA2}}}}{\Longleftrightarrow} \mathrm{FA} + \mathrm{S}_2$$

$$THFA.S_1 \overset{\frac{1}{K_{THFA}}}{\Longleftrightarrow} THFA + \mathrm{S}_1$$

$$2 - MF.S_1 \overset{\frac{1}{K_{2-MF}}}{\Longleftrightarrow} 2 - MF + \mathrm{S}_1$$

$$2 - MTHF.S_1 \overset{\frac{1}{K_{2-MTHF}}}{\Longleftrightarrow} 2 - MTHF + \mathrm{S}_1$$

$$4 - \mathrm{HCP.S}_1 \overset{\frac{1}{\mathrm{K_{4-HCP1}}}}{\Longleftrightarrow} 4 - \mathrm{HCP} + \mathrm{S}_1$$

$$4 - \mathrm{HCP.S}_2 \overset{\frac{1}{\mathrm{K_{4-HCP2}}}}{\Longleftrightarrow} 4 - \mathrm{HCP} + \mathrm{S}_2$$

$$2 - \mathrm{CP.S}_1 \overset{\frac{1}{\mathrm{K_{2-CP}}}}{\Longleftrightarrow} 2 - \mathrm{CP} + \mathrm{S}_1$$

$$\mathrm{CP.S}_1 \overset{\frac{1}{\mathrm{K_{CP}}}}{\Longleftrightarrow} \mathrm{CP} + \mathrm{S}_1$$

$$5 - \mathrm{H2P.S}_1 \overset{\frac{1}{\mathrm{K_{5-H2P1}}}}{\Longleftrightarrow} 5 - \mathrm{H2P} + \mathrm{S}_1$$

$$5-\mathrm{H2P.S_2} \overset{\frac{1}{\mathrm{K}_{5-\mathrm{H2P2}}}}{\Longleftrightarrow} 5-\mathrm{H2P} + \mathrm{S_2}$$

$$1,4-\mathrm{PD.S_1} \overset{\frac{1}{\mathrm{K}_{1,4-\mathrm{PD}}}}{\Longleftrightarrow} 1,4-\mathrm{PD} + \mathrm{S_1}$$

With the assumption of irreversible heterogeneous hydrogenation reactions[10], we have:

Surface reactions:

Reaction 1: $\mathrm{FUR.S_1} + 2\mathrm{H.S_1} \overset{k_1}{\rightarrow} \mathrm{FA.S_1} + 2\mathrm{S_1}$

Reaction 2: $\mathrm{FA.S_1} + 2\mathrm{H.S_1} \overset{k_2}{\rightarrow} 2-\mathrm{MF.S_1} + 2\mathrm{S_1} + \mathrm{H_2O}$

Reaction 3: $\mathrm{FA.S_1} + 4\mathrm{H.S_1} \overset{k_3}{\rightarrow} \mathrm{THFA.S_1} + 4\mathrm{S_1}$

Reaction 4: $\mathrm{THFA.S_1} + 2\mathrm{H.S_1} \overset{k_4}{\rightarrow} 2-\mathrm{MTHF.S_1} + 2\mathrm{S_1} + \mathrm{H_2O}$

Reaction 5: $2-\mathrm{MF.S_1} + 4\mathrm{H.S_1} \overset{k_5}{\rightarrow} 2-\mathrm{MTHF.S_1} + 4\mathrm{S_1}$

Reaction 6: $\mathrm{FA.S_1} + \mathrm{S_2} \overset{k_6}{\rightarrow} \mathrm{FA.S_2} + \mathrm{S_1}$

Reaction 7: $\mathrm{FA.S_2} \overset{k_7}{\rightarrow} 4-\mathrm{HCP.S_2}$

Reaction 8: $4-\mathrm{HCP.S_2} + \mathrm{S_1} \overset{k_8}{\rightarrow} 4-\mathrm{HCP.S_1} + \mathrm{S_2}$

Reaction 9: $4-\mathrm{HCP.S_1} + 2\mathrm{H.S_1} \overset{k_9}{\rightarrow} 2-\mathrm{CP.S_1} + 2\mathrm{S_1}$

Reaction 10: $2-\mathrm{CP.S_1} + 2\mathrm{H.S_1} \overset{k_{10}}{\longrightarrow} \mathrm{CP.S_1} + 2\mathrm{S_1}$

Reaction 11: $\mathrm{FA.}S_2 + 4\mathrm{H.}S_1 \overset{k_{11}}{\longrightarrow} 5-\mathrm{H2P.}S_2 + 4S_1$

Reaction 12: $5-\mathrm{H2P}.S_2 + S_1 \xrightarrow{k_{12}} 5-\mathrm{H2P}.S_1 + S_2$

Reaction 13: $5-\mathrm{H2P}.S_1 + 2\mathrm{H}.S_1 \xrightarrow{k_{13}} 5-\mathrm{H2P}.S_1 + 2S_1$

Based on our previous work on furfural hydrogenation using Pd-TiO_2 on activated carbon support, small to zero yields of 2-MTHF, CP, 2-CP, 4-HCP and 1,4PD were observed. Therefore, reactions 4, 5, 7, 9, 10 and 13 are eliminated. It can also be assumed that reactions 6, 8 and 12 occur rapidly and are not rate-limiting. Therefore, the only reactions participating in the model will be reactions 1, 2, 3 and 11. The model simplifies as follows:

$$\mathrm{H}_{2(g)} + 2\mathrm{S}_1 \overset{\mathrm{K_{H_2}}}{\Longleftrightarrow} 2\mathrm{H}.\mathrm{S}_1$$

$$\mathrm{FUR} + \mathrm{S}_1 \overset{\mathrm{K_{FUR}}}{\Longleftrightarrow} \mathrm{FUR}.\mathrm{S}_1$$

$$\mathrm{FUR}.\mathrm{S}_1 + 2\mathrm{H}.\mathrm{S}_1 \xrightarrow{k_1} \mathrm{FA}.\mathrm{S}_1 + 2\mathrm{S}_1$$

$$\mathrm{FA}.\mathrm{S}_1 \overset{\frac{1}{\mathrm{K_{FA1}}}}{\Longleftrightarrow} \mathrm{FA} + \mathrm{S}_1$$

$$\mathrm{FA}.\mathrm{S}_2 \overset{\frac{1}{\mathrm{K_{FA2}}}}{\Longleftrightarrow} \mathrm{FA} + \mathrm{S}_2$$

$$\mathrm{FA}.\mathrm{S}_1 + 2\mathrm{H}.\mathrm{S}_1 \xrightarrow{k_2} 2-\mathrm{MF}.\mathrm{S}_1 + 2\mathrm{S}_1 + \mathrm{H_2O}$$

$$2-MF.S_1 \overset{\frac{1}{K_{2-MF}}}{\Longleftrightarrow} 2-MF + \mathrm{S}_1$$

$$\mathrm{FA}.\mathrm{S}_1 + 4\mathrm{H}.\mathrm{S}_1 \xrightarrow{k_3} \mathrm{THFA}.\mathrm{S}_1 + 4\mathrm{S}_1$$

$$THFA.S_1 \overset{\frac{1}{K_{THFA}}}{\Longleftrightarrow} THFA + \mathrm{S_1}$$

$$\mathrm{FA}.S_2 + 4\mathrm{H}.S_1 \overset{k_{11}}{\longrightarrow} 5-\mathrm{H2P}.S_2 + 4S_1$$

$$5-\mathrm{H2P}.\mathrm{S_2} \overset{\frac{1}{\mathrm{K}_{5-\mathrm{H2P_2}}}}{\Longleftrightarrow} 5-\mathrm{H2P} + \mathrm{S_2}$$

Total site balance for fractional coverages (θ = fractional coverage of each compound):

S_1: $^{\theta 1}_{free} + {}^{\theta 1}_{H} + {}^{\theta 1}_{FUR} + {}^{\theta 1}_{FA} + {}^{\theta 1}_{THFA} + {}^{\theta 1}_{2\text{-}MF} = 1$ Equation 6.1

S_2: $^{\theta 2}_{free} + {}^{\theta 2}_{FA} + {}^{\theta 2}_{5\text{-}H2P} = 1$ Equation 6.2

If the rate-limiting step is surface reaction and adsorption/desorption steps occur rapidly, the quasi equilibria for rapid steps is applied as follows:

For adsorption reactions: $r_{Ad_i} = k_{Ad_i} C_i \theta_{free} - k_{revAd_i} \theta_i$ Equation 6.3

For desorption reactions: $r_{Des_i} = k_{Des_i} \theta_i - k_{revDes_i} C_i \theta_{free}$ Equation 6.4

Where $\frac{k_{Ad_i}}{k_{revAd_i}} = \frac{k_{revDes_i}}{k_{Des_i}} = K_i$ and i is the participating compounds (except H_2) in the reaction system.

At equilibrium: - $r_{Des_i} = r_{Ad_i} = 0$. Therefore,

$^{\theta 1}_{j} = {}^{\theta 1}_{free} * K_j * C_j$ where j are compounds that are adsorbed at S_1 except H_2 Equation 6.5

$^{\theta 2}_{m} = {}^{\theta 2}_{free} * K_m * C_m$ where m are compounds that are adsorbed at S_2 Equation 6.6

For hydrogen, using the partial pressures, given that hydrogen dissociatively adsorbs at the active site:

At equilibrium : $k_{Ad_{H_2}} P_{H_2}\ \theta_{free}^2 - k_{revAd_{H_2}} \theta_H^2 = 0$ where $\frac{k_{Ad_{H_2}}}{k_{revAd_{H_2}}} = K_{H_2}$ Equation 6.7

Therefore, $\theta_H = \sqrt{K_{H_2} P_{H_2}}\theta_{1free}$ Equation 6.8

Applying Henry's law: $P_{H_2} = \frac{C_{H_2}}{H}$ (H is Henry's law constant in unit of mol/L.atm) and replacing P_{H_2} in Equation 6.8:

$$\theta_H = \sqrt{\frac{K_{H_2} C_{H_2}}{H}}\theta_{1free}$$ Equation 6.9

Now rewriting Equation 6.1 and 6.2 based on Equation 6.5, 6.6 and 6.9, ${}^{\theta 1}_{\text{free}}$, ${}^{\theta 2}_{\text{free}}$ can be solved:

$${}^{\theta 1}_{\text{free}} = \frac{1}{1+\sqrt{\frac{K_{H2} C_{H_2}}{H}}+\sum K_j C_j}$$ where j is FUR, FA, THFA, 2-MF adsorbed at S_1

Denominator denoted by R: ${}^{\theta 1}_{\text{free}} = \frac{1}{R}$ Equation 6.10

$${}^{\theta 2}_{\text{free}} = \frac{1}{1+K_{FA2}.C_{FA}+K_{5-H2P2}.C_{5-H2P}}$$

Denominator denoted by S: ${}^{\theta 2}_{\text{free}} = \frac{1}{S}$ Equation 6.11

Now rewriting surface reactions (Reaction 1, 2, 3 and 11) in terms of active sites:

$$r_1 = k_1 [{}^{\theta 1}_{\text{FUR}}] [{}^{\theta 1}_{\text{H}}]^2$$

$$r_2 = k_2 [{}^{\theta 1}_{\text{FA}}] [{}^{\theta 1}_{\text{H}}]^2$$

$$r_3 = k_3 [{}^{\theta 1}_{\text{FA}}] [{}^{\theta 1}_{\text{H}}]^4$$

$$r_{11} = k_{11} [{}^{\theta 2}_{\text{FA}}] [{}^{\theta 1}_{\text{H}}]^4$$

Since pure hydrogen at pressure of 300 psig was applied in this work, it can be assumed that partial pressure of hydrogen and hydrogen concentration in liquid phase is constant. Therefore, ${}^{\theta 1}{}_{H}$ is assumed to be a constant value throughout the reaction. Therefore, rewriting surface reactions, we have:

$$r_1 = k_1'' [{}^{\theta 1}{}_{FUR}] \quad \text{Equation 6.12}$$

$$r_2 = k_2'' [{}^{\theta 1}{}_{FA}] \quad \text{Equation 6.13}$$

$$r_3 = k_3'' [{}^{\theta 1}{}_{FA}] \quad \text{Equation 6.14}$$

$$r_{11} = k_{11}'' [{}^{\theta 2}{}_{FA}] \quad \text{Equation 6.15}$$

Replacing the values from Equations 6.5, 6.6, 6.10 and 6.11 in Equations 6.12, 6.13, 6.14 and 6.15:

$$r_1 = \frac{k_1'' K_{FUR} C_{FUR}}{R}$$

$$r_2 = \frac{k_2'' K_{FA1} C_{FA}}{R}$$

$$r_3 = \frac{k_3'' K_{FA1} C_{FA}}{R}$$

$$r_{11} = \frac{k_{11}'' K_{FA2} C_{FA}}{S}$$

For a packed bed reactor:

$$r_i = \frac{dF_i}{dW}$$

$$F_i = Q_i * C_i$$

Therefore,

$$r_i = \frac{dQ_i * C_i}{dW}$$

With constant Q and $W = \rho_B * V_B$, we have

$$r_i = Q_i * \frac{dC_i}{d\rho_B * V_B}$$

With constant ρ_B and $\tau = \frac{V_b}{Q_i}$,

$$r_i = \frac{dC_i}{\rho_B d\tau}$$

Where F_i is molar flow rate, W is catalyst weight, Q is volumetric flow rate ρ_b is bulk density of catalyst, V_b is packed bed volume and τ is reactor space time.

Rewriting r_1, r_2, r_3, and r_{11}:

$$\frac{dC_1}{d\tau} = \frac{\rho_b k_1^{"} K_{FUR} C_{FUR}}{R}$$

$$\frac{dC_2}{d\tau} = \frac{\rho_b k_2^{"} K_{FA1} C_{FA}}{R}$$

$$\frac{dC_3}{d\tau} = \frac{\rho_b k_3^{"} K_{FA1} C_{FA}}{R}$$

$$\frac{dC_{11}}{d\tau} = \frac{\rho_b k_{11}^{"} K_{FA2} C_{FA}}{S}$$

Then, M = $\frac{R}{\rho_b}$ and N = $\frac{S}{\rho_b}$, Therefore:

$$\frac{dC_1}{d\tau} = \frac{k_1^{"} K_{FUR} C_{FUR}}{M}$$

$$\frac{dC_2}{d\tau} = \frac{k_2^{"} K_{FA1} C_{FA}}{M}$$

$$\frac{dC_3}{d\tau} = \frac{k_3^{"} K_{FA1} C_{FA}}{M}$$

$$\frac{dC_{11}}{d\tau} = \frac{k_{11}^{"} K_{FA2} C_{FA}}{N}$$

Formation/consumption of each compound:

Furfural: -r_1

Furfuryl alcohol: $r_1 - r_2 - r_3 - r_{11}$

2-methylfuran: r_2

Tetrahydrofurfuryl alcohol: r_3

5-hydroxy-2-pentanone: r_{11}

Therefore, based on consumption/formation of each compound, a system of ODEs containing 5 differential equations are formed:

Furfural:

$$\frac{dC_{FUR}}{d\tau} = \frac{-k_1^{"} K_{FUR} C_{FUR}}{M}$$

Furfuryl alcohol:

$$\frac{dC_{FA}}{d\tau} = \frac{k_1^{"} K_{FUR} C_{FUR}}{M} - \frac{k_2^{"} K_{FA1} C_{FA}}{M} - \frac{k_3^{"} K_{FA1} C_{FA}}{M} - \frac{k_{11}^{"} K_{FA2} C_{FA}}{N}$$

2-methylfuran:

$$\frac{dC_{2MF}}{d\tau} = \frac{k_2^{"} K_{FA1} C_{FA}}{M}$$

Tetrahydrofurfuryl alcohol:

$$\frac{dC_{THFA}}{d\tau} = \frac{k_3^{"} K_{FA1} C_{FA}}{M}$$

5-hydroxy-2-pentanone:

$$\frac{dC_{5H2P}}{d\tau} = \frac{k_{11}^{"} K_{FA2} C_{FA}}{N}$$

In order to solve the system of ODEs and determine the rate constants, a series of experiments with starting furfural concentration of 0.42 mol/L at 180 ° C and 300 psi were performed at varying space times. The concentrations of each product were determined after the reaction. Non-linear regression of experimental data with Matlab R2019a using the least square method was applied to solve the system of equations. Nonlinear least square regression of n experimental data points (y_i) with curve function of f (x, θ) is applied such that a θ vector is found to obtain the best curve fit of data in least square sense:

$$Q = \sum_{1}^{n} \left(y_i - f(x_i, \theta)\right)^2$$

Minimum of Q with respect to θ :

$$\frac{\partial Q}{\partial \theta} = \frac{2 \sum_1^n \partial \left(y_i - f(x_i, \theta)\right)}{\partial \theta} = 0$$

In order to measure the goodness of fit, residual sum of squares (RSS) and R^2 are calculated:

$$RSS = \sum_{1}^{n} \left(y_i - f(x_i)\right)^2$$

$$R^2 = 1 - \frac{\sum_1^n \left(y_i - \overline{f(x_\iota)}\right)^2}{\sum_1^n (y_i - \bar{y})^2}$$

6.3.2 Rate Constants

Figures 6.1-6.4 indicates the results of fitting the experimental concentrations as a function of space time. In general, an acceptable agreement was observed between the experimental data and the kinetic model with R^2 and RSS of 0.912 and 0.02, respectively. Table 6.1 shows the 11 kinetic parameters obtained from the kinetic model. These predicted K and k values are in agreement with previous works on furfural hydrogenation.[11-13] The larger value of $k_1^{"}$, compared to $k_2^{"}$, $k_3^{"}$, $k_{11}^{"}$ indicates that the rate of furfural conversion to FA is higher than the rate of 2MF, THFA and 5H2P formation, supporting the theory of quick conversion of FUR to FA. The concentrations of products were predicted slightly higher than the experimental data which can be attributed to the formation of other side products such as 2-methyltetrahydrofuran and cyclopentanone in small concentrations, not included in this model. Among the adsorption constants, 2MF and THFA showed the lowest values indicating the adsorption of reactants (FUR, FA and hydrogen) was preferential. Comparing K_{FA1} (adsorption at Pd site) and K_{FA2} (adsorption at TiO_2 site), a better adsorption of FA at the metal site was observed. This kinetic model, coupled with heat and mass transfer models, can predict the amount of catalyst required for a specified product concentration in furfural hydrogenation reaction over Pd-TiO_2/CACM.

6.4 Conclusions

Kinetics of the multiple reaction system of furfural hydrogenation over Pd-TiO_2 catalyst was determined using two-site Langmuir-Hinshelwood mechanism. The kinetic model showed an acceptable agreement with the experimental data. 11 reaction parameters including reaction rate constants and adsorption/desorption constants were obtained from the model. These reaction parameters are in line with values reported in the literature, previously. The rate constant for furfural consumption was found to be significantly higher than formation of 2MF, THFA and 5H2P.

ACKNOWLEDGMENTS

Support for this research and Maryam Pirmoradi's PhD in Biochemical Engineering was provided by a USDA-NIFA Grant (Carbon Monolith Catalysts from Wood for Biobased Platform Chemicals: 2017-67021-26136).

References

1. Mamman, A. S.; Lee, J. M.; Kim, Y. C.; Hwang, I. T.; Park, N. J.; Hwang, Y. K.; Chang, J. S.; Hwang, J. S., Furfural: Hemicellulose/xylosederived biochemical. *Biofuels, Bioproducts and Biorefining: Innovation for a sustainable economy* **2008,** *2* (5), 438-454.

2. Bartholomew, C. H.; Farrauto, R. J., *Fundamentals of industrial catalytic processes*. John Wiley & Sons: 2011.

3. Piancatelli, G.; Scettri, A.; Barbadoro, S., A useful preparation of 4-substituted 5-hydroxy-3-oxocyclopentene. *Tetrahedron Letters* **1976,** *17* (39), 3555-3558.

4. Fogler, H. S., Elements of Chemical Reaction Engineering, **1999**.

5. Mironenko, R. M.; Talsi, V. P.; Gulyaeva, T. I.; Trenikhin, M. V.; Belskaya, O. B., Aqueous-phase hydrogenation of furfural over supported palladium catalysts: effect of the support on the reaction routes. *Reaction Kinetics, Mechanisms and Catalysis* **2019,** *126* (2), 811-827.

6. El-Sheikh, A. H.; Newman, A. P.; Al-Daffaee, H.; Phull, S.; Cresswell, N.; York, S., Deposition of anatase on the surface of activated carbon. *Surface and Coatings Technology* **2004,** *187* (2-3), 284-292.

7. Toebes, M. L.; van Dillen, J. A.; de Jong, K. P., Synthesis of supported palladium catalysts. *Journal of Molecular Catalysis A: Chemical* **2001,** *173* (1-2), 75-98.

8. Weber, J.; Thompson, A.; Wilmoth, J.; Gulotty Jr, R. J.; Kastner, J. R., Coupling Red-Mud Ketonization of a Model Bio-Oil Mixture with Aqueous Phase Hydrogenation Using Activated Carbon Monoliths. *Energy & Fuels* **2017,** *31* (9), 9529-9541.

9. De Boer, J.; Linsen, B.; Van der Plas, T.; Zondervan, G., Studies on pore systems in catalysts: VII. Description of the pore dimensions of carbon blacks by the t method. *Journal of Catalysis* **1965,** *4* (6), 649-653.

10. Sitthisa, S.; Sooknoi, T.; Ma, Y.; Balbuena, P. B.; Resasco, D. E., Kinetics and mechanism of hydrogenation of furfural on Cu/SiO2 catalysts. *Journal of catalysis* **2011,** *277* (1), 1-13.

11. Srivastava, S.; Jadeja, G.; Parikh, J., Copper-cobalt catalyzed liquid phase hydrogenation of furfural to 2-methylfuran: An optimization, kinetics and reaction mechanism study. *Chemical Engineering Research and Design* **2018,** *132*, 313-324.

12. Rojas, H.; Martínez, J. J.; Reyes, P., Kinetic behavior in the hydrogenation of furfural over Ir catalysts supported on TiO2. *Dyna* **2010,** *77* (163), 151-159.

13. Borts, M.; Gil'chenok, N.; Gurevich, G.; Ignat'ev, V., Kinetics of vapor-phase hydrogenation of furfural on a copper-chromium catalyst. *J. Appl. Chem. USSR (Engl. Transl.);(United States)* **1986,** *59* (1 PT 2).

Table 6.1. Reaction parameters predicted from kinetic model

Temperature	K_{FUR}	K_{FA1}	K_{FA2}	K_{2MF}	K_{THFA}	K_{5H2P}	K_{H2}	$k_1^{"}$	$k_2^{"}$	$k_3^{"}$	$k_{11}^{"}$
°C	L/mol	L/mol	L/mol	L/mol	L/mol	L/mol	1/atm	mol/gcat.h	mol/gcat.h	mol/gcat.h	mol/gcat.h
180	0.113	0.585	0.144	0.002	0.001	0.182	0.17	1.925	0.506	0.269	0.973

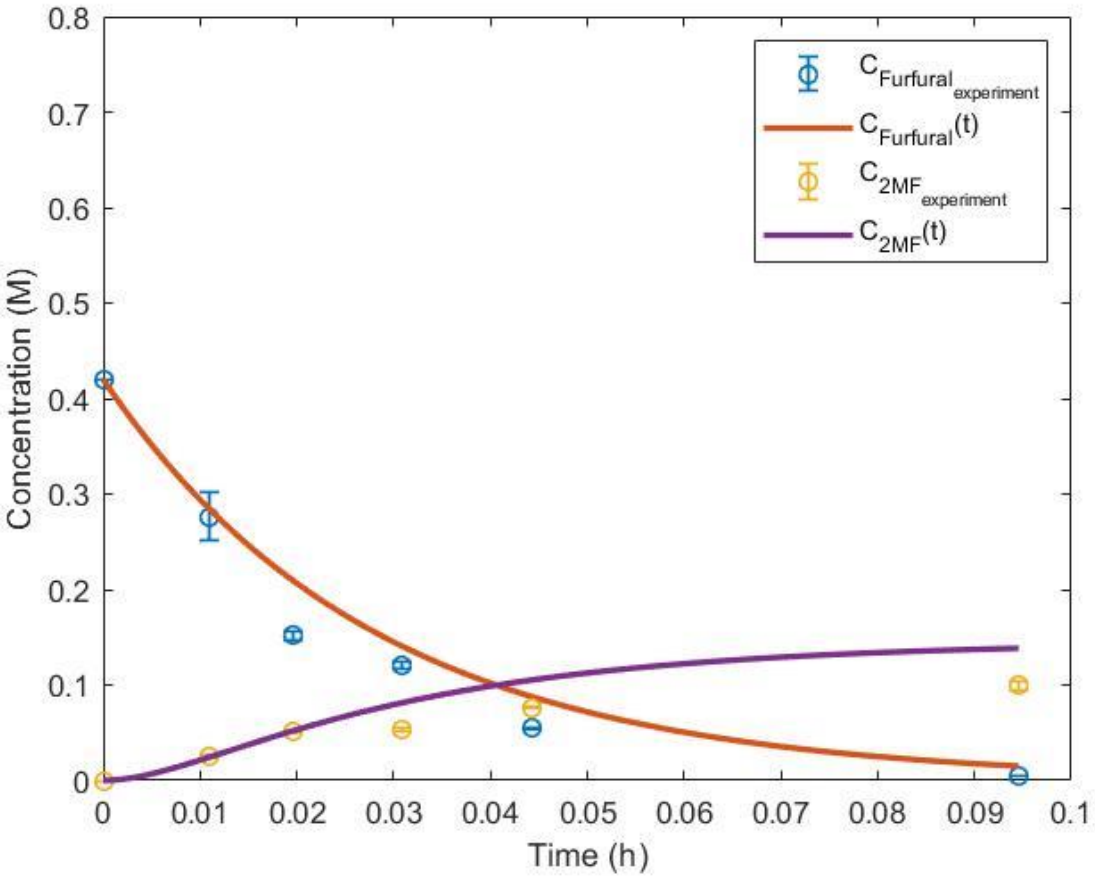

Figure 6.1. Comparison of predicted and experimental concentrations of 2MF.

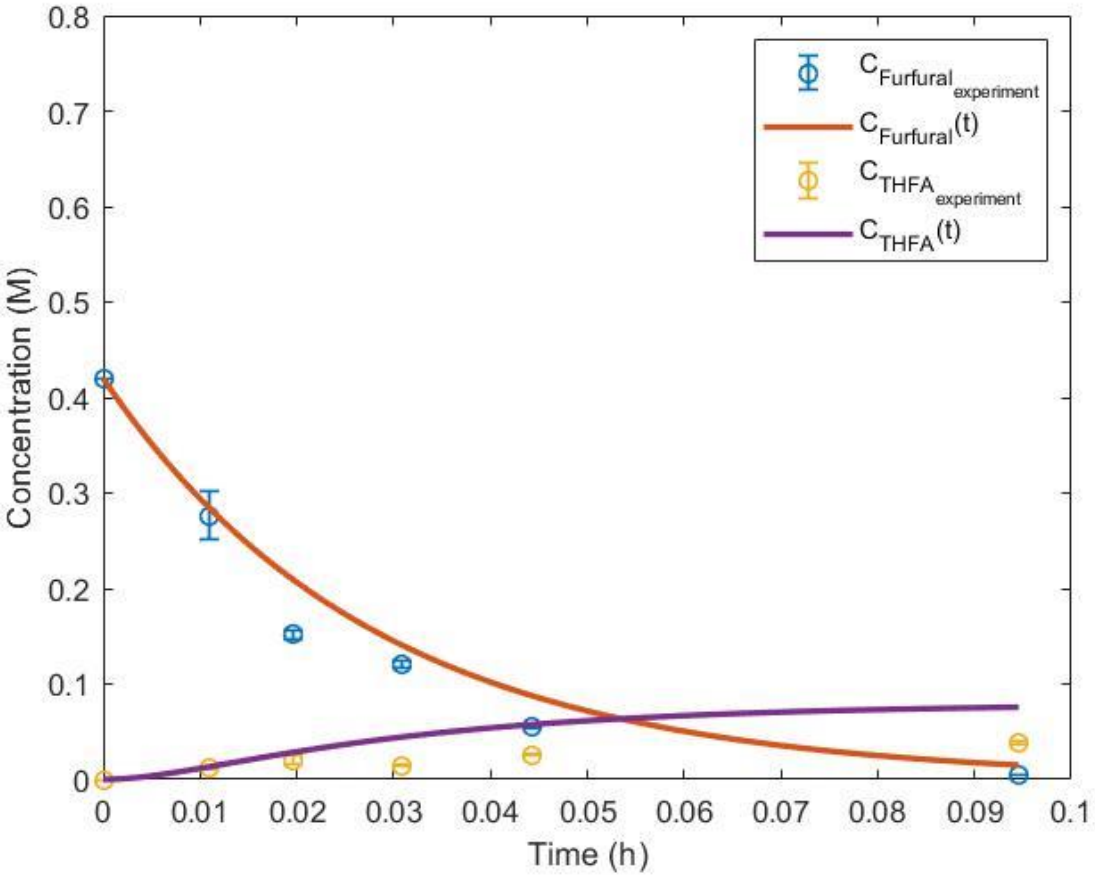

Figure 6.2. Comparison of predicted and experimental concentrations of THFA.

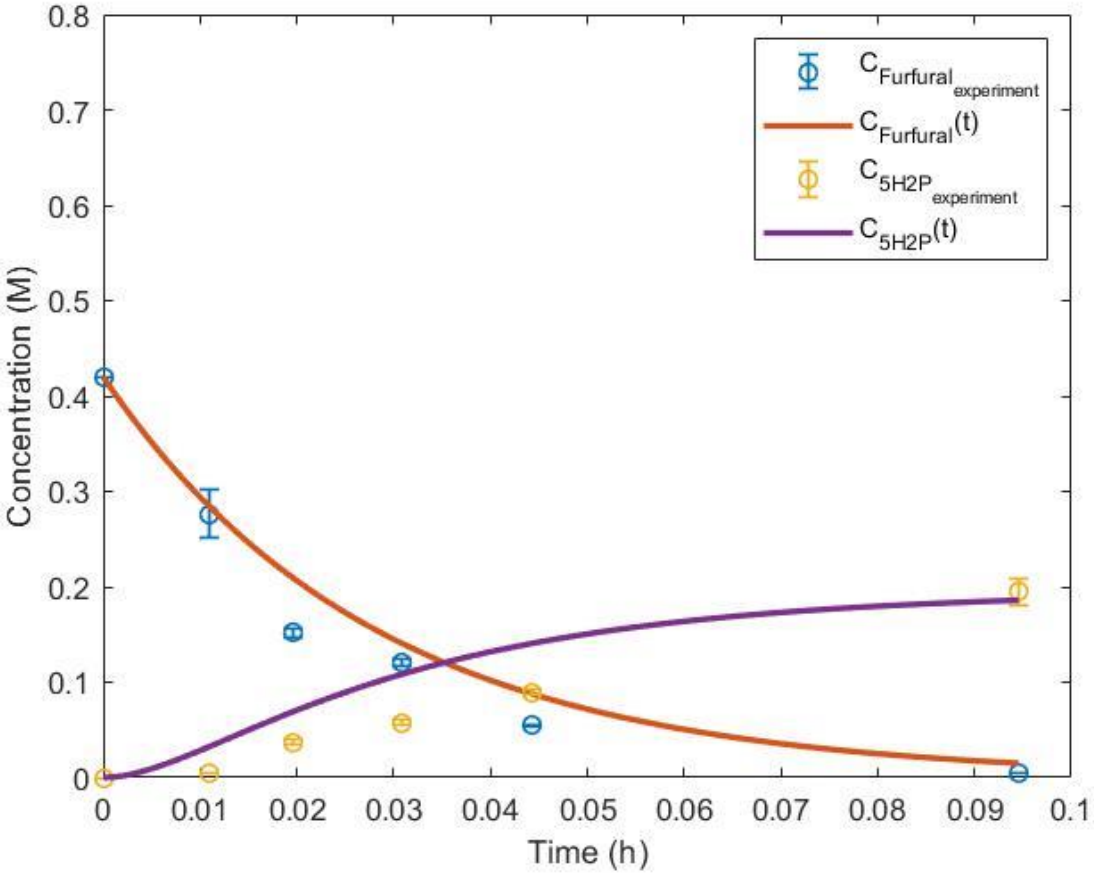

Figure 6.3. Comparison of predicted and experimental concentrations of 5H2P.

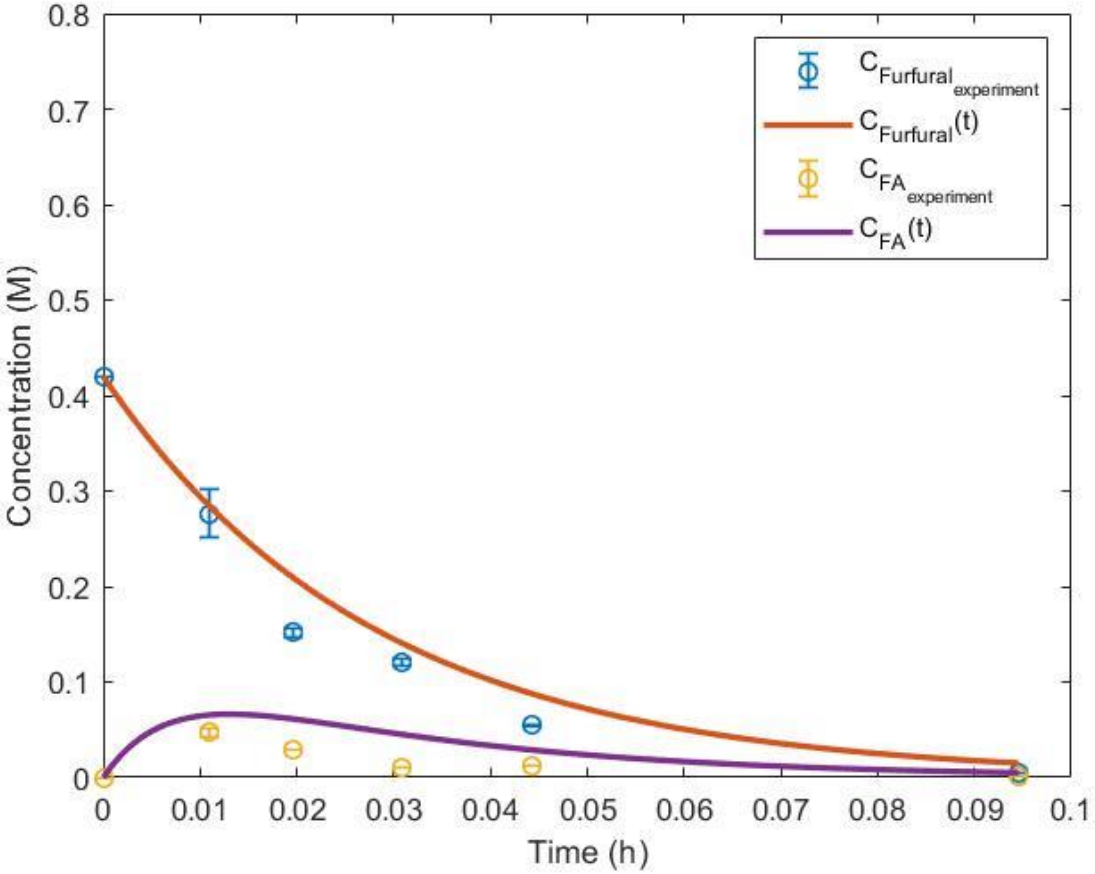

Figure 6.4 . Comparison of predicted and experimental concentrations of FA.

CHAPTER 7

CONCLUSIONS AND RECOMMENDATIONS

7.1 Conclusions

This work was aimed at contributing to the knowledge of activated carbon monolith catalysts as a substitute for conventional packed beds in three-phase hydrogenation reactions. Aqueous furfural, which can form a series of valuable products through hydrogenation reactions, was selected as a green and inexpensive feedstock. The results from this work is divided into four studies. The first study compares the powder, granular and monolith forms of Pd catalyst for furfural hydrogenation. Among the three catalysts, monolith was the only catalyst that did not show external mass transfer resistance for both hydrogen and furfural, which contributed to a lower activity loss and coke for monolith. These results make monolith catalyst, derived from activated carbon, a promising alternative for conventional granular or powder packed bed reactors. The second study involves selective hydrogenation of furfural to furfuryl alcohol and tetrahydrofurfuryl alcohol by adding a second metal to the Pd monolith carbon catalyst. Adding Cu and Fe as a second metal to Pd monolith catalyst resulted in the highest furfuryl alcohol and tetrahydrofurfuryl alcohol at 180 °C and 300 psig. The presence of these second metals on monolith catalyst stabilized Pd particles and reduced leaching. The third study is another selective hydrogenation of furfural using Pd-TiO_2 on crushed activated carbon monolith. TiO_2 added weak acid sites to Pd catalyst resulting in furan ring opening and formation of 5-hydroxy-2-pentanone. The highest yield of 5-hydroxy-2-pentanone was achieved at 180 °C and 300 psig.

The last chapter involves developing a rate law for hydrogenation of furfural over Pd-TiO_2 catalyst using Langmuir-Hinshelwood mechanism. A satisfactory agreement was observed between the experimental data and the kinetic model. The reaction parameters including adsorption constants and reaction rate constants were derived from the kinetic model.

7.2 Recommendations

Transitioning to Pd-TiO_2 activated carbon monolith catalyst from the crushed form, the kinetic model can be coupled with monolith heat and mass transfer models to predict the required number of monolith catalysts for future furfural hydrogenation works using Pd-TiO_2 on activated carbon monolith catalyst. Due to high reactivity of titanium (IV) isopropoxide during catalyst synthesis, it is difficult to reach high dispersions of TiO_2 using direct air-hydrolysis method, especially for monolith structures. Therefore, it is recommended to test other methods such as incipient wetness impregnation of TiO_2 followed by calcination for synthesis of the activated carbon monolith catalyst. It is important to determine the effect of catalyst preparation method on product selectivity.

Additional studies on scalability and economics of activated carbon monolith for hydrogenation of furfural are necessary. In industrial scale reactions, catalyst deactivation is an important factor in economic analysis. The cost of a new catalyst, lower reaction rates during deactivation and reactor shut down during replacement or regeneration of the catalyst are factors that affect the economy of a catalytic process. Studying the catalyst deactivation by continuous operation of the reactor system for at least 360 hours, where the reaction rate is measured every 12 hours, is recommended to perform activity analysis. In addition, physical and mechanical durability of monolith structure needs to be tested for scale-up.

There have been very few studies in the literature on application of activated carbon monolith catalysts for three-phase reactions. Other than hydrogenation of furfural, there are other important hydrogenation reactions such as hydrogenation of muconic acid to adipic acid, that can employ activated carbon monolith catalysts. It is important to consider that depending on the type of carbon source and binder employed in the structure of the activated monolith catalyst, different active sites can be involved in the reaction. Therefore, the catalyst characterization results of activated carbon monolith in this work does not translate to other types of activated carbon monolith with different carbon source and binder.

APPENDIX A

SUPPLEMENTARY DATA FOR CHAPTER 3

Mass Transfer Analysis

Mears and Weisz-Prater (Equation S3.1 and Equation S3.4) criteria were applied for mass transfer analysis (Fogler, 1986). Hydrogenations using the granular activated carbon and Powder C forms in the packed bed reactor were considered as a trickle bed reactor. Therefore, we considered external and internal mass transfer as the two major resistances in the system. The large particle size of the Pd on granular activated carbon catalyst (d ~ 3 mm) indicated that furfural hydrogenation may have been affected by external and internal mass transfer. Based on Mears criterion if the following equation is smaller than 0.15, the system is not limited by external mass transfer resistance (eq. S3.1).

$$\frac{r_{furfural}\,\rho_b R\,n}{k_c\,C_{furfural}} < 0.15 \qquad \text{Equation S3.1}$$

where, r is the reaction rate of the furfural or hydrogen (mol g^{-1} s^{-1}), ρ_b is the bulk density of the catalyst bed (g m^{-3}), R is the particle radius (unit: m; R = 2.5* 10^{-4} m for the Pd/Powder C and 3 * 10^{-3} m for Pd on granular activated carbon), n the order of the reaction (usually assumed to be first or second order), k_c (m s^{-1}) the mass-transfer coefficient (Equation S3.2), D_{AB} is the effective diffusivity of the furfural or hydrogen in water (Equation S3.3; Wilke and Chang 1955), C is the bulk liquid phase concentration of the furfural or hydrogen (mol m^{-3}).

$$k_c = 0.266\left(\frac{D_{AB}}{d_p}\right)\mathrm{Re}^{1.15}\, Sc^{1/3} \qquad \text{Equation S3.2}$$

$$D_{AB} = 1.17x^{-13}\left(\frac{\left(M_B\xi\right)^{1/2}T}{\mu_B V_A^{0.6}}\right) \qquad \text{Equation S3.3}$$

The total moles of product (furfuryl alcohol [FA], tetrahydrofurfuryl alcohol [THFA], 2-methyl furan [2MF], cyclopentanone [CP], and 5-hydroxy-2-pentanone [5H2P]) produced per mass of catalyst per time were used to estimate hydrogen reaction rates. We assumed 1, 2, 2, 1, 2, and 2 moles of H_2 were consumed per mole of FA, THFA, 2MTHF, 2MF, CP, and 5H2P.

To study internal mass transfer resistance the Wiesz-Prater criterion (C_{WP}), Equation S3.4, was applied (Fogler, 1986). Based on Weisz-Prater criterion if the following equation is much smaller than1, the system is not limited by internal mass transfer resistance:

$$C_{WP} = \frac{r_{furfural}\,\rho_p R^2}{D_{eff}\,C_{furfural,s}} << 1 \qquad \text{Equation S3.4}$$

r is the furfural or hydrogen reaction rates, ρ_p is the bulk density, D_{eff} is the effective diffusivity and R is the catalyst radius. Equation S3.5 was applied to estimate effective diffusivity.

$$D_{eff} = \frac{D_{AB}\varepsilon_{particle}}{\tau_{particle}} \qquad \text{Equation S3.5}$$

For activated carbon monolith, the gas to liquid velocity ratio was ranged from 71.4 to 6.3, an indicator of film and annular flow patterns. In film flow, gas transfer occurs through a thin film. Based on the presence of thin film, mass transfer coefficient was estimated using Equation S3.6 (Han and Shikazono, 2009).

$$k_{GS} = \left(\frac{D_{AB}}{\delta_F} \right)$$ Equation S3.6

where, k_{GS} is the mass transfer coefficient; D_{AB} is diffusivity of the furfural or H_2; δ_F is the film thickness.

The results of Mears and Wiesz-Prater criterion calculations are shown in Table S3.2 and S3.3.

Table S3.1. Elemental analysis of fresh and spent carbon catalysts

Elements	**Pd/ACM**	**Pd/ACM**	**Pd/GAC**	**Pd/GAC**	**Pd/Powder C**	**Pd/Powder C**
(ppm, mg/kg)	Fresh	Spent	Fresh	Spent	Fresh	Spent
Aluminum (Al)	548	ND	11.9	ND	191	ND
Boron (B)	17.8	ND	3.87	ND	2.59	ND
Cadmium (Cd)	<2	ND	<1	ND	<2	ND
Calcium (Ca)	<100	ND	291	ND	586	ND
Chromium (Cr)	27	ND	<1	ND	19.3	ND
Copper (Cu)	<10	ND	6.98	ND	11.2	ND
Iron (Fe)	2229	ND	17.8	ND	126	ND
Lead (Pb)	<0.77	ND	<0.39	ND	<0.77	ND
Magnesium (Mg)	<20	ND	331	ND	366	ND
Manganese (Mn)	<10	ND	6.81	ND	<10	ND
Molybdenum (Mo)	<2	ND	<1	ND	<2	ND
Nickel (Ni)	7.37	ND	<1	ND	3.79	ND
Palladium (Pd)	**11,932 (1.2%)**	**9,539 (0.95%)**	**5609 (0.56%)**	**3.0 (3x10^{-4}%)**	**47604 (4.8%)**	**29,042 (2.9%)**
Phosphorus (P)	351	ND	236	ND	126	ND
Potassium (K)	105	ND	6808	ND	<100	ND
Silicon (Si)	125	ND	109	ND	<100	ND
Sodium (Na)	1199	ND	668	ND	3550	ND
Sulfur (S)	25.6	ND	61.6	ND	1187	ND
Zinc (Zn)	<10	ND	<5	ND	<10	ND

ND – not determined

Table S3.2. Estimated Mears criterion for Pd/Powder C, Pd/GAC, and Pd/ACM

	Pd/Powder C			Pd/GAC			Pd/ACM			
Q_g/Q_l	LHSV (h^{-1})	Mears FUR	Mears H_2	LHSV (h^{-1})	Mears FUR	Mears H_2	LHSV (h^{-1})	Mears FUR n=2	Mears H_2 n=2	Mears H_2 n=1
200	1.5	0.15	1.7	1.3	1.02	10.2	-	-	-	-
100	3.0	0.13	2.45	2.6	0.83	13.9	-	-	-	-
71.4	-	-	-	-	-	-	1.3	$1.1x10^{-6}$	$1.9x10^{-5}$	$9.5x10^{-6}$
50	6.1	0.10	0.84	5.3	0.58	6.7	1.9	$1.7x10^{-6}$	$3.1x10^{-5}$	$1.5x10^{-5}$
25	12.2	0.07	0.38	10.6	0.45	5.4	3.8	$2.4x10^{-6}$	$2.5x10^{-5}$	$1.2x10^{-5}$
12.5	-	-	-	-	-	-	7.7	$4.7x10^{-6}$	$6.1x10^{-5}$	$3.1x10^{-5}$
6.3	-	-	-	-	-	-	15.4	$5.6x10^{-6}$	$4.2x10^{-5}$	$2.1x10^{-5}$

Q_g is gas flow rate; Q_l is liquid flowrate; LHSV = $(Q_l*\rho_B)/W_{cat}$; W_{cat} is amount of catalyst
$D_{AB(furfural)} = 9.42x10^{-9}$ m^2/s; $D_{AB\ (H2)} = 4.6x10^{-9}$ m^2/s
$D_{eff\ (furfural)} = 1.2x10^{-9}$ m^2/s; $D_{eff\ (H2)} = 5.7x10^{-9}$ m^2/s
Tortuosity Factor = 4; Internal Void Fraction = 0.5; n or reaction order = 2, except where noted
Bulk Liquid Phase Concentrations: $C_{FUR} = 0.5$ mol/L; $C_{H2} = 0.009$ mol/L
kc is the mass-transfer coefficient, m/s; δ is the film thickness, m
σ is surface tension and was assumed as 0.06 N/m (for water)
$\rho_B = 0.254$ g/ml, bulk density of Pd/Powder C; $\rho_B = 0.22$ g/ml, bulk density of Pd/GAC
$\rho_P = 0.25$ g/ml, packing density of Pd/ACM , $R = d_p/2$ for granules and Wall thickness/2 for ACM

Table S3.3. Estimated intraparticle mass transfer limitations for Pd-carbon catalysts (300 psig, 180 °C)

	Pd/Powder C			Pd/GAC			Pd/ACM		
Q_g/Q_l	LHSV (h^{-1})	$C_{WP,FUR}$	$C_{WP,H2}$	LHSV (h^{-1})	$C_{WP,FUR}$	$C_{WP,H2}$	LHSV (h^{-1})	$C_{WP,FUR}$	$C_{WP,H2}$
200	1.5	0.006	0.04	1.3	0.7	4.1	-	-	-
100	3.0	0.011	0.124	2.6	1.24	12.3	-	-	-
71.4	-	-	-	-	-	-	1.3	0.005	0.08
50	6.1	0.02	0.10-0.17	5.3	1.93-1.96	13-14	1.9	0.007	0.13
25	12.2	0.03	0.095	10.6	3.3	23.7	3.8	0.01	0.10
12.5	-	-	-	-	-	-	7.7	0.019	0.25
6.3	-	-	-	-	-	-	15.4	0.022	0.16

Q_g is gas flow rate; Q_l is liquid flowrate; FUR is furfural; LHSV = $(Q_l*\rho_B)/W_{cat}$; C_{WP} = Wiesz-Prater criterion.

W_{cat} is catalyst weight.

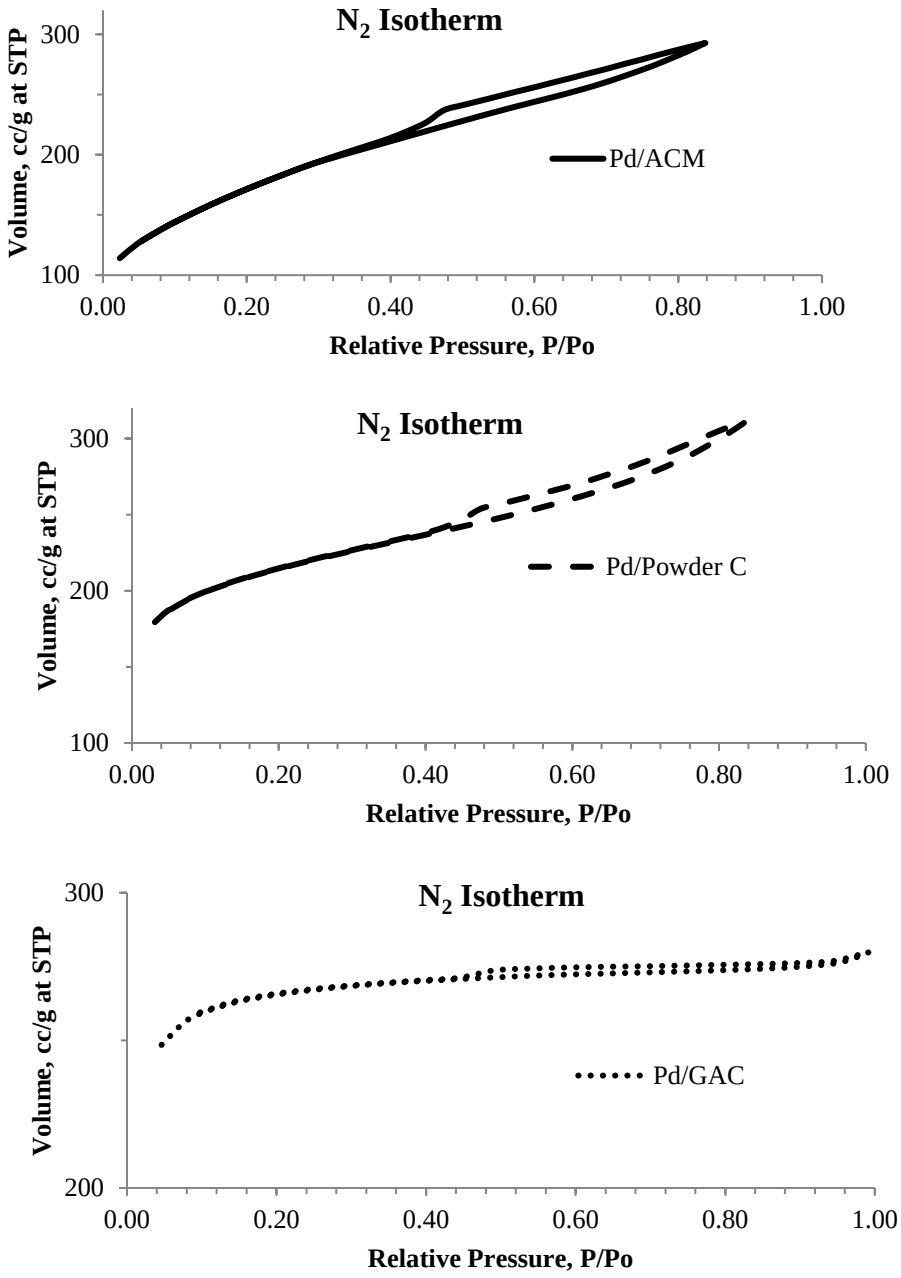

Figure S3.1. Isotherms of fresh Pd on carbon catalysts (ACM, GAC, and Powder C).

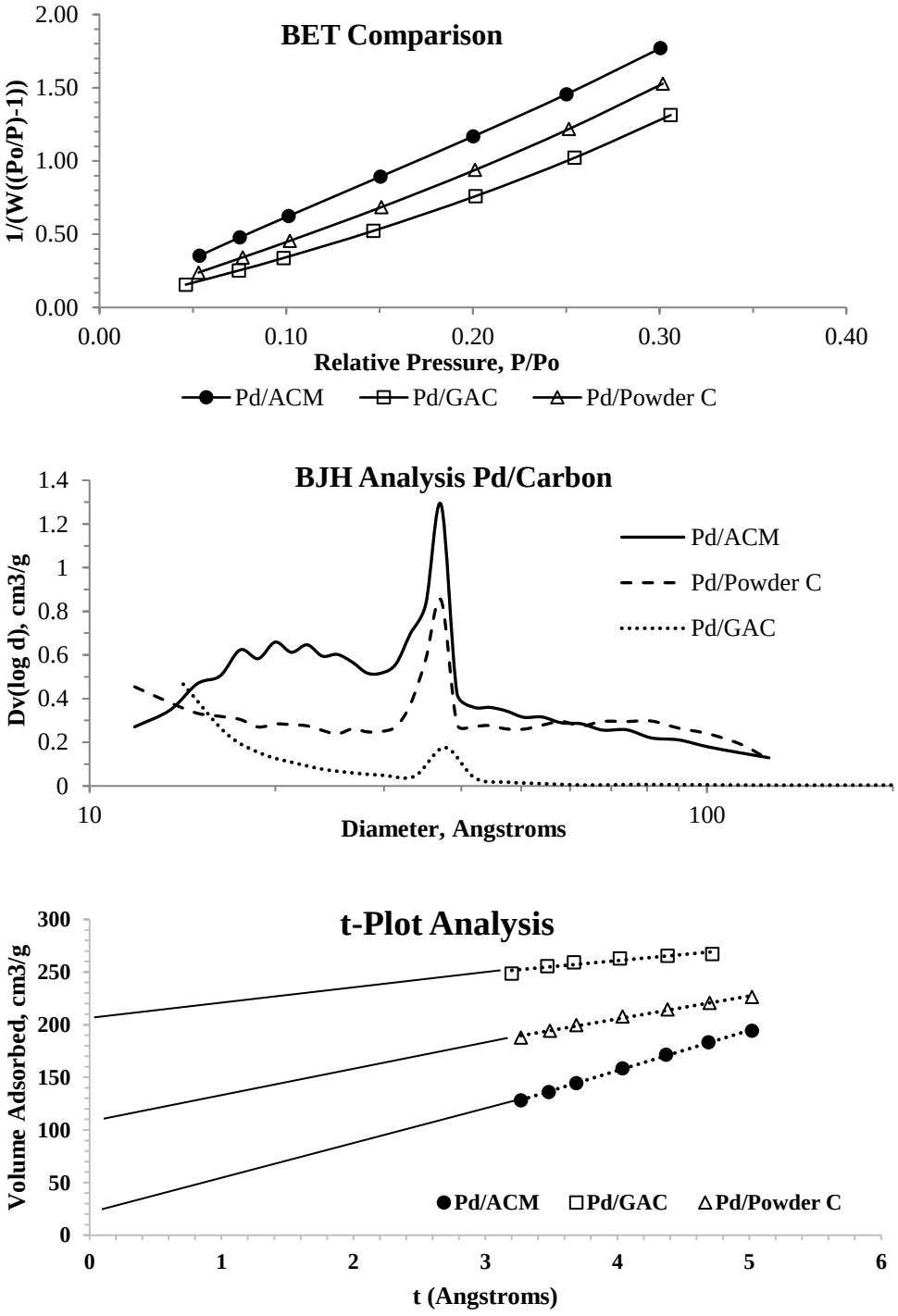

Figure S3.2. Surface area, BJH and t-plot analysis of fresh Pd on carbon catalysts (ACM, GAC, and powder). Intercepts for the t-plots were 3.2, 214, and 118 cm^3/g for Pd/ACM, Pd/GAC, and Pd/Powder C, respectively.

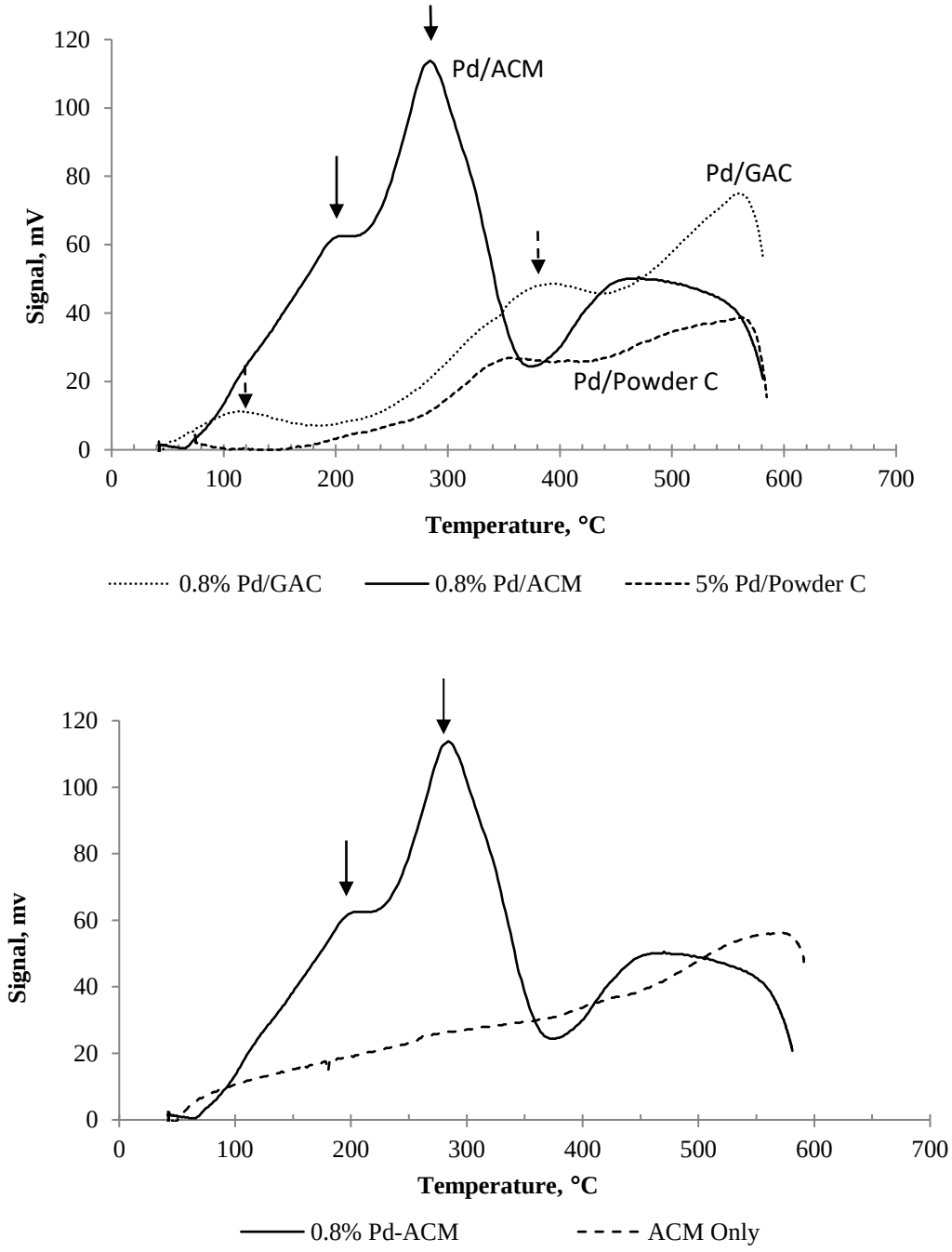

Figure S3.3-A. Temperature programmed hydrogen reduction (H_2-TPR) of Pd on carbon catalysts and the base activated carbon monolith only (ACM).

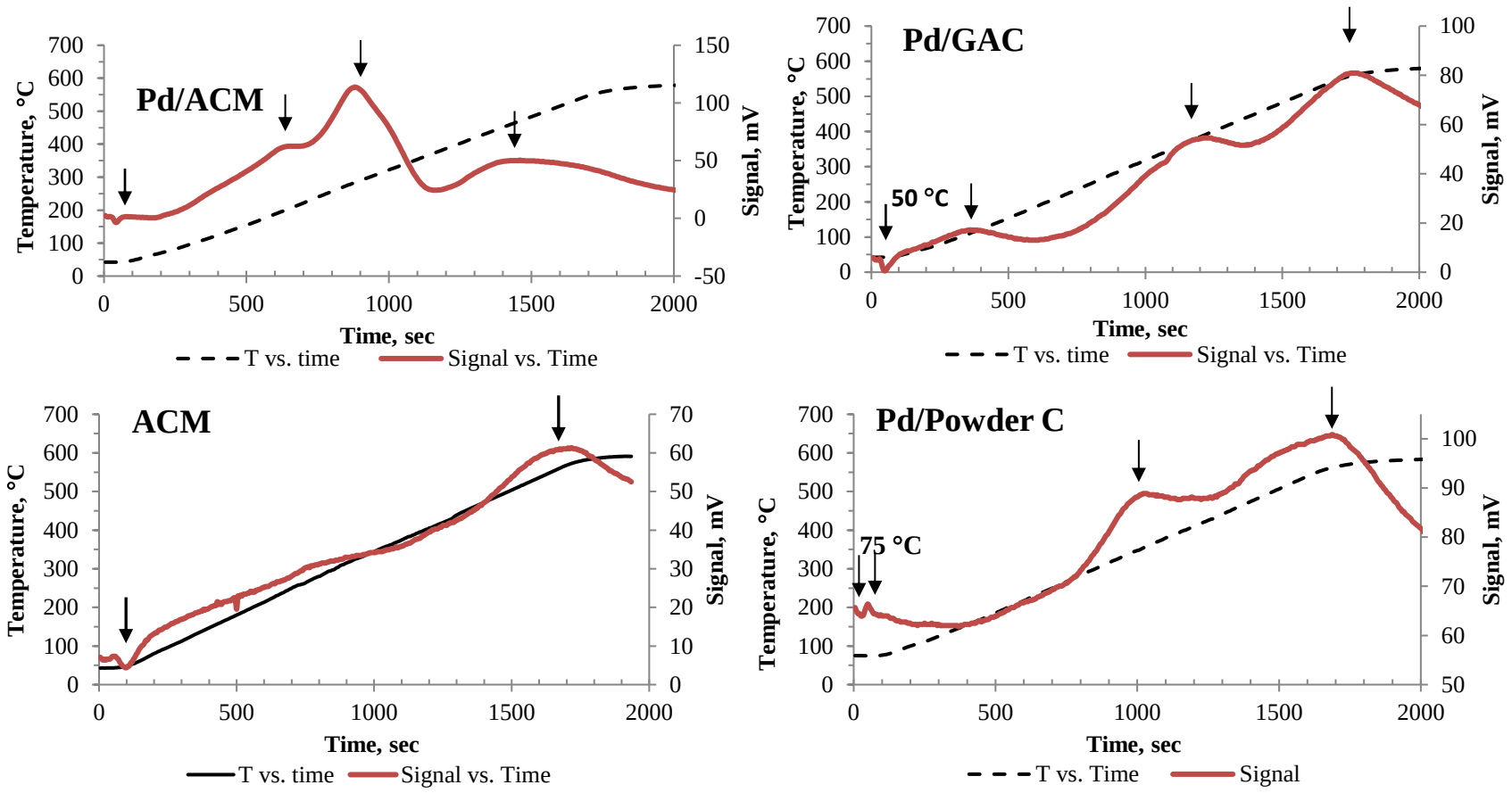

Figure S3.3-B: Temperature programmed hydrogen reduction of Pd (temperature vs. time and signal vs. time) on carbon catalysts and the base activated carbon monolith only (ACM).

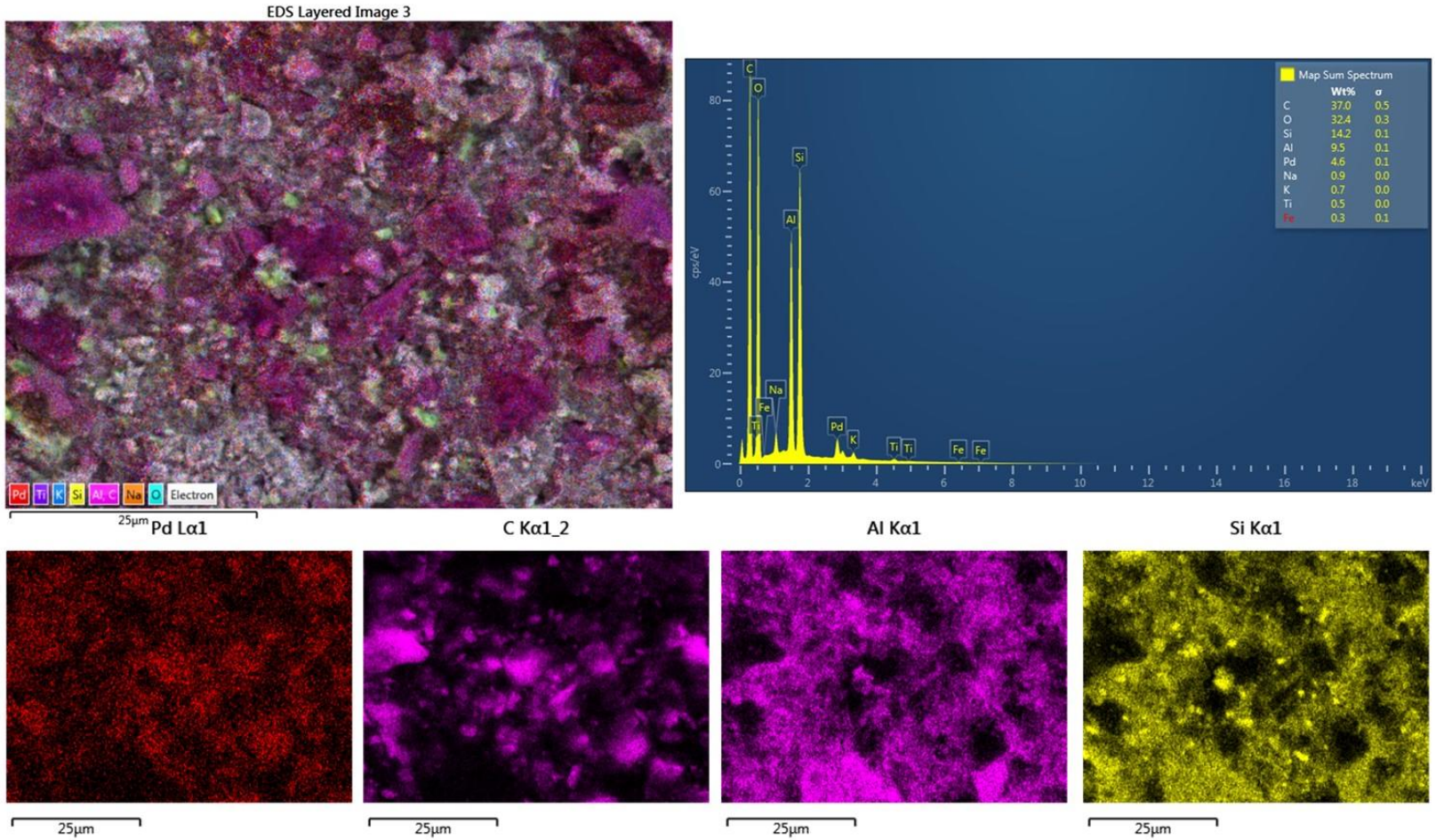

Figure S3.4. SEM-EDS analysis of the Pd/ACM catalysts (fresh). Pd is concentrated on the carbon, but also distributed on Al and Si indicative of locations in some areas of the ceramic binder.

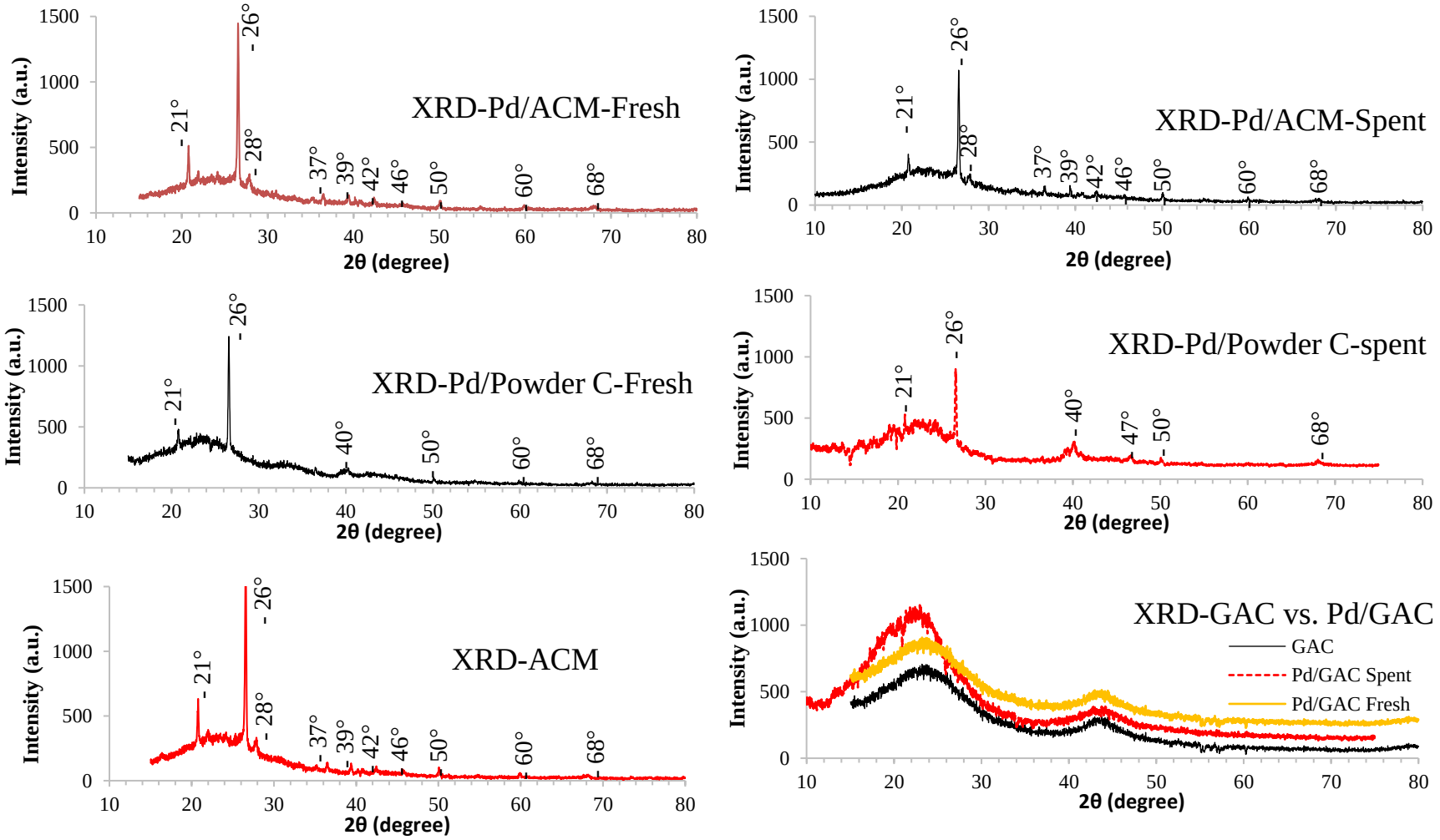

Figure S3.5. XRD analysis of Pd catalysts.

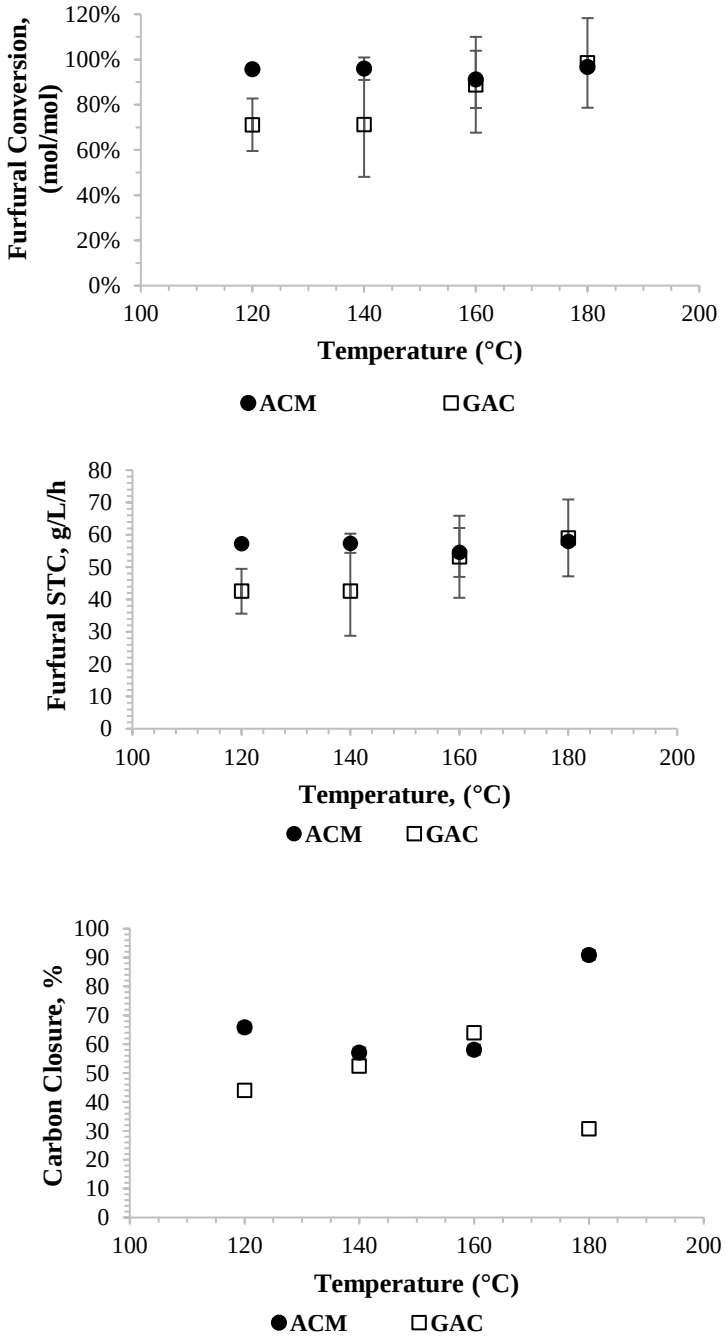

Figure S3.6. Effect of reaction temperature on furfural conversion, carbon closure, and furfural space time conversion.

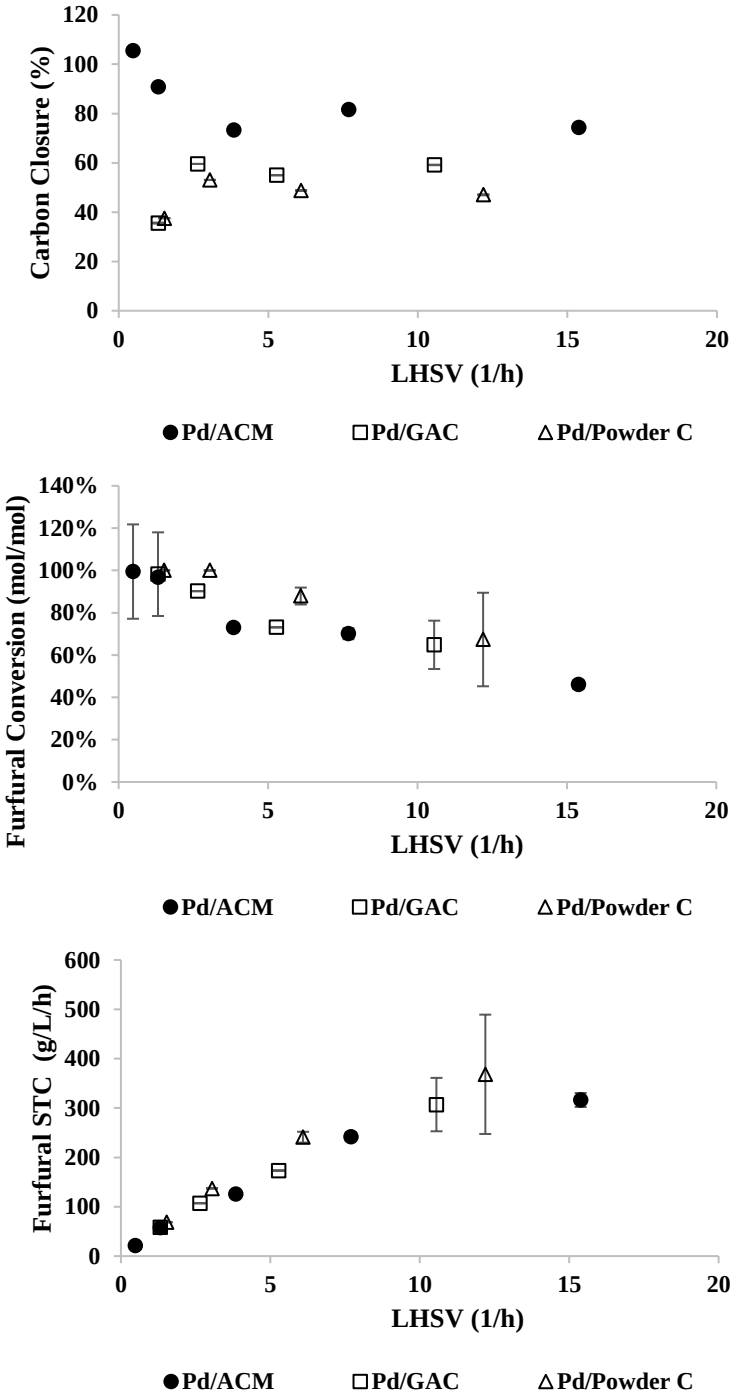

Figure S3.7. Effect of liquid residence time on furfural conversion and carbon closure for hydrogenation at 180°C and 300 psig (2 MPa) using Pd/ACM, Pd/GAC, and Pd/PowderC. LHSV is liquid hourly space velocity based on inlet conditions. STC is space time conversion, g furfural converted/L-cat./h.

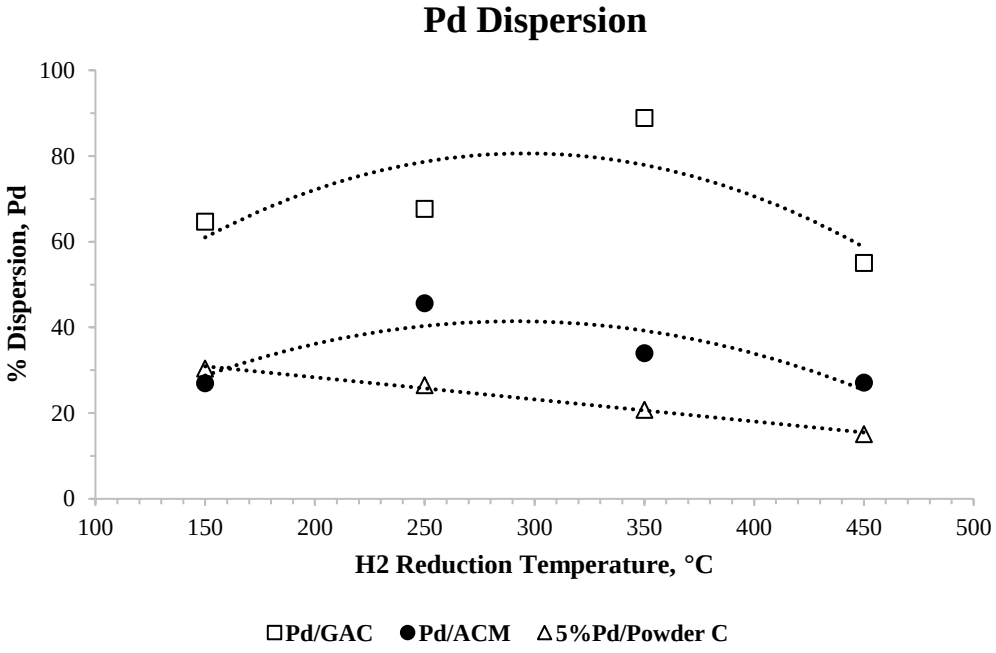

Figure S3.8. Effect of H_2 reduction temperature (as reported in section 3.2) on Pd dispersion measured by CO pulse titration on carbon supported catalysts (~0.8 wt% Pd on GAC and ACM).

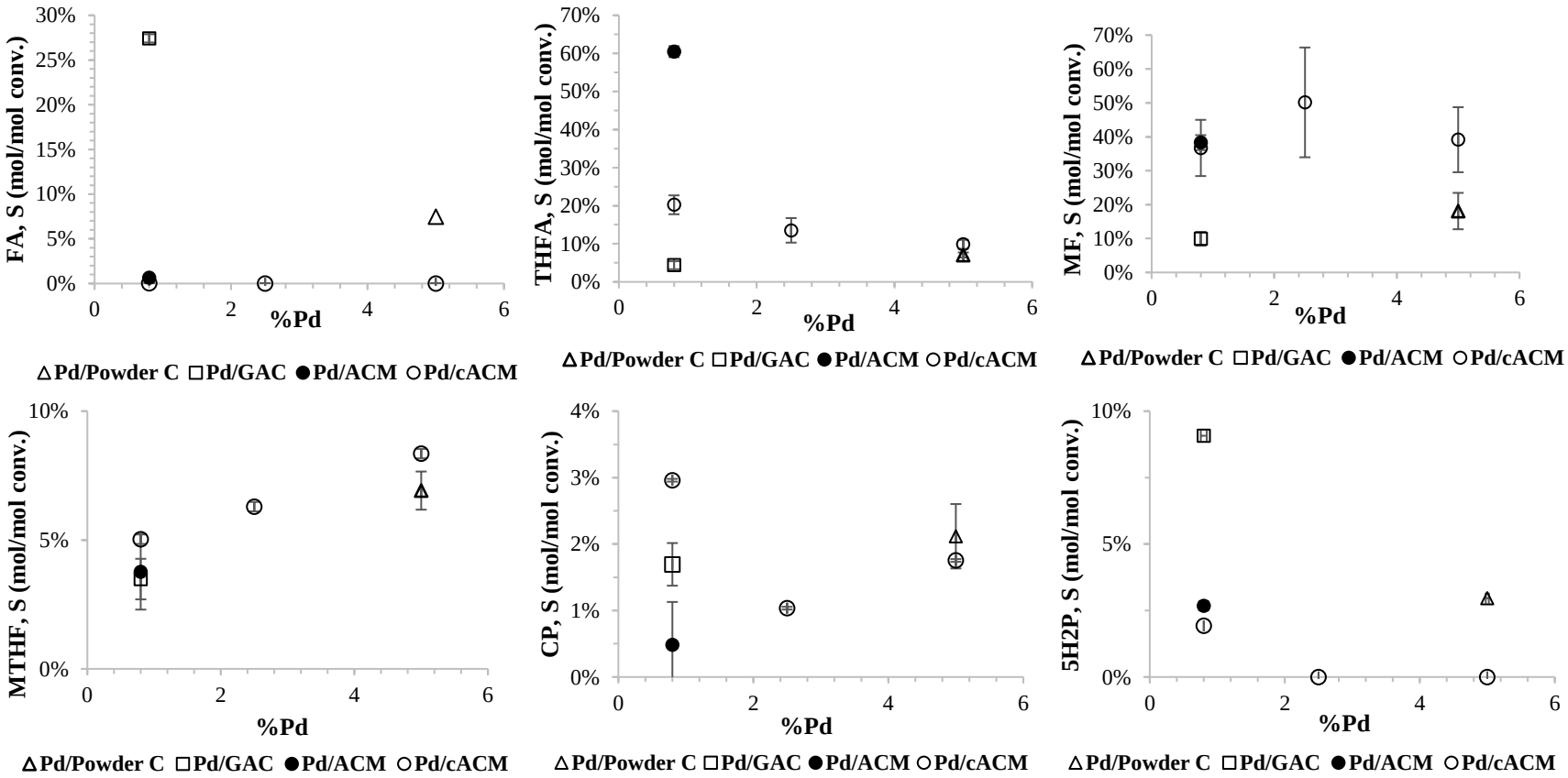

Figure S3.9. Effect of Pd loading on product selectivity using carbon supported catalysts (FA, furfuryl alcohol; THFA, tetrahydrofurfuryl alcohol; 2MF, 2-methyl furan; 2MTHF, 2-methyltetrahydrofuran; 5H2P, 5-hydroxy-2-pentanone; CP, cyclopentanone). Reactions were performed at 180°C, 300 psig (2.07 MPa), and LHSV from 1.3-1.5 h^{-1}. cACM indicates crushed ACM.

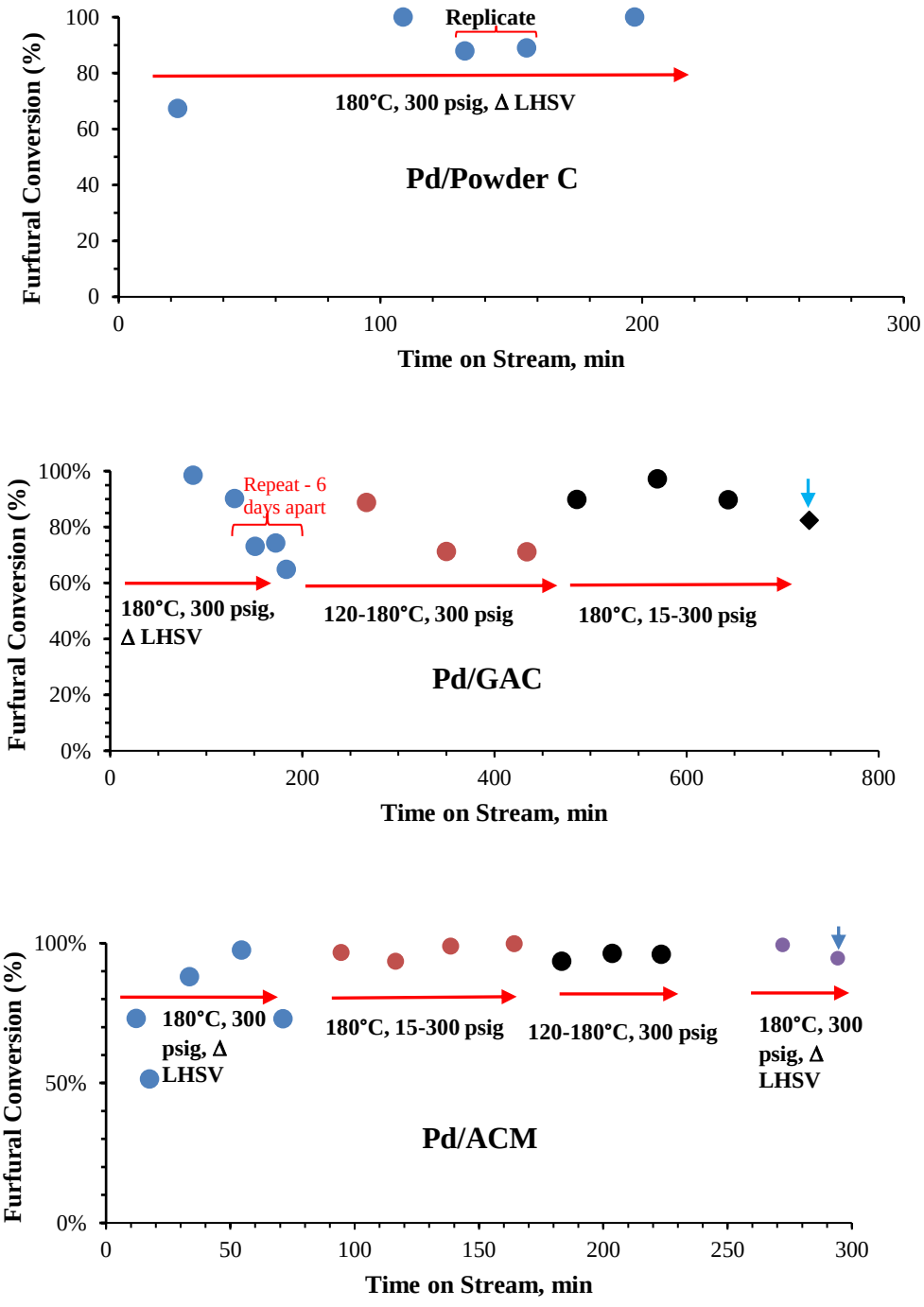

Figure S3.10. Time on stream analysis for furfural hydrogenation using Pd/carbon catalysts. The arrows indicate the experiment in which acetic acid was added to the feed.

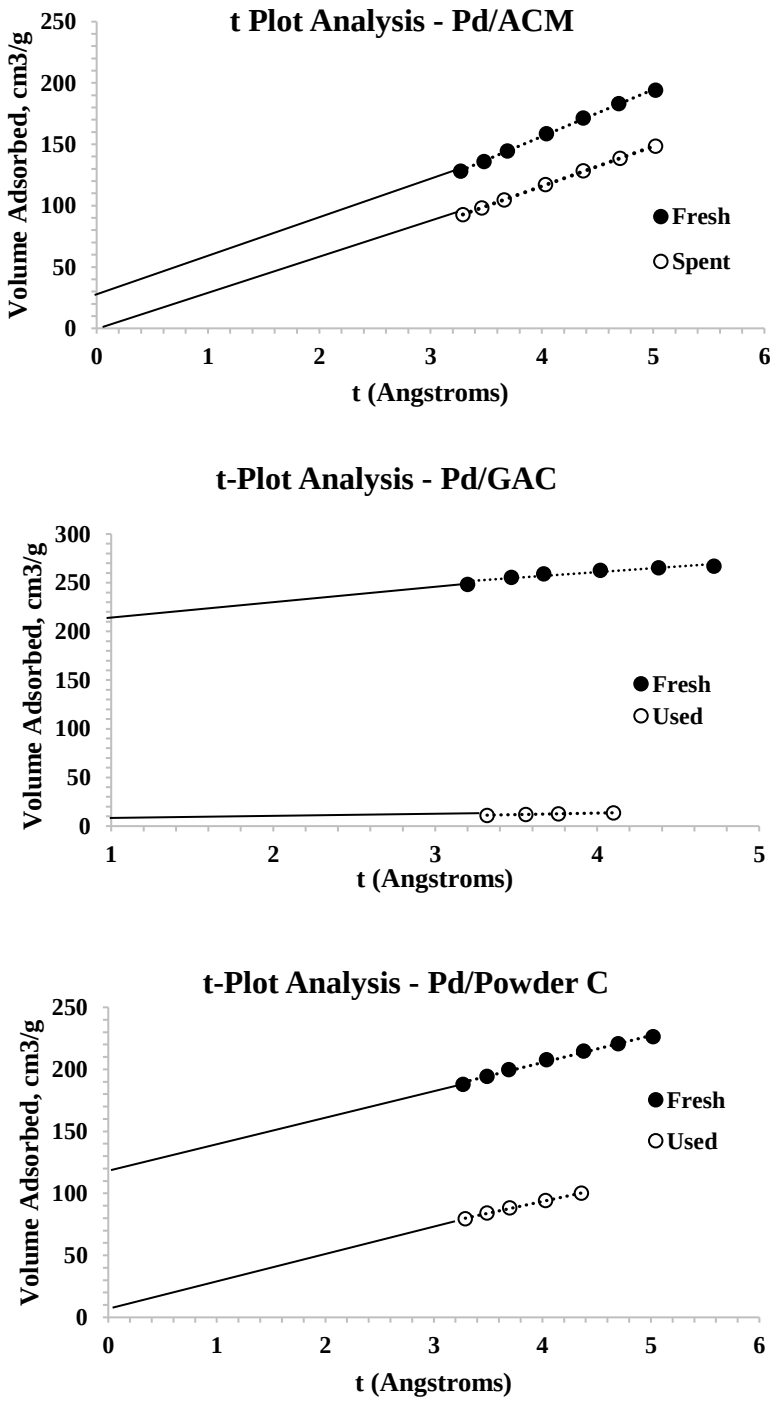

Figure S3.11. t-plot analysis of used/spent and fresh Pd on carbon catalysts (ACM, GAC, and powder C). Intercepts for the t-plots and used catalysts were 10.3, 0.0, 0.0, and 17.0 cm^3/g for, Pd/ACM, Pd/GAC, and Pd/Powder C, respectively.

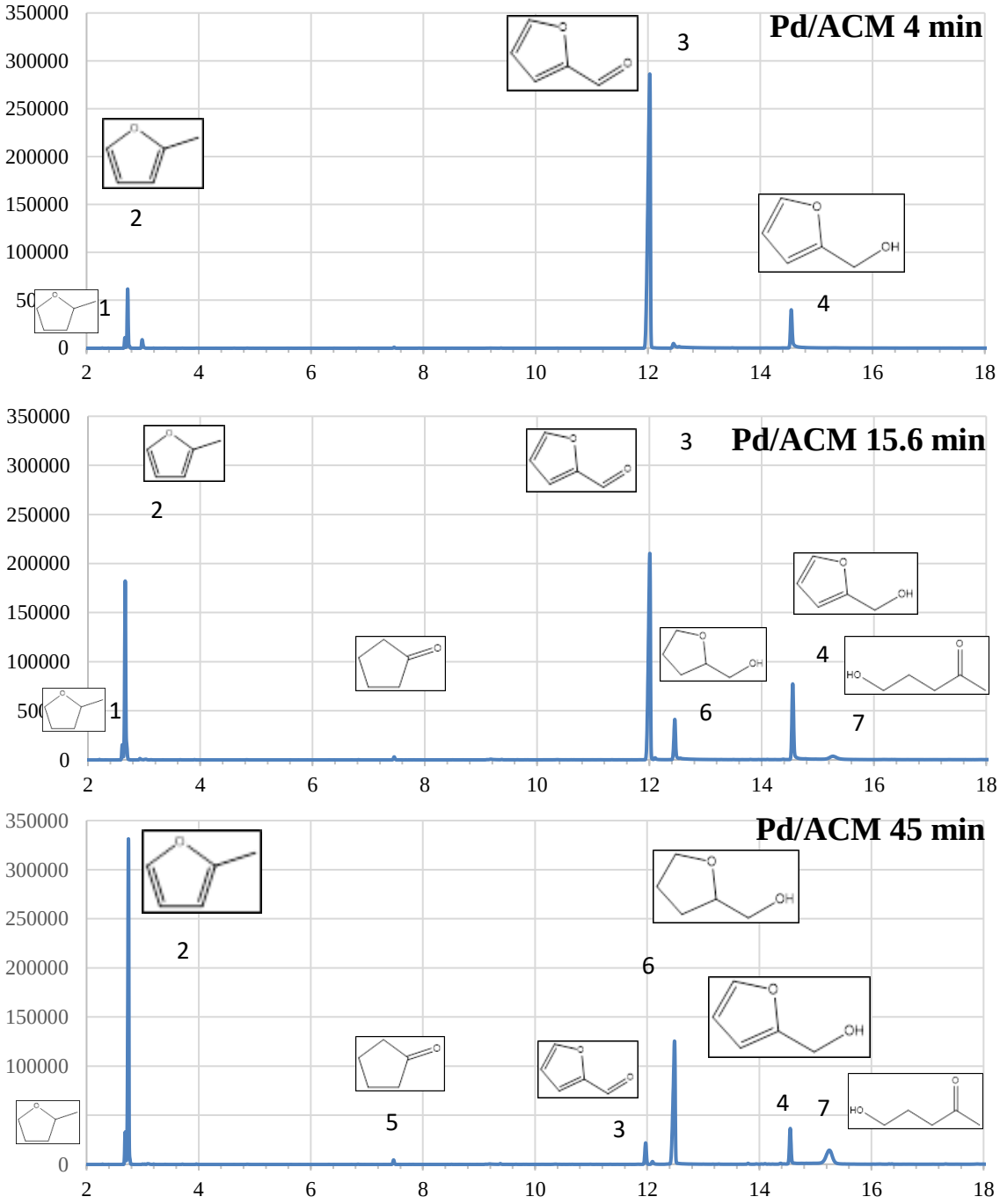

Figure S3.12. GC/FID chromatograms (signal vs. time) of samples at different LHSV's or liquid contact times from the continuous catalytic hydrogenation of furfural using Pd/ACM. Compounds shown are 1) 2-methyl tetrahydrofuran, 2) 2-methyl furan, 3) furfural, 4) furfuryl alcohol, 5) cyclopentanone, 6) tetrahydrofurfuryl alcohol, and 7) 5-hydroxy-2-pentanone.

APPENDIX B

SUPPLEMENTARY DATA FOR CHAPTER 4

This section contains chapter 4 supplementary information:

1. Expanded TPR analysis

2. Expanded SEM-EDS analysis

3. XRD analysis

4. Effect of temperature, pressure and liquid hourly space velocity on furfural conversion and carbon balance

5. Effect of temperature and pressure on product space time yield

6. Effect of acetic acid on furfural conversion

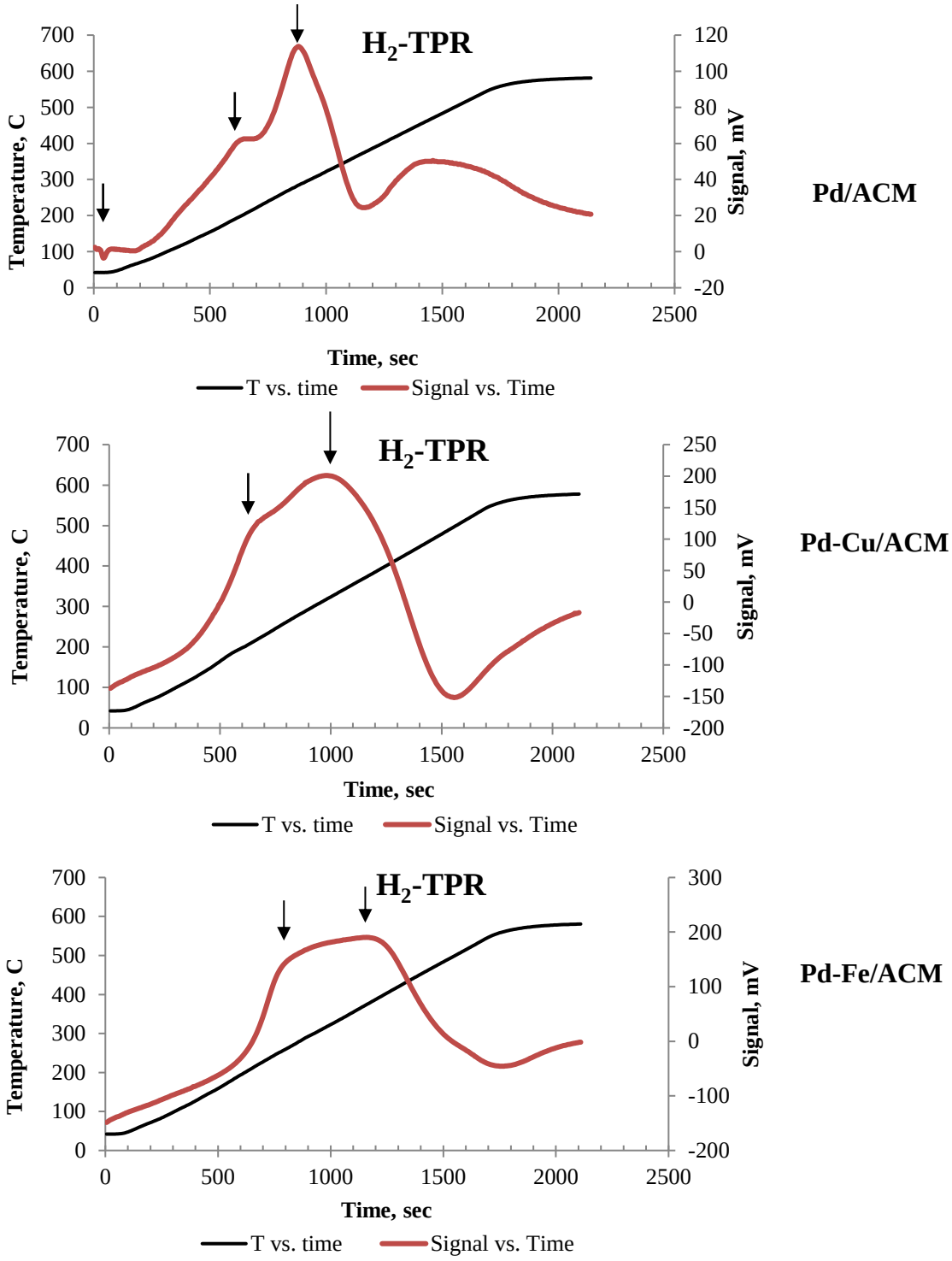

Figure S4.1. Expanded TPR analysis of monolith catalysts.

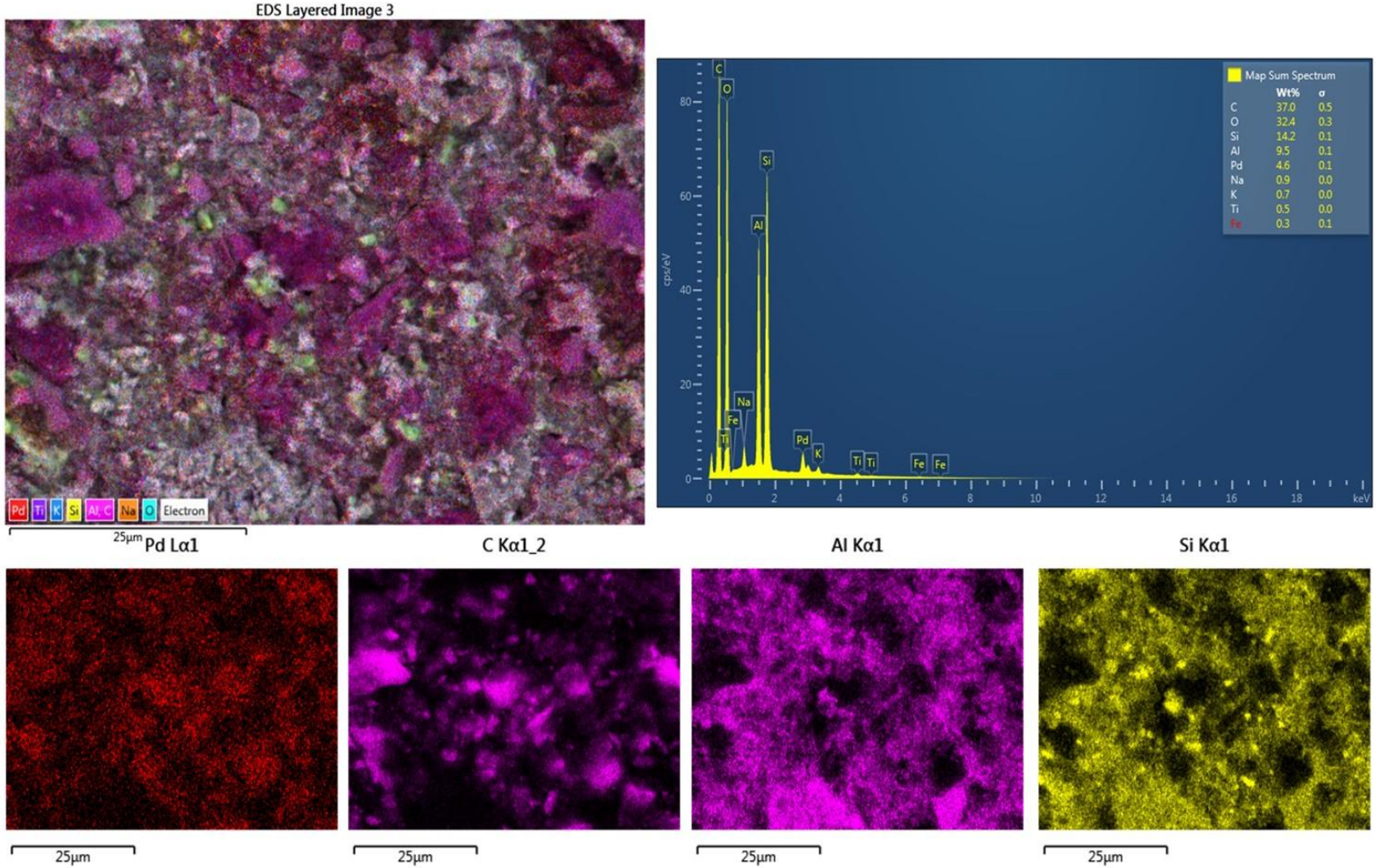

Figure S4.2. SEM-EDS analysis of the Pd/ACM catalysts (fresh). Pd is concentrated on the carbon, but also distributed on Al and Si indicative of locations in some areas of the ceramic binder.

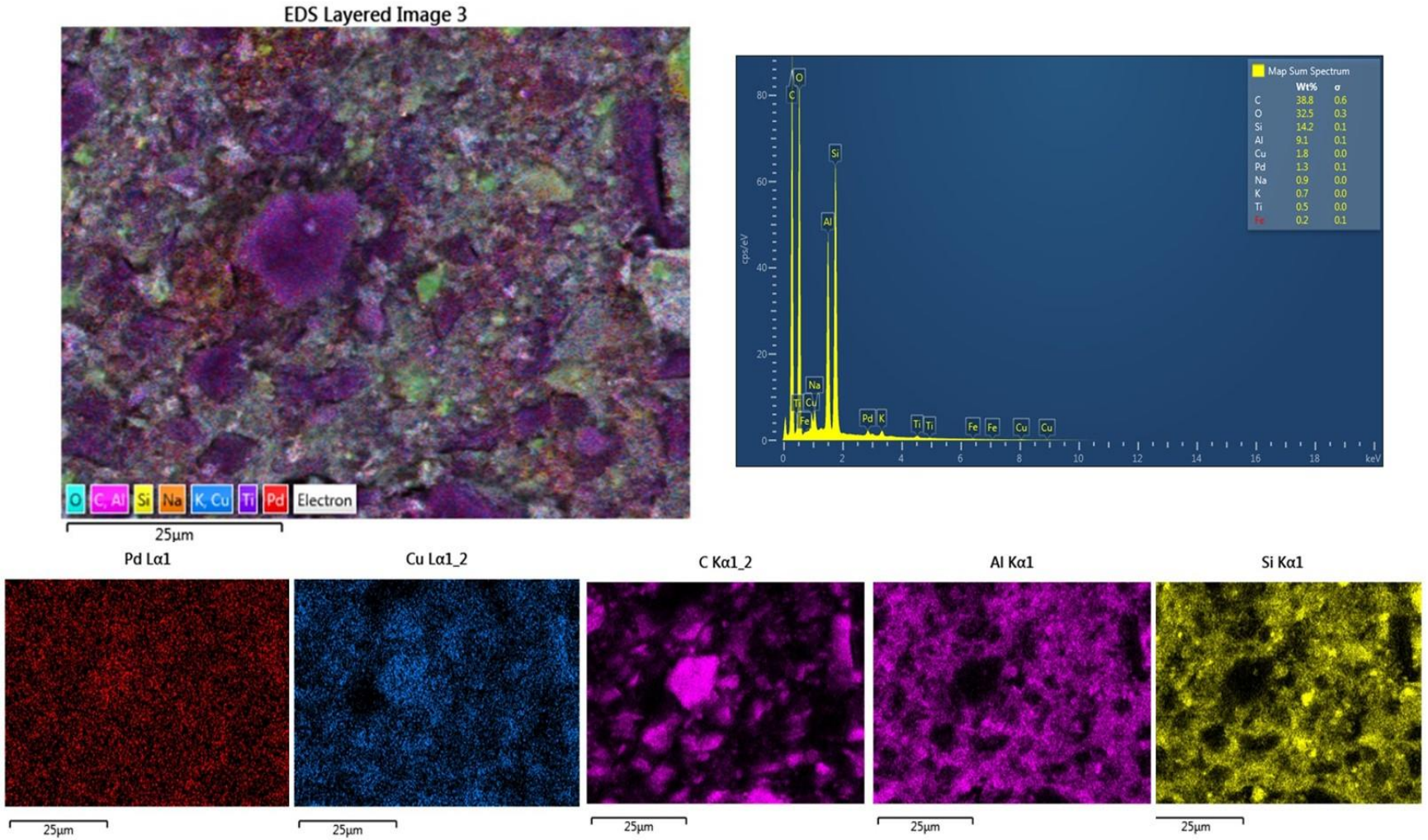

Figure S4.3. SEM-EDS analysis of the Pd-Cu/ACM catalysts (fresh). Pd and Cu is concentrated on the carbon, but also distributed on Al and Si indicative of locations in some areas of the ceramic binder.

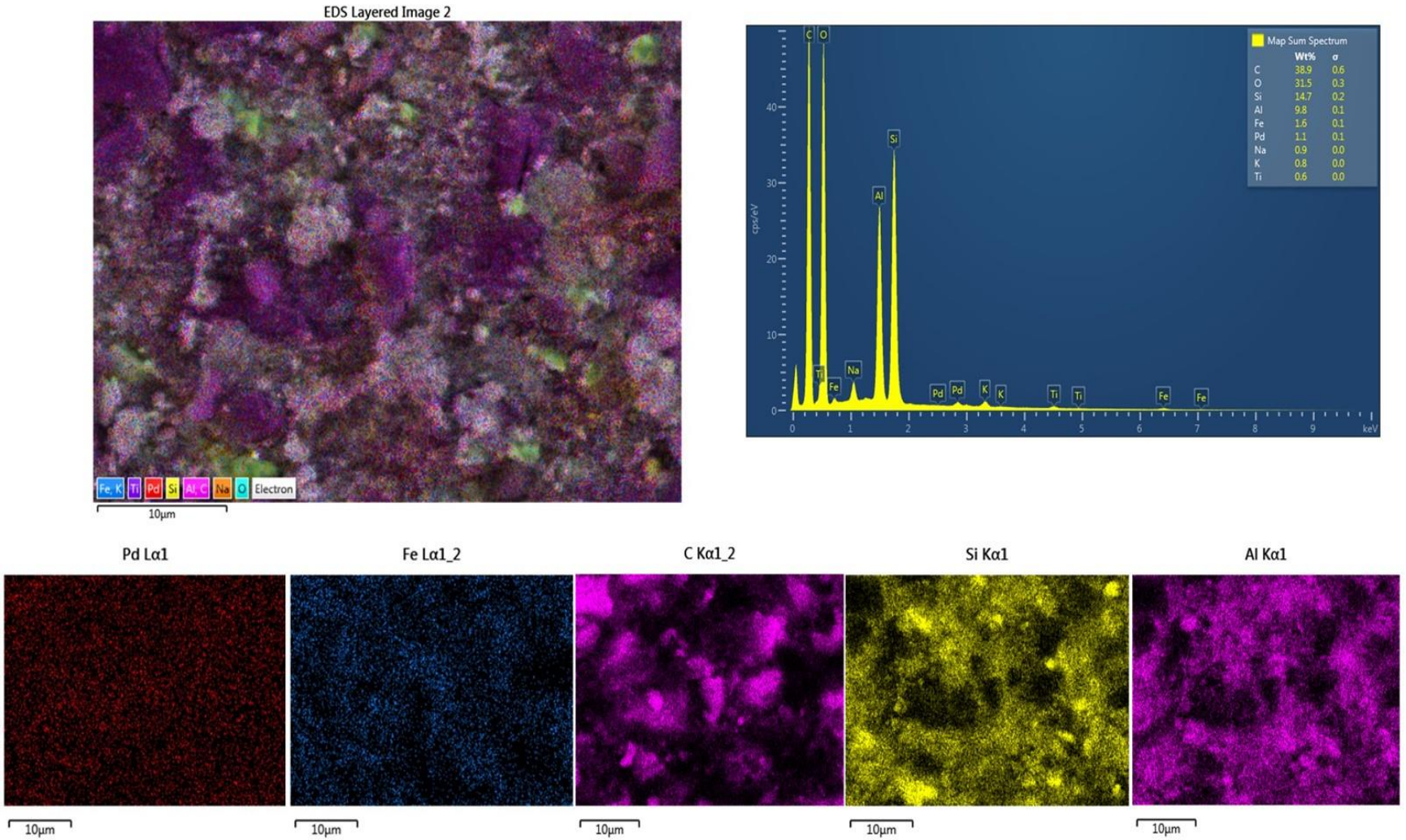

Figure S4.4. SEM-EDS analysis of the Pd-Fe/ACM catalysts (fresh). Pd and Fe is concentrated on the carbon, but also distributed on Al and Si indicative of locations in some areas of the ceramic binder.

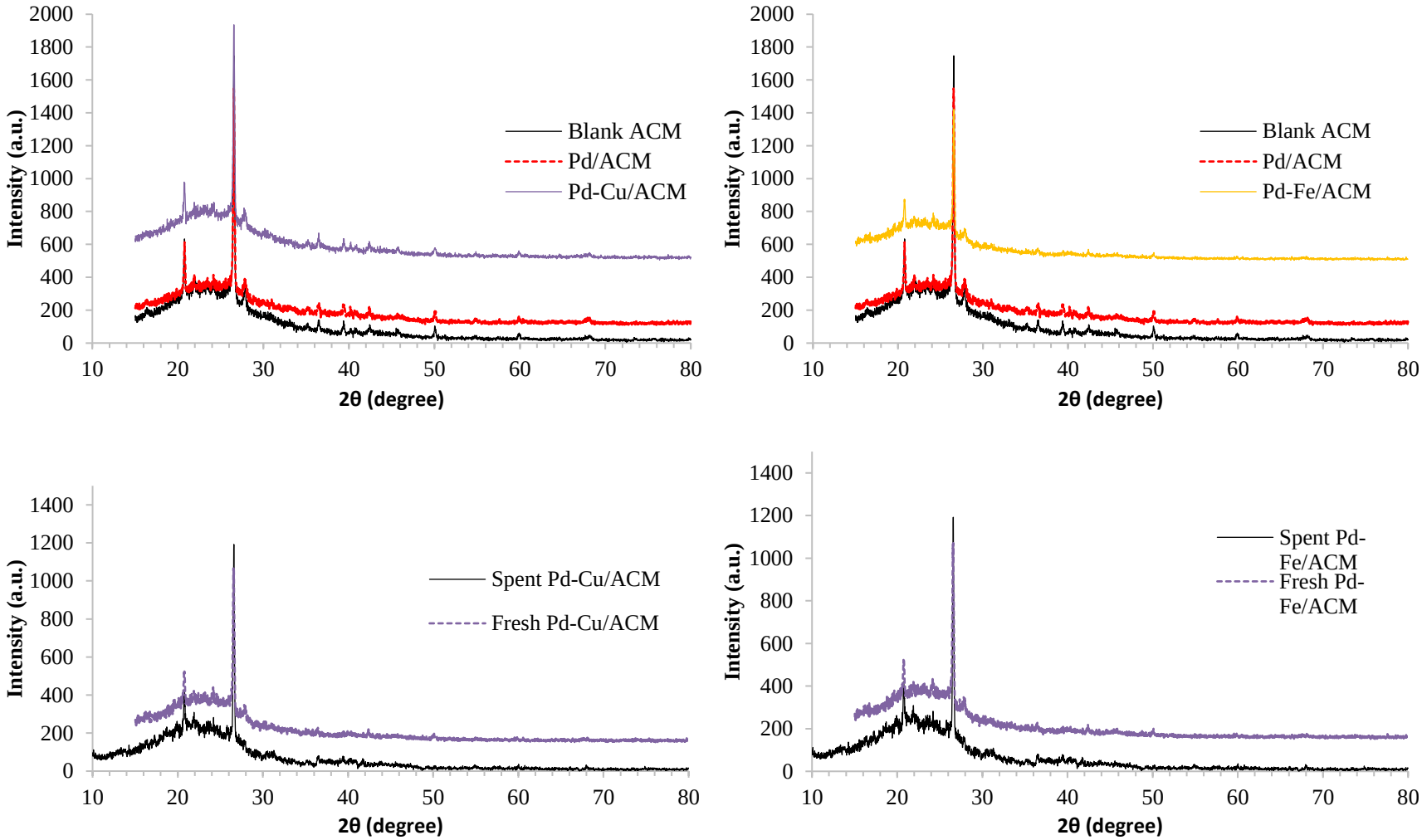

Figure S4.5. XRD analysis of ACM catalysts.

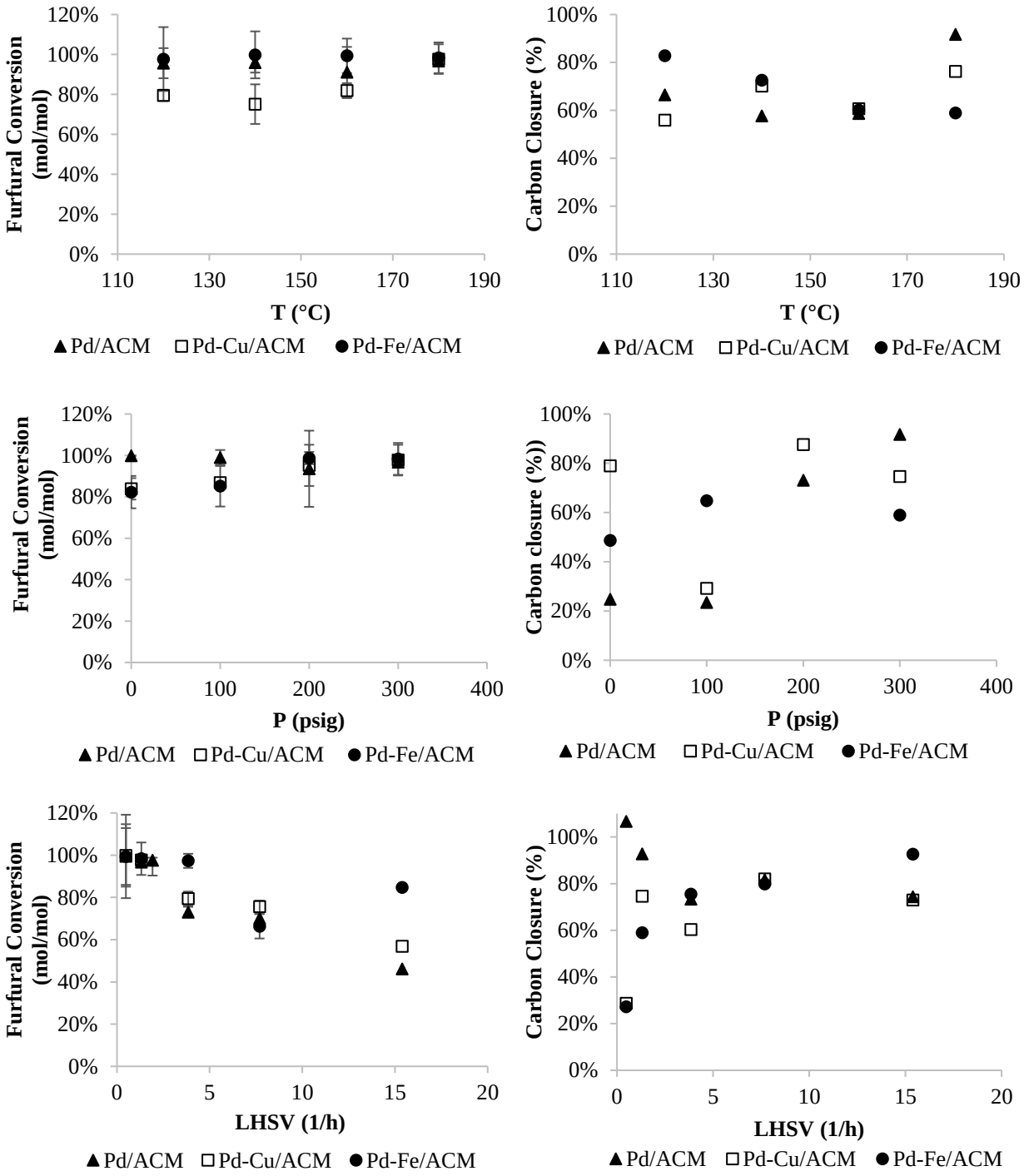

Figure S4.6. Effect of temperature, pressure and LHSV on furfural conversion and carbon balance.

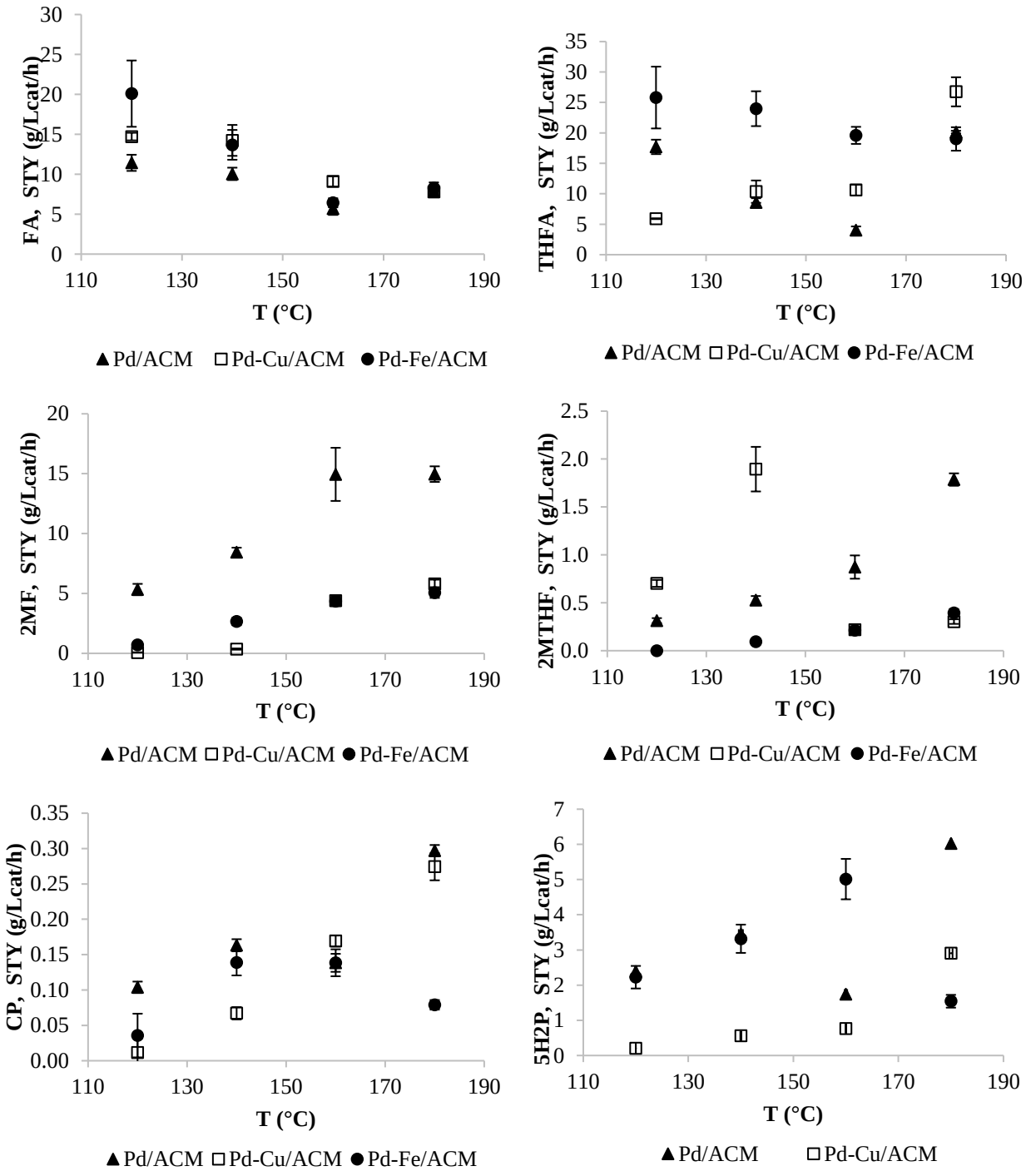

Figure S4.7. Effect of temperature on product space time yield.

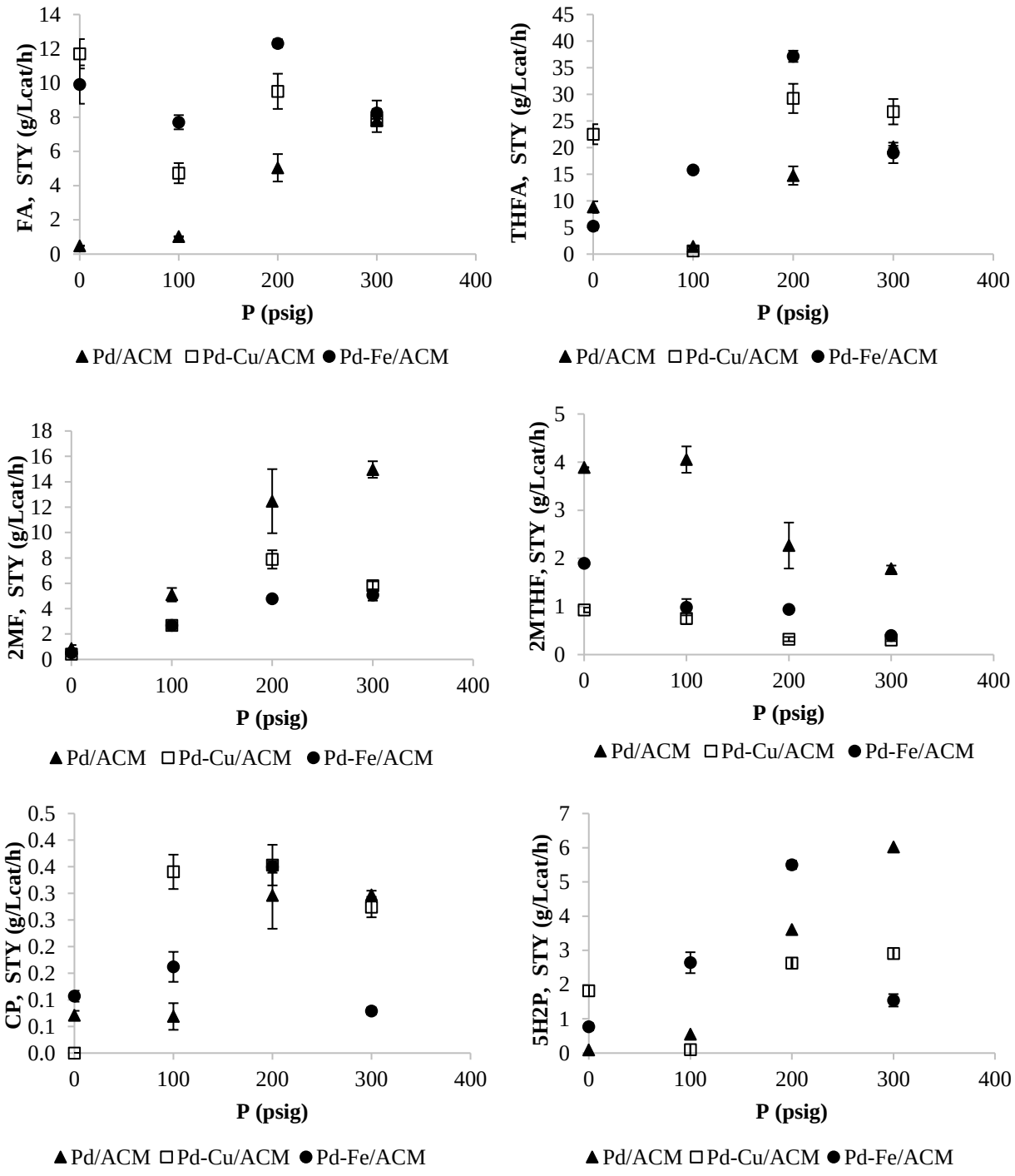

Figure S4.8. Effect of pressure on product space time yield.

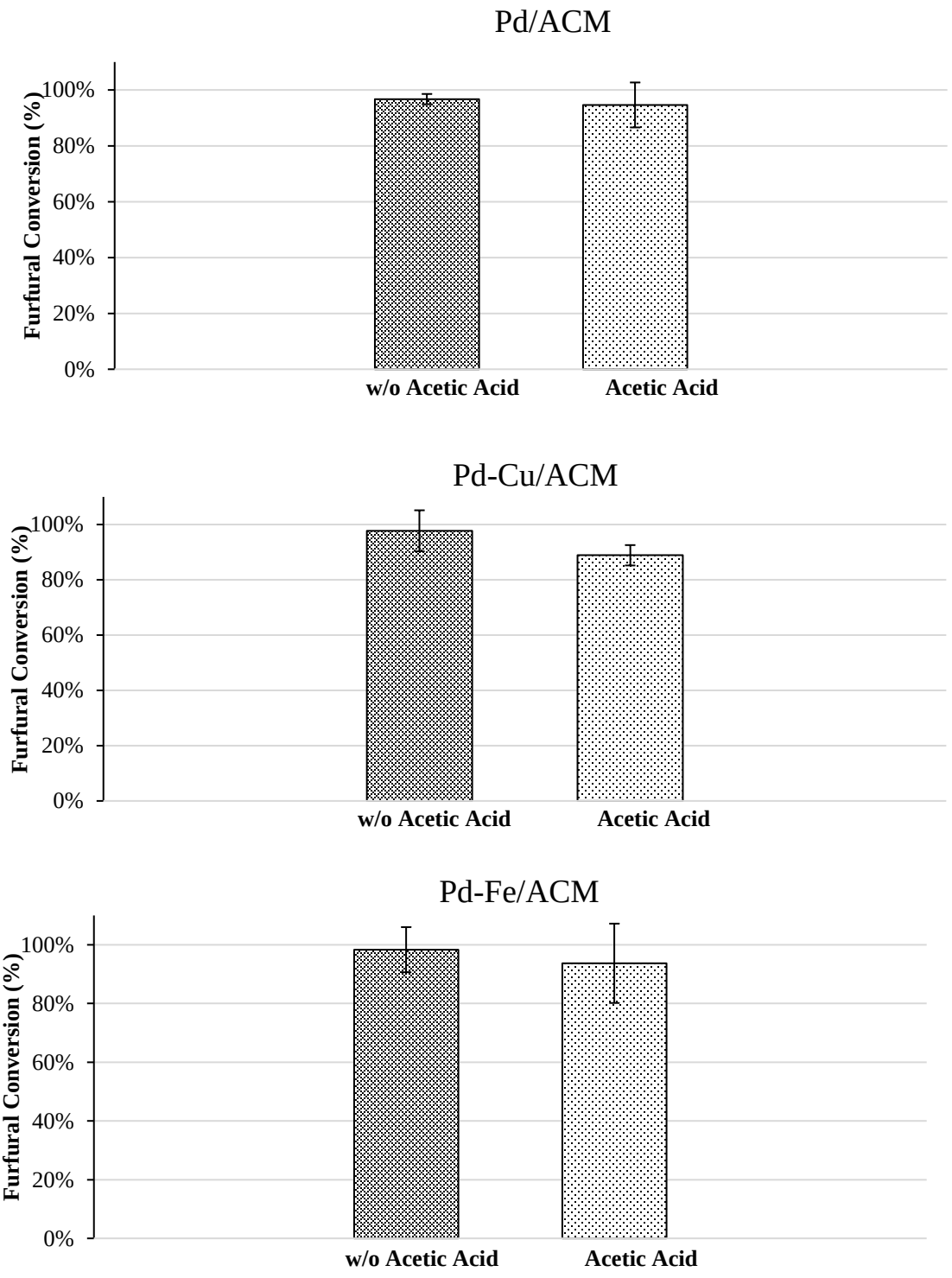

Figure S4.9. Effect of acetic acid on furfural conversion.

APPENDIX C

SUPPLEMENTARY DATA FOR CHAPTER 5

This section contains chapter 5 supplementary information:

1. FTIR analysis of blank CACM

2. Expanded TPR analysis

3. Effect of temperature, pressure and liquid hourly space velocity on furfural conversion and carbon balance

4. Effect of temperature and pressure on product space time yield

5. Effect of acetic acid on furfural conversion

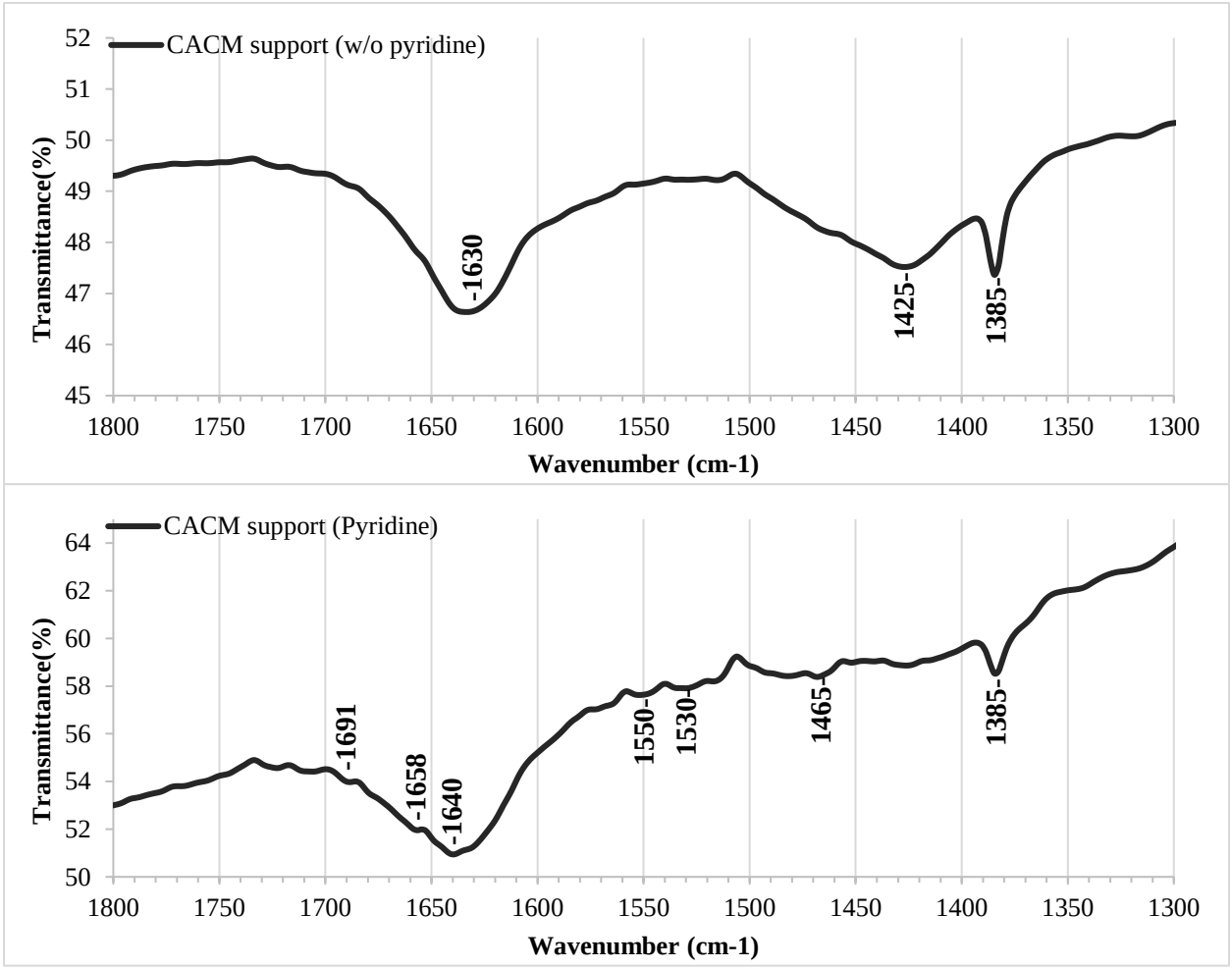

Figure S5.1. FTIR analysis of CACM support.

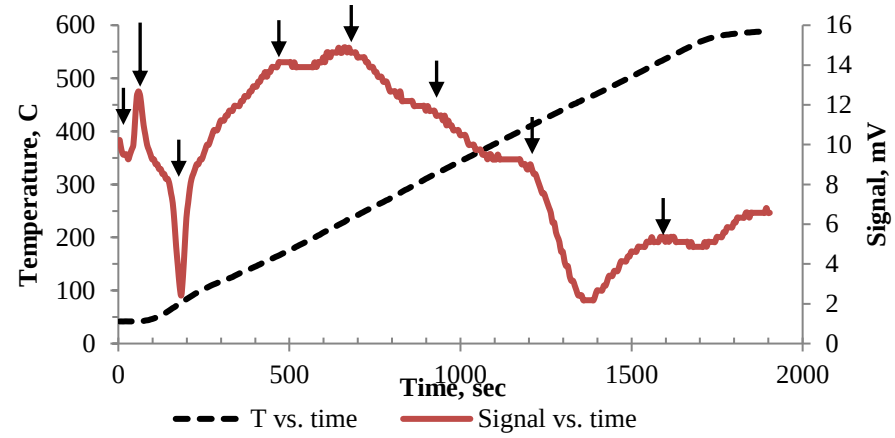

Pd-TiO2/ACM

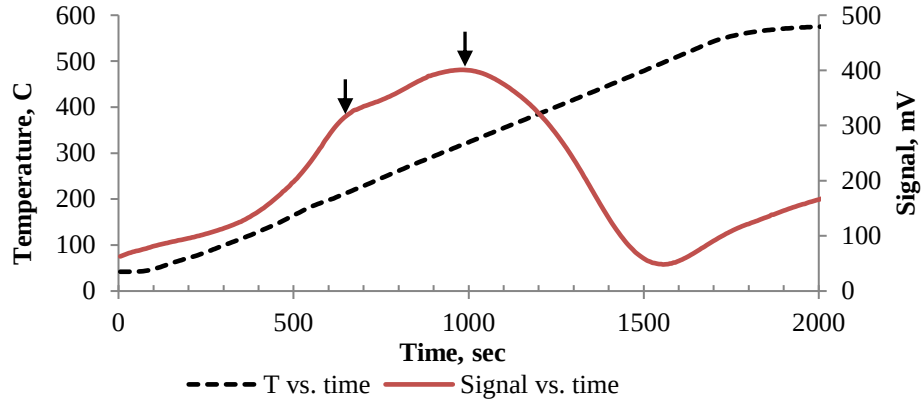

Pd-Cu/ACM

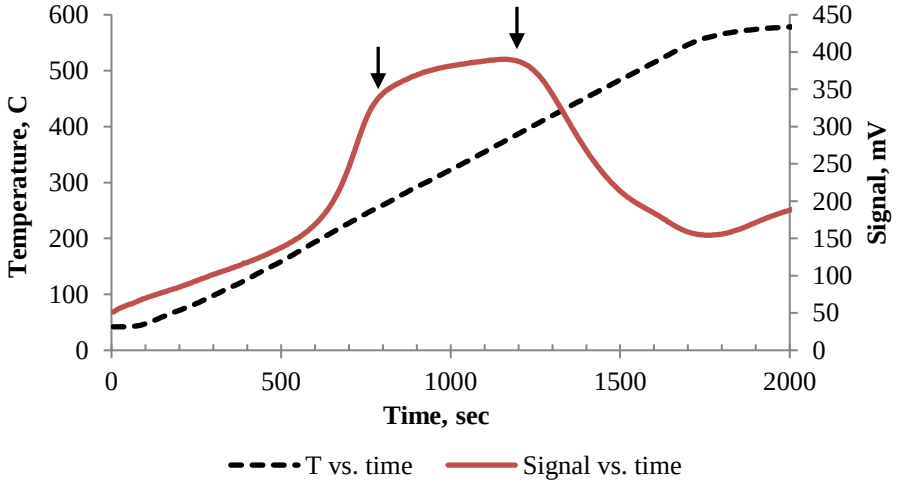

Pd-Fe/ACM

Figure S5.2. Expanded TPR analysis of the carbon catalysts.

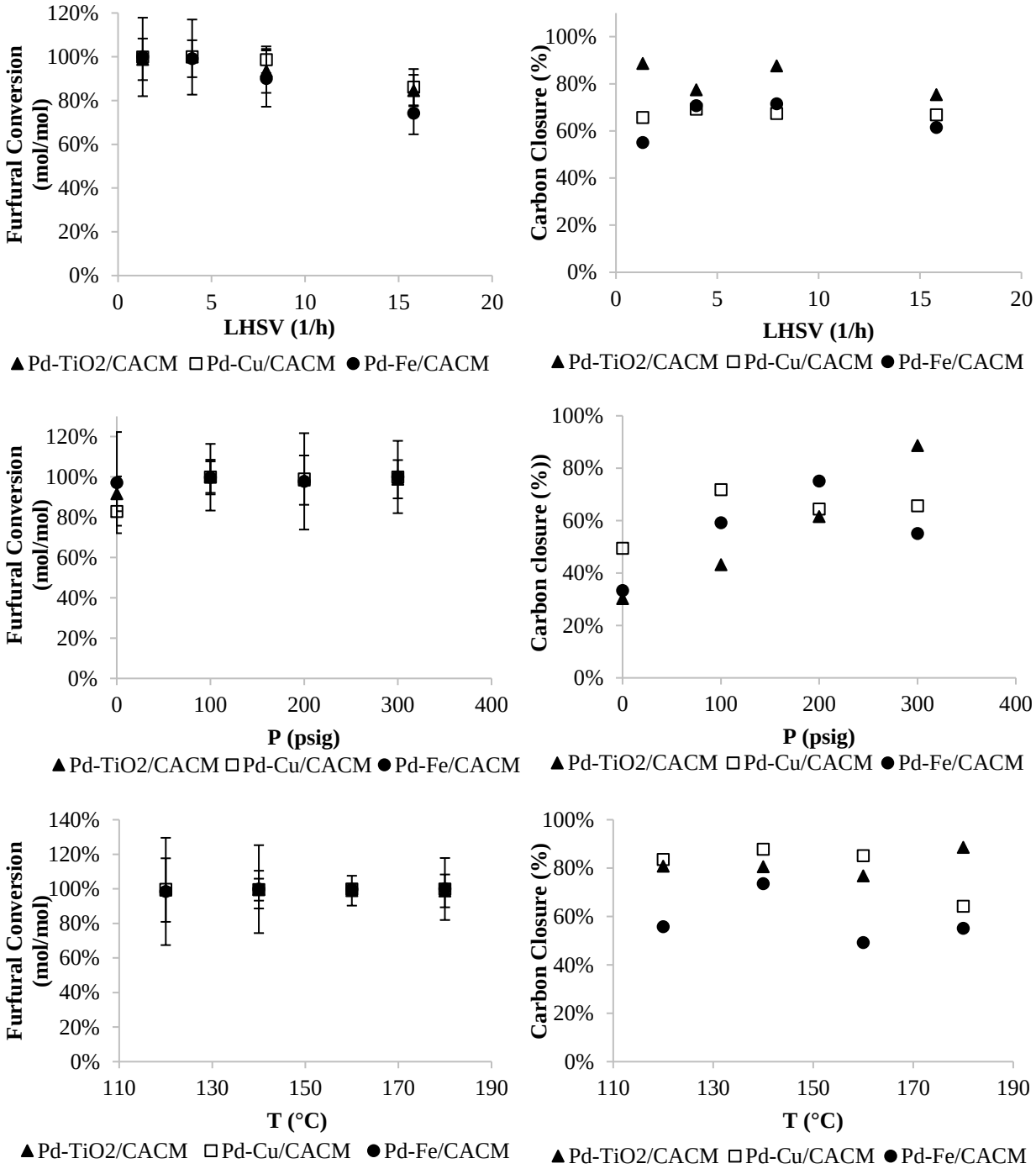

Figure S5.3. Effect of LHSV, pressure and temperature on furfural conversion and carbon closure.

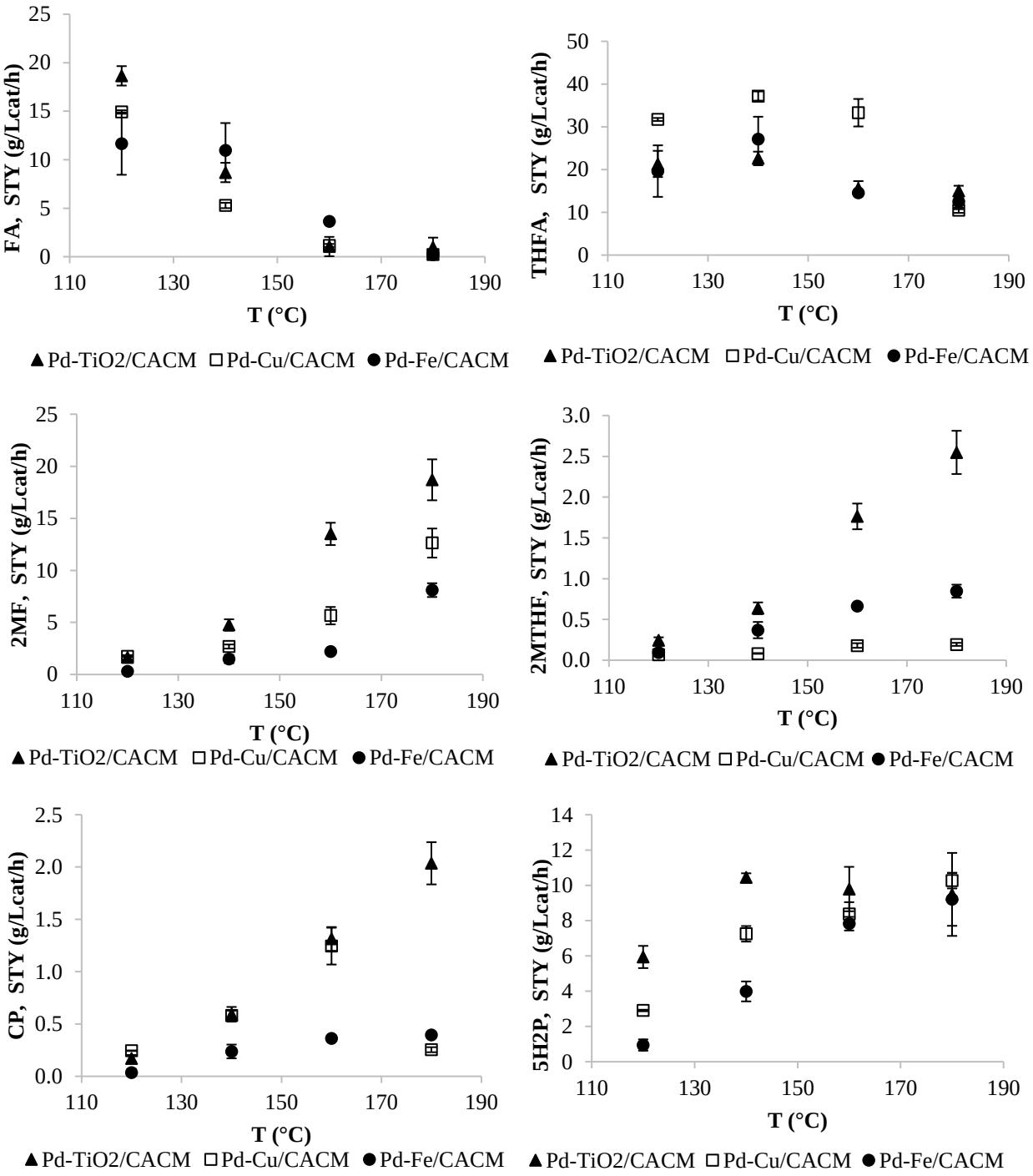

Figure S5.4. Effect of temperature on product space time yield.

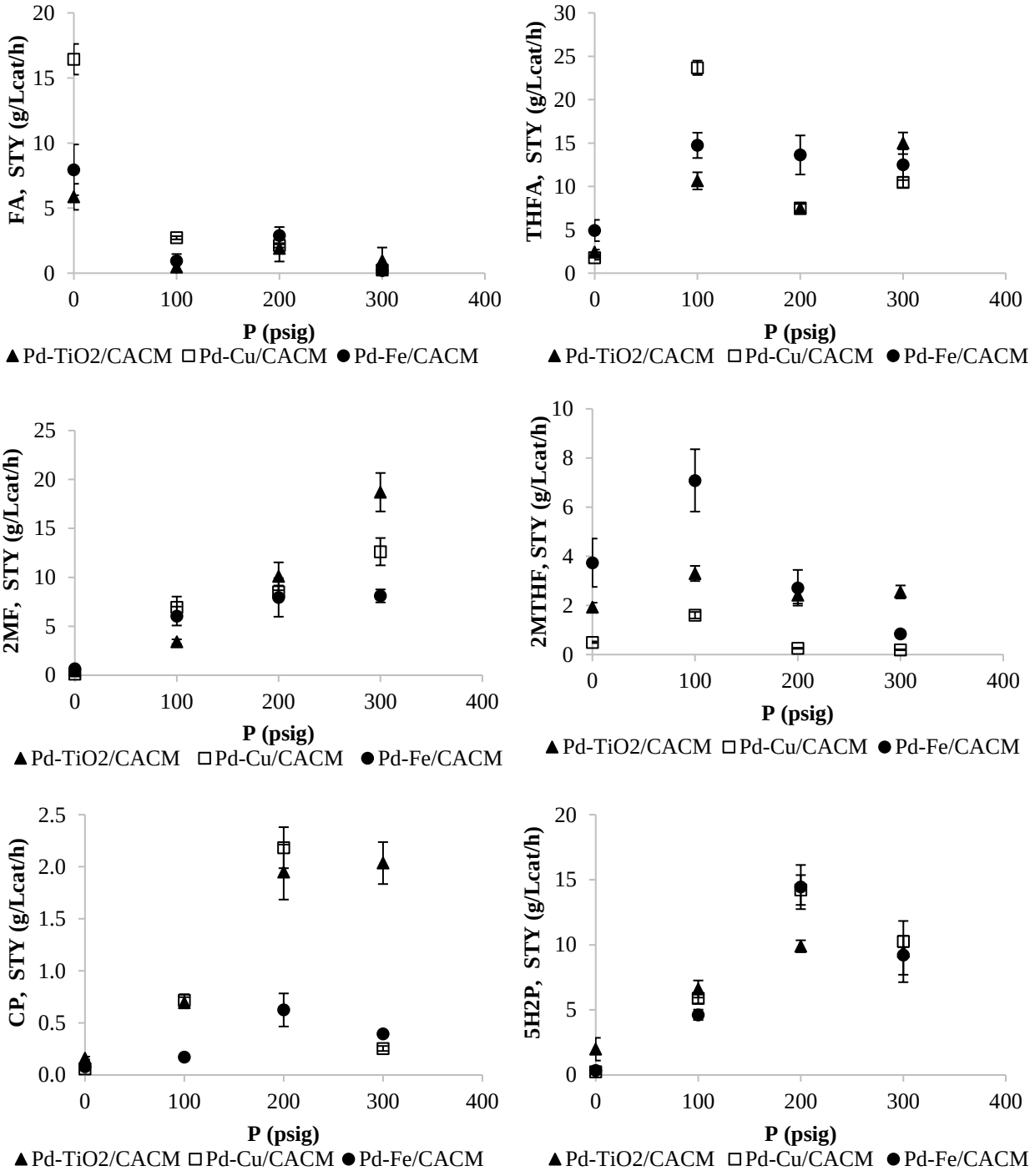

Figure S5.5. Effect of pressure on product space time yield.

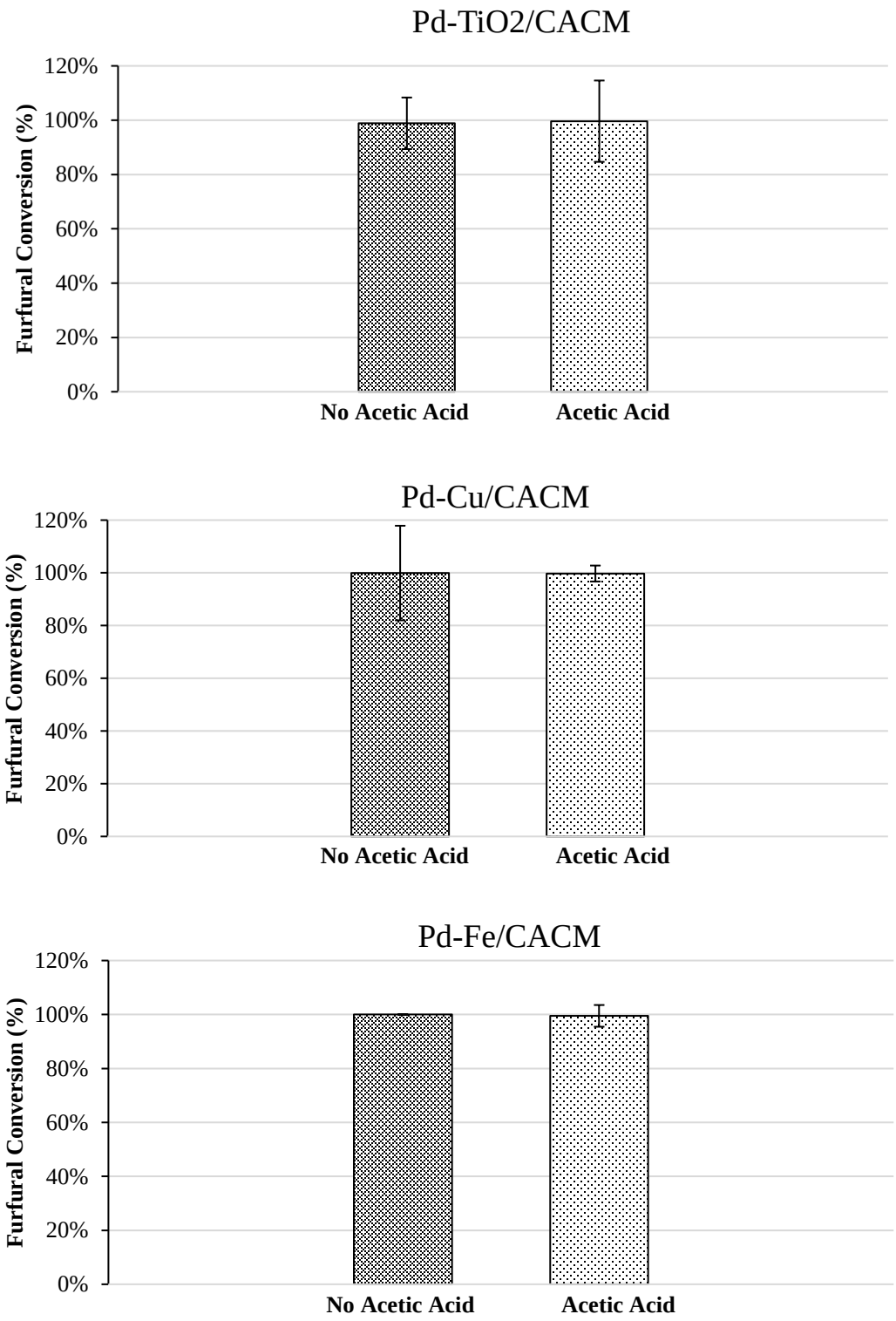

Figure S5.6. Effect of acetic acid on furfural conversion.